Measuring Area and Volume of Leg Ulcers by Structured Light

Peter Plassmann

A thesis submitted in partial fulfilment of the requirements of the Council for National Academic Awards for the degree of Doctor of Philosophy

September 1992

The University of Glamorgan in collaboration with the Royal National Hospital for Rheumatic Diseases, Bath and the Fachhochschule Hannover, Germany

Meinen Eltern

Declaration

This dissertation has not been, nor is being currently submitted for the award of any other degree or similar qualification.

Peter Plassmann

Copyright Statement

This work is partly supported by the German Academic Exchange Service (DAAD).

Acknowledgements

I am most grateful for the outstanding supervision of my Director of Studies, Dr. B.F Jones. He combined careful guidance, continuous help and unequivocal interest throughout the project with genuine warmth and humour and created the motivating and inspiring atmosphere which helped me to quickly overcome the rare phases of doubts and frustration. Working with him was a pleasure and often great fun and I can hardly imagine a better supervisor.

I am also greatly indebted to my second supervisor Dr. E.F.J. Ring from the collaborating establishment, the Royal National Hospital for Rheumatic Diseases in Bath. It was his initiative that induced the project and the fruitful discussions with him were of essential value, assuring that the project resulted in an instrument which is tailored for the real needs of a physician.

My gratitude to Mr. R.J. Williams. His constructive criticism and his valuable suggestions were of great help for the completion of this work.

I am thankful to Prof. Dr.-Ing. W. Heinecke for his initial encouragement to come to Wales and embark on this project. His assistance and expertise throughout the project, especially with financial and organisational problems arising from the collaboration between the Fachhochschule Hannover and the Polytechnic of Wales, were of eminent value.

I gratefully acknowledge the support by Dr. K. Harding from the University Hospital of Wales, College of Medicine in Cardiff. He provided access to patients in order to test the equipment. His challenging and inspiring questions significantly helped to define the strengths and limitations of this work.

I thankfully acknowledge the assistance from all the University's employees whose work and expertise helped to overcome a lot of obstacles. I especially wish to thank Viv Cole for his advice in photographic problems, John Rees for his help with 'C' and Dr. Lawrence Dooley for his special tutorials on digital filtering.

Thanks to all my friends, especially Menna Jones for her listening, understanding and sharing of all my unpredictable moods and problems, for her support and for being there when she was needed.

Finally in these acknowledgements but at a prominent place in my heart I wish to thank my family. I dedicate this thesis to my parents in gratitude for their reassuring support and their encouragement throughout the project.

Abstract

Ulcers of the human skin are difficult to cure and a massive burden to patients. Their treatment costs in the UK are in excess of £ 100 million annually (1989). Both suffering and costs can be reduced significantly by establishing if an ulcer is responding to treatment. Any measurement device must not make any contact with the patient in order to avoid pain, damage or infection of the wound.

This work describes a novel non invasive measurement method for superficial skin ulcers. Measurement is carried out using a new version of colour coded structured light method to obtain three dimensional surface data. A set of parallel stripes of light is projected onto the ulcerated skin and observed by a camera. The stripes are displaced by an amount which is related to the shape of the skin. It is shown how stripe parameters such as colour, distance, width and coding may be optimised with respect to the object of interest to maximise the performance of the method. Two newly developed stripe extraction algorithms ensure that the centre positions of the projected stripes are found with a precision better than 0.1 mm. From the position of the stripes on the skin a computer then calculates a representation of its shape by triangulation. This is stored in a three dimensional surface map. The volume of a skin ulcer is the difference between the measured base of the lesion and the original healthy skin. The work demonstrates that the original shape may be simulated by a specialised spline interpolation method which is based on the surroundings of the ulcer.

The technique is implemented in a portable instrument which is capable of measuring the area and volume of a wide range of different ulcers and pressure sores with a standard deviation of less than 5% of the total figure. With the current equipment the measurement is made in half a second and its result is available after less than 5 minutes.
The technique works well in subdued ambient lighting and on most ulcers. In cases where the ulcer is wet, specular reflection may cause problems but the system is usually able to correct for them. The instrument is suitable for a large variety of ulcers but is not able to measure wounds which undermine the skin, extend outside the normal field of view or are highly flexible.

Table of Contents

page

Chapter D: Software and Principles

Chapter E: Experimental Results

Chapter F: Error Analysis

A: Introduction

A.1 Background of the Work on 3-D Measurement of Skin Ulcers

Many chronically ill people suffer great physical pain when parts of their skin become ulcerated. Skin ulcers develop from minor injuries when a number of factors and circumstances combine. Minor skin injuries are favoured if the elasticity of the skin is decreased by age or as the side effects of medication used to treat other diseases. In combination with insufficient blood perfusion which may be aggregated by smoking, varicose veins or damaged or blocked vein valves, a small injury may quickly develop into an ulcer. A weakened immune system is often an additional complication.
Closely related to skin ulcers, but of a different origin are pressure sores. They are a common problem in bedridden or chairbound patients. Pressure sores appear where the skin is constantly exposed to high pressure, normally over bony prominences. First signs of a developing pressure sore is a slight discolouration of the skin. If the pressure is not relieved a sore appears, the skin surface is destroyed and a cavity may develop.

Skin ulcers and pressure sores respond slowly to treatment, and little is known about the pattern of healing. The study of effective treatment regimes is hampered by the lack of non contact measurement. A means of deciding whether an ulcer is healing by becoming shallower or smaller in area and volume would be useful for the clinical management of the patient. Any measurement method must not entail physical contact due to the need for an aseptic technique and the heightened pain sensitivity around the wound experienced by many patients.

From the medical point of view ulcers and pressure sores are two different illnesses since they are caused by different mechanisms and require different approaches for their treatment. In this work, however, they are treated with little distinction because their physical appearance is very similar and the need for area and volume measurement arises with both.

A.1.1 Incidence of Skin Ulcers and Pressure Sores

Several studies [16,8] have shown that the prevalence of pressure sores in a hospital population is in the region of 6% to 8%. Venous ulceration, especially with elderly people, is extremely common, and vasculitis ulceration as a complication of diseases such as rheumatic arthritis, represents a challenging and expensive clinical problem. The costs of ulcer management in the developed countries are in excess of several billion pounds annually.
In terms of human suffering these conditions also represent a massive burden. The mortality rate of patients with pressure sores was found to be five times as great as usual in a hospital population [8].

A.1.2 Assessment of the Status of Ulcers and Pressure Sores at Present

Due to the lack of any accurate measurement method physicians tried to establish an objective scale for the classification of ulcers and sores. Different schemes for grading have been proposed and reviewed. Some researchers describe a grading schedule with 4 points [113]. Others with 5 points are more descriptive with reference to the diameter of the lesion. In venous ulcers of the leg the lesions are rarely regular enough to measure a diameter. Furthermore the practice of tracing ulcer edges through plastic sheet is painful, imprecise, and always open to infection hazards. This commonly used method is capable of providing area measurement errors of 25% and more [26].
Volume measurement is of great interest to the physician because ulcers tend to heal at their bottom rather than their border. With a fast and accurate volume measurement device doctors could decide at once whether the patient is responding to their treatment.

Volume measurement is impossible with most techniques available at the moment. Raw assessments have been made by filling the ulcer with saline from a calibrated syringe. The method may produce errors of more than 20% [19]. Other approaches uses stereophotogrammetry [26,48] which produces accurate results but is slow since the processing of the photographs and the subsequent manual tracing is very time consuming.

The great variety of treatment regimes and medications which are currently in use arises mainly due to the fact that no fast, accurate and uncomplicated means of assessing the status of healing of skin ulcers and pressure sores is available at present. An accurate and objective measurement device would quickly reduce the number of treatment methods to the most effective ones thus reducing hospitalisation times, costs and patient's suffering.

A.2 Aim of this Work

A.2.1 Formulation of the Problem

In 1988 representatives of the collaborating establishment for this work, the Royal National Hospital for Rheumatic Diseases in Bath, approached the sponsoring establishment, the Polytechnic of Wales, and expressed the need for an objective means for the measurement of leg ulcers. Discussions with the physicians at the hospital resulted in a list of standard specifications. It was agreed that a clinically valuable means of assessing the status of healing of skin ulcers and pressure sores must satisfy a number of constraints:

- the measurement process must not make any contact with the patient to avoid pain and the risk of infection
- the instrument has to be exact, fast and easy to operate
- the measurement process must not require special environmental conditions other than those normally found in a hospital

Since most ulcer patients are confined to a bed or a wheelchair a measurement device would gain additional value if it were relatively small and portable to allow measurements directly at the patient's bed.

The above constraints drastically limit the amount of possible ways to measure skin ulcers. An extensive literature survey into existing measurement methods (see section B.2) revealed that no method or system which is currently available is able to satisfy all the above constraints.

A.2.2 Proposed Solution

In this work a new approach to the problem is proposed.

- The method in use is based on the **structured light technique** in order to obtain three dimensional surface data of the ulcerated skin. The structured light systems which are currently in use are unable to process surfaces with complicated optical properties such as ulcerated human skin, since they are mainly designed for the use of industrial objects with constant (and often lambertian) reflection. Therefore some new procedures have to be developed to deal with problems arising from varying and specular reflections, and the irregular shape of the wound.
- The structured light system comprises of a relatively small portable **3-D sensor** which acquires the structured light images of the lesion and an attached **computer system** where image processing and calculations take place.
- Volume measurements require some kind of definition of what the volume of a skin ulcer actually is. In this work the volume of an ulcer is defined as the difference between the measured ulcerated surface and the original healthy skin. Therefore a procedure has to be found that reproduces the original surface by interpolating from the unaffected skin which surrounds the ulcer.

The proposal outlined above embodies the original contribution to knowledge which is claimed by this work. This is documented in the following section.

A.2.3 Achievements of this Work

The original contribution of this work is the development of the following single techniques and methods and their amalgamation into a combined system:

- the identification of vital parameters of a structured light pattern which is in use with the three dimensional measurement system and a method for the optimisation of these parameters with respect to the object of interest,
- techniques for the localisation and extraction of structured light patterns on an optically inconsistent object using two different sets of image data and specialised image processing algorithms,
- methods and correction algorithms to either avoid or eliminate the influence of significant error sources,
- the design and testing of a virtual reconstruction algorithm for damaged parts of human skin that simulates the mechanical behaviour of the skin.

Section B.2 of the following literature survey gives an overview of existing measurement techniques in order to support the above claims.

In addition to the actual design of a measurement device based on the above innovations this work claims to contribute

- an investigation into possible error sources of the structured light method and an assessment of their significance and influence on the performance of the method,
- and a proceeding to assess accuracy and precision of a three dimensional measurement instrument for skin ulcers considering that the performance of such an instrument depends on connected factors such as the area, the volume and the area/volume ratio of the lesion.

Section B.3 and B.4 of the following literature survey give an overview on the components and methods in use with the structured light technique and their respective error sources. These isolated error sources are analysed later towards their combined influence within the framework of a structured light measurement device.

B: Literature Survey

It is this survey's aim to find the best possible approach for a three dimensional measurement system for skin ulcers. Sources in this survey are discussed in the light of the specifications for the instrument which are outlined before in section A.2.1.

Since the method to be developed inevitably incorporates information, principles and techniques from a wide range of scientific fields this survey is divided into 5 sections.

B.1 The first section investigates biomedical data on ulceration and the human skin. Existing measurement methods for ulcers are discussed. Optical and mechanical properties of the skin are also studied in order to gather underlying information on the object of interest.

B.2 The second section examines existing three dimensional measurement methods considering their applicability to skin ulcers. It provides the rationale for applying the structured light technique for the measurement of skin ulcers and pressure sores.

B.3 In the third section of the survey potential equipment for the structured light technique is investigated. Advantages and limitations of system components are examined.

B.4 This section looks at existing methods and software algorithms which are important for structured light techniques and image processing in general.

B.5 The last section summarises the findings of the preceding survey and draws conclusions relevant to the development of the ulcer measurement system.

B.1 Ulcers, Pressure Sores and the Skin

B.1.1 Incidence of Ulcers and Pressure Sores

There are many reasons why skin ulcers develop. One factor is a weakened immune system which can be caused simply by age, certain diseases or as a side effect of medical treatment. Another contributory cause is poor blood perfusion in certain regions of the skin induced by diseases such as varicose veins, but also by behaviourial influences such as smoking. Other influential factors can be anaemia, diabetes, vitamin deficiencies and metabolic disorders. These multiple factors may all contribute to the likelihood of an ulcer developing on the skin.

Pressure sores are created when a patient has to remain nearly motionless for a longer period of time. Those parts of the body which are weightbearing are then under a constant pressure. These are generally focal areas over bony prominences. In an average hospital population, up to 8% of all bedridden or chairbound patients suffer from ulcers and pressure sores [16] resulting in chronic pain and discomfort. According to a study by Knight [76] in 1988 another 12% are at risk when they have been confined to a bed for longer than one week.

Skin ulcers and pressure sores heal very slowly. Many months rather than weeks are often required for the healing process. Due to difficulties of treatment some patients suffer even longer and may have to live with the lesion for several years. Patients with pressure sores stay between 3.5 and 5 times longer in hospital than usual [8]. The costs for this are an enormous burden to the N.H.S, and are believed to be in excess of £ 100 million annually (1989). An American survey [33] revealed that the costs for one patient alone are between $2,000 and $10,000. The total figure for the United States was estimated being $3 billion to $5 billion (1980).

B.1.2 Treatment

There is general agreement on two main phases for ulcer treatment:

- The first **cleansing phase** is characterised by the presence of necroses, pus or fibrin covering the wound [15]. During the first phase which lasts approximately two weeks, surgery and cleaning by the application of enzymes can be used. The wound is usually treated with 0.9% sodium chloride solution (saline) or dextranomer beads [43].

- The second **granulation/epithelialisation phase** of ulcer treatment may last several months but *"...there is surprisingly little agreement about subsequent management ..."* [19]. Treatment techniques may vary from hospital to hospital. The choice is wide and includes even exotic medicaments such as sugar and honey [109], gold leaf, bismuth and titanium[1]. A 1988 survey concludes that *"there are literally hundreds of agents that are touted to improve healing, but until adequate trials can prove the efficacy of these agents, conservative treatment remains the preferred method"*[2].

At present there are few well-controlled studies to overcome this dilemma. Some of these attempts for objective assessment of the healing status of ulcers and pressure sores are reviewed in the following section.

---

1 for an overview on the more established agents, see Knight, *Medical Management of Pressure Sores* [76] p.97 and 98

2 Knight, [76], p.99

B.1.3 Existing Ulcer Measurement Methods

B.1.3.1 Grading Schemes

Table B.1 shows the oldest and more descriptive method[3] that uses grading schemes for the assessment of ulcers and pressure sores:

Grade	Description
1	discolouration of the skin
2	superficial score
3	destruction of the skin without a cavity
4	destruction of the skin with a cavity

Table B.1: Grading scheme of Jordan and Clark

Another scheme by Lowthian (1985)[3] puts more emphasis on the actual size of the lesion. Grade 1 is a sore with less than 5 mm diameter, grades 2 to 4 if larger. Grade 5 is a *"necrotic or bursal lesion of more than 40 mm diameter overall with a skin opening of less than 15 mm diameter"*.

Unfortunately ulcers of the leg are rarely regular enough in shape to allow simple measurement of diameter. This problem led to an approach using transparent films which is described in the next section.

B.1.3.2 Measurement by Transparent Films

Berg et al. [19] describe a method where a transparent and adhesive film is placed on the skin, completely covering a pressure sore. The volume between the film and surface is then filled with saline solution. The amount of saline necessary to fill the volume is measured, indicating the volume of the sore. Compared with the subjective grading schemes above, this method is more advanced and provides objective measurement.

Pressure sores and ulcers tend to heal from the base rather than the boundary. For this reason volume measurement delivers more evidence on the effectiveness of the applied treatment than area or diameter estimation.

---

3 source: Ring,E.F.J, Clarke,A.K, *"Non invasive ulcer measurement by digitised video"* p.2.
A proposal made by the Royal National Hospital for Rheumatic Diseases, Bath, to the Polytechnic of Wales, Dep. of Electronics & I.T. June 1988. It was this proposal that initiated this project.

Pressure sores may stretch well beneath the visible surface and form a cavity. This is caused by the greater sensitivity of subcutaneous tissue to pressure compared with the skin. By filling the wound with saline, these invisible areas may be measured. The accuracy of the method depends on the size of the sore: Small cavities (ca. 1 cm^3) may be measured with an uncertainty of approximately 10%, bigger ones (ca. 20 cm^3) with up to 5% repeatability. Berg actually states that the above figures characterise the accuracy of the method but this statement must be treated with caution since he does not report how much of the water is absorbed by the wound during the measurement process. Furthermore the method makes contact with the patient and therefore may be painful. It also risks an additional infection due to contamination or damage of the fragile healing tissue.

B.1.3.3 Measurement by Digitised Video

The Department of Clinical Measurement and the Rehabilitation Unit at the RNHRD[4] have made recordings of ulcers by infrared thermography [107]. Figure B.1 shows an infrared linescan through an ulcer.

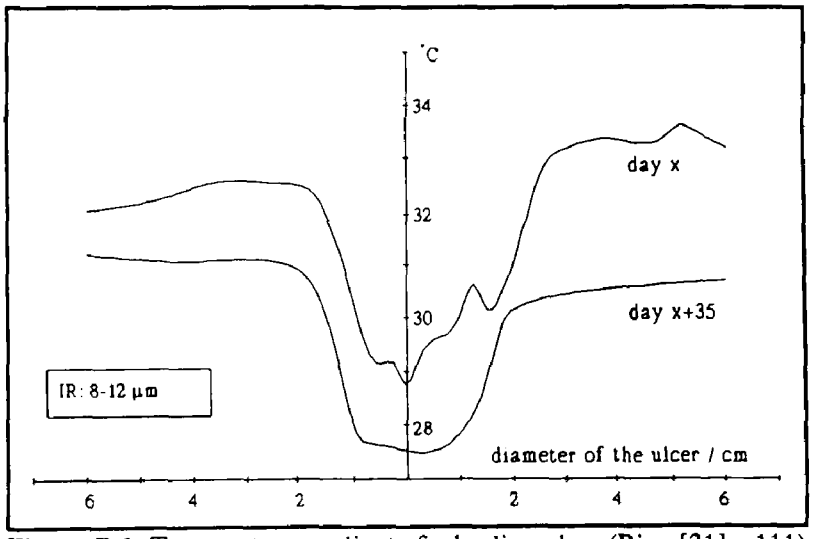

Figure B.1: Temperature gradient of a healing ulcer (Ring [31] p.111)

Inside the lesion the thermogram shows reduced temperature caused by the absence of skin (which has an extremely high IR-emitance) and the presence of evaporating (and thus cooling) fluids. Little information may be extracted from this area as the presence of fluids is more dependant on the dressing of the wound than a certain state of healing.

---

[4] RNHRD: Royal National Hospital for Rheumatic Diseases, Bath. The collaborating establishment for this work.

More useful is the perimeter of the ulcer. The temperature there indicates the effectiveness of blood perfusion. Inflamed areas appear warmer, those with reduced blood supply cooler than normal.
Area measurement by thermograms is not attempted as the boundary of the lesion rarely coincides with the isothermal lines of the thermogram.

The area is measured using a video camera (operating within the visible spectrum) linked to a *pdp11* computer based image processing system. A tracker ball marker is used to follow the perimeter of the digitised ulcer image. From the marked region the system then calculates the area of the ulcer.
As in older methods which use photographs the method is reliable provided that the skin is relatively flat and either the distance from the camera to the skin is known or a scale is visible within the field of view of the camera to provide a means for calibration. Skin curvature inevitably leads to miscalculation as 3-D data can not be processed. Volume measurement is not possible.

B.1.3.4 Stereophotogrammetry

The most advanced approach to measure area and even volume of ulcers was undertaken by Bulstrode et al. [26] and Eriksson et al.[43,44]. Both use a method called stereophotogrammetry where two photographs of the lesion are taken by a special stereo camera that is both camera and projector. After processing the film the transparencies are placed in the camera again. The back of the camera is replaced by a strong projecting light source. Polarising filters are then mounted to each of the two lenses. An operator observes the projected scenes through polarising spectacles. The image from the left lens only reaches his left eye and the image from the right lens passes only to his right eye. Thus a true stereo impression is generated. The observer then traces this virtual image in three dimensions by a mechanical device connected to a computer system. The operator adds data on the boundaries of the ulcer to the tracing. Using this information the surface is reconstructed by a third order curve. The coordinates of the floor of the ulcer are then subtracted from the interpolated curve to calculate its volume. Area calculation uses the boundary information and also the 3D data.

The accuracy of volume measurement is *"5% with a precision of under 2%"*[5]. It will be shown later in this work that statements about the accuracy or precision of volume measurements have to be treated with care since the various factors such as the area of the lesion and its distance from the measurement device influence the reliability of the result. The major disadvantage of the stereophotogrammetry method results from the need to process the film with the stereo images before the scanning process. After processing a skilled operator needs approximately 20 minutes for manually scanning the stereo data into a computer.

B.1.4 Optical Properties of Ulcers

B.1.4.1 Prediction of the Healing Time by Colour Ratios

An approach using digitised video to assess area and volume of a skin ulcer or pressure sore offers not only the advantage of highly accurate measurement but also the possibility to obtain some additional data from certain optical properties of healthy and damaged skin. From this data it may also be possible to forecast the healing time. For burn injuries, which apparently are very similar in their optical properties to skin ulcers this has already been carried out by Afromowitz and his group [3]:

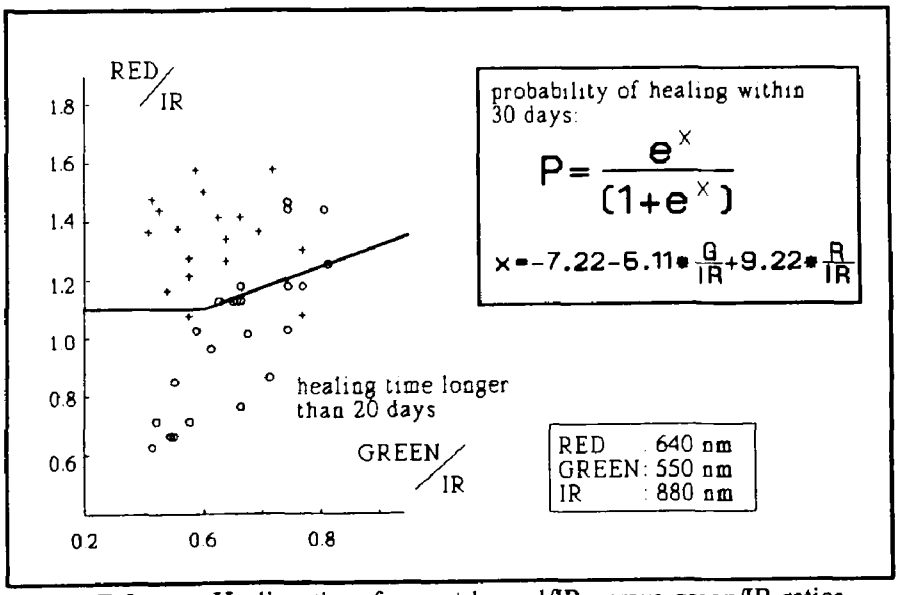

Figure B.2: Healing time forecast by red/IR versus green/IR ratios. (The figure is based on fig.3 on page 116 of [3])

Using the ratio between red and infrared radiation versus the ratio between green and infrared radiation they were able to predict the time necessary for the wound to heal. Afromowitz claims that the

5 Bulstrode et al. [26] p.440

predictions are significantly better than those of experienced physicians [2][6]. The group did not use digitised video but a simple photodetector. Light emitting diodes were used as light sources. Nevertheless the results might be reproduceable using a video camera (which is also sensitive to the near IR, see C.2.2, fig. C.4) and a tungsten halogen light source.

Since the above results are obtained on burns where the pattern of healing differs significantly from skin ulcers, it is doubtful if such a prediction method may be transferable.

B.1.4.2 Classification of Ulcers

Arnqvist and his group [15] attempted to classify healing ulcers by a method involving image processing of colour photographs. They indexed the wound by 16 different parameters. This was achieved manually using three basic classes obtained from the colours of the wound:

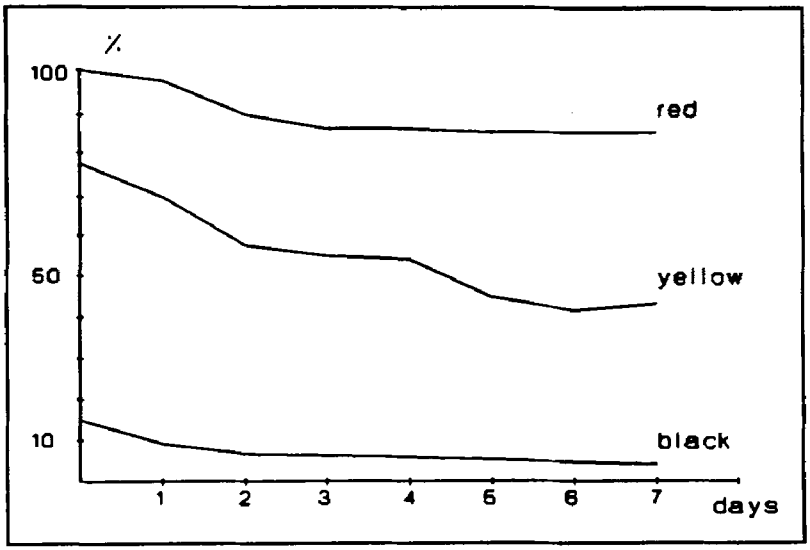

Figure B.3: A typical tracing of a healing process of a venous ulcer. The figure shows the percentage each colour covers on the area of the ulcer. (Based on fig.2 on page 460 of [15])

- Class 1: **Black** necrotic eschar
- Class 2: **Yellow** necrosis and fibrin
- Class 3: **Red** granulation tissue

The amount of red, yellow and black surface was traced while the ulcer was healing as shown in figure B.3. This method may be improved by using pictures of the ulcer directly without intermediate photography and under controlled and constant lighting conditions.

---

[6] [2] table 1 and 2 p.503

B.1.5. Optical Properties of Healthy Human Skin

The human skin is a complex organ. It is extremely inhomogeneous with many different cells and structures. It varies between individuals and race. Even in one individual the variations in thickness, colour and other properties are very large. The varying colour properties of the skin are of special interest in this work.
While some groups tried to solve the problem using a mathematical model [14] many research groups have measured the reflectance or absorbance spectra of skin for all skin types [13,35,73,77] providing well founded information about this crucial factor. Typical measurements were made by Kuppenheim and Heer:

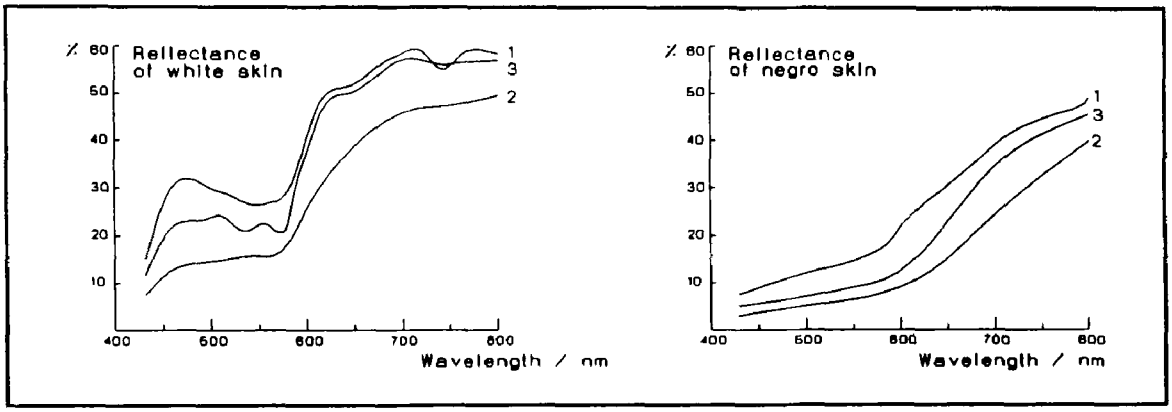

Figure B.4: Spectral reflectance of white (left) and negro skin (right) (after fig.1&2, p.801, [77])
1 untanned **2** most tanned **3** medium tanned

Figure B.4 shows the spectral reflectance of white and negro skin. The local minimum between 530 and 590 nm may be attributed mainly to haemoglobin, oxy-haemoglobin (in the red blood vessels) and bilirubin, while the underlying slope of the curve is caused by the change of the melanin[7] content of the skin [46]. Figure B.5 shows their absorbance spectra.

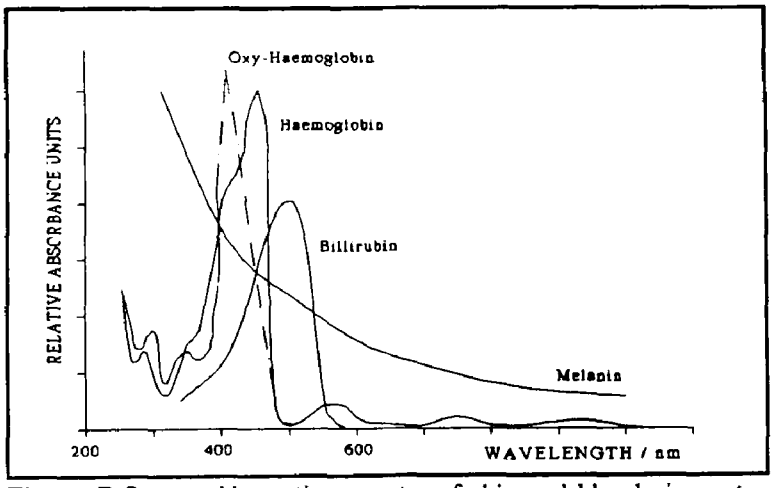

Figure B.5: Absorption spectra of skin and blood pigments (based on fig. 28.1, p.254, [13])

[7] The production of the pigment melanin in the skin is stimulated by ultraviolet light and is the cause for suntan.

According to Anderson and Parish [13] the differences between "black", "white" and other colours of human skin are solely caused by this pigment in the epidermis. The other layers of the skin (stratum corneum, dermis) are identical for all races. These layers contain the haemoglobin and the pigments bilirubin and carotene [46] and are not affected either by suntan or race. This fact is important as ulcers totally destroy the epidermis with the melanin that is mainly responsible for the difference in skin colours.

The ulcerated area uncovers the deeper layers of skin and flesh where colours are identical for all individuals. Thus ulcers of all patients, regardless of skin colour, may be classified by the same colour based scheme.

Skin is not an ideal reflector for visible light. A sharp beam of light is scattered, absorbed and reflected by the different layers of the skin. A measurement technique, based on light, has to take these factors into account. In particular it is necessary to deal with the widening effect caused by scattering that blurs the pattern projected onto the skin. Figure B.6 illustrates this. Only a small amount of light (4% - 7%) is regularly reflected over the entire visible spectrum due to the change in the refractive index between air (n_D=1.0) and stratum corneum (n_D≈1.55). Transmission through the epidermis is 10-15% in white skin and 2-5% in black skin. The rest is scattered and absorbed leading to the reflectance spectra shown in figure B.4.

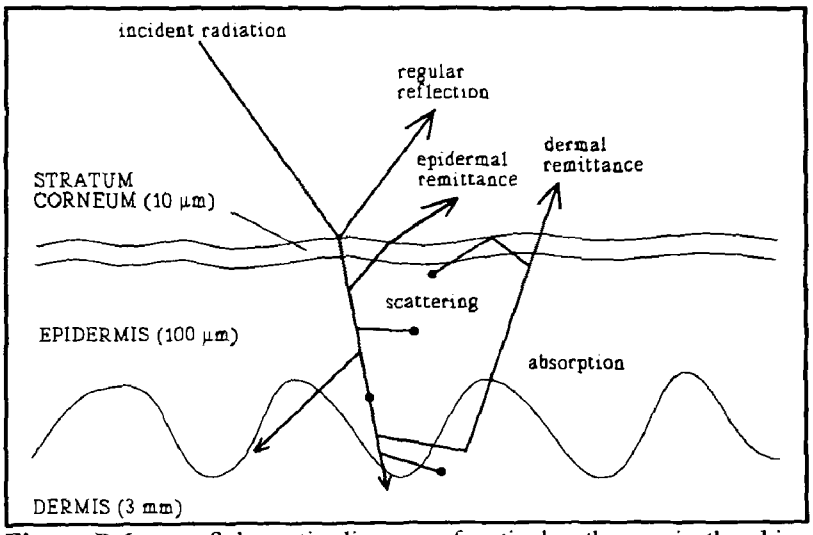

Figure B.6: Schematic diagram of optical pathways in the skin (based on fig.1, p.14, [13])

B.1.6 Mechanical Properties of Skin and Subcutaneous Tissues

As already mentioned in B.1.3.4 the reconstruction of the former healthy skin is essential for volume measurement of an ulcer as the lesion's volume is the difference between the reconstructed and the actually measured skin surface.
Human skin is a composite elastic tissue. The elasticity is caused by both its micro- and macrostructure. On the molecular level the elasticity is provided by collagen and elastin fibres that are embedded in an amorphous matrix of mucopolysaccharides and arranged in two planar networks [78]. The collagen fibres gain their ability to stretch from being highly twisted while the elastin fibres have elastical properties. The fibres' network may stretch isotropically.

The macrostructure are the visible wrinkles on the outside and the undulation of the dermo-epidermal junction inside the skin. Both provide a reserve of tissue during normal body movement allowing the epidermis to stretch without damaging the cell matrix. The macrostructure is anisotropic to tension which is apparent on skin covering the fingers. The skin stretches more readily in a longitudinal direction. On the inside of the forearm the limit of strain in a longitudinal direction is approximately 28% while in transverse direction it is only about 10% [47][8].

Subcutaneous tissues are also anisotropic. Apart from a layer of fat directly under the skin, muscular texture has a preference for stretching in the longitudinal direction. On the legs and arms this anisotropy is identical to that of the skin.

An ulcer interrupts the matrices of flesh, fat and skin. The lines of tension change their position and become more dense around the lesion tearing it apart. This effect may be observed in a small scale on a minor accidental cut. As a result the parts of the skin which are close to the wound become slightly elevated. The higher the tension in the skin, the higher the elevation appears. Any method that attempts to reconstruct the former undamaged skin must take this behaviour into consideration.

---

[8] see figure 10.1 on page 84 of [47]

B.2 3-D Measurement Techniques

Three dimensional objects may be measured with a variety of sensors, systems and methods. Normally the measurement process is selected to comply with the circumstances imposed by demands of accuracy, the environment in which the measurement has to take place, safety requirements, and of course, the object of interest itself. This chapter gives a brief review of several existing techniques in the light of the findings of the preceding chapter on ulcers and pressure sores.

All existing methods of three dimensional measurements may be systematically classified by the sensor channel and the principle they use. Figure B.7 below gives an overview of the most common methods with special emphasis placed on optical techniques. The following analysis will show that the structured light technique is the most promising for the non-contact measurement of skin ulcers and pressure sores.

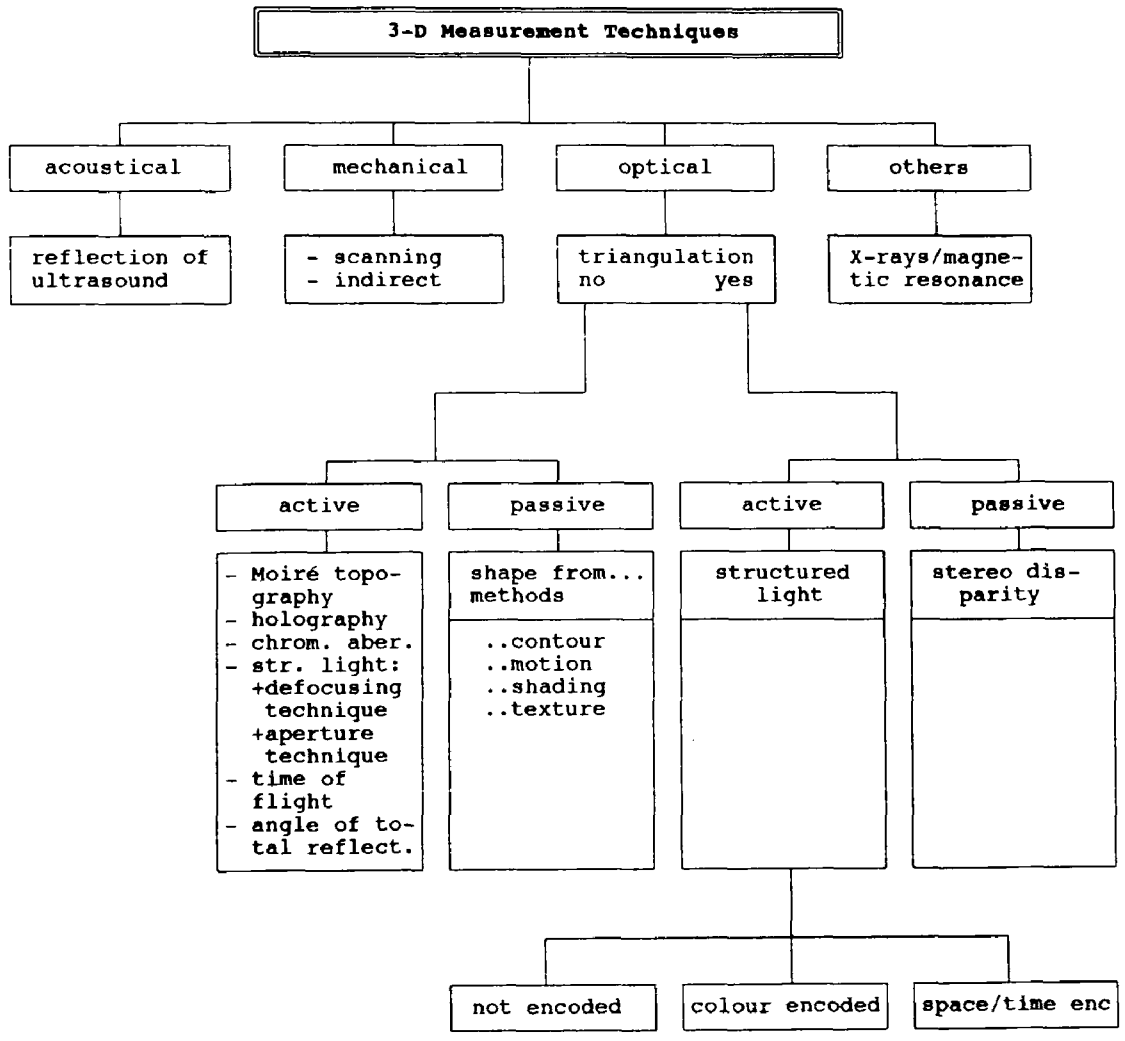

Figure B.7: 3-D measurements methods with emphasis on optical techniques

B.2.1 Non - optical Measurement Techniques

B.2.1.1 Acoustic

Acoustic methods mainly depend on ultrasound rather than audible sound as the possible resolution increases with shorter wavelengths. Acoustic scanners do not have to make contact if distance measurement is required. This is only necessary if the inner structure of an object is of interest. Common applications in industry are the quality control of welding joints and the detection of faults in the inner structure of metals. In medical diagnostics ultrasonic scanners are standard equipment for soft tissue scans within the body. The reflected ultrasound is interpreted to form a picture which may be displayed in real time onto a monitor. Unfortunately the density differences within the human body especially the flesh are very small. As acoustic waves, like light waves, are only reflected where density changes occur in the transmitting medium, the images are often vague, have poor contrast and are affected by noise.

Woodcock [130] describes another medical application where the Doppler effect is exploited to measure the flow of blood within the vessels. Blood which is flowing towards the ultrasound sensor slightly increases the frequency of the reflected wave, while blood which moves away from the sensor decreases the frequency. The frequency shift is then used to determine the velocity of the bloodflow.
To obtain such information from within a body or structure the ultrasound emitting and receiving head has to be placed directly onto the surface. A gel is used to guarantee good acoustic coupling. For that reason an ultrasonic *depth* scanner cannot be used for ulcer measurement.
An ultrasonic *surface* imager is possible but compared with a normal camera its resolution is always relatively low since ultrasonic waves are difficult to focus to a single narrow beam. Even the latest developments which use phase shift arrays, a technique adapted from microwave range finders (radar) [96] still have relatively poor resolution [65]. Resolution may be increased by taking multiple "pictures" from different positions [29]. However this process is time consuming and not suitable for skin ulcer measurement since a patient must remain motionless during the scanning procedure. Due to the limited speed of ultrasound waves in air (approximately 330 m/s) a sequential scan of a surface with 100 times 100 points at a distance of 20 cm takes approximately 13 seconds.

B.2.1.2 Mechanical

All mechanical measurement systems have one major disadvantage: they make contact with the patient. The plastic-sheet-method of Berg's group [19], mentioned earlier, nevertheless has the advantage of measuring an ulcer's volume even when it undermines the skin and the internal surface is not totally visible. This is clearly impossible for all optical techniques. As the technique is simple and cheap it undoubtedly has advantages when there is a need to assess the status of healing in ulcers with cavities under the epidermis.

Mechanical scanners are very popular in industry for measurements and quality control. But for medical tasks a mechanism where a sensor device glides over the inflamed surface combines all the possible disadvantages of other techniques: it is slow, inaccurate as the patient may move while scanning, painful, risks infection and does not trace cavities under the epidermis. Therefore this technique is totally inadequate for ulcer measurement.

B.2.1.3 X-rays and the Magnetic Resonance Effect

Two or three dimensional scanners (tomographs) for medical use are based either on the absorption of X-rays or on nuclear magnetic resonance.

The X-ray tomograph scans a slice of the human body from different angles. A computer reconstructs a complete image of the slice out of the multiple scans. Scans of many slices may be added to a three dimensional representation of the body's inside.

Richard et al. [104] use a CT-9800 scanner with a scan time of 1.3 seconds for one slice of approximately 1.5 mm thickness. A 3-D scan of an area of 15 cm thickness (approx. necessary for a skin ulcer) would therefore last more than two minutes. During this period the patient is exposed to X-rays and must not move. This is probably the reason why Richard and his team used post mortem material for their experiments.

The magnetic resonance effect may also be used to obtain 3-D data [90]. The patient is placed within an extremely strong (0.5 to 2 Tesla, superconducting) electromagnet and irradiated with a high frequency electromagnetic field. The magnet makes the instrument very bulky and no metals (heart pacemakers, watches) must be present within the area influenced by its field.
The output of the scanner is processed by a computer in pseudo colour pictures. Each picture represents a thin cross section through the body. Multiple scans may be added for a full three dimensional picture. The latest scanners are able to take 128 cross sections through any part of the body in 10 minutes or less [74]. During this scanning time the patient must not move. An average resolution of 0.6 mm^3 may be achieved.

Thus tomographic scanners provide an excellent means to obtain information from inside the human body. They are highly accurate and harmless[9] as no X-rays or radioactive rays are used.
But as before, scanning time where the patient must not move is a problem. Additionally magnetic resonance scanners are prohibitively expensive (ca. 1 million pounds) and therefore rare equipment in a normal hospital.

Another disadvantage is the sheer physical size of the scanners. They are not portable and the patient has to be carried to the instrument rather than the preferable other way round.

B.2.2 Optical, Non Triangulation Techniques

Optical measurement techniques mostly involve some kind of a computer vision approach. General introduction into the area of computer vision and image processing may be found in [23,39,62]. Jarvis [71] gives a specialised discussion on range finding techniques.

---

[9] This is currently being questioned. Side effects may be produced by the high frequency radiation that heats the body or the presence of recently discovered tiny magnetic particles in the brain.

B.2.2.1 Active Non-Triangulation Techniques

In active methods the measurement device is involved in a certain kind of activity i.e. the projection of some kind of pattern onto the object. A method is passive when the measurement device only observes[10]. It is the general advantage of active methods that the projected patterns create a well known and controlled lighting environment. Changes in brightness or colour of the ambient roomlight can normally be ignored.

1. Time of flight method. The underlying principle of this method is the speed of light in a medium. The time from transmission to reception of the reflected wave is directly proportional to its distance. Agin [6] (p.37,38) discusses this method. The major obstacle, however, is the need for a scanning process that will last several seconds. No information other than distance is obtainable by this method.

2. Moiré topography. This method uses the Moiré interference effect to produce depth contour following fringes on an object. The method may be applied to the whole human body [123] or to small industrial components [24]. The method is very accurate. Errors are within 0.2% of the total distance to the object. The main problem with this technique is to determine the direction in which the change in depth occurs.
It is impossible to code the fringes or stripes. Coding of stripes is necessary as a labelling process for all fringes is essential for later image processing. As soon as the reflectivity of the object is not completely ideal stripes will be blurred or partly invisible. This makes the labelling process difficult if not impossible.

3. Holographic interferometry. The principle of this method is the same as the one of the Moiré technique. The difference is that the fringe pattern will be produced by a hologram [59](p.608). The disadvantages are the same [68,69].

This is not a generally agreed definition. Some researchers would call an observer that is involved in some kind of activity (like automatic adaptation to the level of illumination, focusing on certain points of interest and movement of the sensor (human eye, camera)) an active observer. For this work, however, this definition is believed not to be suitable.

4. Angle of total reflectance. This method projects a tiny spot of laser light onto the surface to be measured. A critical angle prism, a convex lens and two photodiodes, followed by a differential amplifier are used to measure the distance of the spot. Details may be found in [87]. But again, a time consuming scanning process is necessary, and no information other than distance may be obtained.

5. Aperture technique. A mask in the aperture of a lens is used to produce a double image of a stripe which is being projected onto an object [20]. The distance of the two stripes is directly proportional to the distance of the observed surface. Since the distance between two stripes may be considerably their number is limited to allow their identification and to prevent overlapping. This restricts the total number of stripes to less than 10. In order to obtain higher resolution, multiple pictures with the stripe pattern slightly moved must be taken. This again is a scanning process with the disadvantages mentioned above.

6. Defocusing technique. When a pattern is projected onto a surface it will be in focus for a certain distance only. Increasing or decreasing the distance will cause the pattern to defocus. The amount of defocusing may be measured and interpreted as a change in distance [52]. This method works on objects with homogenous reflectivity only. Skin with its variations due to scattering and absorption can not be measured. The object must not vary too much in its height as this would cause the pattern to defocus beyond recognition.

In table B.2 the advantages and disadvantages of non-triangulation techniques are compared. The disadvantages are so relevant that these systems are inappropriate for the purpose of skin ulcer measurement.

METHOD	ADVANTAGES	DISADVANTAGES
time of flight method [6]	-direct measurement of distances	-depth resolution less than 1 mm -mechanical scanning system -slow -only depth information obtainable -no colour information
Moiré topography [24,123]	-only 0.2% depth error -additional information from colour available	-difficult to derive the direction of the change of depth -stripe labelling problems
holography [59,68,69]	-accurate	-as Moiré topography -no colour information available
angle of total reflectance method [87]	-extremely accurate	-scanning process --> slow -polished objects only -object has to be fixed relative to the system -no colour information
aperture technique [20]		-scanning process --> slow -limited resolution and accuracy have to be overcome by processing multiple images
defocusing technique [52]		-scanning process --> slow -homogeneous surface required -depth changes of object limited

Table B.2: Non-triangulation 3-D vision systems

B.2.2.2 Passive Non-Triangulation Techniques

Passive Non-Triangulation Techniques mainly cover the big group of *Shape From .....* methods [9]: shape from shading, contour, texture and motion. Generally all these methods are more descriptive than accurate measurement methods.

1. Shape from Shading, was proposed first by Horn [62] and adapted by other researchers such as Houken and Korsten [64]. The method calculates a 3-D surface representation from shades on the object. It requires knowledge about certain physical properties of the surface such as reflectivity and specularity: It assumes that

- the surface is smooth,
- the surface reflectance characteristics (usually Lambertian) are the same throughout the surface,
- the lighting, usually one-point lightsource, is the same throughout the surface,
- and the image is nearly noise free.

It works well on certain homogenous objects while human skin produces a huge variety of surface properties. A refined version by Pentland [98] does not need such a priori information but also suffers from *"the intrinsic difficulty related to the inability to obtain depth cues"* [31] (p.366).

2. Shape from contour is normally restricted to planar objects. Work on nonplanar contours can be found in the work of Aloimonos et al. [9] (p.342). Contours on ulcerated skin are smooth and blurred rather than sharp and exact. Therefore the method can not be considered for ulcer measurement.

3. Shape from texture suffers from the same problems as shape from contour. Again the lack of clearly defined boundaries and contours in the image of an ulcer make this method unfit for this special task.

4. Structure from motion is similar to stereo vision. Depth information may be obtained by either moving the object or the observer or both. Pictures from different angles have to be matched using the knowledge of the position of the observer and the object relative to each other. The main problem is to find corresponding points in all the images. This is easy for objects with defined contours but, again, not for an object such as an ulcer or a pressure sore.

The above list is just a brief summary of the *Shape From* .... methods. An elaborate discussion may be found in [9]. Nevertheless it should be clear that none of the methods is suitable for ulcer measurement.

B.2.3 Optical Triangulation Techniques

B.2.3.1 Passive Triangulation (Stereo Vision)

Stereo Vision is a well known approach to obtain a three dimensional representation of an object. It is similar to the way of human range perception and normally uses two cameras as sensors. To improve the performance of the technique three cameras are in use in some applications [30]. This reduces the occlusion- and missing-part-problem as well as the probability of incorrect matching of corresponding points in pictures from one object taken from multiple angles.
As already mentioned the corresponding-point-problem is the major obstacle in stereo vision [32]. Although an easy task for the human brain it is difficult for a computer. Being comparatively easy when there are clearly defined geometrical objects with sharp edges [67] it becomes more and more difficult with smoother object textures. Ulcers therefore are the most unsuitable objects for this technique.

To overcome the corresponding-point-problem some systems have been invented using both, structured light (see next section) **and** stereo vision [82,84]. Structured light provides reference marks which act as corresponding points. With these points allowing for definite identification, the distance of these points to the measuring system can be calculated by triangulation [30].
The corresponding-point-problem is the main reason why **stereo vision is not appropriate for the measurement of skin ulcers**.

B.2.3.2 Active Triangulation (Structured Light)

Structured light is an active triangulation technique. One optical sensor of the passive stereo vision method is replaced by an active projector. The projector produces a pattern of light through lasers or slides onto a surface. Using knowledge of the geometry of the equipment (positions and angles of camera and projector towards each other, angle of the projector beam) the position in space for all those points of the observed surface that intersect with the pattern may be calculated.

The difficulties of this technique are not immediately obvious. They will be evaluated on the following pages. Figure B.8 demonstrates the principle of the structured light technique:

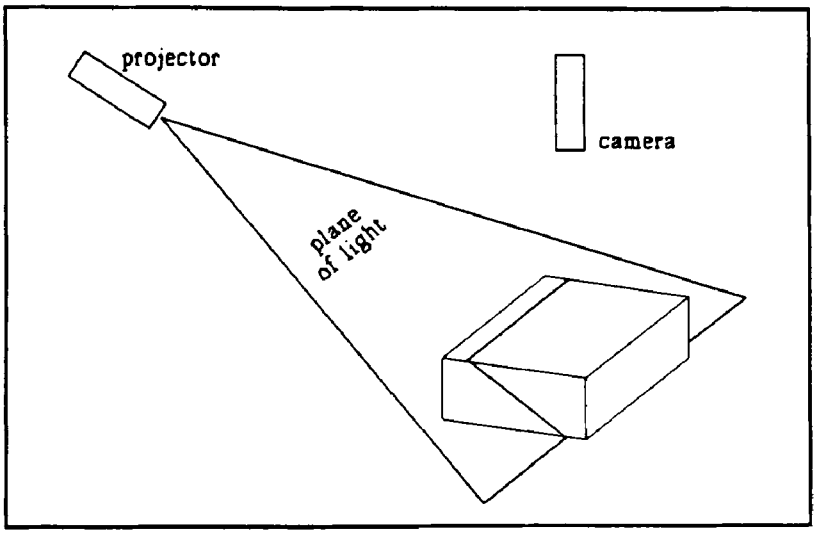

Figure B.8: The principle of the structured light technique

A great variety of projecting and sensing equipment is used in many applications. A summary on several of these may be found in a paper by Wang et al. [127]. Some researchers use a mechanical system to drive the optical scanner [5,6,80,99,112]. Scanning is necessary when depth information cannot be captured into a video frame in a parallel process, i.e. either the projector or the sensor works serially (beam of laser light [4,10,68,88] generated by diodes or tubes, single line camera).

The main disadvantage of a mechanical scanning system is that the process is time consuming. During the scanning time the object must not move relative to the system. Other difficulties occur from mechanical imprecision which can never be totally avoided even with very accurate (expensive) devices. Mechanical scanning systems also need to be calibrated often which makes them inappropriate for use outside a laboratory.

An approach using a projecting system that generates the whole pattern at once [22,131] does not have this disadvantage.

The underlying principle of the structured light method is triangulation. Triangulation anticipates a priori knowledge about the position of the triangles edges relative to each other. Two of these edges are the projector and sensor device. Their positions in space are easily obtainable. The third edge is a point of the pattern projected onto the object of interest. (This, of course, also works the other way round, when only the camera's position is unknown [57].) The problem is now to identify this point with respect to other points of the pattern. The point has to be labelled in some way.

1. Uncoded Structured Light

If the pattern is not coded in a certain way, systems using this method run into difficulties when the pattern is occluded by edges, or disappears occasionally due to poor reflection properties of parts of the object. This is called the labelling problem in structured light techniques. It can partially be overcome in certain cases by special algorithms and labelling techniques, which are elaborate and not always satisfactory [119]. The majority of research to date has been done with uncoded structured light[11]. The problem of labelling was avoided by using objects of high homogenous reflectivity without occlusions.

Two techniques are known to overcome the labelling problem: time/space coding and colour coding.

2. Time/Space Coded Structured Light

This technique is also known as binary encoding. A binary code word is assigned to each projected stripe. A series of multiple stripe projections carry the code for each stripe. When the pattern consists of N stripes, $\log_2 N$ projections are necessary. Different patterns may be produced by a transparent LCD array [7,53], a rotating disk with different slides on it, or simply by several slides in a common slide projector.

---

11 [4,6,36,49,50,55,69,75,79,81,88,97,99,105,108,114,122,162]

This method has its drawbacks:

- multiple pattern projection is time consuming and has the disadvantages of all the other scanning techniques
- many image frames have to be stored in the imaging system for later processing
- the alignment of all patterns has to be extremely precise which requires intricate mechanical projection systems (not with a LCD array)
- the scene illumination changes due to the different patterns making stripe detection more difficult
- decoding may be difficult on scenes or objects with varying reflectivity

Time coding is sometimes also named space coding because the binary information is encrypted in spatially varying patterns [80]. Typical examples of the time coding technique may also be found in [7,10,100].

3. Colour Coded Structured Light

The introduction of colour as a means for labelling makes better use of the visual channel. Colour cameras can clearly distinguish several colours on objects with homogenous reflection properties. When the objects themselves are coloured the use of colour may be restricted, e.g. if an object absorbs red light completely the projection of a red stripe makes no sense. Mainly due to this disadvantage the method introduced by Yanh, Boyer and Kak in 1984 [131] and further developed in 1987 [22] may have been neglected for a long time. In C.3.3 the main constraints under which the method works are discussed. In C.4 a method to adapt the colours of the projected pattern to the object and the equipment itself is discussed. Colour adaption allows the use of colour coding techniques areas where it would be otherwise impossible.

The accuracy of the structured light technique is limited by the number of stripes which the system can project, locate and clearly distinguish from each other. This is a major problem especially when the technique is being used to measure objects with sharp edges and corners. A quantisation error is inevitable. The surface of the human skin is, even in regions with ulcers, smooth and missing depth data between stripes may be assessed by interpolation with reasonable accuracy.

B.2.4 A Method to Measure Ulcers and Pressure Sores

The above survey examined examples of all three dimensional measurement methods which are currently available. Most of them are unsuitable for a measurement system for human skin ulcers:

- **acoustic** methods are too slow and offer only limited resolution,
- **mechanical** methods make contact with the patient and are inaccurate,
- **tomographic scanners** are relatively slow, not portable and expensive,
- **optical, non-triangulation** techniques also have their disadvantages: the time-of-flight and the angle-of-total-reflectance methods are time consuming, Moiré topography and holographic interferometry encounter stripe labelling problems, the aperture technique has insufficient resolution and the defocusing technique needs homogeneous surfaces.
- The **shape from ...** techniques are more descriptive rather than accurate measurement methods,
- and **stereo vision** suffers from the corresponding point problem.
- Using **uncoded structured light** results in stripe labelling problems
- and **space/time coded structured light** requires multiple stripe patterns to be projected onto the surface.

After considering all the methods and techniques which have been discussed above it becomes clear that an instrument designed for ulcer measurement should incorporate the only remaining method: **the colour coded structured light technique.**

The **advantages** of a such a system are:

- it is a stereo vision concept avoiding the need for two cameras and the matching-point-problem
- information other than range data may be acquired
- it is fast, no scanning is necessary
- it has higher tolerance to noise than *shape from ...* techniques
- few mechanical components are needed
- it is sufficiently accurate for the task

The **disadvantages** of the method are its limited resolution and restrictions in the number of useable colours.

In the light of this decision the following pages take a closer look at the physical requirements for the color coded structured light technique. The following section of this literature survey will therefore focus on the structured light technique alone. It investigates equipment which may be used with the technique and discusses their respective advantages, disadvantages and possible equipment induced error sources which might affect the performance of the method.

B.3 Equipment for the Colour Coded Structured Light Technique

Irrespective of which methods, algorithms or principles are used a 3-D measurement system based on the structured light technique has to consist of the 3 blocks shown in figure B.9.

A computer controls the whole arrangement by its software. Recently, personal computers became powerful enough for image processing and can now perform better than systems especially built for this purpose some years ago. They are already being used in some applications [54,61]. The computer also provides the interface for the user and eventually to an external system for data exchange and storage if the internal storage capacity is too limited. Despite data compression methods [28,91] colour images occupy a fair amount of space on a storage medium. The computer is not discussed in the following as PCs are becoming increasingly a part of every day life and no special requirements other than sufficient speed and storage capacity are needed.

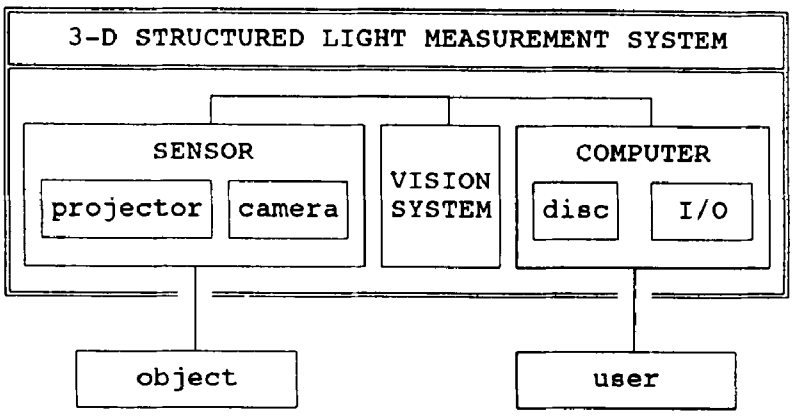

Figure B.9: Components of a structured light measurement system

The following paragraphs therefore focus on the other components of the system: projector, camera and vision system.

B.3.1 The Projector

As proposed by Schroeder [110] and Hopwood [61] the projector has to be carefully adapted to the task taking into account:

- the object of interest (skin, ulcers)
- the optics (lenses, mirrors, filters)
- the image sensor (camera)
- and the control and image capturing electronics.

The source of light and the pattern to be projected onto the surface are of particular importance.

1. Light Source. The choice of a colour coded structure light technique significantly reduces the number of possible light sources. Lasers and light emitting diodes are monochromatic. A laser for each colour is too expensive and LEDs are not bright enough for projection purposes. The luminance of fluorescent lamps is too low for projection. The bandwidth of neon and sodium lamps is too limited to allow the extraction of multiple colours. Therefore flash tubes and tungsten lamps are left for consideration.

Flash tubes are broad banded which make them suitable for the production of coloured stipes, e.g by slides. Unfortunately they are very fast: the synchronisation between the camera and the flash tube requires an additional electronic circuit. Further electronics is necessary to control the amount of light emitted by the flash which otherwise fluctuates greatly.

Another candidate is the tungsten lamp. Especially **quartz halogen lamps** emit a lot of light at shorter wavelengths. This makes quartz halogen lamps more suitable for the illumination of human skin which has relatively poor reflectance for short wavelengths of light and more "blue" components are needed to counteract this effect.

2. Pattern giving device. Common colour slides are excellent multi colour filters. Most of them hold three different pigments (e.g. yellow, magenta and cyan) to produce colours. By carefully controlling the photographing and processing of a specially selected film the colours may be adapted to the task.

The use of a quartz halogen lamp in combination with a slide is commonly available in slide projectors. The combination is inexpensive, flexible and does not involve highly specialised manufacturing skills and safety measures required when a laser is in use.
Nevertheless a special projector design is necessary: it has to be much smaller and lighter than a common slide projector. The design is shown in chapter C.3.1.

B.3.2 The Camera

An elaborate discussion of the performance of several camera types including possible errors and defects may be found in [120], where some methods to figure out properties of cameras by experiments are also given. Table B.3 gives a brief overview of the advantages and disadvantages of the most common camera types:

CAMERAS		
TYPE	ADVANTAGES	DISADVANTAGES
CCD [11,42]	-fast, small quiet, rugged -high sensitivity [32] -low power consumption -most common	-irregular spectral response -signal loss at saturation -limited resolution, especially CCD -blooming
CID [42]	-better antiblooming than CCD -nondestructive readout -as CCD	-expensive -only one manufacturer (1990) (CID Technology Inc.) -complex control circuit -limited resolution
CCPD / CPD [42]	-regular spectral response -no signal loss due to saturation -as CCD	-expensive -limited resolution
IR [20,106,107,122]	-identification of ulcers by changes in skin temperature(?)	-extra cooling -limited resolution -expensive -big
vidicon tubes [68]	-high resolution -no dead zones between pixels -inexpensive -good availability	-power consumption -big -geometric distortion -burn-in -limited filament life -jitter, thermal drift -fragile

CCD = Charge Coupled Device CID = Charge Injection Device CPD = Charge Primed Device
CCPD = Charge Coupled Photodiode Device IR = InfraRed Camera

Table B.3: Overview of several camera systems

CCD cameras are relatively cheap, small and easy to handle and most researchers prefer them. Tube cameras are ruled out by their disadvantages. Other sensors such as photosensitive diodes and transistors are used in very special applications only [3].

An ulcer measurement system should take advantage of a colour CCD camera because it is small, light, low in power consumption and relatively cheap. But all colour CCD cameras have some disturbing properties which are not immediately obvious. Many researchers who use imaging systems pay little or no attention to camera distortions and errors. Intuitively they assume the camera to be ideal in most of its properties. This may be caused by the fact that a scene captured by a camera and displayed on a monitor is very close to the scene observed in reality. On the following pages eight of the most important irregularities are listed.

1. Non linearity. An ideal camera response is linear. According to Novak et al. [93] the output m_i of a certain camera pixel depends on the spectral distribution function of visible light illuminating that pixel $L(\lambda)$ (luminance, [candela/m^2]) and its spectral sensitivity $s_i(\lambda)$:

$$m_i = \int_{\lambda=400nm}^{\lambda=700nm} L(\lambda)\, s_i(\lambda)\, d\lambda \qquad \text{(B.1)}$$

Normal CCD cameras are adapted to normal monitors which again are adapted to human visual perception which is non-linear. The perceived brightness B of a given point on a monitor is dependent on its input voltage V and the two parameters picture brightness α and contrast γ :

$$B = \alpha V^{\gamma} \qquad \text{(B.2)}$$

Camera manufacturers consider this relationship and design their devices in order that

$$V = m_i^{1/\gamma} \qquad \text{(B.3)}$$

where m_i is the value expected from equation (B.1) and V is the actual camera output voltage. Thus the displayed brightness will be directly proportional to the real brightness of the scene.

There are two consequences for image processing resulting from this effect. Firstly, brightness ratios between areas of an image are not correct. Secondly, the ratio between colour output channels shift with varying brightness. A pink surface for example might have a RGB ratio of 0.5 : 0.25 : 0.25 (in a camera output ranging from 0 to 1), when measured with little illumination. The same surface might have a RGB output ratio of 0.70 : 0.50 : 0.50 when measured under brighter conditions. On a colour monitor the colour would still appear as pink because of equation 2. Image processing hardware normally has linear rather than such a nonlinear dynamic characteristic. Knowing this, the effect may be overcome by appropriate programming of the image processing unit.
Another obstacle is hidden in $s_i(\lambda)$ in equation (B.1). The spectral sensitivity of a certain pixel is anything but linear. Common CCD cameras have a set of three (sometimes four or more) types of pixel with different sensitivities. Each type has a non linear characteristic for a fraction of the visible spectrum (normally red, green and blue). The sensitivities of red and green and those of the blue and green sensitive pixel overlap. But as before, these non-linearities and channel overlapping can be partly eliminated in later image processing.

2. Clipping. Equation (B.1) assumes that the dynamic range for brightness of the camera is unlimited. In reality, however, there is a certain brightness at which the maximum output of the camera is reached. A further increase in brightness does not result in a further increase in output voltage. The consequence again is a possible colour shift. A pink surface, for instance, might have a 0.50 : 0.25 : 0.25 ratio and is observed by a **linear** camera. Under extremely bright conditions the red channel may become saturated whilst the green and blue channels are not. A possible output might be 1.0 : 0.9 : 0.9. The green/blue ratio is still correct but the red/green and red/blue ratios have changed. The surface will appear nearly white. This effect is called clipping [93].
There is no way to correct this error by subsequent image processing. The only answer to the problem is to avoid any part of the image being 'clipped' to the maximum value by closing the aperture by some stops.

3. Blooming is an effect also caused by saturation of the parts of the CCD sensor due to extreme brightness. Parts of the charge in the saturated pixel may leak into other pixels causing a halo of brighter areas surrounding the overexposed spot. The size of the affected area and the direction in which the leakage spreads depends on the type of CCD camera and the amount of overexposure. There is no way to correct this flaw without a priori knowledge of the observed object.

4. Grey-level-shift is similar to blooming. This time the overall brightness of the whole picture affects the charge in each pixel. It should influence all pixels in an equal fashion. This may not be quite correct and there might be an individual shift for each pixel dependent on its neighbours but the results of McLean [85] indicate that the model is quite appropriate. Furthermore a correction for each pixel value would result in time consuming correction calculations and suitable techniques for measuring individual grey-level-shifts are not available at present. McLean also suggests an experiment to measure the grey level shift. From the results a look-up table may be produced to largely counteract the effect.

5. IR sensitivity. Equation (B.1) assumes that the integration is performed within the wavelength range of human visual perception, i.e. from ca. 400 to 700 nm. CCD cameras, however, are also able to respond to wavelengths in the near infrared band in an unexpected manner. All three types of pixel in a common CCD camera (not only the red-sensitive ones) respond to wavelengths longer than approximately 680 nm. All colours appear lighter and less saturated than expected by the human observer. A simple way to avoid this error is the use of an IR-cut filter. Figure C.4 in section C.2.2 shows the spectral response of a camera with and without IR-cut filter.

6. Colour imbalance. The response of a common CCD camera is adapted to human visual perception. The human eye is most sensitive in the middle of the visible spectrum (between yellow and green at approximately 570 nm). Cameras simulate that by increasing the amount of green sensitive pixels at the cost of the red and blue ones. When observing a light source emitting light with equal intensity over the whole visible spectrum the camera will produce a higher output at the green channel than the red and the blue channel.
This error may be corrected in later image processing when the characteristic of the camera sensitivity for each channel is known.

7. Moiré beats occur with any high frequency information in the image. They are caused by the design of the CCD array[12] where parallel stripes of aluminium are placed vertically over the readout zones of the array forming a very fine grating. *"This aliasing cannot be removed by subsequent image processing"* [51].

---

12 This problem occurs in Interline Transfer Imagers only. Since they are the most common ones this effect is mentioned here.

[132]. The term edge response describes the camera's ability to reproduce sudden changes in contrast in the observed scene as it might occur on edges of an object. Edge response is limited by pixel noise and the need for spatial quantisation on the CCD array. It does not pose a severe problem as images of ulcers do not have any sharp edges and structured light stripes are diffuse and blurred due to the scattering properties of human skin.

B.3.3 Lenses

Lenses are an important part of the measurement system. Unfortunately they suffer from many possible errors. They may be divided into two main groups: monochromatic and chromatic errors. An elaborate discussion may be found in [59]. The effect of these errors depends on how and where the lenses are used. Some of them may be minimised by environmental conditions or eliminated by image processing techniques.

B.3.3.1 Monochromatic Errors

Monochromatic errors of lenses are faults that affect all parts of the visible electromagnetic spectrum in the same way. They are caused by certain physical properties of the optical media and may be corrected only partly. Normally the correction of one error increases another one. A typical lens is therefore a compromise designed to achieve optimum performance in a certain application. Monochromatic errors fall into two categories: aberrations and distortions. In this application the camera's lens works as a wide angle 'macro' lens where distortions cause a far greater error than aberrations. Distortions affect the image geometry while monochromatic aberrations merely cause a certain degree of blurring.

Distortion arises because different areas of a lens have different focal lengths and different magnifications [59] (p.230). Figure B.10 shows the consequence of the effect on a rectangle which is affected by positive (barrel-) and negative (pincushion-) distortion respectively.

For a single lens the displacement of each image point may be calculated using the

For a single lens the displacement of each image point may be calculated using the fact that distortion is proportional to the third power of the distance of a given image point from the optical axis [128] (p.108, equ.6.57). In addition to distortion each lens shows a certain amount of field curvature. It blurs off-axis image points and also shifts these points either towards or away from the optical axis. Field curvature of a single lens may also be calculated.

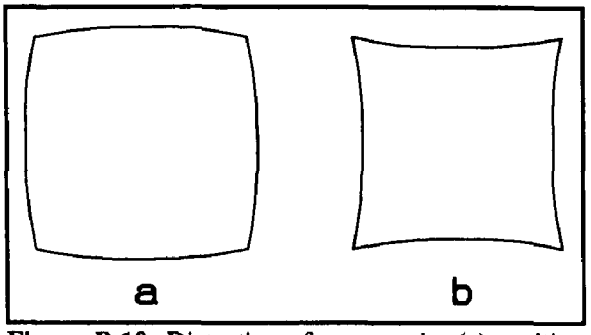

Figure B.10: Distortion of a square by (a) positive (barrel) and (b) negative (pincushion) distortion

For a whole camera lens which is a combination of several single lenses the calculation of these errors is difficult as the distortions and field curvatures of several different lenses with different falsifying attributes add together in a complex way. Furthermore it is impractical to dismantle the whole lens and try to extract the relevant parameters for each single lens. Instead of such an in-depth analytical approach in order to find parameters for the correction of distortions and field curvature by image processing a more straightforward approach may be used to tackle the problem.

In chapter D.5.1 a correction equation for these errors is derived from the simplifying assumption that distortion and field curvature are caused only by different distances of points on the object from the camera's focal point. Other causes are neglected. Experiments show that this simple model enables the displacement of image points in corners of the image (where the error is worst) to be corrected from 7 pixel widths down to 1 pixel width.

Other **monochromatic errors** (spherical aberration, coma and astigmatism) all produce blurring of image points. The centre of a blur represents the real position of an image point. Monochromatic aberrations degrade the image quality but they do not cause distortions.

Chromatic aberrations exist in all lenses because the refractive index of a lens is a function of wavelength. Some manufacturers offer achromatic lenses where the effect is partly eliminated by using pairs of lenses with different refractive indices. Unfortunately it is impossible to eliminate the aberration completely even with such pairs of lenses. It may be done for two wavelengths only. Additionally the elimination works perfectly for only two points in the image field. These are normally the optical axis and a certain radial distance from the axis. Chromatic aberrations have two consequences:

- It is impossible to focus the lens perfectly for each colour channel. Due to the different refractive index the image obtained from the red channel of the camera may be in focus but those for blue and green are not (longitudinal chromatic aberration).
- As a result of the impossibility of focusing rays of all wavelength at the same focal plane, images of all but one colour appear blurred radially from the lens centre (lateral colour). This causes colour shifts especially at the edges of the image.

B.3.4 The Vision System

The vision system is the part of the whole system where special hardware is used to process the picture information and capture it from the camera. Some researchers use special hardware to find the projected pattern on the image [99,122] to filter off noise or to perform an edge detection algorithm [70].

Hardware implementations are extremely fast but expensive and very specialised. Alterations take a long time and are costly. Software implementations can be changed to new tasks, are inexpensive, but are not as fast as hardware. This is not an obstacle for this work as there is no need for real time processing. A reasonable processing time (some minutes) is definitely acceptable.

The elementary component of any vision system is the *frame grabber* that captures pictures from the camera and stores them either in the host computer or its own memory for subsequent processing. The output from the camera undergoes two significant conversions:

1. Sampling. Most frame grabbers synchronize themselves to the line or frame frequency of the camera rather than to the stream of pixel readouts from the camera pixel by pixel. A line from the camera may contain 400 pixel (PAL standard) which the frame grabber converts into a line of with a multiple of 256 pixels (usual for frame grabbers for obvious reasons : $2^8 = 256$) in its memory. There is no 1:1 ratio between a CCD imager pixel and a frame grabber pixel[13] ! Therefore the frame grabber pixels are called *virtual pixels.*

2. Quantisation. The camera provides the frame grabber with an analogue signal. For digital storage it has to be converted into binary code. The code is normally 8 bit long resulting in 256 shades of brightness for each colour channel. This limits the total amount of available colours to $256^3 = 16{,}777{,}216$ colours. Other quantisations (5 bit, 16 bit) are also in use.

Both procedures inevitably add a certain amount of error to the signal. Compared with the output noise of the camera they may be ignored as they contribute little to the already existing noise from the camera.

There are several methods of representing colour information within an image processing system. The most common one defines colour to be a combination of the additive primaries red, green and blue (RGB)[14]. The disadvantage of the RGB method is the need to always process all three channels. This may be overcome by a representation in the HSI (hue, saturation and intensity) format [89]. Some image processing applications (for example distinguishing a red from a blue object) may be performed by processing one channel (the hue channel in this example) only. Edge detection can be performed by looking only at the intensity values. Some image processing hardware does support the HSI format and should be preferred to RGB if possible.

---

[13] As discussed in Chapter C.2.3 there is not even a 1:1 ratio between the CCD array and the output of the camera. The camera's electronics performs a similar conversion.

[14] In contrast to this additive method stand the subtractive colour mixing method used in the area of publishing printed media: CYMK (cyan, yellow, magenta and black) is in use. This representation is adequate for printing but not for image processing because camera outputs are normally in RGB and four instead of three channels have to be processed.

B.3.5 Result of the Literature Survey into Equipment for the Colour Coded Structured Light Technique

This section investigated several literature sources in order to find the most suitable equipment for the measurement of skin ulcers by structured light. The analysis of technical background information on cameras, projectors and frame grabber cards together with a review of different approaches which use the structured light technique leads to the following component configuration for an ulcer measurement device:

- **Projector.** A specially designed slide projector with a quartz halogen bulb and colour slides as a pattern giving device.
- **Camera.** A common colour CCD camera. Some precautions must be taken to avoid or eliminate the effects of error sources such as clipping, non-linearity and blooming. Both, projector and camera will have to sit in a compact and portable sensor housing.
- Normal close-up or macro **lenses.** Errors, introduced by the lenses in use with the projector and the camera must be taken into account.
- **Vision system.** A colour frame grabber card which is able to store and process colour TV pictures obtained from the camera will be in use. Effects such as sampling and quantisation must be considered in the design of the system.
- **PC.** A personal computer which also houses the frame grabber card is the central control and calculation unit. It should also be portable.

The components outlined above are only the physical manifestation of the measurement system. The measurement process itself is controlled and carried out by computer programmes in the PC. The software has to control the system, compensate for errors introduced by the hardware and process the pictures in the frame grabber card in order to produce the measurement results. In the light of the above findings the following section reviews software (programmes, methods, procedures and algorithms) which is currently in use in other image processing applications as far as they are relevant for skin ulcer measurement.

B.4 Software in Use with the Structured Light Technique

When using the structured light technique the measurement process is broken up into several steps. The first step - image acquisition - is carried out by the camera in combination with a frame grabber. All the following steps, are performed by computer programmes. Some structured light applications use specialised hardware to perform subsequent image processing steps in order to achieve greater speed. As already mentioned this hardware can always be replaced by software which is cheaper and offers greater flexibility.
Many different approaches to each of the steps may be found in literature. In the light of the findings of the previous chapters the relevant ideas are resumed in the following sections.

B.4.1 Image Pre-processing

The original picture of an ulcer is obtained from the camera and stored in the computer memory. It is inevitably corrupted by noise from different sources. Camera electronics, long cables and signal quantisation are the main contributors. Denq and Bergen [38](p.142) assume image noise to be white Gaussian with zero mean. Using this assumption an appropriate convolution filter may be designed to reduce noise.
Spatial variations in the reflectance properties of a surface influence the appearance of a projected pattern. In areas with low reflectivity the pattern will appear darker. The orientation of the surface towards the light source and the viewer also influences the scene radiance. Horn and Sjoberg [63] discuss methods of calculating a reflectance map of the scene that provides correction data for subsequent image processing, especially the determination of the exact positions of the centres of the projected stripes which form the structuring pattern.
LeMoigne and Waxman [81](p.205) use a similar approach called '*albedo normalisation*'. They use the measured brightness of given points of a projected pattern and the average brightness around them to asses the reflectance (albedo) of the surface at the position of those given points.

B.4.2 Thinning Projected Patterns

For triangulation purposes the accurate position of certain features of the projected pattern must be found. Since this pattern consists mostly of stripes of light it is the centre of the stripes which has to be found. This process is commonly called line thinning.
In a first step of line thinning a set of rules has to be designed defining the kind of image pattern that is acceptable as a stripe. Alexander and Chew Ng [7] propose four rules which also consider noise superimposed on the image and variations in surface reflectance.
In a second step the accurate position of the stripe has to be found by thinning the broad lines of light. The original application of thinning algorithms was the optical recognition of characters. Applications then spread into automated fingerprint recognition, analysis of chromosomes and counting asbestos fibres in filters. Thinning is performed by "*...successive erosion of the outermost layers of the pattern*" [37](p.53) in order to extract a skeleton preserving its shape. The skeleton does not necessarily coincide with the brightest parts or the centre of the pattern. Therefore this approach is not suitable for the structured light technique where the position of a stripe rather than its form is of importance.

The approach by Takaki and Hata [122](p.236, fig.3) is more appropriate: they calculate the centroid of the intensity distribution of a stripe of light to find the centre. This determines the stripe's position with higher precision than purely looking for the brightest pixel of its image. In fact sub-pixel accuracy may be achieved.
The approach has to undergo two significant changes before it can be incorporated into a measurement system for a surface with non-uniform reflectance properties:

- the fixed threshold that defines beginning and end of a stripe has to be replaced by a dynamic one and
- the reflection properties of the surface have to be considered when calculating the centroid.

Denq and Bergen [38] investigate the influence of quantisation, thresholds, sampling rates and noise on the accuracy of the centroid finding method. They found that the maximum error is never more than 16% of the width of a detector unit (camera pixel).

The centroid finding algorithm also reduces the influence of surface roughness addressed by Jalkio, Kim and Case [68](p.972). Together with the reflectance map obtained from image pre-processing the centroid finding algorithm should produce much better results than skeleton thinning.
Another more sophisticated method to find the stripe's centre uses a priori information about the expected intensity distribution of the stripe [55][15][75][16]. This approach is unfortunately restricted to surfaces with uniform reflectance properties and cannot be used with ulcerated skin.

B.4.3 Linking Patterns

Gaps in the imaged pattern may occur due to low reflectivity, occlusions or gaps in the object's surface. Before starting the linking process the corresponding ends of the stripes in the pattern have to be identified by a labelling process, a method used by Lapreste et al. [79]. The need for labelling is the main reason for coding the pattern either by colour [22,131] or by a binary space/time coding technique [80,108,126].
Alternatives to pattern coding are rare. A different approach by Stockman and Hu [119] uses some assumptions about the observed scene and geometric and topological constraints in the pattern. The results are *"...reasonably acceptable..."* [119](p.606) but sometimes not unequivocal leaving it to the human operator to decide whether the labelling is correct.
After the labelling process it is easy to link the identified pieces together. Missing bits in between may be filled using straight lines [6] (small gaps only), quadratic polynomial approximation [79] or any other approximation method such as splines and Bezier functions.
The result of all the preceding steps is a pattern of stripes closely following the contours of the surface to measure. The position of a given point of this pattern is a direct representation of the spatial position of the corresponding point on the surface. This information is used to create a representation of the surface in the computer.

---

[15] [55] p.2: *"The instability distribution of a laser follows the normal distribution"*

[16] [56] p.98 *"...the laser stripe has a Gaussian intensity profile, a least square fit weighted by the intensity (after thresholding) was used to get more accurate line fit."*

B.4.4 Measuring Area and Volume

For **area calculation** it is necessary to extract the zone which is occupied by the open wound. This may be achieved by the use of certain colour properties of the ulcer (see B.1.4 and B.1.5) [2,3,15,122]. Edge detection algorithms [1,70,123] are not suitable for specifying the boundary of an ulcer since the lesions normally have very vague and indistinct (colour and brightness) edges.
Infrared information [3,106] could be helpful but since normal CCD cameras are only sensitive to the near infrared part of the spectrum it is unlikely that additional information may be achieved. An additional infrared camera could deliver the temperature data but is not considered in this work due to the reasons previously mentioned in B.1.3.3 and the limited resolution of IR cameras (B.3.2).

Volume calculation depends on information about the whole area affected by the ulcer. This is not only the open wound extracted for area measurement but also the indirectly affected tissue around it. The volume of an ulcer is the difference between the measured surface and the former healthy surface. Therefore it is necessary to define the affected area and reconstruct the healthy surface. The information about the affected area may not be derived from skin colours because the colour of swollen or otherwise affected skin might not appear to be sufficiently different from that of healthy skin. Instead a structural analysis is necessary.
The rims of the ulcer are often slightly elevated as a result of the inner structure of the tissue as mentioned in chapter B.1.6. It might be possible to detect and recognise such a feature by structural filters [79] or transformation of the surface data into the gaussian sphere [114]. Perhaps a scene analysis according to Duda [40] might be a successful approach.
These possibilities have to be considered but it is believed that none will work really successfully under all circumstances as even for physicians it is often impossible to define the boundaries of the ulcerated area precisely. When a huge 'database' such as a trained human brain is unable to find an accurate boundary it will be extremely difficult to define rules for an automated approach to the problem.

Once the area which is affected by an ulcer is known its former shape has to be reconstructed. This is necessary because the volume of a skin ulcer needs an upper confinement. The lower confinement is established by the actual measured surface while the upper one has to be reconstructed to imitate the former healthy skin surface.

Cubic spline approximations which may be implemented by multiple one dimensional [25,83] curve fittings or by a single two dimensional [72,117] surface fitting should be a perfect method to reconstruct the original surface of the skin. The Spline interpolation produces curves with minimum curvature. Splines may be designed that certain variables may simulate parameters such as tension and curvature. The working hypothesis of this work is that skin under normal tension from all sides forms a surface with minimum curvature. This hypothesis is based on the findings of B.1.6 which show that the lines of tension within the skin are anisotropic. This is exactly the sort of curve cubic splines are able to produce. The similarity between the real surface behaviour and the reconstruction algorithm should result in a reasonably accurate reconstruction.

B.4.5 Calibration and Accuracy

For any measurement device there is an obvious need for a means of calibration and for assessing the overall accuracy. Quite a variety of different strategies for the **geometrical calibration** of the whole equipment or only parts of it are known:

- A calibration technique using pattern with known geometry is mentioned by Takagi and Hata [122]. The pattern is measured and the results are compared with reality. From the differences between the measurement data and the real data correction tables may be produced.

- Puskorius and Feldkamp [102] discuss a camera calibration methodology for stereo vision. The method delivers a correction matrix for the geometrical errors of cameras.

- McVey et al.[86] present a method to calculate the accuracy of a 3-D measurement system. They investigate the influence of parameters such as object height and distance, sensor array size and focal length of the camera. Their error analysis results in a formula showing a proportional relationship between measurement error and distance between object and instrument.

Some investigations and experiments are necessary to actually decide if (and which of) the above methods may be applicable to an ulcer measurement system.

For this work it is also necessary to perform a **colour calibration** of the system:

- Healey and Binford [58] propose a colour metric independent of subjective human colour perception. The metric considers underlying spectral properties and noise characteristics of the sensors being used.

- Goharla'ee and Raaberg [53] give a list of possible systematic errors of imaging systems, including ways to overcome them.

The calibration method used for an ulcer measurement depends on the actual construction of the instrument and is influenced by parameters such as desired accuracy, object distance, lighting conditions, camera type and computing hardware.

B.5 Results and Conclusions Drawn from the Survey

The findings of this literature survey strongly suggest that the colour coded structured light method which uses a slide projector and a colour CCD camera is the best choice for skin ulcer measurement. This work is not the first attempt to develop a method for three dimensional measurement of skin ulcers. It can build on well known approaches for the three dimensional measurements of objects in general and some investigations into the feasibility of non-contact measurement of skin ulcers in particular. From these studies some techniques and methods may be adopted and included into the system with minor changes only. These include:

- standard input/output operations for the computer system and the camera
- and certain image processing techniques for noise reduction, image capturing and edge detection.

Other already known techniques will need major alterations and tests to prove their suitability. These are:

- linking algorithms,
- a centre of line finding method, including reflectance maps and adaptive threshold techniques,
- a suitable calibration method,
- and image processing algorithms to correct or overcome limitations of the camera/frame grabber hardware.

Some techniques will be subject to new investigations and experiments. These include:

- a method to optimise colour and spatial properties of the projected pattern to different kinds of skin,
- a method of recognising the ulcer's surface,
- an interpolation algorithm for reconstructing the healthy surface of the skin
- and a classification method based on colour and colour distribution in the ulcer.

The following chapter C describes the design of a new measurement system which does not only incorporate the findings and results of the above literature survey but also some original features such as filter adaptation, image acquisition techniques and a specially designed pattern projector.

C. The Measurement Sensor

C.1 General

This chapter gives a description of a novel specialised measurement sensor for the three dimensional scanning of skin ulcers. The sensor is the physical manifestation of the findings obtained from the literature survey and a number of new methods and principles developed in a successive refining process.
The measurement sensor consists of a colour CCD camera and a projector system. Both are housed in a box which is 50 cm high, 30 cm wide and 10 cm deep. Two mirrors are used to reduce the size of the sensor. Figure C.1 shows a photograph of the sensor, figure C.2 a schematic diagram. To allow for easy disinfection the housing is completely closed and has a smooth surface. The maximum voltage in the sensor is 48 V making it safe even in the case of electrical failure.

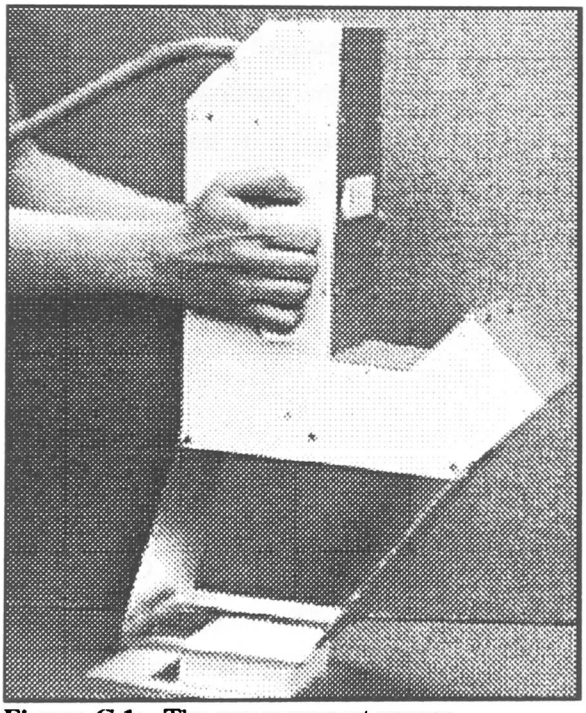

Figure C.1: The measurement sensor

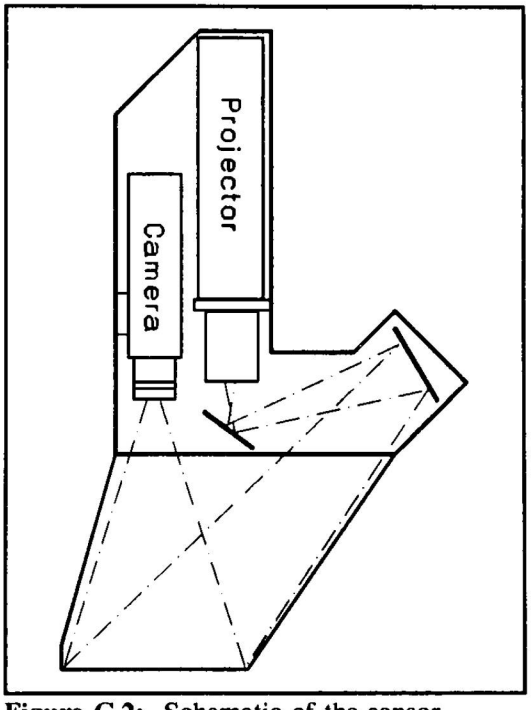

Figure C.2: Schematic of the sensor

A rectangular frame is mounted underneath the housing. When it is slightly above the skin and the ulcer is visible within the rectangle, the optimum distance and field of view for measurement is guaranteed. This may be observed on a video monitor attached to the system. The rectangle also acts as a fixing for a plate to calibrate the system. The measurement process may be started from the controls on the handles of the housing or directly from the computer.

On the following pages the two main components of the sensor, camera and projector are characterised and those attributes which are of special importance for a structured light image sensor are highlighted.

C.2 The Camera

C.2.1 General

The camera in use is a PAL colour CCD camera (TMC76S RGB (PAL), manufacturer: PULNiX America Inc.). It is small and compact (160 × 56 × 50 mm) and weighs only 350 grams. Its ability to work with a minimum illumination of 25 lux (at F=1.4, colour temperature = 3200 K) makes it very suitable for measurement purposes by structured light as it requires less brightness from the pattern projecting equipment. This reduces the power consumption of the projector and thus its size and weight (mainly caused by the transformer). The camera can resist shock of up to 70 g and will not be damaged when dropped to the ground. This and the ability to work within a temperature range from 0°C to +40°C exceeds the environmental conditions normally found in a hospital.
The camera provides two different outputs: a common composite video PAL output and a RGB output (2:1 interlace, 50 frames / second). These features, together with an additional synchronisation input and output allows the camera to be connected to virtually every frame grabber card available at present.

C.2.2 The CCD Array

The CCD array is an *interline transfer imager*. The name is derived from the readout method in use with this kind of array. For details see [51].The CCD imaging array has a resolution of 756 horizontal and 581 vertical pixel. They are arranged on a rectangular chip that is 8.8 mm wide and 6.6 mm high as shown in figure C.3. The vertical pixel columns alternate between purely green sensitive and

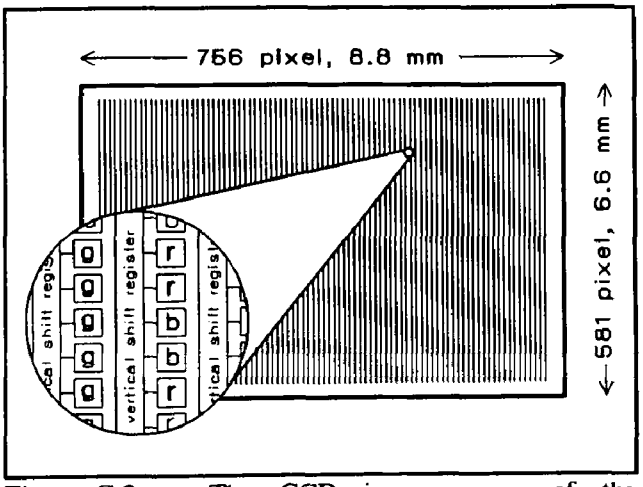

Figure C.3: The CCD imager array of the PULNiX TMC76S (PAL) camera

mixed red and blue sensitive columns. This arrangement simulates the sensitivity of the human eye which responds much more to green, and less to red and blue light. By imitating human visual perception the array has a lower vertical resolution for pictures obtained from the red and blue channel of the camera.

The **horizontal resolution** is identical for all channels: 43 pixel / mm (756 pixel × ½ / 8.8 mm). The **vertical resolutions** for the three channels are

- 88 pixel / mm for the **green**, (581 pixel / 6.6 mm)
- 44 pixel / mm for the **red** and the **blue** channel (581 pixel × ½ / 6.6 mm)

The main consequence resulting from the different resolutions in horizontal and vertical direction is that the camera is used in such an orientation that the projected stripes of light fill the CCD array **horizontally**. In this orientation the crucial depth information may be obtained from the image by the **vertical** displacement of the stripes using the higher vertical resolution of the CCD array.

The light sensitive pixels have a finite size and a certain distance from each other. Inevitably this leads to quantisation errors. This problem and the effects of errors of CCD imagers such as noise, saturation, and blooming are addressed in F.1.3.

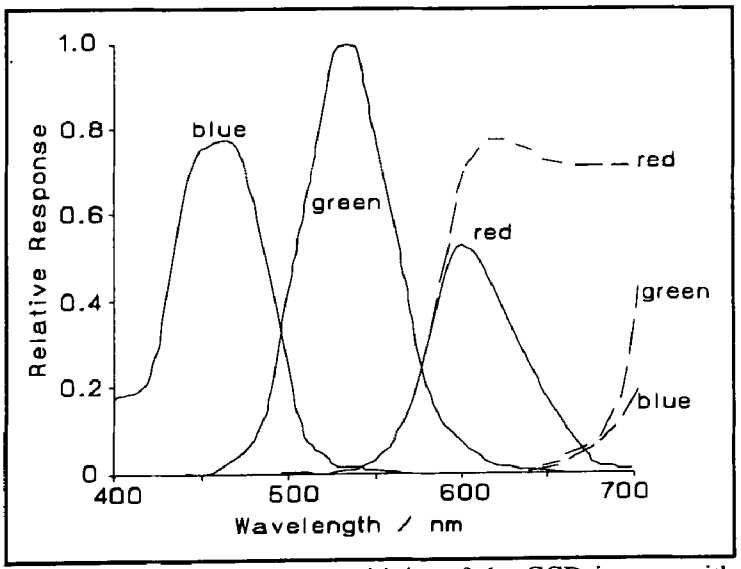

Figure C.4: Spectral sensitivity of the CCD imager with (full lines) and without (dashed lines) infrared cut-filter

The CCD imager is designed to simulate the sensitivity of the human eye. This condition can not be met for the near infrared part of the spectrum as shown in figure C.4. In contrast to the human eye the camera is also sensitive to wavelengths longer than 700 nm. Therefore an infrared-cut filter has to be introduced to prevent IR rays from reaching the camera. This is essential as neither the pattern giving slides nor the other optical components (lenses and mirrors) are able to filter out infrared rays. Without an IR-cut filter, the IR sensitive pixels of the imager would constantly be stimulated. This would result in a steady offset mainly in the red channel limiting the dynamic range and worsening the signal/noise ratio.

C.2.3 Camera Electronics

The camera electronics convert the output of the pixel array into a standard PAL TV signal with 575 columns vertically and 330 lines horizontally. Again the vertical resolution is higher than the horizontal one. This confirms the correctness of the vertical orientation of the camera towards the projected pattern implicated by the CCD array resolution. This output is used by the frame grabber as input.

A crucial parameter which is highly dependent on the quality of the camera's circuits is the dynamic range of the three colour channels. The dynamic range is a qualitative description of a camera's ability to respond to the full brightness range of an observed scene. Compared with the human eye cameras generally perform poorly. The dynamic range for light intensity of the human eye [27] (p.339) is $10^{10}/1$ (200 dB), CCD cameras have approximately 300/1 (50 dB). Small dynamic range causes dark areas of a scene to be displayed completely black while brighter areas appear entirely white causing blooming and clipping effects discussed in B.3.2.

Different CCD cameras have different dynamic ranges. Figure C.5 shows the output of one CCD column of the PULNiX TMC60 camera observing a set of horizontal multicoloured stripes. A stripe of a specific colour is represented by a peak in the respective colour channel. Figure C.6 shows the output of the TMC76S camera which is in use with this equipment, observing the same scene under the same conditions.

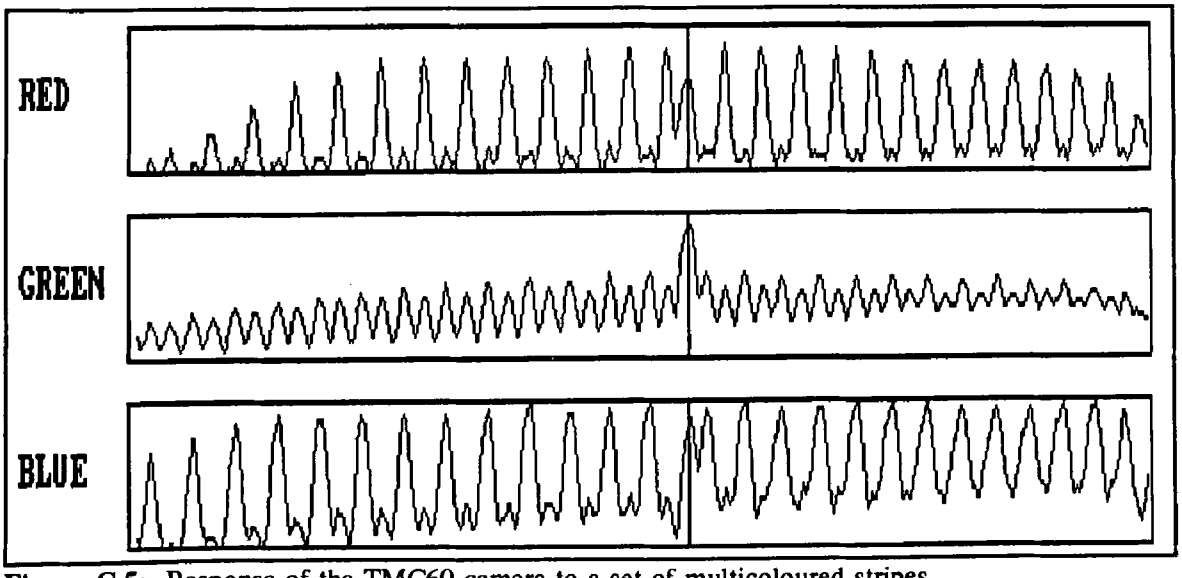

Figure C.5: Response of the TMC60 camera to a set of multicoloured stripes

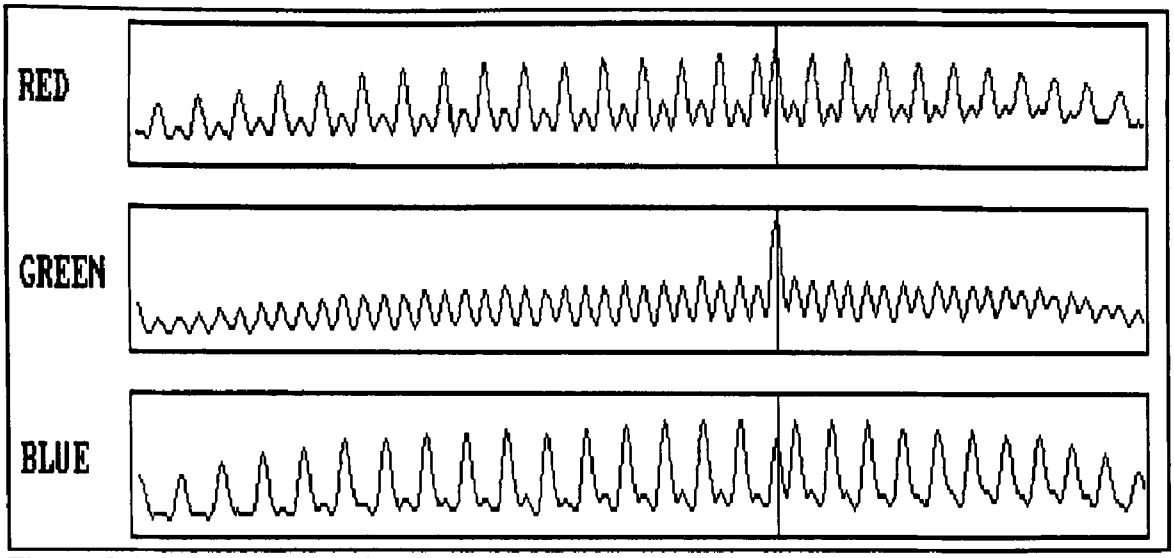

Figure C.6: Response of the TMC76S camera to a set of multicoloured stripes

While the dynamic range of the TMC60 is already fully used the TMC76S still has some reserves. Note the small peaks in the green channel which are caused by crosstalk from the red and the blue channel. Similar but smaller crosstalk peaks appear in the red and blue channels. The problem of channel crosstalk and ways to deal with it will be addressed in later chapters.

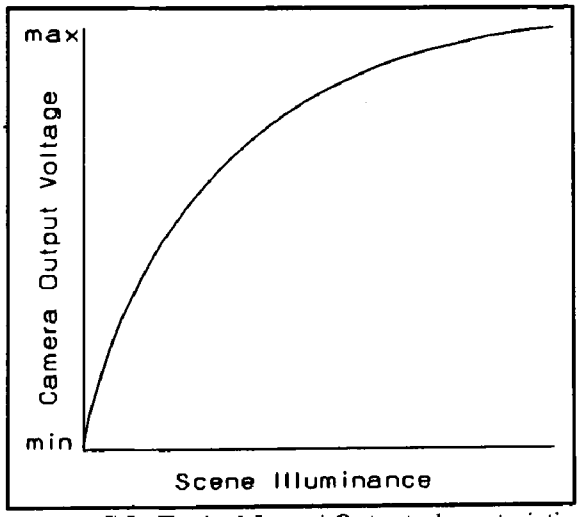

Figure C.7: Typical Input/ Output characteristic of a camera caused by the gamma correction factor

Neither the CCD imager nor the camera electronics are linear. The camera is designed to be used in conjunction with a colour TV monitor which also normally has a non linear response. Both non-linearities cancel each other out giving the correct impression of brightness on the monitor (see B.3.2). A frame grabber normally has a different I/O-characteristic. It uses an input look up table to convert the analog camera input into a digitised video. For accurately converting the picture brightness into a digital representation the knowledge of the *gamma correction factor* γ is vital. This factor describes the non-linear relationship between picture brightness m_i and the camera's output voltage V: $V = m_i^{1/\gamma}$. The gamma correction factor may be obtained by measurements suggested by [93] (p.55ff). A typical gamma characteristic is shown in figure C.7.

Figure C.8 compares the output of the red colour channel of the TMC76S camera for two cases: (above) gamma correction circuit in operation and (below) the circuit switched off. As in figures C.5 and C.6 before a stripe pattern is observed.

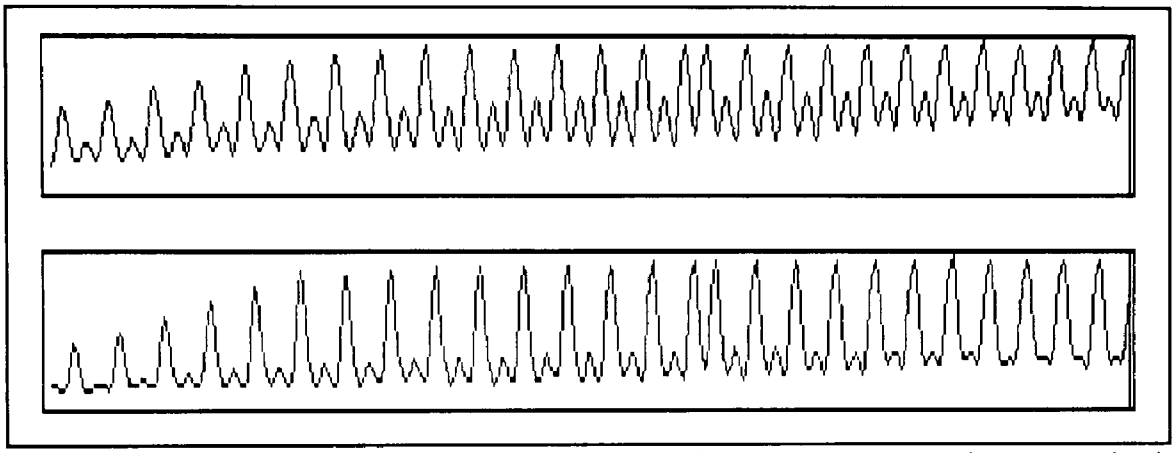

Figure C.8: The output of the red channel of the TMC76S camera (above) with gamma circuit on and (below) gamma circuit off.

As expected from the gamma curve in figure C.7 darker parts of the curve are shifted upwards when the gamma circuit is in operation. If the gamma circuit is in use it has a gamma factor of $1/\gamma = 0.45$. The advantages and disadvantages of the gamma circuit will be discussed later in those chapters where it is of relevance.

According to the manufacturer's technical description the camera electronics (TMC76S) has a signal/noise ratio (SNR) of 46 dB. This could not be confirmed by own measurements as additional noise on cables and in the frame grabber electronics (temperature noise, quantisation error: 5 bit coding -> 30.1 dB SNR) significantly decreases the SNR down to approximately 28 dB.

The camera is equipped with potentiometers allowing to adjust the colour balance between the red and the green channel and between the blue and the green channel. During the colour calibration process (see D.1.2) the camera is adjusted so that the colour temperature of 3300 K produces an equal output in each channel.
It is tempting to adjust the camera to varying skin colours in order to achieve a better performance. Skin normally reflects less blue and green than red light. Increasing the sensitivity of the blue and green channel would secure a better brightness resolution for these channels. This is not advisable for the following reasons:

1. The gamma correction factor changes when readjusting the colour ratios via the potentiometers. Therefore the whole input look up table of the frame grabber would have to be reprogrammed every time.

2. The dynamic range of all three sensor types is at its maximum when being adjusted to a colour temperature around 3200 K. By adjusting the camera much differently the dynamic range of at least one channel inevitably decreases causing a worse SNR.

3. The repeatability for different adjustments is difficult to achieve and proper adjustment of the tiny potentiometer knobs is intricate.

4. The ratio between the three primary colours is shifted causing an image appear to be tinted red, for example. If the observed object is an ulcer, a overall reddish tint would give the observer the impression of the wound being more severely inflamed than it really is.

Ulcer classification by colour, which is a further feature of the instrument, becomes difficult to achieve.

An additional electronic feature is the *Automatic Gain Control (AGC).* It automatically adapts the camera electronics to varying ambient lighting conditions. Being very helpful under normal circumstances, AGC would significantly endanger the measurement process as the colour coded structured light method used in this work is based on two differently bright pictures which both require to be taken with exactly the same gain. Fortunately AGC can be switched off.

C.2.4 The Lens

The camera's lens is a common surveillance camera lens with an angular field of view of 54.7° and a focal length of 8.5 mm. It is able to focus on objects from 0.2 m to infinity. From 25 cm distance an object of approximately 25 × 30 cm just fills the screen. Due to the system always operating at the same distance to the object under fixed lighting conditions no autofocus or auto-iris facility is needed. The lens is not fully astigmatic and causes chromatic aberration. Both errors are analysed in F.1.2 and are fully corrected during later image processing (D.5.1 and F.2.2.1).

C.3 The Projector

C.3.1 Design of the Projector

The projector is a crucial part of the instrument. It is specially designed for use in this instrument. Figure C.9 shows its design.

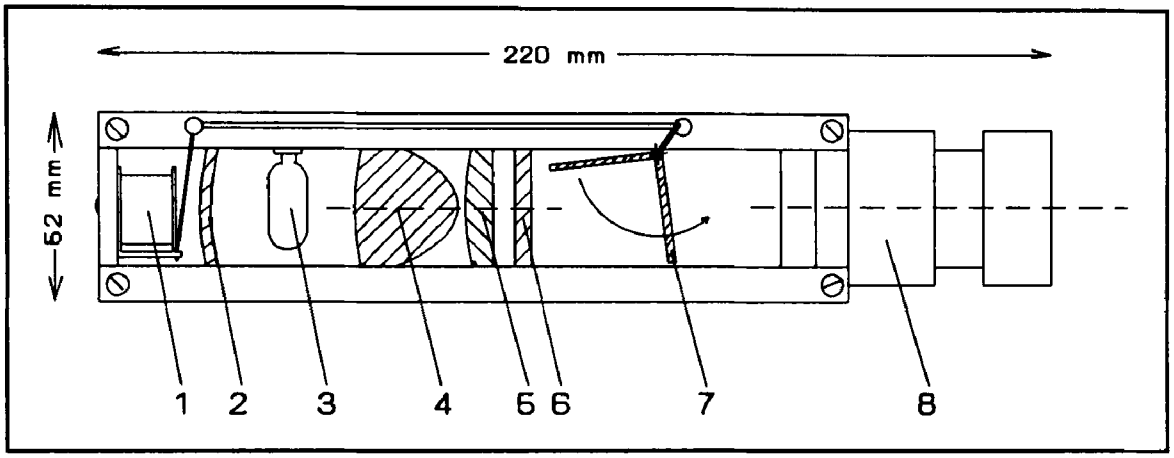

Figure C.9: The projector: **1** electromagnet **2** reflector **3** halogen lamp **4,5** collimator lenses **6** IR-cut filter **7** rotatable slide holder **8** focusing lenses

This special projector is similar to a common slide projector but with three significant differences:

1. It is much smaller. Reduction in size was possible because neither a transformer (which is located outside the sensor) nor a cooling fan is incorporated. A cooling fan is superfluous as the halogen lamp is not used for longer than 1 second with at least 30 seconds pause until activated again (This is equivalent to a 8.3 Watt lamp in constant operation).

2. The mechanism for changing the slides is completely different. Instead of slowly rotating a carousel with a lot of slides its task is to switch between two slides only. This in contrast has to be done as fast as possible. The mechanism, operated by an electromagnet, exchanges the slides by rotating a light but rugged fixing for two slides within a tenth of a second. This speed is required because two frames of the ulcerated skin with two different patterns of light projected onto it have to be taken. Both frames should show exactly the same part of the skin. This allows simplified image processing without angle- and position correction which is inevitable if too much time is lost between both frames and the patient or the sensor moves slightly.

3. The orientation of the slides is not orthogonal to the main axis of the beam of light as illustrated in figure C.9. The deviation is forced by the projection of the pattern onto the skin under an angle of 45°. By also mounting the slide under a certain angle (approx. 10°) the projected pattern remains focused better over the field of view.

The task of the projector is the production of two different patterns of light which will be projected onto the ulcerated skin[17]. These patterns are specially designed for the colour coded structured light technique. They are examined on the following pages.

C.3.2 Projector Pattern One

The first pattern is only a homogenous beam of light with defined spectral properties to obtain two things:

- Firstly, underlying information about the ulcer: its colour in certain areas and its boundaries. This information is necessary for automatic colour extraction (see D.4.2) and the measurement process itself.

- Secondly, the brightness value of each pixel of the ulcers image in the red, green and blue domain. The brightness values are vital for later image processing especially the detection of the centres of the projected stripes of pattern two.

C.3.3 Projector Pattern Two

The second pattern is the structured light pattern itself. It allows the 3-D scanning of the skin. The colour properties of the pattern have to be well defined in order to make the colour coding technique work. The colours of the measurement pattern have to fulfil the following three criteria:

---

17 The projector is controlled via a special interface board to switch the light source on and off and to select the slides.

1. The colours have to be clearly distinguishable. This is essential for image processing. When measuring a surface which might absorb parts of the visible spectrum **completely**, non primary colours[18] should be avoided. A green absorbing surface for example would turn yellow light into red, a red absorbing surface magenta into blue. Even with the knowledge of the reflection and absorption properties of the surface (obtainable from the first pattern described above) it is impossible to decide whether a spot of light reflected in red was caused by a purely red source of light or perhaps a yellow source with the green fraction being absorbed completely.
Fortunately ulcerated skin does not absorb any part of the visible spectrum completely. Thus a spot of red light with a hint of blue in it is clearly identifiable as purple if only few selected mixed colours are in use. Especially mixtures between two out of the three main colours are appropriate. Therefore the total maximum number of clearly distinguishable colours is 6 (red, green, blue, yellow, magenta and cyan) plus two non-colours (black and a shade of white). The use of more colours is possible but very likely to confuse the system mainly due to noise and quantisation errors in the camera and frame grabber electronics.

2. The different colours should generate nearly the same response in the camera. If one colour is too dominant all the other colours will appear very dark because the aperture of the camera has to be adapted to the brightest pixel of the image to prevent blooming. The darker a colour appears the worse the signal to noise ratio becomes.

3. Neighbouring stripes must not influence the precision of the centre of line detection. Figure C.4 shows the spectral sensitivity of each channel of the camera. The channels overlap significantly. Normally a coloured stripe is not absolutely monochromatic but relatively broad banded. A red stripe, for example, would also excite green sensitive CCD pixels. This effect reduces the accuracy of the centre of stripe finding algorithm:
if a red stripe is the direct neighbour of a green stripe both will partly overlap due to the scattering effect of skin (see figure B.6 in B.1.5). They will both

[18] In this context primary colours are understood to be the three colours that the three different types of photosensitive silicon of the camera's CCD sensor respond to. These are red (ca. 550 - 700 nm), green (ca. 450 - 600 nm) and blue (ca. 400 - 525 nm).

add to their neighbours brightness distribution curve. Both curves will be shifted towards each other. Their centroid is not the real centre of the stripes. Preceding image processing can theoretically overcome this effect if the spectral distribution of the stripe colours, the sensitivity distribution of the CCD array, the gamma correction factor and the reflectance properties of the skin are known. But as all the above factors may vary slightly and due to the presence of noise in the picture an error will always be introduced. Experiments revealed that in spite of such pre-processing the error may be well above the width of one pixel[19].

To avoid this the stripes have to be separated either spatially (greater distance) or spectrally. Greater distance unfortunately reduces the resolution and therefore the accuracy of the measurement and spectral separation also has its drawbacks. It may be achieved in two different ways:

- Extremely narrow banded stripes of light will not interfere on the CCD imager. In order to obtain sufficient output of the imager they have to be extremely bright[20]. Producing a slide with narrow banded colours can not be achieved with normal slide material.
- Using only two broad banded stripes on the opposite end of the visible spectrum. As the characteristic curves for red and blue sensitivity of the camera do not overlap there will be no interference. This limits the amount of usable colours to two: red and blue.

The constraints mentioned above led to a compromise using three colours, red green and blue. They are clearly distinguishable. Red and blue stripes appear alternating and very closely to each other on the pattern. Only one green stripe, necessary as a reference is used. It has sufficient spatial distance to the red and the blue stripe to avoid interference by channel crosstalk.

In order to achieve the same response in the camera the colours have to be adapted to the object of interest. This procedure is described in the following section.

---

[19] Anticipating an object difference of 20-25 cm to the camera this error is equivalent to an error in depth of approximately 0.5 to 0.8 mm. This might appear small but has significant effects on later calculations, especially surface reconstruction.

[20] Each colour susceptible CCD pixel integrates over its range of sensitivity. Wide banded and relatively dark light generates the same output as narrow banded bright light.

C.4. Adaptation of Slide Colours to Equipment and Skin

The three constraints above, may be met by carefully adjusting the slides with the patterns to the equipment and the object of interest. This can be done by analysing the spectral properties of the equipment and the human skin[21].

C.4.1 The Influence of the Equipment on the Shift of Colour

Figure C.10 shows the transmission spectra of the system's optical components.

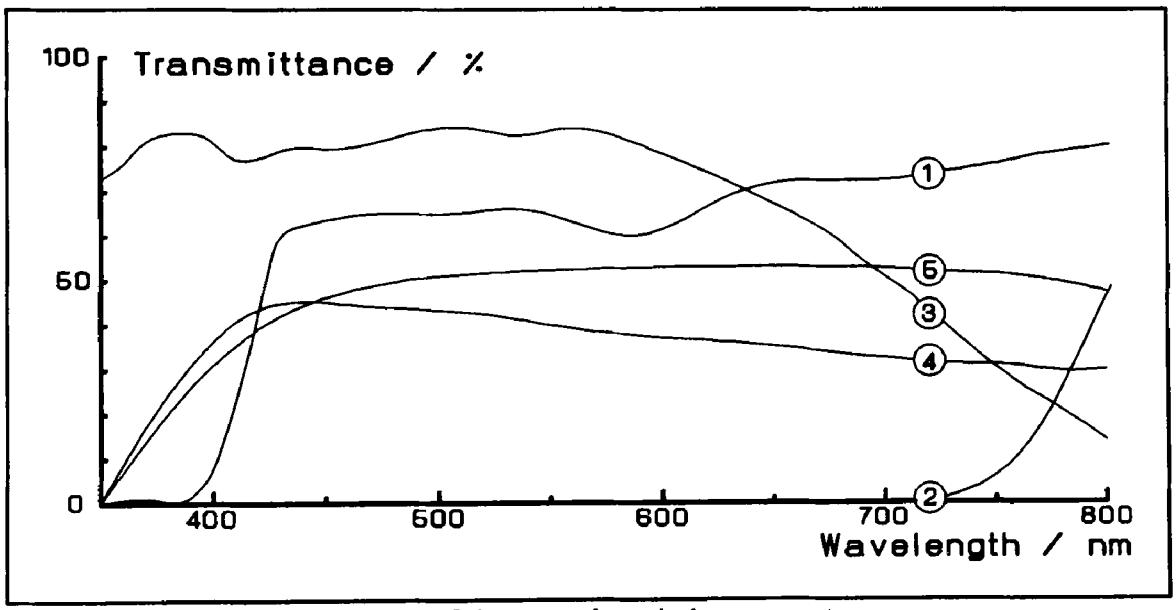

Figure C.10: Transmittance spectra of the system's optical components:
1 transparent slide **2** black slide **3** IR-cut filter **4** camera lens **5** projector lenses and glasses

The slide material

Curve 1 in figure C.10 shows the transmittance spectrum of the slide material $T_{slide(\lambda)}$ (a common Ektachrome™ slide) when fully transparent and curve 2 when completely black.

---

[21] All transmittance spectra in this work are obtained using a SERIES 5000 Spectrophotometer (issue 5011) by CECIL INSTRUMENTS LTD.

The material entirely absorbs all ultraviolet light under 400 nm but transmits almost all infrared wavelengths over 800 nm. The 400 nm limit does not pose any problem at all as the cameras CCD sensor sensitivity ends at exactly the same wavelength. The transmittance of infrared radiation over 750 nm wavelength through the completely black slide makes it impossible to use this part of the spectrum for pattern producing purposes. With a different slide material this part of the spectrum could also be used but would not produce any advantages as the camera converts the near IR part of the spectrum (up to 750 nm) into a red (and even a bit of blue and green) output signal if not blocked by an IR cut-filter.

Lenses and glasses in the projector and the camera

The light emitted from the lamp then passes through the collimator lenses, the focusing lenses and the two glasses which hold the slide. The combined transmittance spectrum of all lenses and glasses $T_{proj(\lambda)}$ of the projector is curve 5 in figure C.10. Curve 4 shows the transmittance spectrum of the camera's lens $T_{cam(\lambda)}$. It is similar to the one of the projector lens.

IR - cut filter

The IR-cut filter is a very important component. Curve 3 in figure C.10 shows its transmittance spectrum $T_{IR(\lambda)}$. The IR-cut filter has two functions:

- It protects the slide from the concentrated heat from the projector lamp. Without the filter the slide would melt down within a few seconds. Shorter exposure to heat does not damage the slide material but the colour quality deteriorates significantly.

- It reduces those parts of the projector lamp's IR-spectrum which may fool the CCD array. Figure C.4 illustrates the spectral sensitivity of the array with and without an IR-cut filter.

Projector lamp

The light source of the system is a 24 V 250 W halogen tungsten lamp commonly used for overhead and slide projectors. Figure C.11 (a) shows the entire emittance spectrum $\mathbf{E}_{\mathbf{lamp}(\lambda)}$ and (b) shows the visible part at 3380 K colour temperature (which is equivalent to a coil temperature of 3300 K).

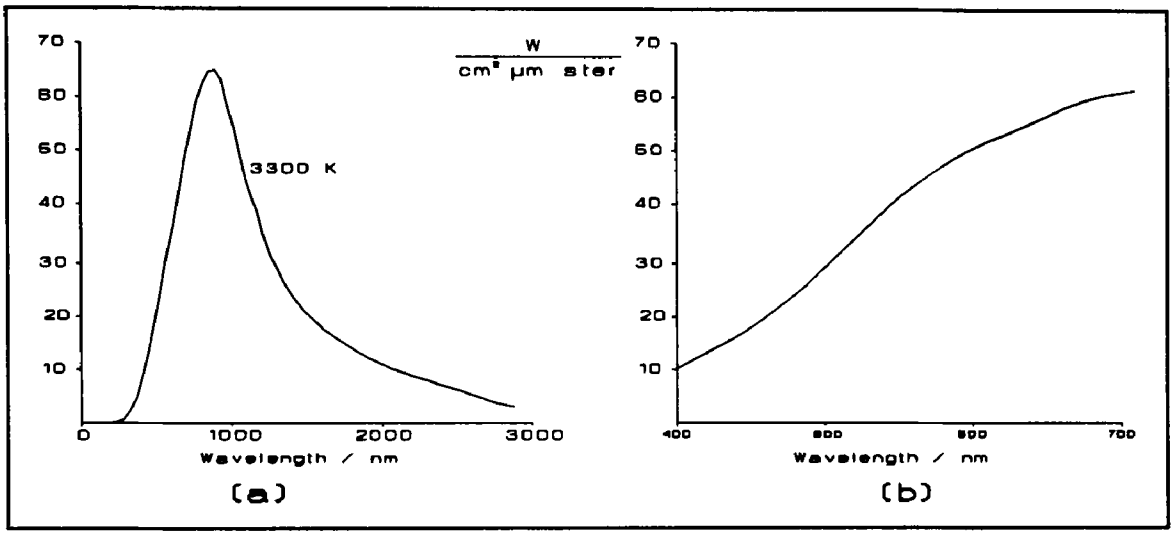

Figure C.11: (a) Full emittance spectrum of the halogen lamp and (b) visible spectrum of a halogen lamp , at a coil temperature of 3300 K (source: OSRAM).

Mirror system

Both mirrors are surface aluminised and show an absolute constant and linear reflectance for all wavelengths. Surface aluminised mirrors are necessary to prevent double reflections on both the glass surface and on the coated back which occur with ordinary mirrors. The mirrors therefore do not influence the colour appearance of the pattern and are ignored in the following. Only a constant reduction (ca 5%) over the whole of the spectrum may be observed.

CCD array

The spectral response $\mathbf{SR}_{(\lambda,\mathbf{colour})}$ of the CCD array has already been discussed in C.2.2. It is shown in figure C.4.

The above discussion indicates how the **equipment** components influence the appearance of colours. The influence of **skin colours** is analysed in the following. Both equipment and skin attributes may then be combined to determine optimised colours for the projecting slide.

C.4.2 The Influence of the Skin on the Shift of Colour

Human skin shows no constant absorption and reflectance behaviour. To allow an optimised adaptation of the slide colours to the object a colour orientated classification of the skin into white (caucasian) skin and black (negro) skin is useful. Both groups may be subdivided further according to different types of shading or tanning. Figure C.12 below shows two examples of reflectance spectra $\mathbf{R}_{skin(\lambda)}$ for untanned white and negro skin.

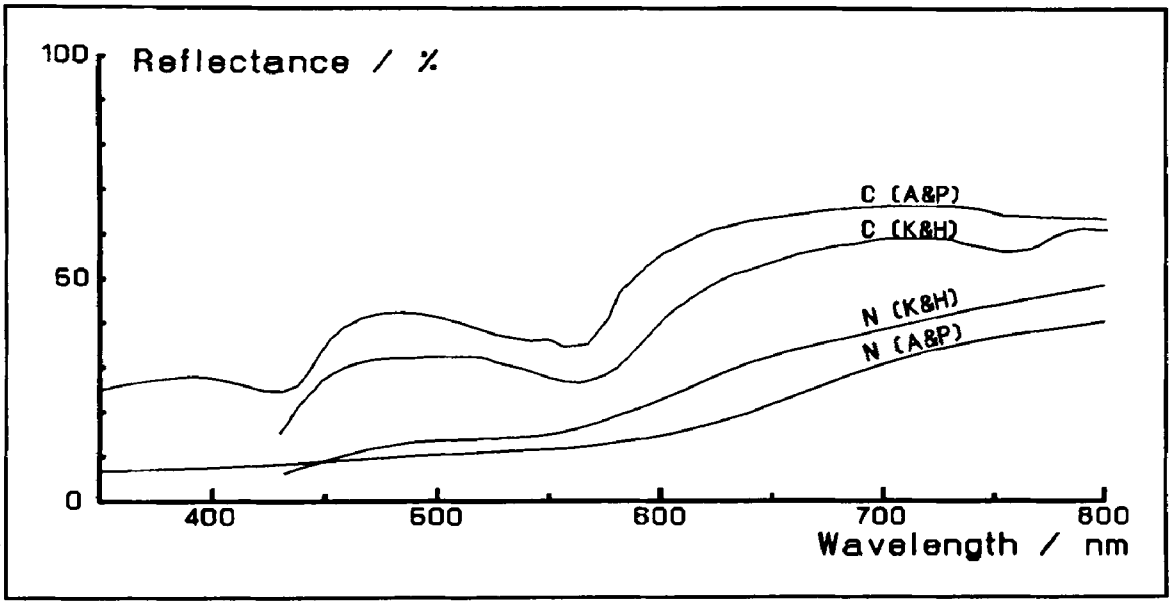

Figure C.12: Reflectance of untanned Caucasian and Negro skin N Negro, C Caucasian skin **(A&P)**=Anderson & Parish [86],p.16 **(K&H)**=Kuppenheim & Heer [93],p.801

The corresponding curves for caucasian and negro skin are parallel for both research groups. They differ only in brightness rather than colour. These findings theoretically allow the production of slides which have their colours especially optimised and adapted to a certain type of skin. The optimising method is explained in the following.

C.4.3 Optimising the Colours of the Pattern Giving Slide

The optical properties of all the spectra above may be combined and integrated over each of the three colour channels of the camera. For simplicity let $\mathbf{T}_{equip(\lambda)}$ be the combined transmission spectrum of all optical components: lenses, IR-cut filter and slide holding glasses in the projector and the camera's lens.

$$T_{equip(\lambda)} = T_{proj(\lambda)} \cdot T_{cam(\lambda)} \tag{C.1}$$

The illuminance $\mathbf{I}_{(\lambda)}$ finally reaching the CCD array is

$$I_{(\lambda)} = E_{lamp(\lambda)} \cdot T_{equip(\lambda)} \cdot R_{skin(\lambda)} \cdot T_{slide(\lambda)} \tag{C.2}$$

The camera electronics converts this illuminance of the CCD array into an output voltage for each colour channel $\mathbf{V}_{out(colour)}$

$$V_{out(colour)} = A_{(colour)} \cdot \gamma \cdot \int_{\lambda=400nm}^{\lambda=750nm} SR_{(\lambda,colour)} \cdot I_{(\lambda)} \, d\lambda \tag{C.3}$$

where $\mathbf{A}_{(colour)}$ is the amplification for each colour channel, γ the gamma correction factor and $\mathbf{SR}_{\lambda,colour)}$ the spectral response of each colour channel[22].

Apparently a certain output voltage $\mathbf{V}_{out(colour)}$ may be achieved by an infinite variety of slides. With all factors of the above equations fixed and only the parameter $\mathbf{T}_{slide(\lambda)}$ being variable, the colours of a slide may be either extremely narrow banded but intense or broad banded and dim to achieve the same output.

---

22 The spectral response is a very complex term in itself. In F.1.3 it will show that the colour balance is influenced by effects such as noise, leakage, sampling and channel crosstalk. Since these effects are either too small to significantly affect the output voltage or are statistically distributed and may be eliminated by averaging over large numbers, they are ignored in this context.

In C.3.3 the three criteria for the colour properties of the projection slide, distinguishability, identical camera response and non-interference, were evaluated. The ideal stripe colour should therefore be bright and narrow banded[23].

A common colour slide has relatively broad banded colours. This is caused by the colour producing method of the films. Normally there are only three types of granules in the slide material. One for each primary colour. The photographer can only control the density of each granule type (brightness of the colour). It is not possible to influence the bandwidth or any other parameter of the transmittance curve. As an example typical curves for several shades of blue are shown in figure C.13. Compared with five other slide materials *Ektachrome™ Professional* films appear to be the narrowest banded ones. Additionally the location of the Ektachrome™ colours coincides well with the colour sensitivity of the CCD array.

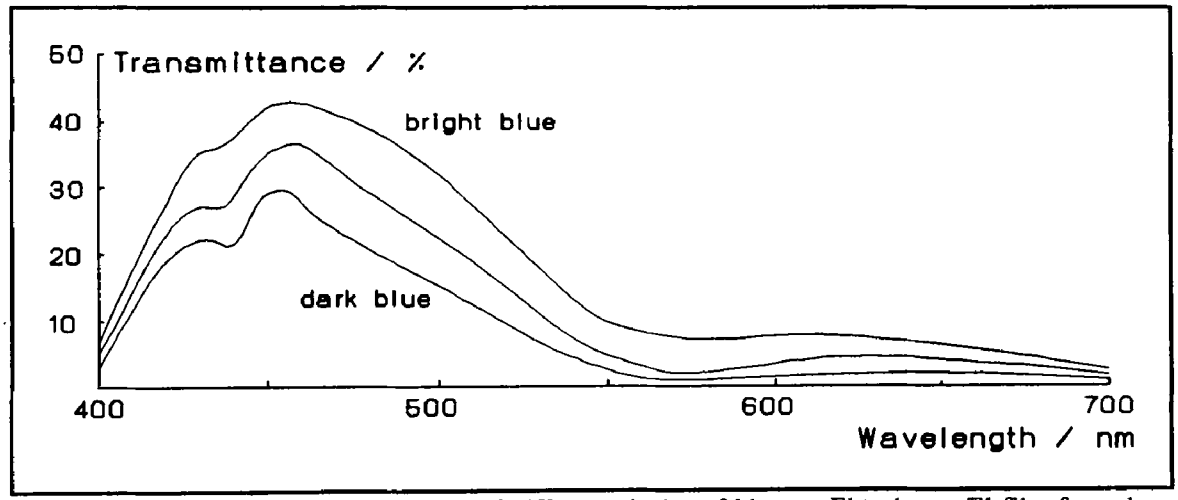

Figure C.13: Transmittance spectra of different shades of blue on Ektachrome™ film for colour slides

Due to these reasons experiments with varying exposure times and different film materials were carried out rather than trying to produce made-to-measure slides. The experiments resulted in a set of filters for every colour. Each of the filters was scanned for its transmission spectrum. The spectra $T_{slide(\lambda)}$ were then used in equation C.2 and subsequently C.3 to find the best fitting candidates.

---

[23] Such filters are *interference filters* which have a bandwidth of around 10 nm only. Unfortunately they are expensive (around £ 200 at 1992 prices) and technologically they can not be arranged in a way to form a multicoloured stripe slide. In chapter G.1 some suggestions are made on how to use interference filters in combination with common slides to produce narrow banded multicoloured stripes.

C.5 Summary

The design of the measurement sensor described in this chapter is based on the experience obtained from a first laboratory version and clinical trials with two further experimental prototypes. The hardware features which are described in this chapter significantly influence the performance of the instrument.

- **Camera** resolution and spectral response are important underlying characteristics of the instrument. Theses hardware characteristics and further information about special properties of the camera's electronics such as gamma adaption, colour balance and automatic gain control are vital parameters for the design of appropriate computer programmes which process the output of the camera.

- Since the **projector** is especially build for this instrument it is much easier to influence its characteristics than those of the camera. Optimised slide colours may be produced to achieve the maximum performance of the instrument and to make subsequent image processing as accurate and simple as possible.

The following chapter describes the processing of the pictures which are obtained by the sensor. Image processing is not only used for the calculation of the area and the volume of the measured skin ulcers but also for the correction of some significant errors which are inevitably introduced by the components of the sensor.

D: Software and Principles

D.1 General

This chapter describes the ideas and principles necessary for the measurement system which are not found in the hardware design of the sensor but are implemented in computer algorithms.

The chapter follows the flow of data through various processing steps. Figure D.1 illustrates how the data from the ulcer images are processed to extract the relevant information.

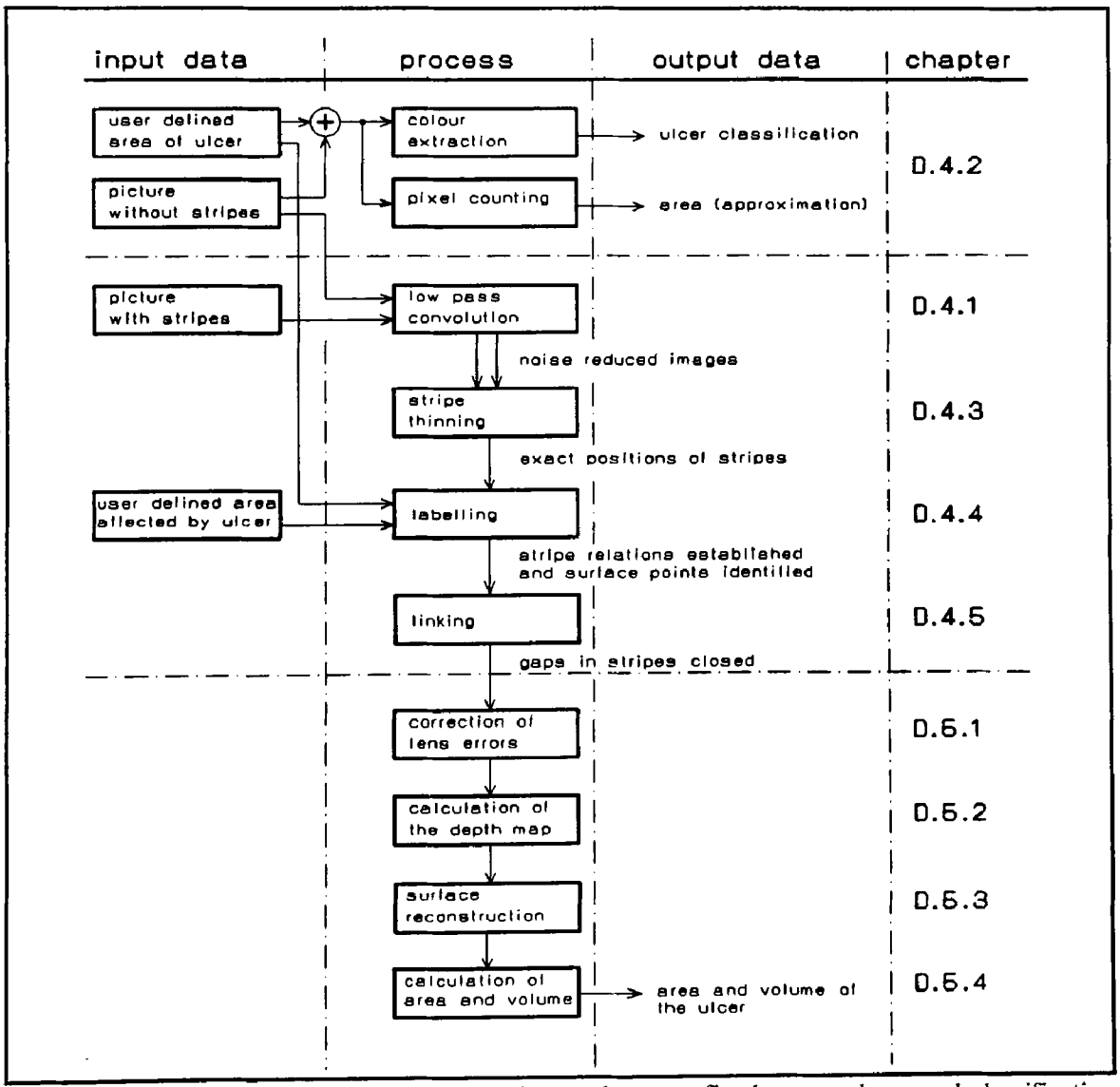

Figure D.1: The flow of data from raw image data to refined area, volume and classification information

In addition to the two ulcer images, two other sets of input data are needed for processing: the border of the ulcer and the skin area which is affected by the ulcer. For reasons discussed later this information cannot be extracted automatically from the ulcer images. It has to be provided by the operator.
Varying consecutive processing steps convert the input data into the information the physician is interested in. The system delivers a colour analysis of the lesion which may assist its classification and give the final area and volume figures of the wound.

Before the actual measurement commences the system has to be calibrated to ensure the accuracy of the measurement and to standardise the colour properties of the acquired pictures.

D.2 Calibration

D.2.1 Colour Calibration

Colour calibration is necessary because the amplifications of the three colour channels of a standard RGB camera are separately adjustable to adapt the camera to varying colour temperatures[24] of light sources. Daylight, for example, has a colour temperature of approximately 5200 K while a common tungsten lamp for room lighting has a colour temperature of around 3000 K.

If a camera which has been colour balanced for outdoor use is operated under artificial lighting the resulting pictures will show a yellowish tint. A camera calibrated for indoor use produces blueish pictures in daylight.
Some CCD cameras utilise a compensation circuit for this effect which produces acceptable results for home video. For colour measurement purposes, however, the circuit is not accurate and fast enough in some cameras. In order to achieve reproducible results the camera in use with the measurement sensor is calibrated to the colour temperature of the halogen light source of the projector: 3300 K.

---

[24] The colour temperature of a light source is expressed as an equivalent black-body temperature in Kelvin. The radiation of a black body is a homogenous spectrum and only depends on its temperature. If the spectrum of a given light source is close to the radiation of such a black body the colour temperature of the light source is approximately the temperature of the black body.

For calibration a thin chip of compressed magnesium oxide is used. Due to its pure and extreme whiteness and its diffuse reflection properties magnesium oxide is a common white standard.
The magnesium oxide chip is placed at the centre of the rectangular aluminium frame of the sensor and illuminated by the projector's halogen lamp. The camera observes the chip and its output is monitored. The colour controls in the camera's circuit are tuned until the outputs of all the three colour channels of the camera are exactly the same.
This process should be repeated from time to time to adjust the camera to the change in the colour temperature of the light source which is mainly caused by aging processes of the filaments and condensation of coil material at the quartz body of the lamp.
Thus the constancy of the colour balance of the acquired pictures may always be guaranteed and the pictures may be compared and reproduced without colour errors.

D.2.2 Geometrical Calibration

The geometrical calibration of the sensor is a measurement process to obtain the accurate positions of the two main components, camera and projector, with respect to each other. Since the structured light method uses triangulation each error in determining these figures inevitably causes errors in the measurement results of the sensor.
One distance and the positions of only two points relative to each other have to be determined: the distance of the camera's focal point relative to a reference plane[25] and the focal points of camera and projector. Due to the geometrical constraints of the sensor, all other information (angle of incidence of light rays, angle of camera and projector towards each other, position and angle of mirrors) may be derived from these figures.
It will be shown in later sections (F.2.4.1, F.2.5.1) that a change of ±1 mm of each figure causes errors of 3% of the total area and volume in the worst case. This is significantly less than errors introduced by other sources. An accuracy of ±1 mm is therefore sufficient and makes geometrical calibration easy to realise.

---

[25] The reference plane is a flat plate placed in the rectangular frame at the bottom of the sensor (see figures C.1 and D.11). It is used to produce a reference pattern for the measurement process.

The robustness of the system towards geometrical displacement is of great advantage for an instrument which has to be mobile and subsequently subject to shocks and vibrations which might slightly change the geometrical setting.

The positions of the focal points of the camera and the projector are two fixed corners of a triangle which is used to calculate the depth map of the observed surface by triangulation. The third corner of the triangle which is also necessary for calculation is given by those points on the scanned surface which are hit by the stripes of light. Other than the positions of the focal points the position of the stripe pattern is highly sensitive to mechanical disturbances.
Even if the focal point of the projector moves only slightly due to transportation or shock the stripe pattern may be shifted by a considerable amount since it is projected onto the surface from approximately 55 cm distance.
As a consequence a new reference pattern[26] has to be produced after each transportation to adjust the computer's internal representation of the geometrical situation to reality.
Once the calibration process has been performed and a reference pattern has been produced the actual ulcer measurements may commence.

D.3 Image Acquisition

The measurement process begins with the acquisition of two pictures of the ulcerated area of the skin. These pictures form the basis for subsequent image processing. Image acquisition is controlled by software which drives the interface to the camera in order to synchronise the camera with the frame grabber. It also drives the interface board that controls the slide projector.
Both pictures have to be taken in a fraction of a second. This guarantees that a certain point on the observed surface appears in the same position in both images which is necessary for the accuracy of subsequent image processing steps. The consequences of a shift between the two pictures are discussed in F.2.2.5.

---

[26] The reference pattern is a set of colour coded structured light -the same pattern which is projected onto the ulcer- projected onto the flat reference plate. The position in space of a given point of a stripe of light which has been projected onto an ulcer is then calculated by measuring the distance of this point relative to the corresponding point in the reference pattern. This procedure is described in detail in D.5.2.

The acquisition of both pictures takes 0.45 seconds. Most of this time is consumed by the process of slide changing (approximately 0.1 second) and a certain delay time (approximately 0.2 seconds) to ensure that vibrations caused by the changing process have settled down. The remaining time is consumed by synchronising camera and frame grabber and acquiring the pictures into the frame grabber memory.

Figure PI.1 on plate I at the end of this chapter (page 93) shows the first image, an ulcer illuminated by the homogeneous white halogen light of the projector, and figure PI.2 the same ulcer, this time with stripes projected onto it.

Immediately after image acquisition a number of pixels around the centre of the pictures (where the image is brightest) are checked to see whether they are clipped, i.e. one or more of the three colour components of a pixel displays its maximum value. If this is the case a warning is displayed and the acquisition should be repeated with a slightly closed camera aperture.

If the acquisition process is successful the operator may display brightness scans through the pictures at any position to assess if the dynamic range of each channel has been optimally exploited. Figure D.2 shows such a scan along a line indicated by the white line in the scanned image in figure PI.2.

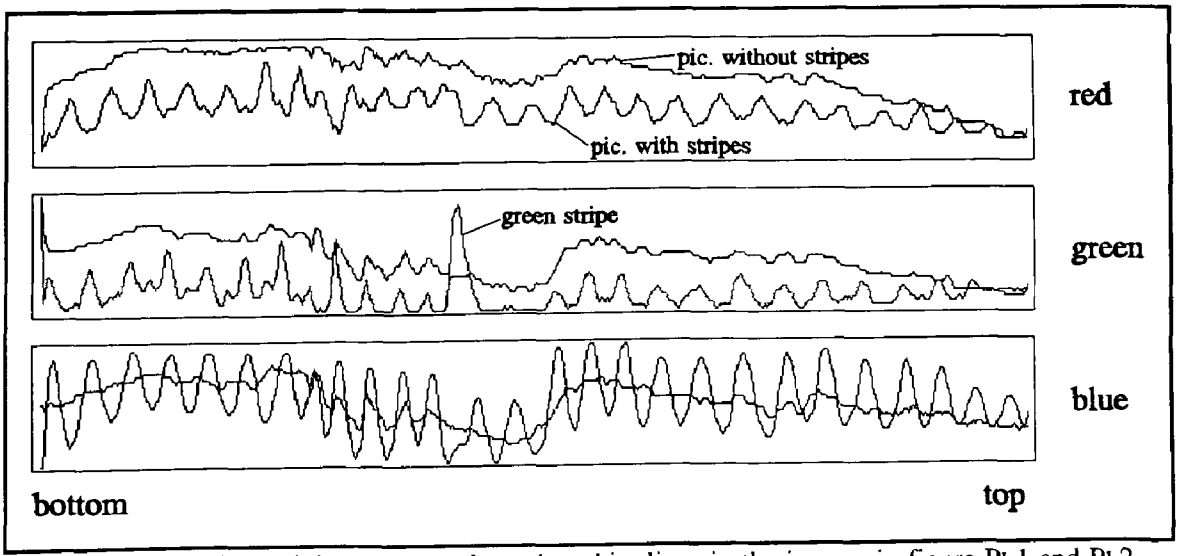

Figure D.2: Vertical brightness scan along the white lines in the images in figure PI.1 and PI.2

The three boxes show the red, green and blue channels respectively. The strongly oscillating lines represent a scan through the picture with stripes in figure PI.2 while the smoother line is a scan through the image without stripes in figure PI.1.
One effect which influences later image processing is clearly observable: in the green channel the scan of the picture with stripes shows a value higher than the scan of the picture without stripes at one location only: at the position of the green stripe. The scan of the picture without stripes acts as a threshold for detecting the green stripe. For the blue stripe this behaviour may also be observed almost everywhere whereas the red stripe is always below the threshold line.

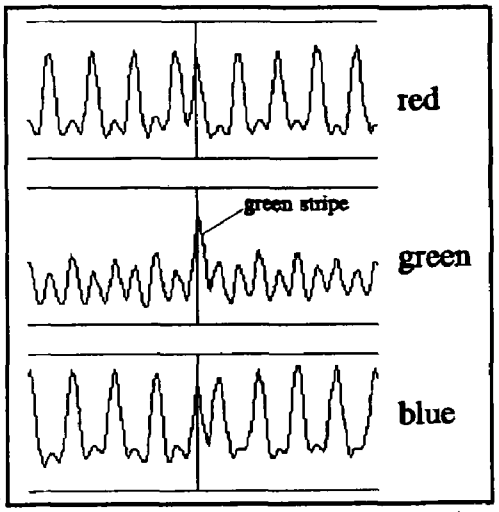

Figure D.3: Extract of a scan showing channel crosstalk

Another effect, similar to the channel crosstalk effect discussed in C.2.3, becomes more obvious when looking at the scan of the homogeneously coloured reference plate in figure D.3: colour crosstalk which is caused by overlapping bands of the colour filters in the slide material and the CCD array rather than by electronic deficiencies. The peaks of the red and blue channels also appear in the green channel. Only the peak in the middle of the green scan indicates a real green stripe, the other peaks are phantom peaks caused by the colour crosstalk. The green stripe also causes a strong impulse in the other two channels. The colour crosstalk effect is strong enough that even the relatively separated blue and red channels cross-influence each other.

D.4 Image Processing

D.4.1 Noise Reduction

For a number of reasons, such as quantisation and performance of electronic circuits, the picture in the frame store is noisy (see F.1.3 for a detailed analysis). In order to reduce noise and enhance the quality of the pictures a large variety of algorithms have been designed by computer vision researchers. Since a picture is two-dimensional, most techniques employ two dimensional convolutions of some kind.
In this work noise reduced image information is necessary as an input for two algorithms: the colour extraction and the centre-of-stripe-finding algorithm (COS-algorithm). The COS-algorithm works solely on a one dimensional basis, i.e. it uses the image information of only one column of the picture at a time. Therefore a one dimensional low-pass filter rather than a two dimensional one is used to prepare the image data for the COS-algorithm. This has the advantage of increased computing speed. The upper scan in figure D.4 shows the unfiltered output of the camera's blue channel for a scan along the white line in figure PI.2.

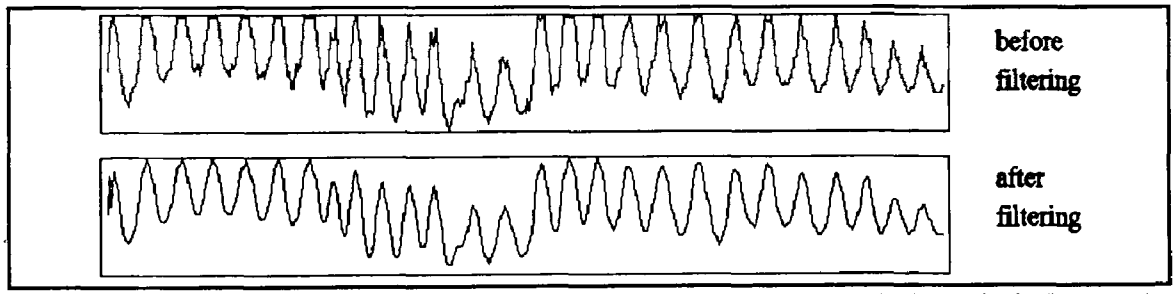

Figure D.4: (above) unfiltered scan of the blue channel along the line in figure PI.2, (below) the same scan but filtered by a moving average filter

The scan discloses two characteristic features: the scan line is not smooth but rippled due to noise and its peaks are partly cut off due to clipping.
The lower line in figure D.4 shows the same scan after passing it through a moving average filter which has some similarities to a low pass filter. While moving from pixel to pixel the filter averages the grey values of the actual pixel at position y and two pixels to the left and to the right using the following expression

```
out[y] = (in[y-2] + in[y-1] + in[y] + in[y+1] + in[y+2]) / 5.
```

This filter rather than a real digital lowpass filter is used due to two advantages: it is fast to compute and it preserves the locations of the peaks and troughs of the scan. It will be shown later (G.1.1) that a specially designed lowpass filter has better filtering qualities, but is unsuitable in this context due to its tendency to shift the peak and trough positions.

D.4.2 Colour Extraction

Before the actual measurement process takes place it is already possible to extract some basic information from the unstriped image of the ulcer. As mentioned in the literature survey (see B.1.4.2) the ratio between black/yellow colours indicating necroses and granulation tissue expressed by red colour is of some value to the physician. After encircling the ulcerated area by the means of a computer mouse (see figure PII.1 at the end of this chapter, page 94) the software starts checking the marked area pixel by pixel for their respective colours. Each pixel carries the colour information of a specific point of the surface. In order to reduce noise the colour of a given pixel is calculated by a 3x3 moving average filter.

Table D.1 shows the convolution matrix of the filter. The central cell of the matrix is moved from pixel to pixel within the user defined boundary of the ulcer. For every centre pixel $\mathbf{P}_{(2,2)}$ the value of each colour component is calculated by

1/16	1/8	1/16
1/8	1/4	1/8
1/16	1/8	1/16

Table D.1: Convolution matrix used for noise reduction by the colour extraction algorithm

$$P_{(2,2)} := \frac{1}{16}P_{(1,1)} + \frac{1}{8}P_{(1,2)} + \frac{1}{16}P_{(1,3)} + \frac{1}{8}P_{(2,1)} + \frac{1}{4}P_{(2,2)} + \frac{1}{8}P_{(2,3)} + \frac{1}{16}P_{(3,1)} + \frac{1}{8}P_{(3,2)} + \frac{1}{16}P_{(3,3)} \qquad \text{(D.1)}$$

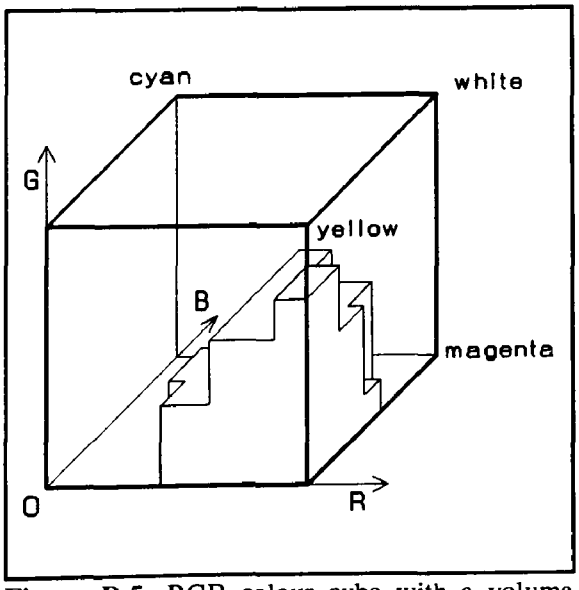

Figure D.5: RGB colour cube with a volume enclosing red granulation tissue colours

After this averaging the colour of the pixel is classified. One method of expressing a colour is the *RGB colour cube* where a colour is represented as a point in a three dimensional coordinate system. Figure D.5 shows a volume in the RGB colour cube enclosing all the coordinates which represent red granulation tissue. The volume was defined after analysing a large number of ulcer photographs manually thus establishing a colour reference base.

It is interesting to note that the impression of 'red' is mainly caused by the balance between the three primary colours of the colour cube rather than the absolute intensity of the red value of a specific point. This may also be observed in the scan in figure D.2 which shows that in the central area of the picture where the ulcer appears in a saturated red the amount of red is actually less than in the surrounding normal skin. There red is balanced by relatively strong blue and green values. Blue and green values drop considerably in the ulcer's centre whereas red values remain on a high level thus causing the impression of a wound in saturated red colours.

Following the proposal of Arnqvist [15] the pixels are divided into three classes: red, yellow and black. (A fourth 'class' is reserved for those pixels which can not be clearly classified as they belong to none or to more than one of the groups). The result of the count is available after a few seconds and displayed graphically in a diagram in figure PI.3 on plate I at the end of this chapter (page 93).

D.4.3 Finding the Centre of a Stripe

The measurement process starts with a procedure to reduce the amount of image data in the image with the stripes. For the measurement process only the accurate positions of the stripes, their centres, are important. The rest of the image data may be ignored.
Finding the centre of a stripe is a common problem in any technique using structured light. Several approaches were made in recent years to design an algorithm for the accurate determination of the centre of a projected line. To the author's knowledge none of them is intended to work on a surface with such complex optical properties as the human skin. A new strategy had to be found to handle ulcerated skin.

The basic problem in finding the centre of a stripe of light is the accurate definition of its width. Previous work into the field of the structured light measurement techniques applies mostly to opaque and homogeneous surfaces with little or no contrast and colour differences.

The objects of interests are mostly uniformly coloured geometrical objects in a laboratory environment. These objects allow some *a priori* knowledge to be incorporated into stripe extraction algorithms to make stripe extraction less difficult. Ulcerated skin, however, is optically inconsistent and irregular in shape, colour and contrast. Experiment E.2 shows that the known approaches[27] to stripe thinning break down when confronted with such an object. New strategies to overcome this problem had to be formulated. Based on the outcome of experiment E.2 the system actually incorporates two methods which are explained in the following two sections.

D.4.3.1 The Dynamic Threshold Method

The dynamic threshold method is used for the extraction of the boundaries of the green reference stripe in the picture with the stripes. The threshold line which defines the width of the green stripe is derived from the picture without the stripes. In the green channel scan of figure D.2 the scan of the picture with stripes breaks through the scan of the picture without stripes only at the position where the green stripe appears in the picture with stripes.

High frequency oscillations in the scan of the picture with stripes are caused mainly by crosstalk from the blue and the red channels. Low frequency oscillation follows the underlying reflectivity of the skin itself. This low frequency oscillation is mirrored in the scan through the picture without the stripes which forms an enclosing hull over the scan through the picture with the stripes.

This stripe extraction method is not merely a stripe detection tool but also a means to take varying surface reflectivities into account which alter the true width of a stripe. Both surface reflectivity and stripe width influence the outcome of the centroid finding process.

---

[27] These approaches are adaptions, variations or mixtures of the two main methods: extraction of a stripe by a fixed threshold which defines its width or a system using a set of rules that defines the properties of a 'valid' stripe. For details see E.2

Once the green stripe is detected its centre has to be calculated with as high a precision as possible. Figure D.6 shows a vertical scan through a horizontal stripe of light. Its centre C may be calculated[28] by

$$C = \frac{\sum_{y=a}^{b} B_{(y)} \cdot y}{\sum_{y=a}^{b} B_{(y)}} \qquad \text{(D.2)}$$

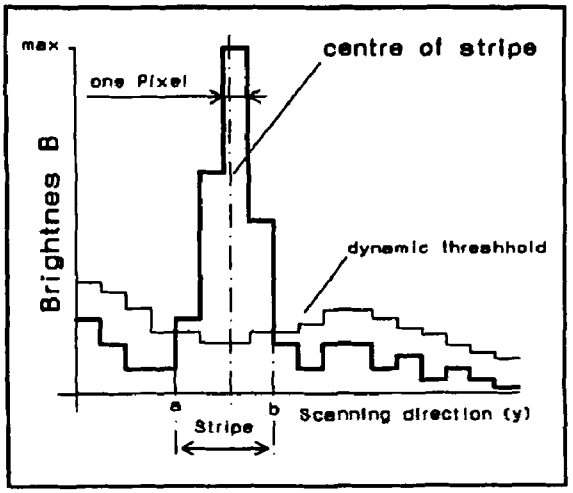

Figure D.6: Vertical scan through a horizontal stripe of light

where $\mathbf{B}_{(y)}$ is the brightness at a given point y, and a and b mark the borders of the stripe as defined by the threshold. The centre-of-stripe equation (COS-equation) actually calculates the centre with sub-pixel accuracy. The accuracy is normally within a tenth of a pixel width.

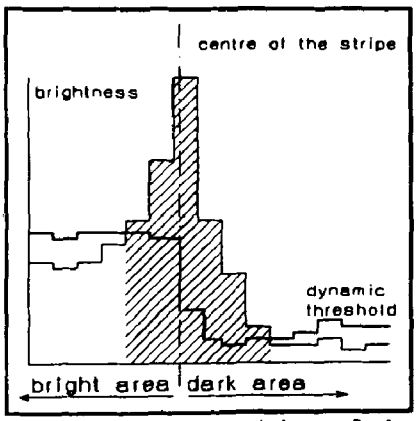

Figure D.7: Maintaining of the stripe width by the dynamic threshold in areas of varying reflectivity

The dynamic threshold maintains the true width of a stripe. In case of a static threshold the stripe's borders a and b would shift their relative positions at places where the reflectivity or the angle of the surface towards the light source change.

As a result the centre is wrongly calculated. If a dynamic threshold is used the original stripe width is maintained and the centre is calculated more correctly. Figure D.7 illustrates this effect. A small remaining error is caused by the lower brightness values of the stripe in regions of lower reflectivity. In F.2.2 it is shown that this error is normally less than 0.4 pixel widths. Theoretically it is possible to eliminate even this small error by correcting the amount of reflected light of a stripe by a factor derived from the reflectivity of the surface measured in the picture without the stripe. This process does, however, not increase the accuracy of the COS-equation for reasons such as noise and the spectra of the colour filters. This is examined more closely in F.2.2.4.

---

[28] [122], p.236

The dynamic threshold detects only the brightest part of the green stripe. In order to increase the accuracy of the COS-equation the darker parts of the stripe are also included in the equation by adding another two pixels to the left and another two pixels to the right of the threshold of the valid part of the stripe. In F.2.2.3 (see table 7) it is shown that increasing the width of a stripe significantly increases the accuracy of the method.

The dynamic threshold method works well with the single green reference stripe but delivers poor results with the red and blue stripes. The reason becomes obvious when looking at the brightness scans of the blue and the red channels in figure D.2. For the red channel the dynamic threshold is located much too high whilst for the blue channel it is too low at some positions. This behaviour is caused by the different spectral intensities and distributions of the white light in the picture without stripes and the coloured light in the picture with the stripes. If, for example, the picture without stripes would be illuminated through a red filter with exactly the same colour properties as the red in the pattern giving slide, the threshold line would appear as a curve connecting the peaks of the stripe representing the scanner line. Designing this red filter slightly darker would lower the line thus providing an excellent threshold line.
As a consequence of such an approach two more pictures (one with a red and one with a blue filter in use) have to be stored and processed. The projector also becomes more complicated. Therefore a new approach is chosen using the fact that the red and the blue stripe are almost identical sinusoidal curves but 180 degrees out of phase: the subtraction method.

D.4.3.2 The Subtraction Method

Figure D.8 illustrates the subtraction method. The oscillating line in the lowest box is calculated by subtracting the red from the blue channel.

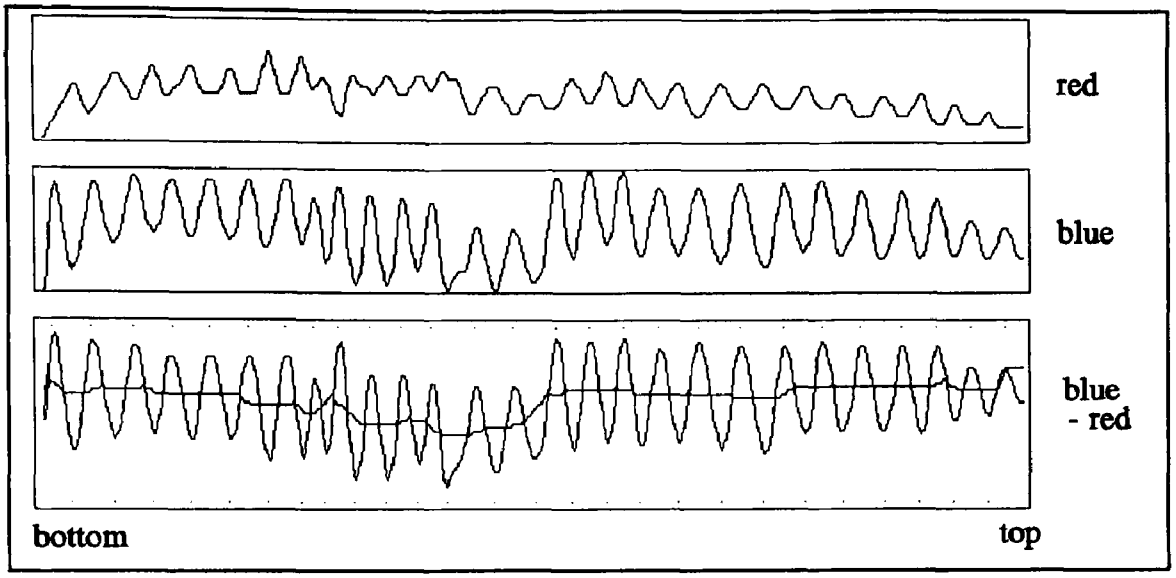

Figure D.8: Vertical brightness scan along the white lines in the images in figure D.2 and D.3

This method has three positive side effects:

1) Crosstalk between the blue and the red channels is reduced since the amount of crosstalk is almost the same in both channels.

2) The dynamic of the resulting signal is significantly higher than in one of the source signals.

3) The original almost sinusoidal form of the stripes is also restored. Even the strong crosstalk signal from the green stripe is fully eliminated.

The resulting graph is an excellent source of data for stripe extraction. Peaks correspond to blue stripes, troughs to red stripes. In order to find the centres of the stripes the peaks and troughs of the curve are found by checking if a given pixel is a local minimum or maximum. This check is based on four rules defining a valid peak or trough:

1. A local peak (trough) exists at a certain position if the grey levels of two points with 4 pixels distance to the left and to the right of this position are 4 units less (more) than the grey level at this position.
2. A peak is followed by a local trough and vice versa.
3. The minimum distance between peaks (troughs) is 15 pixels.
4. The maximum width of a stripe is 30 pixels.

These rules apply for a total number of approximately 50 to 60 stripes in the image and have to be adapted accordingly if a different amount of stripes is projected.

There are two rows of dots in the lowest box of figure D.8 that shows the blue-minus-red scan. The upper row indicates positions where a blue stripe centre has been detected, the lower row indicates where centres of red stripe have been detected. The width of a stripe which is necessary for equation (D.2) is defined by the median curve in the blue-minus-red scan of figure D.8. The intersection of the blue-minus-red curve with the median curve is a boundary of a stripe. Depending on the relative position of the intersection point and the corresponding local extremum it is either the beginning or the end of a stripe. The median curve is found by connecting median points by straight lines. A median point is the middle of a straight line connecting a peak with the next trough.

The experiment in E.2 shows that this method compares favourably with competing approaches in terms of accuracy as well as robustness. Additionally it demonstrates a superior sensitivity in its ability to detect stripes in an image. The overall performance of the method, especially the aspect of accuracy and errors due to specular reflection is discussed in F.2.2. Figure PI.4 shows the result of the two processes which detect the centres of the stripes.

The **combination** of both the above methods, the dynamic threshold method for the green stripe and the subtraction method for the blue and the red stripe is united with the 1-D noise reduction filter of D.4.1 in a single algorithm which is able to process the entire image of ulcerated skin within 55 seconds. Only 10% of this time is consumed by the calculation itself[29], the majority of the time is needed to transfer image data from the frame store on the frame grabber card to the RAM of the host computer. Due to hardware limitations of the frame grabber card the process can not be speeded up by programming techniques (e.g. assembly coding) or a faster host computer.

[29] The calculation time depends mainly on the noise reduction filter which is in use. More complicated filters such as Butterworth or Bessel filters may increase the computing time significantly.

D.4.4 Labelling of the Extracted Stripes

For the human observer the extracted stripes in figure PI.4 are clearly related to each other. For the computer they are at this point of processing only a set of lines. The relation between the stripes, i.e. the position of a given stripe relative to the green reference stripe, has to be established by a labelling algorithm.
The algorithm has to manage irregularities such as missing parts of stripes, and varying distances between stripes. The task is broken up into three stages: vertical labelling, horizontal labelling and consistency checking. The flow chart in table D.2 shows the general structure of the first step of the labelling process: vertical labelling.

Start at the left border of the thinned stripe image			
	scan the column at this position for the green stripe		LABEL=30
	find the first blue stripe over the green stripe		LABEL=31
		go upwards and find the next red stripe	LABEL=LABEL+1
		go upwards and find the next blue stripe	LABEL=LABEL+1
	UNTIL	the upper border is reached	
	go back to the green stripe		LABEL=30
	find the first red stripe under the green stripe		LABEL=29
		go downwards and find the next blue stripe	LABEL=LABEL-1
		go downwards and find the next red stripe	LABEL=LABEL-1
	UNTIL	the lower border is reached	
	move 6 columns to the right		
UNTIL	the right border of the image is reached		

Table D.2: Flow chart of the first of three labelling steps: vertical labelling

For vertical labelling every sixth column in the picture with the extracted stripe centres is scanned for stripes. Firstly, each column is searched for the green reference stripe. Then, starting from this stripe the algorithm searches upwards and then down the column to find the alternating red and blue stripes and labels them.

Apart from doubling the resolution of the instrument the use of two colours for the stripes makes the labelling process more robust against failures in labelling: sometimes the COS-algorithm fails to detect the centre of a certain stripe but it finds the stripes at positions above and below. A gap appears. If stripes of only one colour are used the gap can not be localised by a labelling algorithm analogous to the one portrayed above. If two colours are used the presence of such a gap becomes obvious as two vertically neighboured stripes appear to have the same colour. Since the labelling mechanism does not know if the gap is one, three, five or any other odd number of stripes wide it stops, leaving the problem to subsequent processing steps. The labelling mechanism may be fooled by a gap of two, four or any other even number of stripes. Since the two colours appear alternating no break of the alternation rule may be detected when an even number of stripes is missing. Two or more missing stripes, however, leave a gap of significant size. The labelling mechanism therefore calculates the distance between stripes and stops labelling if the distance between two stripes is more than twice the distance to the preceding stripe.

A labelling algorithm could perform much better if more than two colours could be used to distinguish the stripes. For reasons discussed before (colour separation, channel crosstalk) the use of more than two colours spawns problems in other areas. Figure PI.5 illustrates the result of the first step of the labelling process. Yellow dots indicate the positions where a stripe could be labelled. The positions of the yellow dots are stored in a labelling grid.

In the second step of the labelling process the majority of the remaining unlabelled positions are closed by horizontal labelling: an algorithm checks every yellow dot for a neighbour to the left or to the right. If it does not exist, it tries to follow the respective stripe on which the yellow dot is sitting. It marks every labelling position with a blue dot and also stores its location in the labelling grid. The result of this process is shown in figure PI.6.

In a last step the labelling grid is checked for consistency by following every labelled line from the beginning to the end. All dots which sit on a specific line should carry the same label but in some rare cases the two preceding processing steps produce faulty results. The first labelling step, for example, may be misled if a gap of two stripes is very small and the twice-the-distance rule does not apply. As a result one stripe carries two different labels.

If the checking routine encounters such a contradiction it tries to solve the problem by shifting one set of labels to lines above or below respectively. The labels of these and all following lines are also shifted.
If this shifting causes inconsistencies in stripes which are definitely correctly labelled the other set of labels is shifted. If the problem still exists the system produces a graphical display of all stripes. The user may then decide whether to try a correction of the errors in an interactive process or to start a new measurement.

When the labelling process is successful the y-positions of the stripes at the positions indicated by the yellow and blue dots are stored in a rectangular grid - the labelling matrix. The matrix has 60 rows (the total number of stripes) and 52 columns (widths of the pictures divided by six). The matrix coordinates encodes the labels of the stripes (y-coordinates) and the x-position of a specific labelling point (x-coordinate times six). This labelling matrix alone is needed for further processing. The matrix represents the real surface. It covers the surface like a net with an average mesh size of approximately 2.2 times 2.2 mm.

The intersection points of the grid carry not only labels indicating their relative position towards each other and the spatial information of the respective surface point but also an additional flag that indicates its group classification. Three classifications are possible dependent on whether the point belongs to healthy skin, the ulcerated area or the area affected by the ulcer. The classification flag is set according to the green and the yellow borderlines lines drawn by the operator.

D.4.5 Closing Gaps in Stripes

So far the system deals only with the stripes which can be clearly extracted and identified. Sometimes, however, certain influences such as specular reflection or low reflectivity of the surface cause a stripe to appear too dark or too vague to be detected. A gap appears.
The gap closing algorithm which scans the labelling matrix detects such gaps. In a first step it establishes if the gap is smaller in x- or in y-direction. If the gap is wider than three matrix coordinates in the smallest direction the measurement process fails and new pictures have to be taken. If the gap is smaller the missing matrix points are extrapolated by polynomial approximation using neighbouring points as a base.

At this stage as much information as possible has been extracted from the initial picture with the stripes. For subsequent calculations it is no longer required.

D.5 Calculations

D.5.1 Lens Error Correction

The source of the labelling matrix are the two pictures, with and without stripes, which are influenced by a variety of errors. In F.2 it is shown that most of them, such as noise, quantisation and camera electronics errors, are either negligible or have already been compensated for by the applied image processing steps. Only distortion, caused by lens errors of the camera, significantly influences the outcome of the preceding processing steps and has not yet been compensated for.

The reason why the correction for lens distortion is applied at such a late stage of the processing is influenced by the amount of image data which has to be processed. If the two underlying images are corrected for distortion a total of 2×476×320 pixels have to be processed. The matrix derived from the labelling process has only 52×60 points - nearly 100 times less. Instead of minutes, the correction may be performed in less than 4 seconds. The resulting grid is the same in both cases.

Distortion arises because different areas of a lens have different focal lengths and different magnifications [59] (p.230). Figure B.10 in section B.3.3.1 of the literature survey shows the effect of barrel and pincushion distortion on a rectangle. The distorted rectangle would appear with almost straight borders if it were not drawn on a flat surface but on the inside of a sphere with the camera's focus at its centre. Distortion is then minimised because the distance to the focus is constant and no different magnifications for different distances may occur. Since this model is not an accurate description of the real effect, full correction is not possible, but it will be shown that the reduction in distortion is so significant that the remaining error may be ignored in the context of this work.

The observed barrel distortion of the lens in use may therefore be corrected by an equation derived from figure D.9[30]: a given image point has a real x-y-position $\mathbf{P}_{xy}$ but it is seen by the camera as if it were located at position $\mathbf{P'}_{xy}$. Directly underneath the camera's focal point **C**, at position **M** the distortion disappears. The greater the distance from **M** the greater the distortion. In order to correct the distortion these geometrical constraints may be used to evaluate a correction formula for each image point.

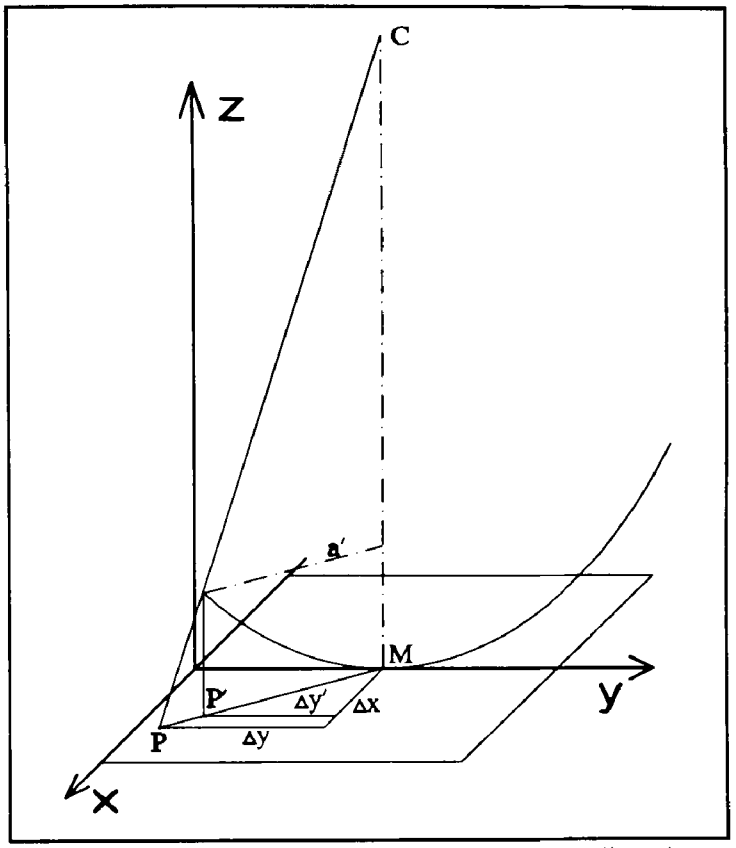

Figure D.9: Model for the correction of lens distortion

In the cartesian coordinate system in figure D.9 the z-position **e** of line **a'** (with a length equal to the distance from point **P'** to point **M**) is given by the equation

$$e = C_z - \sqrt{C_z^2 - a'^2} \tag{D.3}$$

where C_z is the height of the camera's focal point and the radius of the circle. Using the relationship

$$\frac{a'}{C_z - e} = \frac{a}{C_z} \tag{D.4}$$

the distance **a** from **P** to **M** may be found by

$$a = \frac{C_z \cdot a'}{\sqrt{C_z^2 - a'^2}} \tag{D.5}$$

---

30 Notation: lengths are notated in lower, points in upper case. Indices at points (either x,y or z) indicate the coordinate which is used.

Since

$$\Delta x = \Delta x' \cdot \frac{a}{a'}, \qquad \Delta y = \Delta y' \cdot \frac{a}{a'} \tag{D.6}$$

and

$$a'^2 = \Delta x'^2 + \Delta y'^2 \quad \text{with} \quad \Delta x' = |P'_x - M_x|, \quad \Delta y' = |P'_y - M_y| \tag{D.7}$$

the real position of the image point $\mathbf{P}_{xy}$ in x- and y-direction may finally be calculated by

$$P_y = (P'_y - M_y) \cdot \frac{C_z}{\sqrt{C_z^2 - (P'_x - M_x)^2 - (P'_y - M_y)^2}} + M_y \tag{D.8}$$

$$P_x = (P'_x - M_x) \cdot \frac{C_z}{\sqrt{C_z^2 - (P'_x - M_x)^2 - (P'_y - M_y)^2}} + M_x \tag{D.9}$$

The corrected x- and y-values are related to a z-position of zero, the position where the reference plane is located. This is of importance for the following processing step: calculation of the depth map.

As already stated the model in figure D.9 does not entirely reflect the physical reality that leads to distortion. But for the purpose of the correction of stripe positions it is adequate. Figure D.10 shows a stripe of light before (above) and after compensation by equations (D.8) and (D.9). The straight stripe is located at the bottom of the image area, where the distortion is worst. After correction the resulting stripe is within a margin of error of ±0.25 pixel width straight again.

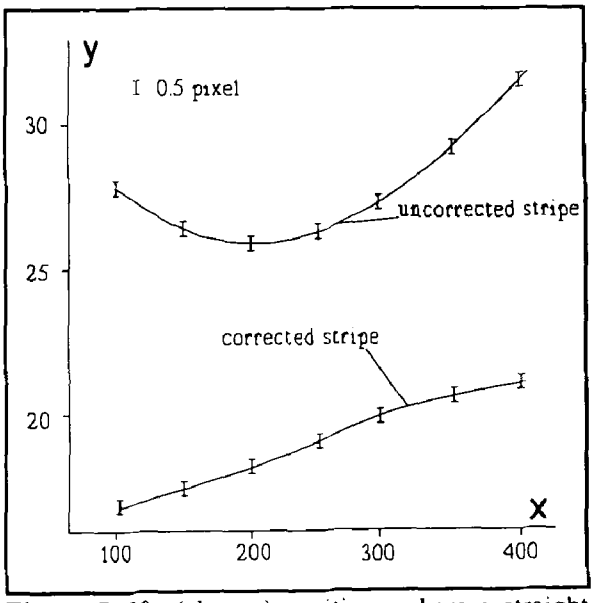

Figure D.10: (above) positions where a straight stripe of light was measured. (below) position after compensation for distortion.

D.5.2 Calculation of the Depth Map

The depth map is the quantised numerical representation of the measured surface. Each point in the labelled surface grid represents a corresponding point on the observed surface. The depth map associates three space coordinates to each of the surface grid points. These space coordinate points are defined relative to a reference plane. In figure D.11 the reference plane is located at z-position zero in line with the x- and the y-axis. The physical position of the reference plane is the rectangular aluminium frame at the bottom of the sensor (see figure C.1). The origin of the coordinate system is therefore the reference plane for the z-coordinate, the x-position of the camera's and the projector's focal points for the x-coordinate and the lower border of the acquired image of the reference plane for the y-coordinate.

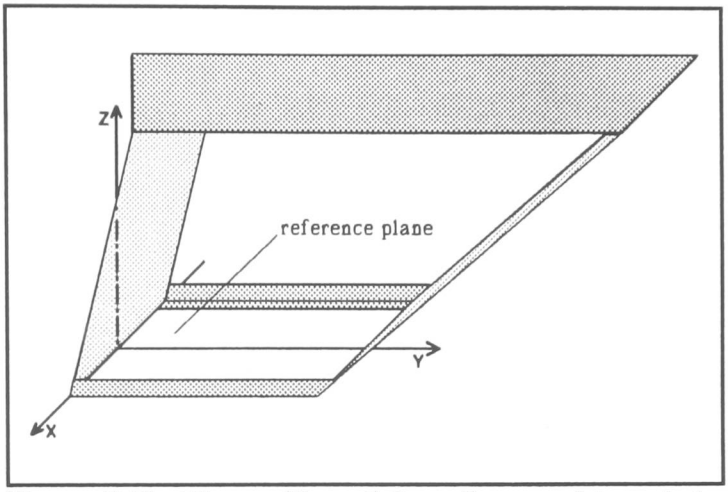

Figure D.11: The position of the reference plate and the coordinate system used for calculations

The reference plane is represented by a labelled reference grid analogue to the labelled surface grid. In order to produce the reference grid, a flat, white, aluminium plate is placed in the rectangular frame and the stripe pattern is projected onto it. This pattern is identical to the pattern which is projected onto the surface to measure. Image acquisition, centre-of-stripe finding, labelling and distortion correction are also performed identically. For measurement both grids, the reference and the surface grid are needed to produce the triangulation data for each point of the surface grid. Figure D.12 illustrates the principle.

A given spot **X** on the surface located at the centre of a stripe is defined by the intersection point of two lines. Two three-dimensional sets of coordinates relative to the reference plane are known to define the run of both lines. At x=0 only two-dimensions have to be considered.

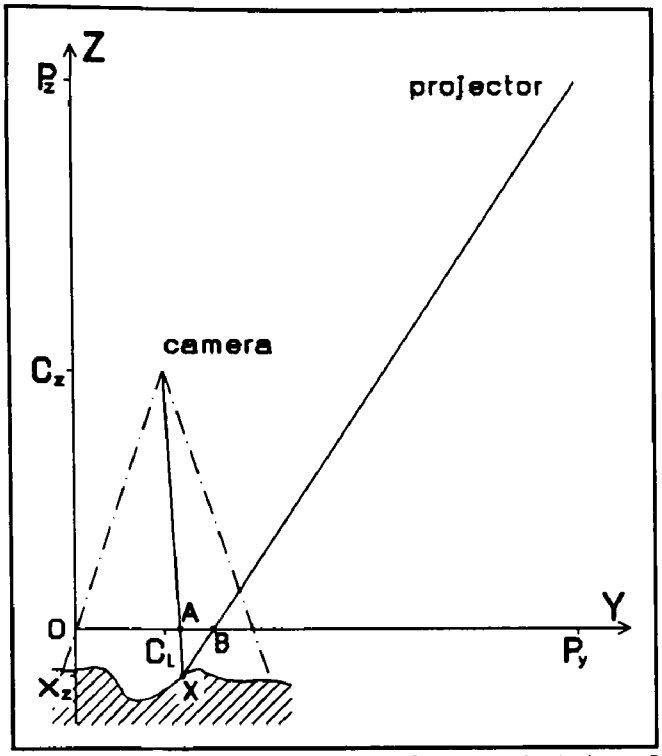

Figure D.12: Geometry used for the calculation of the surface distance by triangulation

For the projector line the first of the two sets of coordinates is the position of the projector's focal point. In the two dimensional case it is defined by $\mathbf{P}_y$ and $\mathbf{P}_z$. The other set of coordinates is the actual y-position of a labelled point **B** of a stripe in the reference grid.

For the camera the first of the two sets of coordinates is also the position of its focal point. The focal point is defined by $\mathbf{C}_y$ and $\mathbf{C}_z$. The other set is the actual y-position of point **A** in the surface grid. Point **A** is the point which corresponds to point **B** in the reference grid. Both points originate from the same ray in a given stripe of light.

The run of the two lines may be described by two equations. For the two-dimensional case the line from the camera to point **X** may be characterised by

$$z = \frac{C_z}{C_y - A_y} \cdot y - \frac{C_z \cdot A_y}{C_y - A_y} \qquad \text{(D.10)}$$

and the line of the stripe of light by

$$z = \frac{P_z}{P_y - B_y} \cdot y - \frac{P_z \cdot B_y}{P_y - B_y} \qquad \text{(D.11)}$$

At their point of intersection both lines have the same y-position. Solving both line equations to their y-parameter and setting them as equal delivers an equation that defines the z-position of point **X**:

$$X_z = \frac{-C_z \cdot P_z \cdot (B_y - A_y)}{B_y \cdot C_z - (C_z \cdot P_y + P_z \cdot (A_y - C_y))} \qquad \text{(D.12)}$$

Knowing $\mathbf{X}_z$ the x- and y-positions of the points are available instantaneously since they are encoded in the x- and y-position of the corresponding pixels in the image. The y-position of point **X** in figure D.12 may be calculated by

$$X_y = -\frac{X_z \cdot (A_y - C_y) - A_y \cdot C_z}{C_z} \qquad \text{(D.13)}$$

Its x- position may be calculated analogously by

$$X_x = -\frac{X_z \cdot (A_x - C_x) - A_x \cdot C_z}{C_z} \qquad \text{(D.14)}$$

The above calculations result in a mesh where every grid point carries a set of three figures: the x- y- and z-position of a given surface point relative to the reference coordinate system. On this mesh the subsequent reconstruction of the ulcerated area is based.

D.5.3 Surface Reconstruction

The volume of an ulcer is the volume enclosed by the former healthy skin surface and the existing ulcer surface. The healthy skin surface is no longer existing and has therefore to be reconstructed.

Prior to reconstruction the system has to be informed which part of the measured skin surface belongs to the ulcer or is affected by it in a way that its shape differs from the original, healthy appearance. Figure PII.1 at the end of this chapter shows a blue line surrounding the ulcerated area. The line is drawn by the operator of the instrument using a mouse. To assist the line drawing an overlay of the extracted stripes is added to the picture of the ulcer. The overlay assists the detections of surface features such as swelling which indicate surface changes induced by the ulcer.

The area inside the yellow borderline is now considered to be ulcerated and has to be reconstructed. The reconstruction algorithm works in two stages. In the first stage the area is divided into cross sections. For each cross section a cubic spline is calculated representing the original surface. In the second stage the array of cross sections is passed through a median filter to create a smooth surface.

Figure D.13 shows a vertical cross section through the middle of the ulcer in figure PI.1. Measured and reconstructed surface enclose positive (for the cavity) and negative (for the swollen areas) volumes.

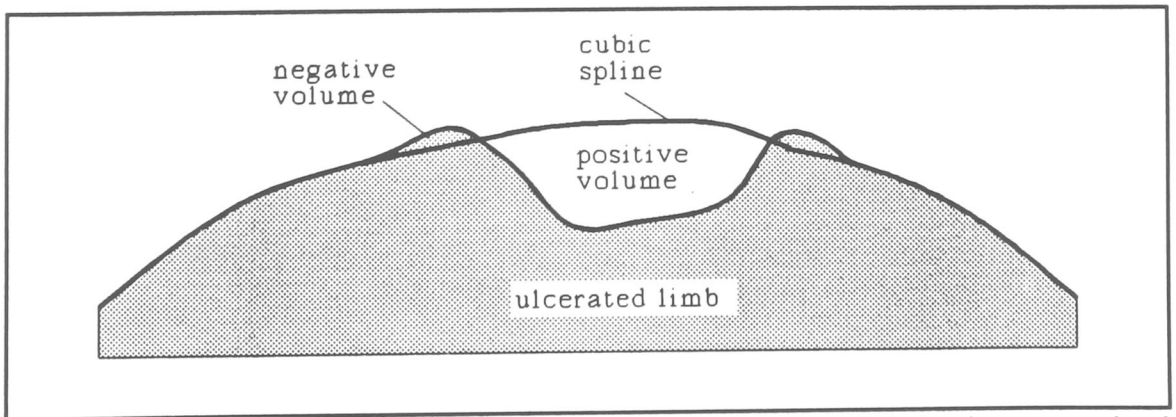

Figure D.13: A cross section out of the middle of the ulcer in figure PI.1 showing measured and reconstructed surface

D.5.4 Calculating Area and Volume of an Ulcer

All the necessary data for the final calculations is now available: a grid representation of the measured and the reconstructed surface and the information about the boundary of the ulcer which has already been defined for colour extraction (see section D.4.2).

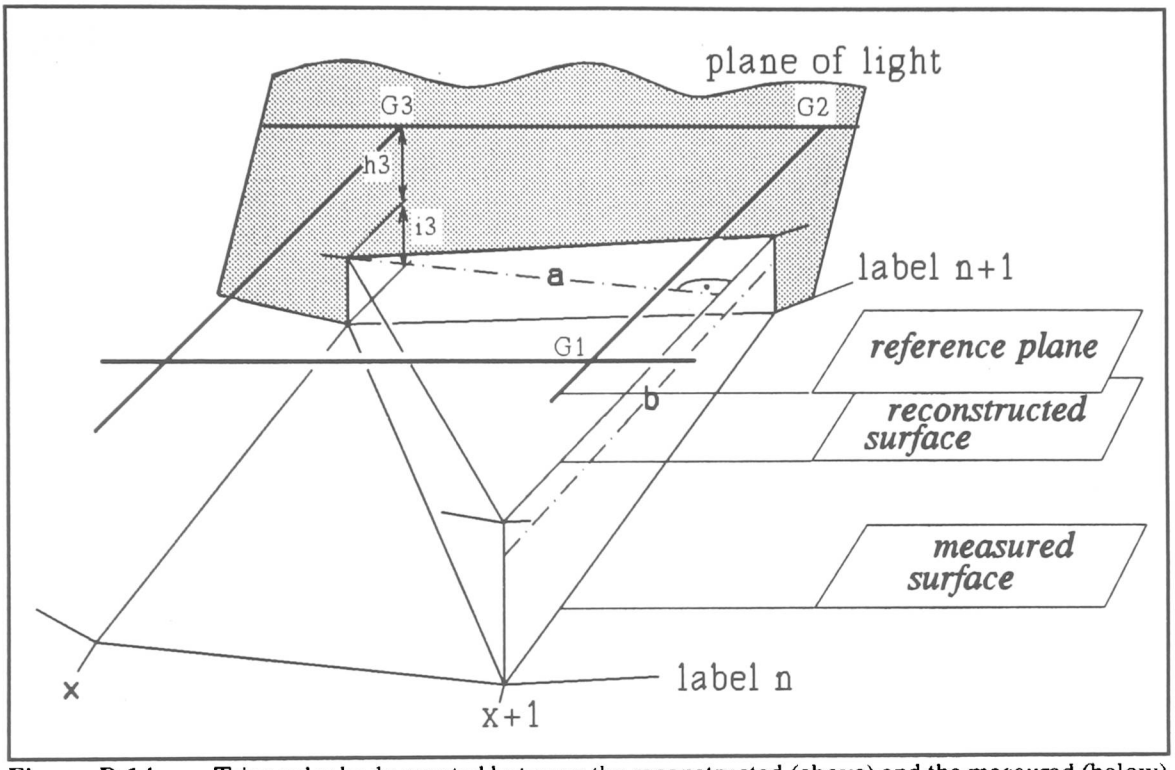

Figure D.14: Triangular body created between the reconstructed (above) and the measured (below) surface

For calculation the rectangular surface grid is subdivided into a mesh of triangles. Figure D.14 shows an extract from the grid somewhere within the ulcer.
If a triangle of the measured surface belongs to the ulcer its area **A** is calculated by:

$$A = \frac{a \cdot b}{2} \qquad \text{(D.15)}$$

where

$$a = \sqrt{(\overline{G3\ G2})^2 + (h3 - h2)^2} \qquad \text{(D.16)}$$

and

$$b = \sqrt{(\overline{G2\ G1})^2 + (h2 - h1)^2} \qquad \text{(D.17)}$$

with 6 pixelwidth being approximately 2 mm. **h1**, **h2** and **h3** are the distances of the respective triangle corner of the reconstructed surface to the reference plane.

The volume of the triangular body between the measured and the reconstructed surface is defined by

$$V = \frac{1}{3} \cdot A \cdot (i1 + i2 + i3) \qquad \text{(D.18)}$$

with **i1**, **i2** and **i3** being the height of the triangular body at the respective corners.

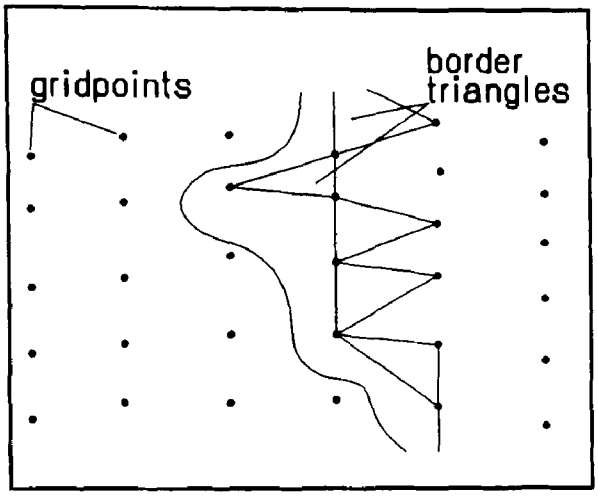

Figure D.15: Measurement triangles close to the border of the ulcerated area

If a triangle is located just inside the borderline of the ulcer and two or three of its corners are located on the outside of the border, its area and volume figures are multiplied by 1.5 to take the quantisation effect into account. Figure D.15 illustrates this. This multiplication sometimes results in too big and sometimes in too small values. On average the large number of borderline triangles produce approximately correct results.

All triangle areas and volumes are added up to the final figures. Figure PII.3 shows the final display.

D.6 Summary

This chapter described the underlying principles and methods of the measurement process which are implemented in computer programmes. Most of the procedures work with satisfying speed and accuracy and produce the expected results (colour extraction, low pass convolution, stripe thinning and labelling). Some procedures, especially the surface reconstruction and the volume calculation algorithm have potential for further development in order to increase their performance. In section H.2.3 some suggestions for changes in these algorithms are made.

The following chapter describes a series of experiments which are designed to assess both the performance of the two underlying algorithms of the instrument stripe extraction and surface reconstruction and the combined performance of the system. Experiences with measurements on patients are also included.

PLATE I: Image Capturing, Stripe Extraction and Labelling

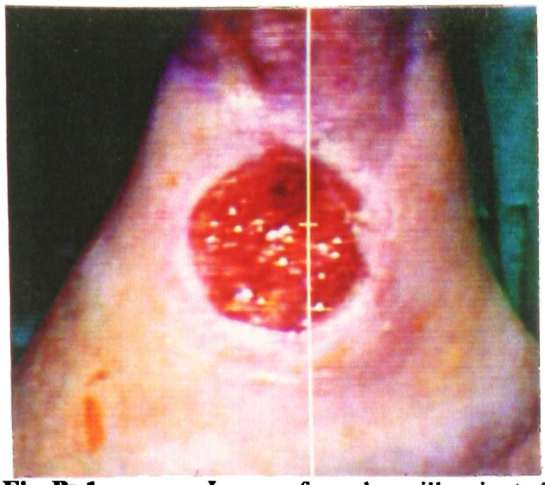

Fig PI.1: Image of an ulcer, illuminated by homogeneous white light

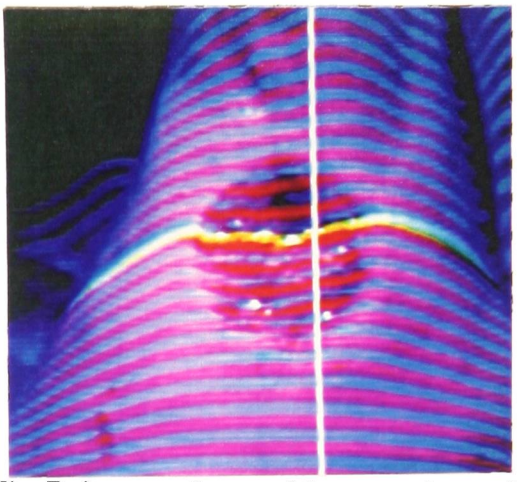

Fig. PI.2: Image of the same ulcer as in PI.1 with projected stripes.

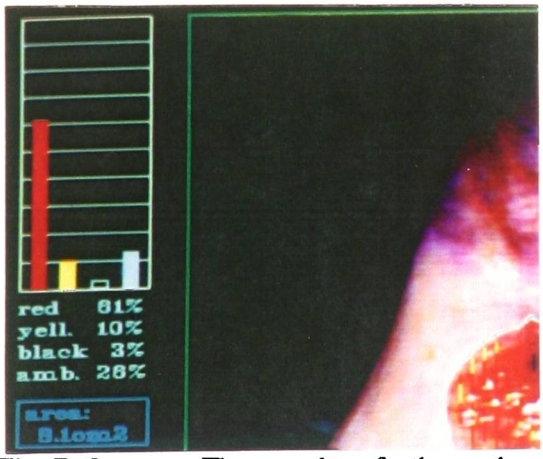

Fig. PI.3: The result of the colour extraction process

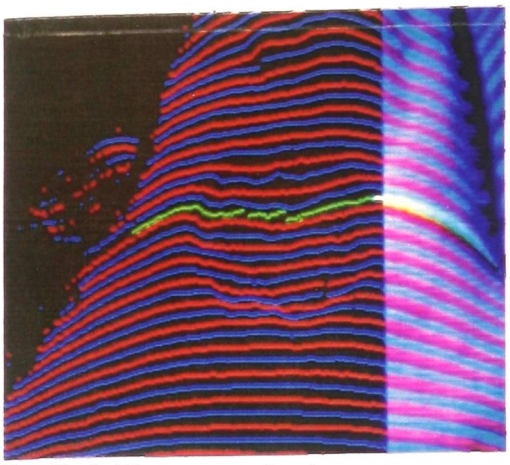

Fig. PI.4: The extracted stripe centres

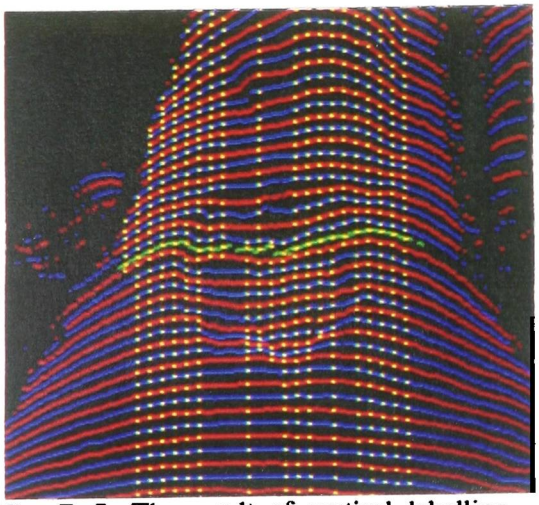

Fig. PI.5: The result of vertical labelling. Labelled points are marked by yellow dots.

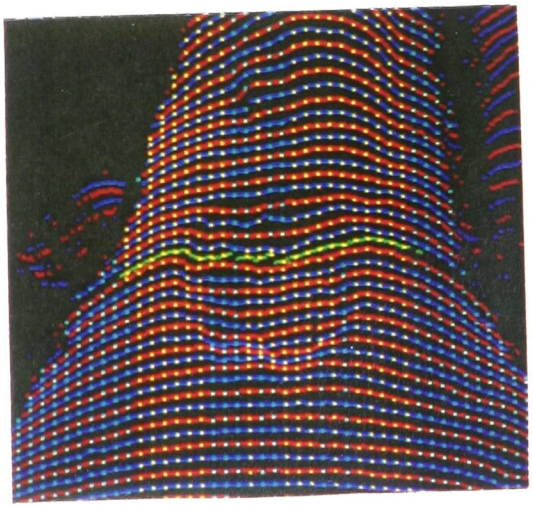

Fig. PI.6: The result of horizontal labelling. Labelled points are marked by blue dots.

PLATE II: Boundary Definitions and the Result of the Measurement

Fig.PII.1: The ulcerated area, marked blue

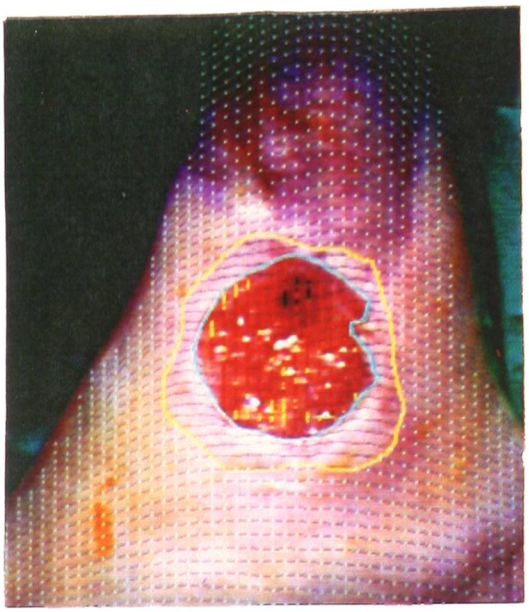

Fig PII.2: The area, affected by the ulcer, marked yellow. Extracted lines are superimposed onto the image area.

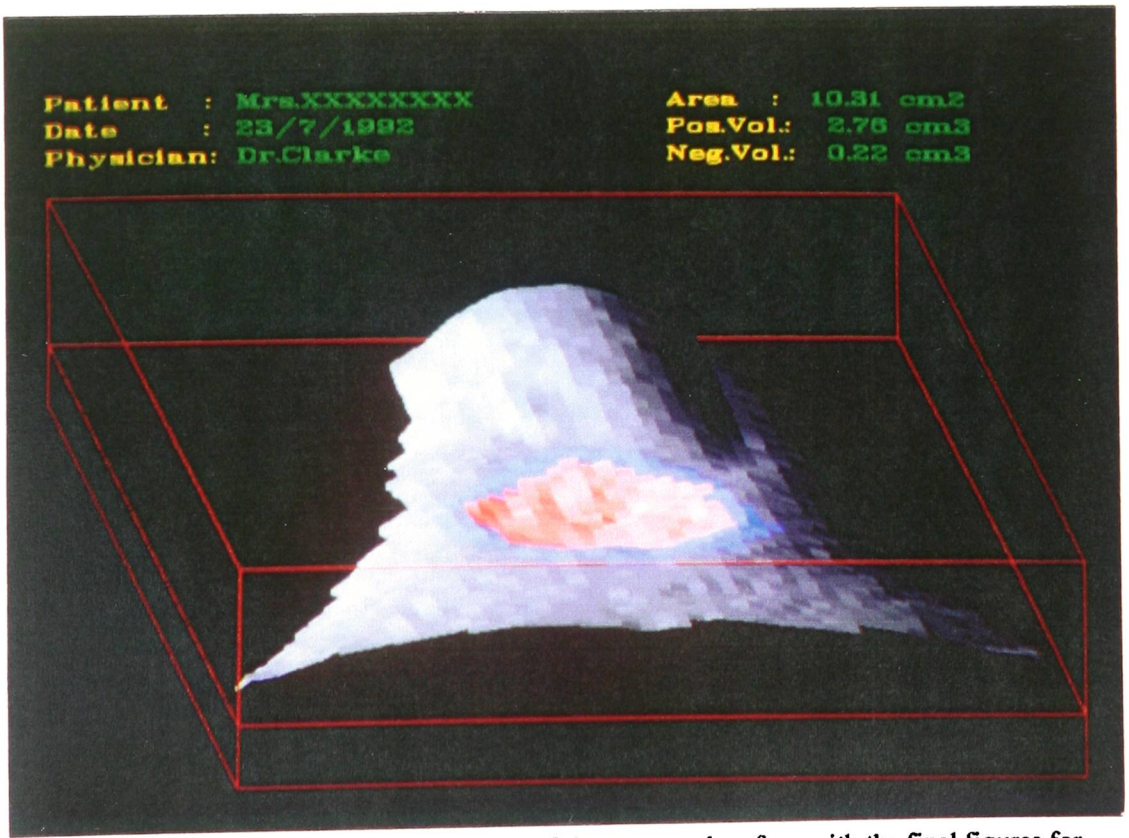

Figure PII.3: Graphical representation of the measured surface with the final figures for area and volume

E: Experiments

E.1 General

This chapter describes a series of three experiments which are designed to assess the capabilities of the two procedures for stripe extraction and surface reconstruction, and the combined performance of the instrument as a whole.

- The first experiment compares the performance of the instrument's core process, the new developed stripe extraction algorithm, with two established methods.
- In the second experiment three different approaches to reconstruct a surface are examined and their usefulness for virtual skin reconstruction is assessed.
- The last experiment of the series assesses the actual accuracy and precision of the instrument when measuring areas and volume of model ulcers to establish how the overall performance of the instrument depends on factors such as the size of a lesion and its area/volume ratio.

An additional section documents a series of measurements on a single patient over a period of some months.

In this chapter the results of the experiments are only considered in their local context. In the next chapter (F) the results are discussed within the framework of the entire instrument, taking error evaluations, crosswise dependencies and the nature of ulcers and pressure sores as objects of interest into account.

E.2 Comparison of Four Stripe Extraction Methods

The extraction of the centres of the projected stripes of light is of substantial importance for the performance of the instrument. Those stripe extraction processes which are in use in existing applications are mostly adaptations or variations of two well established methods: stripe extraction by a fixed threshold or by a rule controlled mechanism. In this section the performance of these conventional approaches is compared with the two new methods described in section D.4.3: the dynamic threshold and the colour channel subtraction method.

The fixed threshold method. Stripe extraction by a fixed threshold has the advantage of being very straightforward and easy to implement in a programme. It uses the assumption that every pixel with a grey level over a certain threshold belongs to a stripe. The method works fine on uniformly coloured and illuminated objects and due to its simplicity it is sometimes implemented in hardware.
The limitations of the fixed threshold method appear as soon as the object of interest is either not uniformly coloured or illuminated: only a fraction of the stripes may then be detected. Figure PIII.2[31] illustrates this on a real ulcer shown in figure PIII.1. Some segments of the stripes are not detected because their grey levels are always below the threshold, other sections have grey levels which are always situated above the threshold.
A severe disadvantage which is not instantaneously apparent is the inaccuracy in centre detection when using the fixed threshold method. If the surface of the object has varying reflectivity the centre of the stripe may have a low reflectivity and therefore may not correspond with the brightest part of the stripe. Inconsistent reflection distorts the stripe's appearance and hence corrupts the accurate detection of its centre. This is discussed in greater detail in F.2.2.4.

Rule based methods. A completely different approach to the stripe extraction problem is based on a set of rules defining the appearance of stripes of light. This approach normally works well on smooth, homogeneously reflecting surfaces where the appearance of a stripe of light may easily be predicted. With increasing complexity of the optical properties of the surface the set of rules have to become more and more sophisticated. Figure PIII.4 shows the result of an attempt for rule based stripe extraction. The algorithm used to produce the figure incorporates a total of eight rules defining distances between stripes and their shape (minimum and maximum width and grey levels). The rules are context sensitive, i.e. their parameters are not fixed but flexible within a certain bandwidth. Their value partly depends on past detections. The allowed distance between stripes, for instance, is always calculated from the already known distances between previous stripes.

---

31 The figures related to this experiment are reproduced on plate III at on page 106 at the end of this chapter

The method suffers from some disadvantages. Firstly, the calculation is more time consuming with every new rule which has been implemented. The more sophisticated the set of rules becomes in order to increase the sensitivity of the method, the more computation time is consumed.
Secondly, the interaction between the rules becomes increasingly difficult for the programmer to understand. The performance of the method increases until approximately eight to ten rules are implemented. More rules actually decrease the stripe detection capability of the algorithm.
A third disadvantage is (as before with the fixed threshold method) that varying surface reflectivity increases the inaccuracy in defining the centre of a stripe.

Due to the disadvantages of the two above methods a new approach to the problem was investigated for this work: the **dynamic threshold method**, which is described in section D.4.3.1. In contrast to the above methods the dynamic threshold method takes varying reflectivities on the object of interest into account. Compared with the above approaches it has two notable advantages: the sensitivity for stripe detection is higher and the centres of the stripes are detected with higher accuracy. An additional benefit is the speed of computation which is about the same as the fixed threshold method but faster than the rule based method. Figure PIII.3 shows stripe centres extracted by the dynamic threshold method. The extraction of blue and green stripes is satisfactory but for reasons already stated in D.4.3.1 red stripes often fail to be detected.

A further improvement to the dynamic threshold method is the **subtraction method** for the detection of red and blue stripes described in D.4.3.2. Even dim sections of the red stripes are now clearly detectable as can be seen in figure PIII.5. In F.2.2.4 it will be shown that the stripe's centres are also detected with high accuracy. Only under extreme conditions does the error in calculating the position of the stripe's centres reach its maximum of 1.5 pixels.
The results of the above experiments clearly prove the superiority of the two new developed methods over the conventional ones for the task of measuring a surface with unstable reflection and colour properties. The methods detect more stripes with higher accuracy and are fast to compute.

E.3 Experiments on Three Different Surface Reconstruction Methods

A virtual reconstruction method for ulcerated skin has to meet two requirements: it has to produce a surface which is very similar to the healthy skin that it simulates and it should to be tolerant against measurement errors. The following two experiments assess the performance of three common interpolation methods, cubic splines, polynomial- and Bezier interpolation in the light of these demands.
The first experiment estimates the error tolerance of the three methods if they are confronted with a set of surface points on a straight horizontal line. As a result of a assumed measurement error one point is located 0.1 mm above the line.
In figure E.1 the horizontal axis represents the straight line. The six points where the skin surface is measured are arranged in two sets of three points each. The first set is located at 0, 10 and 20 mm and the second set at 90, 100 and 110 mm, with a gap of 60 mm between the two sets. At location 20 mm one surface point is not situated on the straight line but is, due to an assumed error, elevated by 0.1 mm. Consequently every interpolation method produces a certain error in the gap between the two sets of measured surface points.

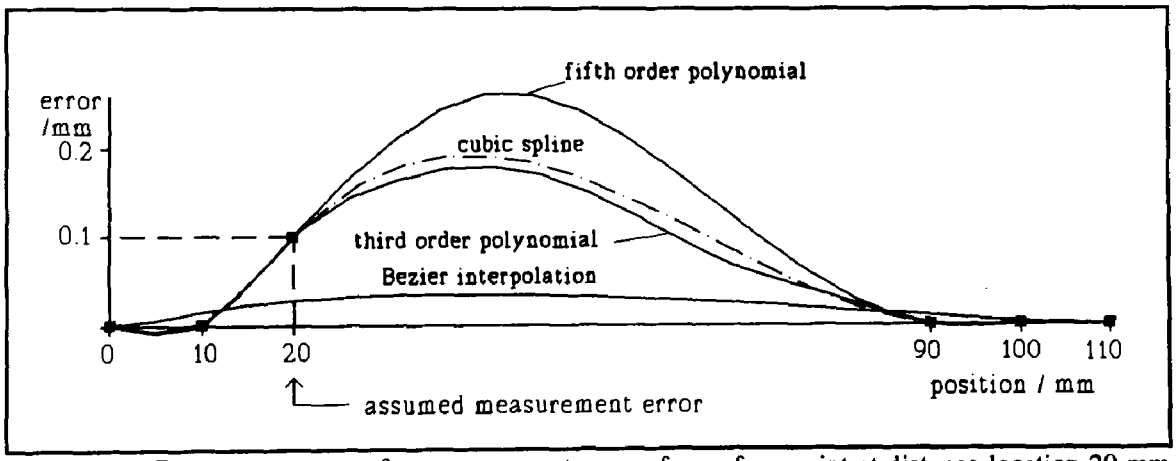

Figure E.1: The consequence of a measurement error of a surface point at distance location 20 mm on the performance of three different interpolation methods.

The worst result is obtained by the polynomial approximation of fifth order, followed by the cubic spline and the polynomial approximation of third order, which perform similarly. The best result is obtained by the Bezier interpolation which, in contrast to the other methods, does not force the interpolated line to pass through the measured points exactly but allows some variance. It is possible to programme polynomial and spline interpolations in order that they, like the Bezier interpolation, also perform a kind of curve fitting (e.g least square method, exponential weighting) in between measured points. This unfortunately causes severe disadvantages which are shown in the following experiment.

In this experiment the three interpolation methods are again used to close a gap of 7 cm between the two sets of measured surface points. This time it is assumed that the points are measured without errors and they are located on a circle of 6 cm radius simulating a skin ulcer of 7 cm diameter on a limb with 6 cm radius.

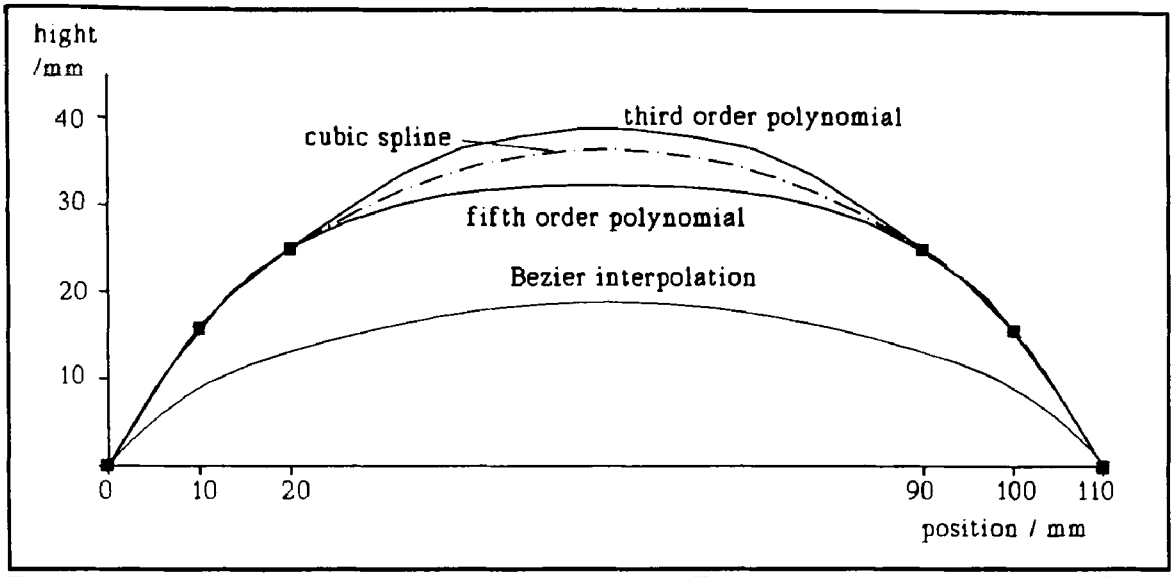

Figure E.2: Interpolation over a 6 cm gap by four different interpolation methods using 2 sets of data points on a circle at 0, 10 and 20 cm and at 90, 100 and 110 cm.

This time the cubic spline method performs best. It accurately follows the circle because a circle is a curve with minimised curvature, exactly the kind of curves a cubic spline generates. Both polynomial interpolations produce some error while this time the Bezier interpolation produces an error of about 2 cm! The same flexibility that is responsible for its error tolerance is now responsible for the poor reconstruction performance which disqualifies it for the task of virtual skin reconstruction. This is the reason why curve fitting methods which use approximated measurement points must not be part of any algorithm attempting to reconstruct skin over a wide gap.

In the preceding experiment the fifth order polynomial approximation show low error tolerance which disqualifies it. Polynomial interpolations of higher order perform even worse. With increasing order they develop a tendency to oscillate which makes them totally unsuitable for surface reconstruction.

The only remaining candidate is therefore the cubic spline interpolation since the cubic spline actually incorporates a third order polynomial (therefore: cubic) with the additional boundary condition that the first derivative is continuous at points where two polynomials are linked. Additionally it has the ability to produce a curve with minimised curvature. A model for this property is a plastic ruler which is fixed at the measurement positions. Its elasticity brings it into a shape which is identical to that of a cubic spline which interpolates between these positions.

E.4 Accuracy and Precision of Area and Volume Measurements

In the context of this work **accuracy** is defined as a measure of any bias in the measurement system. Accuracy is the difference between the mean of repeated measurements and the known real value. **Precision** is a measure for the scatter of single measurements around their mean. It is expressed as the standard deviation of the single measurements and is an assessment for the repeatability of the measurements. In the following experiments precision figures are given in percentages of the mean.

E.4.1 Area Measurements

The measurement of a given area by the instrument is influenced mainly by three factors: the exactness with which the operator can define the area, the quantisation of this area by the grid which describes the surface and the distance of the surface to the instrument.
For this experiment the influence of the operator and the fluctuations caused by grid quantisation may be eliminated by automatically defining an area of constant size and shape at always the same position. Consequently the remaining fluctuations are then caused exclusively by errors in the acquisition and calculation of the surface data. When measuring different areas at varying distances under this regime the accuracy (bias) of the instrument appears to be always less than ±2% of the total area while the precision (standard variation) is within ±0.5% of the total area.

If the experiment is repeated under more realistic conditions with an operator manually encircling rectangular chips of known area the outcome is different. The chips are placed at varying positions and distances from the instrument. In this experiment ten measurements are made for each setting. The results of the ten readings scatter with a certain standard deviation around a mean value. Figure E.3 is a plot of the standard deviation in percentages of the area's size as a function of both distance and area size.
The precision as a percentage increases as the area to be measured increases. Increasing the distance to the instrument also slightly increases the imprecision. The dotted plane in figure E.3 marks the region where measurements have a standard deviation of 5% of the total area. This precision can practically be guaranteed if the measured area is more than 9 cm^2 and less than 3 cm away from the instrument.

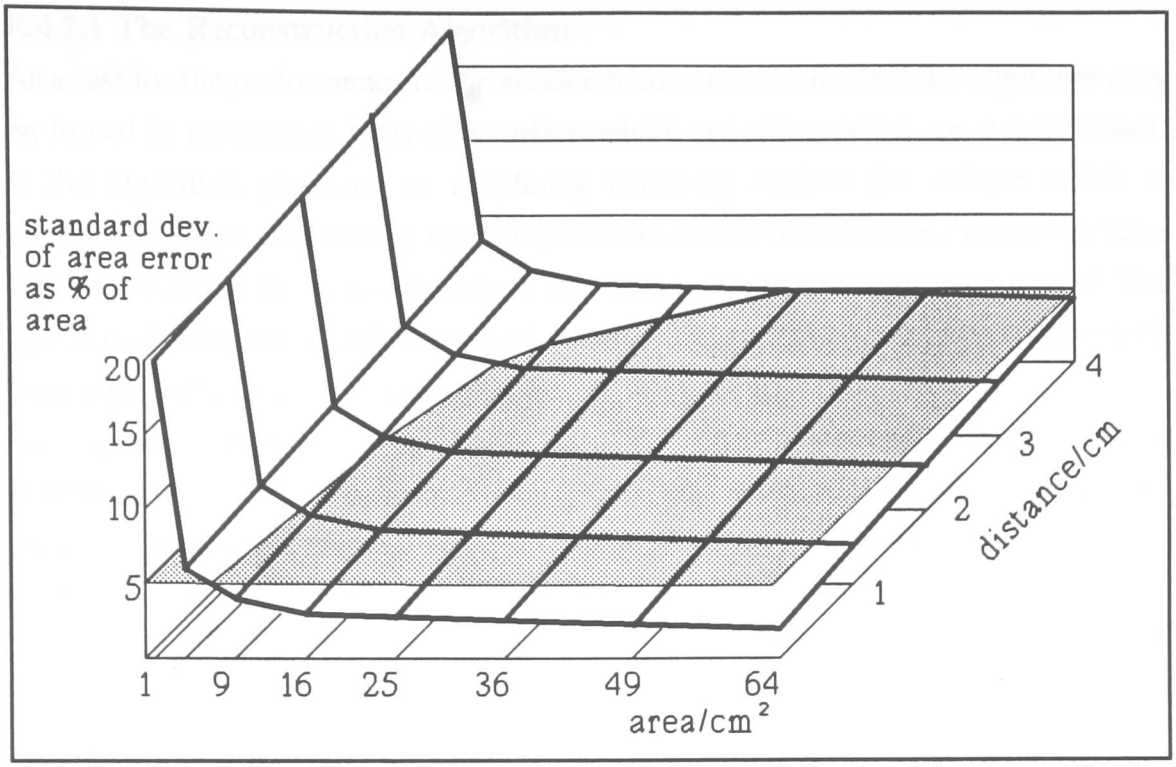

Figure E.3: Standard deviation of the error in area measurement as % of the area as a function of area and distance of the measured object from the instrument.

E.4.2 Volume Measurements

The exactness of volume measurements mainly depends on four factors: the operator defined boundary of the area to be reconstructed, quantisation of the measurement grid, the position calculations for the surface points in the measurement grid and the ability of the reconstruction algorithm to produce a correct surface which is identical to the original. In F.2.4.2 it is shown that the boundary and quantisation errors are small compared with the errors introduced by surface reconstruction and surface measurement.

The volume of a skin ulcer is enclosed by two surfaces: the existing ulcerated surface and the former healthy surface. The instrument obtains the two surfaces by two different methods: The ulcerated surface is directly measured while the former healthy surface is reconstructed. In a first experiment the performance of the reconstruction method is assessed. A second experiment finally shows the overall accuracy and precision of the volume measurement process.

E.4.2.1 The Reconstruction Algorithm

As a test for the performance of the surface reconstruction method the algorithm may be forced to reconstruct parts of a surface which are still existing, i.e. not ulcerated. If the algorithm produces an absolutely matching surface the volume which is enclosed between the actually measured and the reconstructed surface should be zero. Figure E.4 shows the result of such an experiment where a straight plate is used. The figure is obtained by marking areas of varying sizes on the plate and measuring each area repeatedly from varying distances.

The accuracy appears to be greater than 98%: some measurements result in a positive, some in a negative volume, but the mean of a greater number of measurements tends towards zero. A residual offset adds less than 2% on the mean of the measurements. Single measurements, nevertheless fluctuate around the mean. This fluctuation error is a measure for the precision or repeatability of the reconstruction. In figure E.4 the standard deviation of the reconstruction error as a percentage of hypothetical volumes is plotted as a function of the size of the surface area to be reconstructed and the quantity of the hypothetical volumes.

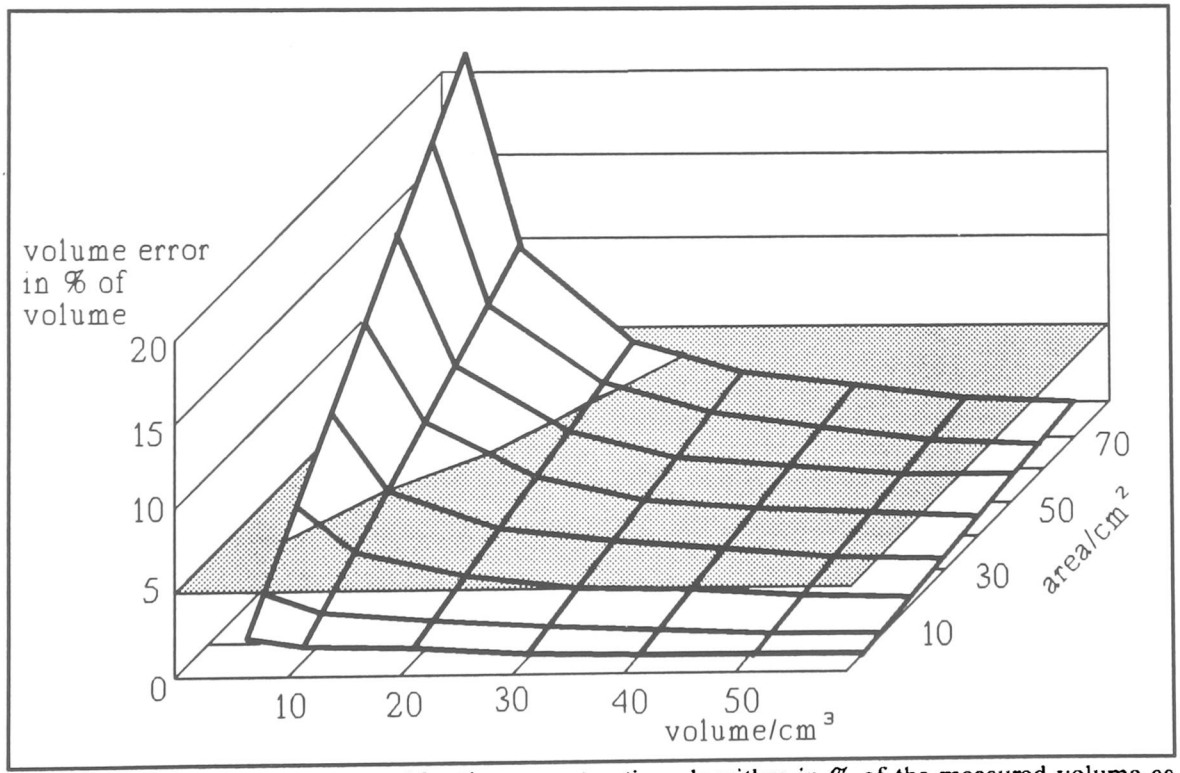

Figure E.4: The error caused by the reconstruction algorithm in % of the measured volume as a function of area and volume of the measured object

If large areas are to be reconstructed the error increases since the cubic splines may fluctuate more freely between widely separated measurement points. For a given area the mean volume error, caused by the reconstruction process, is constant. If this constant error is related to some hypothetical volumes its relative percentage is, of course bigger with smaller volumes than with larger ones.

The experiment may be repeated with other (curved) surfaces but the outcome is the same. Test surfaces which have an irregular feature, i.e. a cavity or elevation that distorts the expected shape of the surface, within the area to be reconstructed, produce the same result as above but with a certain accuracy offset that depends on the volume of the irregular feature. Since human skin normally has only small irregular elevations of significant size (e.g. wrinkles or warts) this effect may be ignored.
The reconstruction error slightly increases with the size of the area to reconstruct. Increasing the distance of the area from the instrument produces a greater error. This is caused by the trigonometrical calculation of surface point positions. The further the distance of the object to the instrument the greater the influence of errors on the result of the calculation.

This experiment gives an assessment of the error produced by the reconstruction method at the upper border of the volume to measure. In the following experiment the complete volumes are measured.

E.4.2.2 Volume Measurements

Figure E.5 shows the precision of the instrument when measuring volumes. Fifteen models of skin ulcers with varying known areas and volumes are measured at a fixed distance of 3 cm. Each model is measured ten times. The standard deviation of the ten volume measurements as a percentage of the volume are plotted as a function of area and volume of the model.
The dotted plane in figure E.5 marks a level where the standard deviation is 5% of the measured volume. The high peak breaking through this plane indicates that the volume of shallow wounds with an volume/area ratio smaller than approximately 0.4 (i.e. wounds which are less than 0.4 cm deep on average) can not be measured with sufficient precision.

The underlying shape of the plot is generated by the reconstruction algorithm which makes the plots in figure E.4 and E.5 very similar. Additional errors in figure E.5 are caused by faults in the measurement of the surface points.

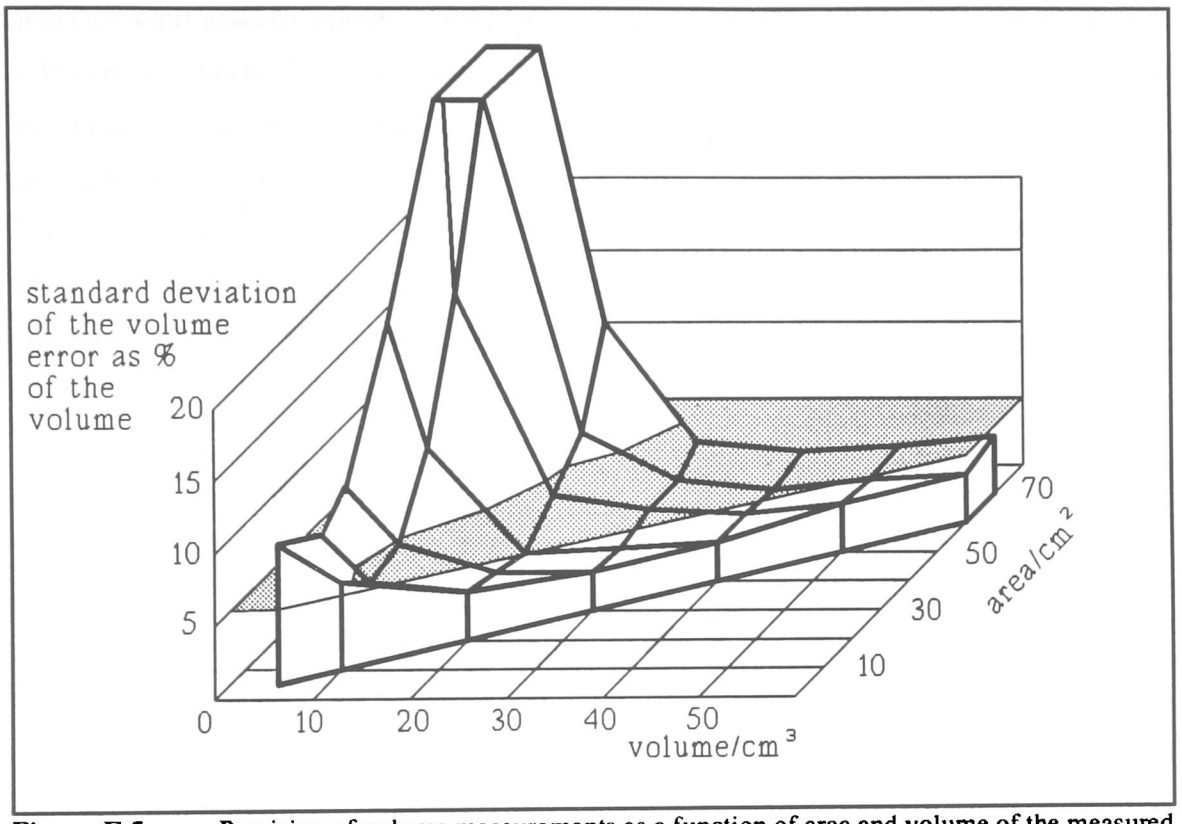

Figure E.5: Precision of volume measurements as a function of area and volume of the measured object.

Apart from the errors, the graph in figure E.5 reveals some limitations of the instrument. Ulcers with an area/volume ratio of less than 1 can not be measured because the slopes of the wound become too steep. Wounds bigger than 70 cm^2 occupy so much area that too little healthy surface is available in the instrument's field of view for a successful surface reconstruction attempt.

The mean of the measurement readings for the volumes is always approximately 3% higher than the real volume of the models. This is partly caused by the accuracy of the area measurement where the results are approximately 2% higher (see E.4.1). Area values are also used for volume calculations. The rest is contributed by an offset in the volume measurement itself.

When a volume is measured by different operators the accuracy changes slightly. When the experiment is repeated with an other operator under otherwise unchanged conditions a different but relatively constant offset is the result. This may be explained by the different ways an operator defines the area to be reconstructed. An operator who always draws a more generous boundary around the ulcerated surface is bound to obtain different results from one who tries to draw the line as close to the ulcer as possible. In order to gain more accurate results the instrument should therefore be calibrated to its operator before the measurement.

The precision of the measurements is also affected by this 'human factor'. Measurements with three different operators on one model resulted in differences in precision of 2% between them whereas the same operator produces results varying approximately 1%.

E.5 Measurements on a Patient

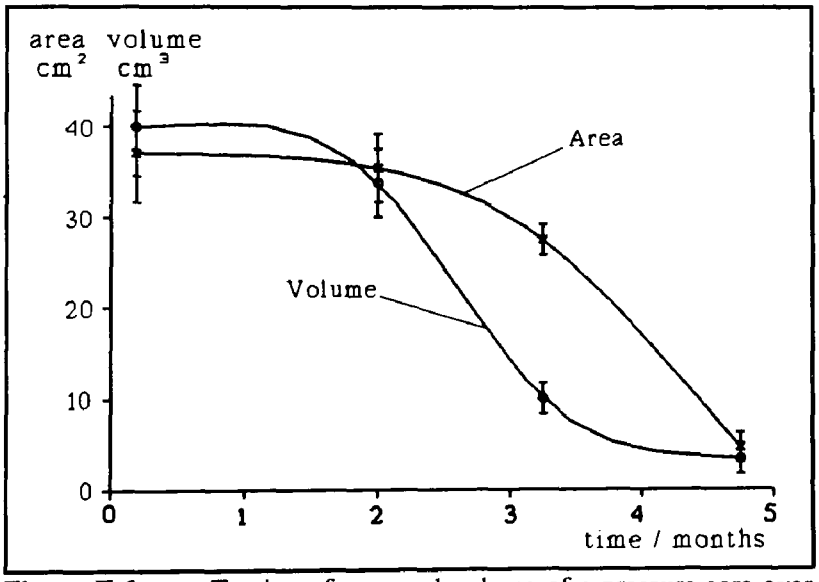

Figure E.6: Tracing of area and volume of a pressure sore over a period of five months

Figure E.6 shows the tracing of area and volume of a patient's pressure sore (located at the buttocks) over a period of 6 months. This example confirms an assumption of some physicians that skin ulcers tend to heal first at their base and decrease in volume before the area shrinks significantly. This isolated single tracing is, of course, not in itself proof of that theory.

Note that the first two measurements have a higher level of uncertainty since they are made with a previous version of both measurement sensor and software where the percentage of error is much higher.

PLATE III: Comparison between four different stripe extraction methods

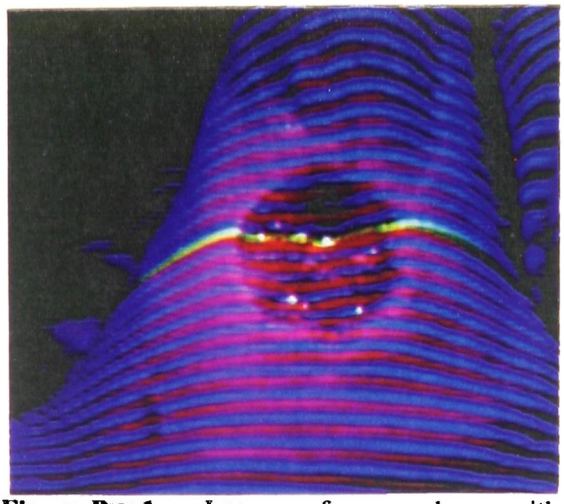

Figure PIII.1: Image of an ulcer with projected stripes to be extracted

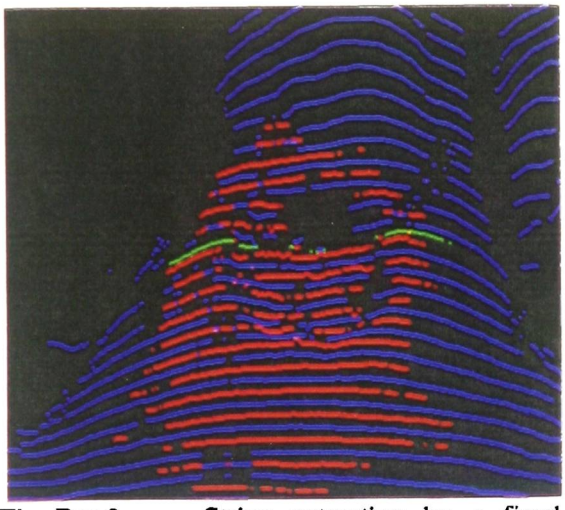

Fig. PIII.2: Stripe extraction by a fixed threshold

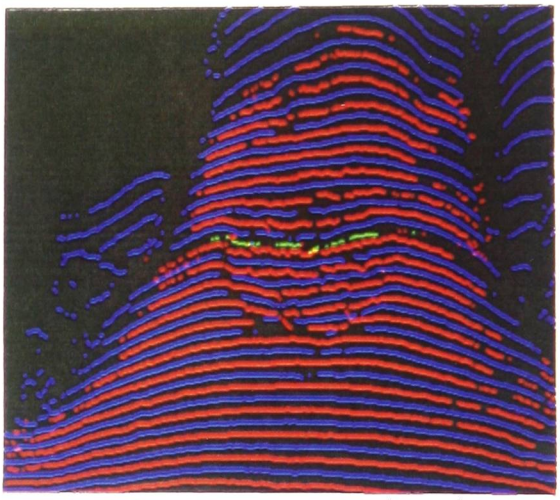

Fig. PIII.3: Stripe extraction by a dynamic threshold

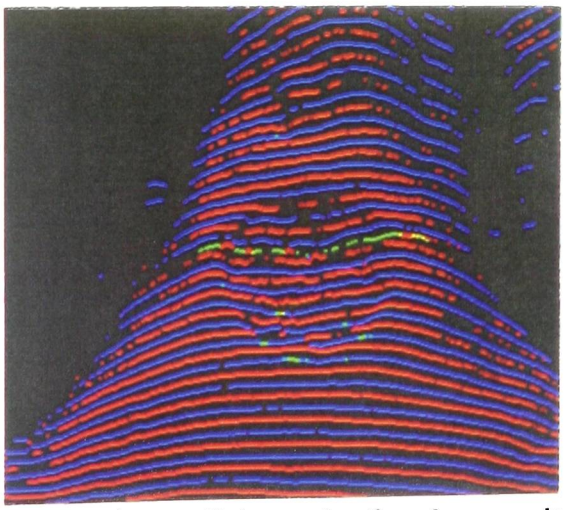

Fig. PIII.4: Stripe extraction by a rule based algorithm

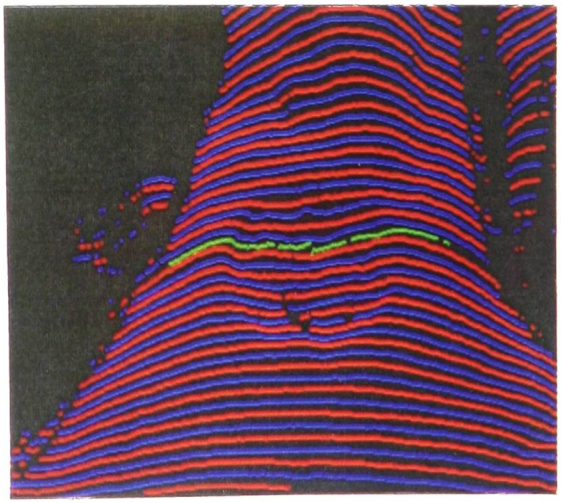

Fig. PIII.5: Stripe extraction by the subtraction method

F: Error Analysis

To understand the experimental results of the instrument's overall performance it is necessary to take a closer look at the underlying factors that influence the results. Based on a comprehensive understanding of these factors, strengths and weaknesses of the structured light method in general, and consequently of the instrument in particular may be estimated. Apart from that this analysis is a general assessment of errors for any instrument based on the same principle such as the one described in this work. The analysis is divided into two sections:

- In section F.1 the five main groups of error sources are examined. These are: mechanical, optical and electronic errors and errors which are caused by certain properties of ulcers, sores and the skin. An additional source for errors is the human operator whose interaction with the system also influences the outcome of the measurements.
- In section F.2 the influence of these errors on programming algorithms and the accuracy of the instrument is discussed. The significance of environmental factors, especially the human skin as the object of interest is analysed.

F.1 Error Sources

The measurement system is a combination of mechanical, optical and electronic components which all contribute a certain amount of error to the measurement process. With some additional errors, mainly caused by the user of the system and the ulcerated skin as the object of interest, there is a total of five main error groups which affect the instrument's precision.

- Errors introduced by imprecisions of mechanical components of the instrument
- Errors caused by optical components
- Errors caused by electronic components in the camera and in the frame grabber card
- Errors caused by the human skin
- Errors introduced by the operator of the system

The sources of these errors together with their consequences and potential ways to counteract their influences are discussed in the following sections.

F.1.1 Errors Caused by Mechanical Imprecisions

Mechanical imprecisions of the instrument give raise to systematic and statistical errors.

For example, systematic errors originate from the inaccurate determination of the exact positions of camera, projector, filters, lenses and mirrors in the sensor and faults in the components themselves.

Statistically distributed mechanical errors are mainly caused by the imprecision of the slide changing mechanism. The error is small: experimental results show that the pattern may be projected with always less than 0.035 mm aberration in y- and 0.06 mm in x-direction.[32] The error in y-direction is equivalent to 0.15 (standard deviation 0.1) pixel width.

Since the stripes run in x-direction a displacement of a stripe in this direction does not influence the accuracy of range finding. It just causes the stripes to be shifted laterally.

Mechanical errors influence the COS algorithm and the calculation of area and volume of an ulcer in different ways. This will be discussed in the sections F.2.4.1 and F.2.5.1 respectively.

F.1.2 Optical Errors

Optical errors may be grouped into two main sections: lens errors and errors due to the circumstances under which the instrument is used. Lens errors subdivide into chromatic and monochromatic errors (or aberrations) whereas errors due to the circumstance under which the instrument is used may be subdivided into errors caused by the user (over- or underexposure, defocusing) and errors caused by the environment (reflections, background lighting).

In section B.3.3.1 the cause and the consequences of **monochromatic aberrations** are discussed. The camera lens in use with the equipment shows positive (barrel-) distortion. Experiments with the camera show that the distortion causes a shift of approximately 7 pixel width in those pixel which are located in the corners of the field of view where the distortion is worst. In section D.5.1 a correction equation for this error is developed which reduces the error down to less than 1 pixel width.

---

[32] A tiny white spot was projected onto a surface at 10 metres distance several times using the slide changing mechanism of the stripe projector. Its position was marked. From the values for aberrations at 10 metres distance the aberrations for the average distance from the projectors' focal point of 57 cm were calculated. This method rather than spot detection via image processing was chosen to exclude errors which are introduced by other parts of the system.

As already discussed in B.3.3.2 **chromatic aberrations** cause errors in all lenses. Fortunately it is possible to assess the amount of chromatic aberrations quite easily by trying to detect the position of a white spot in an image. The position of the spot is detected differently in each colour channel. An experiment[33] testing the lens in use with the system showed that in the corners of the image (where chromatic aberration is worst) the spot was detected at positions varying less than 0.5 pixel widths between the red and the blue channel of the camera. Within a circular field with a diameter of half of the image's height the aberration was less than 0.15 pixel widths, which is less than the present position resolution of the instrument. This error is significantly less than faults which are discussed later and are introduced by other sources. The compensation of chromatic aberrations is possible by following image processing but due to the insignificance of the effect for this work it is subsequently ignored.

F.1.2.1 Errors of the Projector Lens

All the optical errors mentioned above for the camera's lens also appear in the projector's lens system. The situation is even more complicated there because the projector houses additional collimator lenses and a reflector.

Fortunately it is one of the major advantages of the structured light method that it virtually eliminates the influence of optical errors in the projector. As long as the same errors occur while producing the reference pattern and while making a measurement it is neither important if the stripe pattern is projected absolutely horizontal nor if there are distortions caused by the projectors lens. It is not even necessary that the stripes are absolutely parallel or straight. They may also be slightly blurred or show inconstant colours.

The only error may arise by imprecise determination of the position of the focal point of the projector relative to the camera's focal point. This will be discussed later in F.2.5.1.

---

[33] In the experiment a tiny white spot of light is projected onto a diffusely reflecting surface. The position of the spot is detected for the three camera channels by the COS-algorithm described in D.4.3. The experiment takes various disturbing effects, which are discussed later in chapter F.2, into account in order to eliminate influences of noise, camera movement and surface reflectivity.

F.1.2.2 Channel Crosstalk of Stripe Colours

The separation of the three stripe colours in use is important for both stripe detection and the process of finding the centre of a stripe. Figure D.3 in section D.3 shows the effect. Colour crosstalk is caused by the colour filtering properties of the slide and the CCD array. Both colour filters are relatively broad banded and partly overlap. As a result a stripe of a certain colour causes an output in all three channels of the camera. The result is similar to but much stronger than the electronic channel crosstalk which will be examined later in F.1.3.2.

For stripe detection the colour crosstalk effect does not pose a problem. The spectrum of different stripe colours do partly overlap but the difference is always significant enough to distinguish the colours.

The detection of the centres of the stripes in contrast may be strongly affected by the colour crosstalk. If two neighbouring stripes of different colours are so close together that they partly overlap then the brightness (grey level) data from one stripe partly add onto the data from the other one and vice versa. As a result the representation of the stripes in the respective colour channels is corrupted where the two stripes overlap. The algorithm that extracts the centres of the stripes by calculation of their centroids will therefore shift the positions of the stripe centres towards each other.

Unfortunately it is not possible to correct this error by image processing mainly because the accurate absorption and reflectance spectra of a given surface point can not be evaluated. On a uniformly coloured surface compensation would be possible because the colour crosstalk in a given channel is always a constant percentage of another colour channel.

This is the main reason why only three colours are in use with the measurement system and two different extraction methods for the stripes centres are used. Due to this method the errors which are caused by colour crosstalk are minimised. In F.2.2.2 the amount of error will be analysed.

F.1.2.3 Errors Caused by the User

There is little chance for the user to endanger the accuracy of the instrument by wrong adjustment of focus or aperture of the optical systems. A wrong aperture causes the captured image to be either too dark or too bright. If the picture is too dark too few stripes will be detected and the measurement attempt fails. If it is too bright this is detected automatically by the instrument and a warning is given. Defocusing projector and/or the camera causes the stripe pattern to blur. It will be shown later that as long as the stripes stay bright enough to be detected no error will be introduced. If they can not be detected the measurement attempt again fails.

The wrong choice of the lighting conditions in the place where measurement are taken has a similar effect. If the background light is too bright, the contrast of the projected stripes decreases and they may no longer be detected. Again, the measurement fails.

Table F.1 summarises the errors caused by optical effects.

Error	Effect	Influence on *					order of magnitude	compen-sation
		DET	COS	COL	REC	CAL		
distortion & field curvature	displacement of pixels (espec. in corners)				✓	✓	up to 7 pixel widths	possible, necessary
other monochromatic aberration	degrading of image quality			✓			small	not necessary
chromatic aberrations	stripe displacement, colour shift			✓	✓		less than 0.5 pixel width	possible, not necess.
colour crosstalk	overlapping of stripe information	✓					up to 20% crosstalk	impossible
defocusing	blurred image / stripes	✓	✓	✓			may inhibit measurement	better adjustment
background lighting	low contrast of stripes		✓	✓			may inhibit measurement	darker place

* DET=Stripe detection, COS=COS-algorithm, COL=Colour extraction, REC=Surface reconstruction, CAL=Calculation

Table F.1: Errors, caused by optical effects

F.1.3 Errors Introduced by Electronic Components

The schematic in figure F.1 shows the flow of image information from the object to the frame grabber card. The information is subject to a variety of conversions and errors and is influenced by noise.

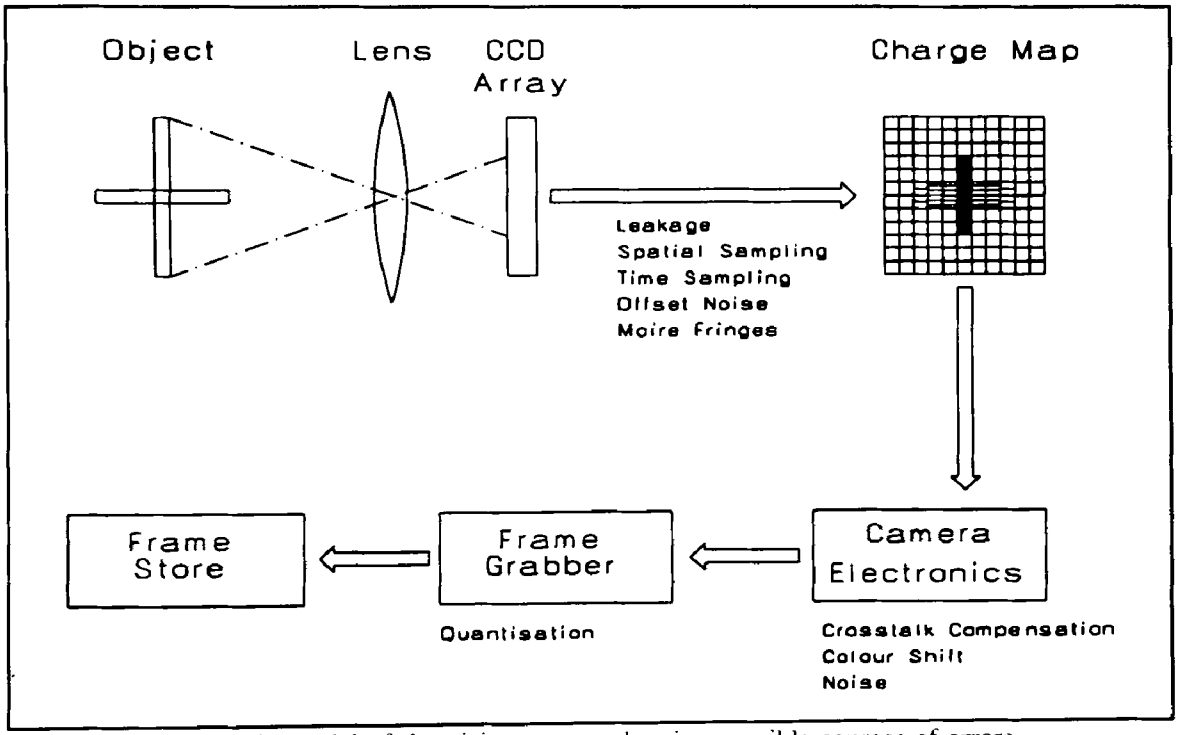

Figure F.1: Schematic model of the vision system showing possible sources of errors

The following three subsections analyses the three main processing blocks: CCD array, camera electronics and frame grabber electronics.

It is possible to describe some parts of the model in figure F.1 mathematically [132] (p.10&11). This is not considered to be worthwhile since most of the parameters needed can not be obtained without time consuming measurements using specialised equipment. Little may be learned from such an analysis because the combined rather than the isolated performance of each component is of importance. The combined performance may be obtained with relative ease and it will be shown in the following that for the given task of ulcer measurement, mainly one figure, the standard deviation of the noise of pixel grey values, is simulating most of the performance of the whole electronics perfectly.

In contrast to the lengthy and complicated experiments necessary to obtain data for each single component in order to find the parameters for a mathematical model, the standard deviation of the grey level noise of a pixel may be obtained by one simple experiment. It is an excellent means to predict most of the performance of the electronic circuits of the instrument.
The standard deviation is a valid measure only if the nature of the processes it summarises is exclusively influenced by randomly distributed effects. In order to validate this assumption and to find the cause of some other subordinate effects the following subsections examine the three main electronic modules of the instrument: CCD imager array, camera electronics and the frame grabber card.

F.1.3.1 Errors Caused by the CCD-Array

According to the manufacturer's datasheet the CCD array in use has a linear response to illuminance. The charge of electrons in each pixel of the array is directly proportional to the illuminance. Nevertheless there are five main errors that influence this ideal linearity:

- spatial sampling
- time sampling
- leakage
- Moiré effects
- offset noise

Errors in the geometry of the sensor such as displacements of pixel cells are found in the magnitude of micrometres. According to the manufacturer's datasheet the absolute displacement of a pixel is never greater than a tenth of the pixel's size. The error introduced by the camera's lens is some orders of magnitude greater. Errors up to 7 pixel width may occur. Pixel displacement on the CCD array is therefore ignored.

- The pixel cells are extremely small but do still have a finite size. One pixel therefore spatially samples light from an area of certain size on the observed object. If the object has features which are smaller than the size of one pixel when being projected onto the array, sampling leads to aliasing of the image information. The effect of sampling is visualised in figure F.1 by varying density of hatching of the charge map.

- The exposure of the CCD array takes a finite time. If the object moves during the exposure, time sampling produces a smeared image. Time sampling poses a problem for fast moving objects only as the CCD array in use has an exposure time of 1/60 second. For the given task of ulcer measurement it is irrelevant.

- In spite of the pixel cells being electrically insulated from each other a certain leakage of electrons into neighbouring pixels occurs. As pixels of different colour channels are neighbours (see C.2.2, figure C.3) channel crosstalk occurs. This leads to a shift in the true colour ratios.

- After the fixed exposure time the CCD array is read out. The readout process shifts the charges from pixel to pixel through the array. In some CCD arrays smear may occur due to exposure to light during shifting. The interline transfer imager in use does not show this effect because the charge of each pixel is first shifted to a neighbouring row of identical but aluminium covered pixels. This row is then read out and due to the opaque aluminium no exposure of these pixels can occur.

  The aluminium covered pixels form a grid of parallel stripes on the CCD array. Any picture with high frequency information (another grid, for example) will therefore be disturbed by Moiré fringes. Since the projected stripes do not occur with high frequency and due to their orientation (the aluminium grid runs vertically, the stripes horizontally) the Moiré effect does appear.

- The readout process nevertheless produces some noise during the shifting process. Sometimes the charge of one pixel is less than 100 electrons. When this charge is being shifted through the array, such a small packet of electrons may easily lose or gain a few electrons giving raise to a certain amount of offset noise.

F.1.3.2 Errors Caused by the Camera Electronics

The camera electronics amplifies the readout from the CCD-array and converts it into a TV signal. It produces three main errors:

- colour shift
- electronic channel crosstalk
- amplification noise

- The gamma adjustment circuit that enhances the camera's dynamic range for darker areas of a scene creates shifts in the colour balance. Correct colour balance, which describes the ratio between the colour channels, is achievable only for a certain illumination of the scene. Figure F.2 shows the effect: a given point with a colour ratio R:G:B of 1:3:5 is observed by the camera. The camera's gamma circuit produces an output of 0.33 : 0.62 : 0.78 (or 1 : 1.9 : 2.3 normalised).

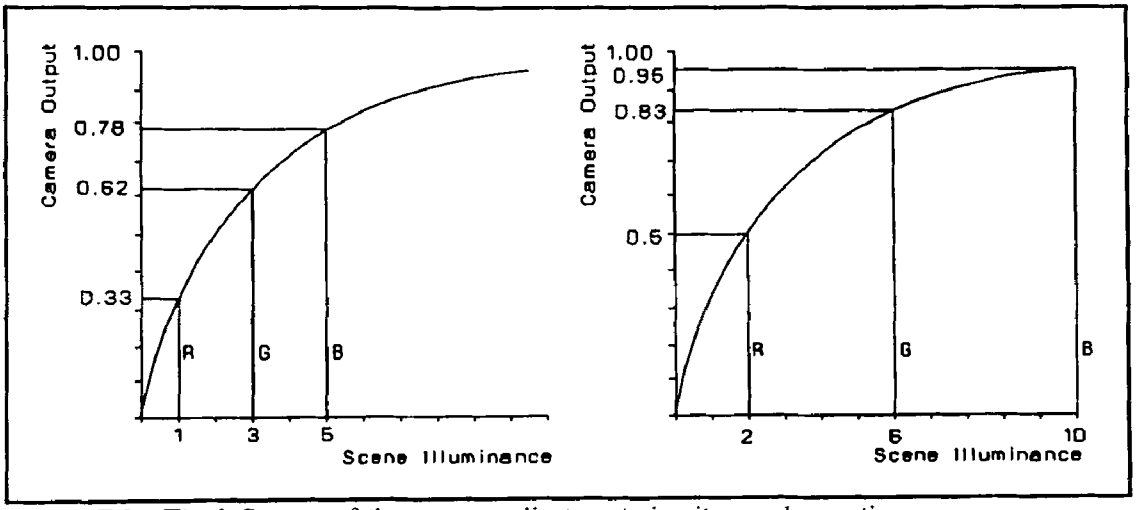

Figure F.2: The influence of the gamma adjustment circuit on colour ratio.

Now the illumination is doubled. The input values still have the same ratio 1:3:5, but due to the gamma curve the output ratio changes to 0.5 : 0.88 : 0.95 (or 1 : 1.8 : 1.9 normalised).This effect does not pose a problem to image processing, provided the gamma curve is known. The original input illumination may be calculated using a gamma correction curve.

The effect is a problem only if a monitor, used for displaying the image, has a gamma correction characteristic different from that of the camera. An object then changes its colour with varying level of illumination. Therefore all images have to be taken by the system under the same lighting conditions, a constraint which is met by the design of the system. With its built-in light source, which is much brighter than normal ambient lighting, repeatable illumination conditions may be achieved.

Otherwise, an objective comparison between a series of pictures in a clinical trial is impossible as, for example, an ulcerated area might appear too red in one picture, giving the impression of being highly inflamed, whilst another appears pale and less inflamed.

If necessary this problem may also be minimised by choosing a camera and monitor without a gamma correction factor. But this would result in less dynamic range for illumination and would make stripe detection more difficult.

A better solution would be to find a monitor with the same gamma characteristic as the camera. If this is not achievable an output look-up-table may be programmed to achieve colour stability. This table has to be re-programmed (or may already exist in a data file) if another camera or monitor is used.

- Additionally the camera in use appears to have a compensation circuit for the electronic channel crosstalk effect caused by leakage between pixel cells in the CCD array. The compensation circuit, however, seems to be a bit over-efficient as the opposite effect can be observed: around an intensely green object on a grey background, for example, pixels surrounding the green object have slightly smaller grey levels (approximately 5%) than those located at some distance. As sharp contrasts like this do not appear on ulcerated skin and due to the insignificance of the effect it is ignored in the following. Compared with the colour crosstalk effect mentioned earlier in F.1.2.2 the electronic channel crosstalk effect is negligible.

- Electronic noise caused at semiconductor barriers, by electromagnetic interference or thermal electron movements, is added by the all component of the circuits in use. Figure C.4 in C.2.2 shows the varying sensitivities of the CCD array for different colours. The camera's electronics have to balance this by amplifying the three colour channels accordingly to simulate the colour response of the human eye. Noise that was added before this amplification is also amplified. This is one of the reasons why the three colour channels show different noise levels.

  Some (negligible) noise is also added by the cable carrying the camera's signals to the frame grabber.

Factors such as temperature and electromagnetic interference may influence the amount of noise of a pixel[34], but under normal circumstances (i.e. room temperature and no interfering equipment around) these factors may be ignored. To detect the amount of noise that is superimposed on a brightness measurement the following simple experiment can be designed.

The CCD camera takes many frames from a scene under stable, unchanged lighting conditions. The output of a particular pixel is stored in the computer (This output is related to a frame grabber pixel (which is not identical to a camera pixel. See chapter C.2). Based on the nature of electronic noise and the fact that the quantisation errors of the frame grabber card are normally distributed, it is assumed (and may be shown by experiments) that the noise which is superimposed on the pixel is normally distributed thermal noise. Standard deviation therefore is an adequate measure for it.

CHANNEL	STANDARD DEVIATION	
RED	0.5	pixel brightness units (0-31)
GREEN	0.25	
BLUE	0.7	

Table F.2: Standard deviation for the three colour channels

Table F.2 shows the results of an experiment on the standard deviation for brightness values of the three camera channels. The experiment may be repeated for different pixels and under different lighting conditions but the results will always be close to those in table F.2. The standard deviations for the three channels are not equal. The green channel shows least noise. This is a consequence of the fact that the green channel has twice as many CCD-array pixels as the red and the blue channel. As the camera's output is produced by a sampling process of the camera electronics, twice as many green CCD-array pixels are available to produce the green output as red and blue ones. Varying noise in the camera's electronic circuits and different noise sensitivities of the red and blue CCD-array pixels themselves also contribute to the difference between the red and blue standard deviations.

Due to the nature of the experiment the quantisation error of the frame grabber card is already included in the figures of table F.2.

---

[34] Increasing temperature causes a slight overall shift in brightness values and the gamma correction factor. It also slightly increases noise. Electromagnetic interference is observable only when experimental electrical appliances without radio noise suppression are in use. Standard motors, monitors or computers do not cause any interference in the equipment.

F.1.3.3 Errors Caused by the Frame Grabber Electronics

The frame grabber is the last module in the row of elements that influence the image information. The analogue TV signal from the camera is digitised and then stored in digital format. The frame grabber in use digitises the input into 32 discrete steps or grey levels for each of the three colour channels. This constitutes a loss in illumination information resolution. The quantisation error σ_Q is normally distributed and has according to [38] a standard deviation of

$$\sigma_Q = \frac{Q_{max}}{2^L \sqrt{12}} \tag{F.1}$$

where L is the number of quantisation levels and Q_{max} is the highest level. In table F.2 on the preceding page the quantisation error has been added to the error caused by noise in other electronic components. Since the quantisation error is normally distributed this is allowed.

The final representation of a given scene in the frame grabber memory is subject to multiple changes and processing steps. They all contribute a certain degree of error or uncertainty to the image data. Table F.3 summarises the five potential sources of error which have been identified.

Error	Effect	Influence on *					importance	compen-sation
		DET	COL	COL	REC	CAL		
sampling & leakage in CCD array	blurring		✓	✓			small	not necessary
electronic channel crosstalk	colour error			✓			small	not necessary
noise incl. quantisation error	noisy base data		✓	✓	✓	✓	0.25 to 0.7 pixel bright-ness units	filtering
gamma	colour shift			✓			considerable	essential

* DET=Stripe detection, COS=COS-algorithm, COL=Colour extraction, REC=Surface reconstruction, CAL=Calculation

Table F.3: Errors, caused by electronic components

After an image is available in digital representation no further errors are added by physical processes. It is up to subsequent programming to eliminate as many errors as possible using appropriate error models and to avoid the introduction of new ones.

F.1.4 Errors Caused by the Human Skin

F.1.4.1 Errors due to Optical Properties of the Skin

Human skin is not a homogenous reflector for visible light (see figure B.6). Incident light is only partly reflected. The skin absorbs, scatters and eventually also emits parts of the light. On a microscopic scale the coefficients for **absorption, transmission and reflection** are different for every single point of the skin due to the random occurrence of cells with varying optical properties. On a macroscopic scale, however, skin appears to be more uniform. Nevertheless a certain amount of inconsistency remains even at a macroscopic scale. Their influence on the accuracy of the COS-algorithm is discussed in F.2.2.4.

Ulcerated skin is often moist. If the wet surface has a certain inclination towards the camera and the light source **specular reflections** may occur. They are a major obstacle for both colour analysis and finding the centre of the stripe. Figure PIV.1[35] shows a piece of moist beefsteak used instead of a real ulcer with highlights caused by specular reflection within the projected stripes. Figure PIV.2 shows the stripe centres extracted from figure PIV.1 with gaps in the stripes at those positions where specular reflections occurs. In the perimeter of the gaps the stripes are bent out of direction and do not mark the real centre of the stripes.

The amount of specular reflection depends on the incidence angle of light with respect to the surface and the refractive indices **n** of the medium in which the light travels. Specular reflection is at its maximum at the angle of total reflection **c** which for the air/water boundary is

$$c = \arcsin\frac{n_{air}}{n_{water}} \qquad c = \arcsin\frac{1}{1.33} \approx 49^{o} \quad \text{(F.2)}$$

The fact that the reflected light is partly polarised may be used to reduce the highlights caused by specular reflection. The elimination is incomplete because the angle of maximum polarisation is not exactly the same as the angle of total reflection. According to *Brewster's Law* the angle of maximum polarisation **i** is

$$i = atan\frac{n_{water}}{n_{air}} \qquad i = atan1.33 \approx 53^{o} \quad \text{(F.3)}$$

---

35 Figures in this section about specular reflection may be found on plate IV, page 147, at the end of the chapter.

The above figures are only approximations since the refractive indices vary with wavelengths and the moisture covering the wound is not pure water.

When using a polarising filter attached to the camera's lens some of the specular reflection may indeed be reduced. Figure PIV.3 shows the result. After image processing the extracted stripe image in figure PIV.4 is slightly better than before when no filter was in use. The same outcome may be produced by placing the polarising filter in front of the projector's lens. Since the specular reflected light is always polarised perpendicular to the surface it is insignificant whether these components are absorbed before or after reflection.

Specular reflection may be completely removed by using two polarising filters: one mounted to the projector's lens the other one attached to the camera's lens. The polarisation axes of the filters are perpendicular. Reflections from the surface are now completely suppressed. Only light which is refracted into the wound and by scattering evades out of it again is visible to the camera since due to scattering the emerging light is no longer plane polarised and may therefore pass the filter at the camera's lens.
The resulting picture in figure PIV.5 is dim and the stripes appear extremely blurred since only the scattered part of the incident light is visible. This is the reason why the location of the stripes centres which are shown in figure D.6 fails in many areas leaving big gaps. In spite of eliminating specular reflection the result is worse than before.

The bad performance of the two filter method is solely caused by the insufficient brightness of the projector. By using a much brighter light source combined with thinner stripes of light this method will produce significantly better results than those achieved with or without one polarising filter only.

Since the present version of the instrument does not have the capability of suppressing any specular reflections their influence on the performance of the stripe extraction and the COS-algorithm, which are most sensitive to it, is analysed in F.2.2.4.

F.1.4.2 Errors Induced by the Mechanical Behaviour of the Skin

Skin is the flexible surface of the body. It responds to a variety of influences: inflammations cause swellings, bandages and dressings compress it, it is shifted under the influence of gravity when a limb changes its position and a wound interrupts the internal matrix of fibres. In the context of this investigation the actual nature of the distortion is of less importance. But it is essential to remember that the surface of the body may change with time.

This change has consequences for the repeatability of the measurement process as it partly depends on the reconstruction of skin areas over a wound. Chapter F.2.4.3 investigates the influence of the mechanical flexibility on the accuracy of the measurement process.

F.1.5 Errors due to Operator Interaction

The experiments in chapter E revealed that both area and volume measurement are sensitive to variations in the user defined boundaries of the ulcer itself and the area which is affected by it. The absolute error increases with the size of the lesion. If the boundary of a circular ulcer of 1 cm radius is defined 1 mm too far outside its area increases by around 0.7 cm^2. If the boundary of a circular ulcer of 5 cm radius is also defined 1 mm too far out the area increases by more than 3 cm^2. The relative error decreases with the size of the area: in the above example the relative error is over 20% for the small area but only 4% for the big one.

The appearance of this error is inevitable. One reason for this is the limited resolution of the TV-picture of the ulcer. The identification of the epithelial edge is difficult since it is always slightly blurred. Another reason is the inability of a human operator of positioning the mouse cursor which is used for defining the boundary of the lesion always at exactly the position where the boundary has been identified.

Even if the operator should manage to define the circumference of an ulcer with high accuracy his endeavours are spoilt by the following spatial quantisation process. The instrument determines the positions of only a limited number of surface points in space. On average these points have a distance of approximately 2.2 mm from each other in horizontal and vertical direction. The boundary is always clipped to the nearest of these surface points, thus producing a spatial quantisation error.

Fortunately both, human positioning and quantisation errors, are statistically distributed. The marked boundary is approximately as often outside as inside the real boundary. Both errors have a tendency to cancel each other out but a certain error always remains.

A completely different error may be produced by the operator in the cause of the image acquisition process. Both pictures, the one with and the one without the stripes, have to be coincident; i.e. a given point on the surface to measure has to be captured into the same x- and y-position in the frame grabber memory. If the two pictures are shifted toward each other the performance of the dynamic threshold method will suffer. This will be analysed in F.2.2.5.

F.1.6 Summary of Relevant Error Sources

This section analysed a large variety and number of possible error sources which affect the measurement process. In the process of assessing the magnitude of the errors some appeared too small to have any significant effect on the measurement while the occurrence of others cause it to fail completely. Table F.4 below summarises those errors which are of significant magnitude and relevance for the measurement process.

Error source	Error	Effect	Influence on *				
			DET	COS	COL	REC	CAL
mechanical	mechanical imprecisions	position errors of focal points of camera and projector cause calculation errors					✓
optical	distortion and field curvature	distortion of image geometry causes errors in calculations of surface point positions					✓
	chromatic aberrations	stripe displacement and colour shift			✓		
	colour crosstalk	up to 20% channel overlap	✓	✓		✓	✓
electronic	noise	noisy image data		✓	✓	✓	✓
	gamma	colour shift			✓		
skin	specular reflection	clipping, endangers stripe detection and finding of the centres of the stripes	✓	✓	✓	✓	✓
	scatter	blurring of stripes	✓	✓		✓	✓
	flexibility	influences repeatability of measurements					
operator	boundary definition	produces fluctuating results in area and volume calculations				✓	✓

* COS=COS-algorithm, COL-Colour extraction, REC=Surface reconstruction, CAL=Calculations

Table F.4: Summary of those error sources which are relevant for the measurement process

F.2 The Influence of Errors on the Performance of the Instrument

In this chapter the influence of the errors which are analysed in the preceding section F.1 are discussed. This section follows the flow of the data from the raw image via the four main processing steps

- stripe extraction,
- COS-algorithm,
- surface reconstruction,
- and calculation

to the final result and investigates the sensitivity of each processing step towards possible errors. An additional paragraph is dedicated to error related problems in the colour extraction procedure.

F.2.1 Errors Affecting Stripe Detection

F.2.1.1 Optical Properties of the Skin

Specular reflections are a severe threat to the stripe detection algorithms. They corrupt the image information by clipping the grey level values of the affected image points to the maximum value. Due to their brightness they also produce some blooming in neighbouring areas.

The dynamic threshold detection method is very sensitive to specular reflections. The clipping effect obviously occurs in both pictures, the one with and the one without the stripes where the threshold is derived from. As a result the value of the threshold is always equal to and never below the value of the stripe. No stripe is detected.

The subtraction method is more tolerant towards specular reflections. A relatively small area of specular reflection (4 pixels or less) might escape the limitations set by the set of rules which define the shape of a valid stripe. Despite this detection the centre of the stripe will not be calculated since the result of this calculation would be inaccurate. The presence of the stripe is of importance only for the rule which requires that a blue stripe is always followed by a red stripe and vice versa. If a stripe is not detected due to specular reflection this would otherwise suppress the detection of the following one.

In opposition to specular reflection is another property of ulcerated skin: poor reflection in certain areas. Insufficient reflection over the entire visible spectrum simply makes stripe detection impossible whilst selective reflection of a specific band of the spectrum suppresses stripes of the respective colours. If the green reference stripe is not detected the subsequent labelling process is jeopardised. If red stripes are not reflected this automatically makes the detection of the blue stripes impossible because a rule in the subtraction algorithm demands that there has to be a red stripe before the blue stripe. The same result is obtained when the blue stripes are completely suppressed .

F.2.1.2 Shape of the Surface

The shape of the ulcerated area is of great importance for stripe detection. If the angle of incidence of the projected stripes on the skin becomes too large the stripes are shifted very closely towards each other. This does not affect the detection of the green stripe since it is the only one of its kind. The detection of the red and blue stripes in contrast becomes increasingly difficult the closer they are together. This is mainly caused by the blurring properties of the skin which tend to smear the appearance of the stripes. Another reason is the digital filter that is designed to suppress high frequency noise. It also contributes a certain amount of blurring to the image information. The image blur suppresses the expression of notable peaks and the stripe detection fails.
In addition to this another effect arises. It will be shown later in this section that the accuracy of the COS-algorithm decreases when the stripes become thinner. In order to avoid high inaccuracy a rule in the subtraction algorithm suppresses stripes which are less than 15 pixel apart.

If the angle of incidence of the projected stripes becomes too small the stripes are separated by greater intervals. Simultaneously they also become wider and more dim. When a stripe becomes too wide or too dim a rule in both stripe detection algorithms suppresses its detection for two reasons. The first reason is noise. The darker a stripe becomes the higher is its sensitivity to noise. This will be discussed in the following subsection. Secondly, the shape of the surface may be such that it produces a dark hole in the stripe, effectively splitting the stripe into two parallel stripes. This would cause severe problems for the COS-algorithm and thus the stripe is suppressed at that position.

Cavities or occlusions caused by ulcers that undermine the skin are not discussed here since the instrument is not suitable to cope with such an obstacle. A method based on direct vision is, in principle, not able to measure anything which is not visible. In such a case the instrument's output is restricted to a depth map of the area visible to both camera and projector.

F.2.2 Errors Affecting the Finding of the Stripe's Centres

F.2.2.1 The Influence of Optical Aberrations

The analysis of optical performance of the instrument in F.1.2 extracted six kinds of optical errors: distortions, monochromatic aberrations, chromatic aberrations defocusing, background lighting and specular reflections. In the following the effect of these errors on the accuracy of both COS-algorithms, the one using the dynamic threshold method and the one using the subtraction method, is examined.
In the context of this chapter the term **relative accuracy** describes the accuracy with which the centre of a stripe **relative** to the pixels of that stripe may be detected. This is different from **absolute** accuracy which describes the stripe's position relative to each other and the whole instrument. Absolute accuracy is essential for later processing steps while in this section only relative accuracy is considered.

Distortion causes a great amount of displacement, it increases with distance of a given image point from the optical axis. The relative position of faraway image points is severely distorted but the relative position of neighbouring image points with respect to each other are only marginally shifted. Since a cross section through a stripe is only a local phenomenon the accuracy of the COS-algorithm is only minimally affected . This can be shown by calculations using worst case assumptions:
assuming a stripe of light with the average width of 6 pixels at the upper border of an image (the worst error occurs here) and applying the correction equation (D.8) for distortion in y-direction (see D.5.1) produces a stripe that is widened in y-direction by 0.8 pixels from 6 to 6.8 pixels. Its centre is therefore shifted approximately by half of the extra distance (0.4 pixels ≡ 0.1 mm) off the real centre.
At a medium off-centre distance where most ulcers normally have their boundary the shift is only 0.1 pixels (ca. 0.03 mm). This shift is less than the error which is inevitably introduced by other factors such as electronic noise and may therefore be ignored.

Monochromatic aberrations introduce a certain amount of image blurring. It is clear that for neighbouring points of a smooth surface the amount of blurring is almost identical. A stripe of light is such a local ensemble of points. Due to the nature of the centroid formula it is unimportant if a given surface point is represented by one pixel with a high grey level or two (or more) neighboured pixels with equivalently reduced grey levels as long as the grey values are spread symmetrically. The centre of a stripe will be located at exactly the same position.

Chromatic aberrations are too small near the optical axis to be measured with the existing equipment. But, as already stated in F.1.2, the maximum error in the corners of an image is approximately 0.5 pixels. This does not affect the COS-algorithms since the stripes are almost monochromatic. Therefore the whole stripe is shifted by approximately the same amount and its appearance is not changed at all. As a consequence the relative centre of a stripe is detected correctly by the COS-algorithms.

As a result of **defocusing**, stripes appear wider and darker. In principle this does not affect the COS-algorithms as the symmetry condition is not violated but problems occur because the dynamical threshold might not identify the stripe as valid. Additionally the accuracy of centre detection decreases due to noise.

A **bright background lighting** decreases the contrast of the stripes. The same problems as caused by defocusing may be observed. In severe cases the measurement may be impossible. In practice this was never found to be a problem as it is always possible to darken a room simply by switching off some lights.

Specular reflections are extremely bright causing the grey level values of all channels to be clipped to their maximum value. In contrast to the above errors specular reflection affect the two COS algorithms in a different way.

- The accuracy of the algorithm that uses the **dynamic threshold** method to extract the green stripe is not affected as it is incapable of finding the green stripe any longer at those points where the grey values are clipped. This is caused by the fact that the picture without stripes where the threshold is derived from is also clipped at exactly the same position. The threshold has the same value as the stripe at positions where specular reflection occurs. The basic condition for the detection of the stripe is not met and a gap in the extracted green stripe is the result.

• For the **subtraction method** the picture is different. If the specular reflection is located at the position of a stripe the programme will detect the clipped grey level values and stops the calculation of the stripe's centre. Again, no error but a gap occurs.

Neighbouring stripes are indirectly affected by the specular reflection due to the subtraction of the red from the blue colour channel. As a precaution the programme therefore suppresses the calculation of stripe centres if a neighbouring stripe is affected by specular reflection and is less than 20 pixels apart.

Thus specular reflections cause gaps in the extracted centres of the stripes but no errors. If the gaps are smaller than approximately 6 mm they are closed by interpolation in later image processing steps.

From the above it may be seen that optical errors hardly affect the accuracy of the COS-algorithms. They are very robust against interference by errors. If a stripe is detected and validated by one of the algorithms its centre will be calculated correctly. The main problem arises from optical errors such as defocusing, bright background and specular reflections which inhibit the detection of the stripe.

F.2.2.2 The Influence of Colour Crosstalk

In F.1.2.2 the overlapping of the filter spectra of both slide and CCD array colour filters was identified as the cause of colour crosstalk. Furthermore it was shown that it is not possible to compensate the crosstalk by image processing. Since the effect is unavoidable with the current hardware it is necessary to assess its consequences on the performance of the COS-algorithms.

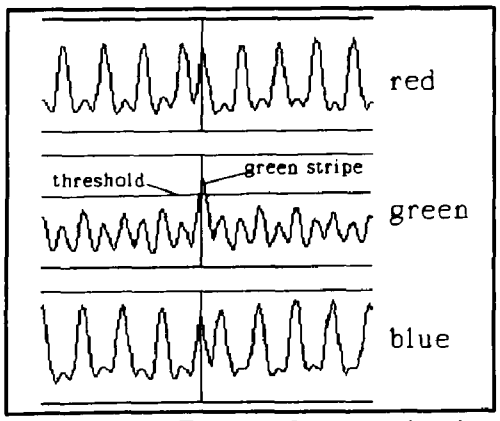

Figure F.3: Extract of a scan showing channel crosstalk

Figure F.3 shows scans of the three channels of the camera. The camera observes a set of stripes which are projected onto a white, plain surface. The vertical line indicates the position of the green reference stripe. Due to colour crosstalk the green stripe also appears strongly in the blue and the red channel. The smaller peaks in the green channel are caused by crosstalk from the blue and the red channels. Some crosstalk from the red channel even reaches the blue channel causing small peaks at the respective locations. In this scan the channel crosstalk has no effect on the accuracy of the two COS-algorithms.

The **dynamic threshold method** which extracts the green stripe's centre is not affected because the crosstalk from the red and the green channel are almost equally strong and they are distributed symmetrically around the green stripe.

The **subtraction method** which extracts the red and the blue stripes is also not affected since the stripes are evenly distributed and the amount of crosstalk from the other channels is approximately the same for both channels. As a result the crosstalk from the green channel totally disappears and the peaks of the stripes are slightly rounded which does not affect the accuracy of the centroid detection. The result of the subtraction is shown in figure D.8 in section D.4.3.2.

In reality the observed object is neither homogenously white nor absolutely plane and errors occur in the cause of the centroid calculation. Experiments with wildly coloured and structured surfaces resulted in centroid calculation errors of up to 2.1 pixels, equivalent to 0.6 mm. For test surfaces which are similar to ulcerated skin the error is approximately halved to 0.3 mm. The error caused by colour crosstalk is by far the biggest error examined in this chapter. In section H.2.1 on future developments a method is proposed how colour crosstalk may be completely eliminated.

F.2.2.3 The Influence of Errors Caused by Electronic Components

The underlying source for all information derived from an image is the pixel. It carries spatial, colour and brightness data of a given point of the image. The emphasis of this chapter is on the brightness data of a pixel. In the analysis of the performance of the electronic components of the camera (F.1.3.2) and the quantisation error of the frame grabber electronics (F.1.3.3) an experiment delivered the standard deviation as a measure of pixel noise. The results of this experiment (table F.2) on pixel noise may be used to simulate the influence of noise and quantisation error on the COS-algorithms by the following procedure: a computer programme generates 1000 stripes and adds the experimentally derived standard deviation for each pixel on it. Form, width and brightness distribution of the stripes are constant and modelled after typical appearances of stripes on skin. The COS-algorithms then calculate the centres of these artificial stripes using a fixed threshold. Table F.5 shows the standard deviations for the three colour channels and the stripe models for simulating bright, medium and dark stripes. The resulting standard

deviations vary between 0.009 and 0.180 pixel widths. The dynamic threshold method used for the green channel produces better results than the subtraction method used for the red and the blue channel since for the subtraction method the noise of both channels is added.

	not-γ corrected			γ-corrected		
STRIPE	bright	medium	dim	bright	medium	dim
RED/BLUE	0.039	0.057	0.079	0.052	0.132	0.180
GREEN	0.009	0.013	0.017	0.013	0.030	0.044

bright medium dark	10 16 30 30 16 10 7 11 20 20 11 7 5 8 15 15 8 5	4 8 29 29 8 4 2 4 12 12 4 2 2 3 7 7 3 2
	not γ-corrected model	γ-corrected model

Table F.5: Top: Simulated standard deviation of centres of stripes caused by pixel noise only. Bottom: Stripe models used in the simulation

Considering the fact that 1 pixel width in the y-direction is equivalent to 0.286 mm on the observed scene this implies that even in the worst case (red/blue channel, dark stripe, γ-correction) a standard deviation of approximately 0.051 mm is achieved. This extremely small error can not be confirmed by measurements on real stripes as the above results are obtained by an idealised simulation that takes only the influence of noise on stripe pixel values into account. It ignores the influence of noise on the threshold that determines whether or not pixels belong to a stripe.

Nevertheless it is interesting to observe that γ-corrected brightness values, which are so helpful for colour detection, produce slightly worse results than uncorrected values. Especially with dim stripes the effect is quite significant. The reason for this becomes obvious when looking at the γ-correction table (table F.6) used by the system:

measured values	0	1	2	3	4	5	6	...	27	28	29	30	31
γ-corrected values	0	1	1	1	2	2	2	...	23	25	27	29	31

Table F.6: Gamma-correction table (corrected values rounded)

Brightness values of dim stripes are converted into even lower values by γ-correction. It is clear that lower values are much more affected by noise than higher values (a pixel with a brightness value of 30 changes only 3.3% when noise adds or subtracts one unit, but a pixel with a brightness value of 2 changes 50%).

This effect also explains why darker stripes show a higher standard deviation in centre detection than bright stripes. As a result of these findings γ-corrected brightness values are not used for centre detection.

For the subtraction method the standard deviations found by the experiment reflect very well the figures found by measurements on real stripes. The standard variations for the green stripes, however, are much better in the experiment than in reality. A refined version of the simulation therefore pays more attention to reality by considering the influence of noise also on the dynamic threshold. The threshold decides whether or not a pixel belongs to a stripe by comparing the brightness of a given point in the striped image with the corresponding point in the unstriped image. A given pixel in the striped image is considered as belonging to a stripe if its brightness value is higher than the corresponding one in the not striped image. Due to fluctuations in reflectivity, angle and noise, neighbouring scans through a stripe might result in a different number of pixels that belong to the stripe.

Figure F.4 demonstrates the consequence of this effect. It shows two neighbouring scans, (a) and (b) through the same stripe. Stripe brightness values are assumed to be identical. Only the threshold varies slightly so that one stripe (a) is 6 and the other one (b) 5 pixels wide. When applying the centroid formula to both scans the centre is found at two slightly different locations. The amount of error introduced by a varying threshold depends on the width and the brightness of the stripe: the error increases with descending stripe brightness levels and widths.

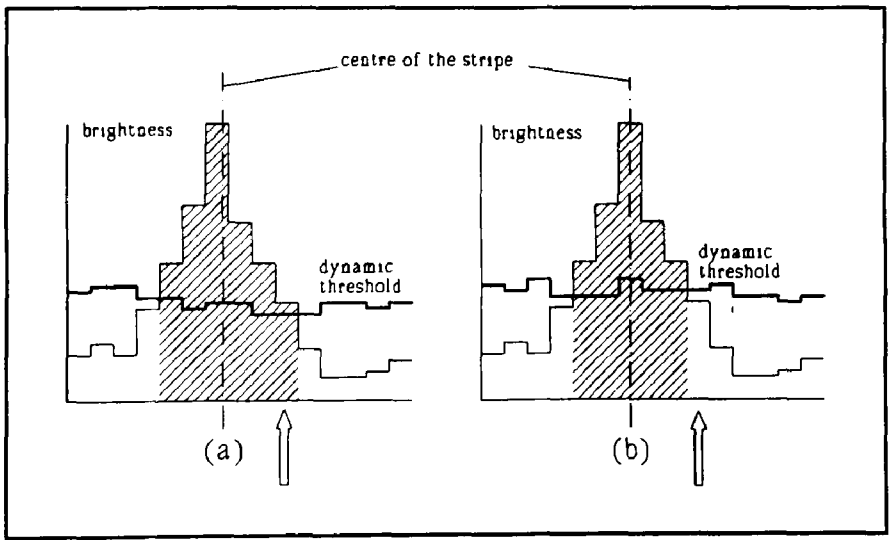

Figure F.4: The effect of varying thresholds on the calculation of the centre of a stripe

When including this noisy threshold into the simulation for the green stripe the results become very close to results obtained from measurements on real stripes: Table F.7 shows standard deviations for medium bright stripes of different widths. Dark and bright stripes are not shown as they only change the results slightly (approximately -0.01 for a bright and +0.01 for a dark stripe). Measurements on real stripes are only slightly worse (approximately 0.05 pixel widths) as other effects like surface roughness, varying reflectivity and quantisation errors are not considered in the simulation. As expected, wider stripes are less sensitive to noise than narrow ones.

STRIPE	width=3	width=4	width=6	width=8	width=10
GREEN	0.15	0.11	0.09	0.08	0.07
RED/BLUE	0.16	0.13	0.08	0.08	0.07

Table F.7: Simulated standard deviations (pixel widths) of stripe centre's caused by noisy threshold and stripe values

These findings imply that it is desirable to project bright and wide stripes onto the skin. Bright stripes do not impose a problem as long as blooming and clipping effects can be avoided. Wide stripes conflict with the demand for high resolution which requires as many stripes as possible. The thinner the stripes become the more of them fit onto the projection slide. Experimental findings suggest a compromise of approximately 30 stripes (per colour) with an average width of 6 threshold detectable pixels. The amount of pixels actually used for the calculation of the green stripe's centre is always greater than this as two pixels to the left and to the right of the threshold are also used adding another 4 pixel. This is possible because stripes of the same colour have an average distance of 20 pixel widths from each other.

For the red and the blue stripe this addition of pixels to both sides is not necessary since the median method which is used for the definition of the width of the stripes always produces much wider stripes than the threshold method.

The above findings on noise (including quantisation noise) generated errors explain the real performance of the centre-of-stripe-finding algorithms. When allowing for additional errors caused by surface roughness and geometrical errors in the projection and imaging system the theoretically expected performance is in reality achieved.

F.2.2.4 The Influence of Varying Skin Reflectivity and Inclination Angle of Light

The algorithm that extracts the stripe's centre anticipates a surface of constant reflectivity over the whole width of a stripe. Obviously this condition can not be met when ulcers or skin act as a reflector. If half of the stripe's width covers a region of high reflectivity and the other half a region of low reflectivity the COS-algorithm will detect the centre in a position which is shifted towards the brighter half of the stripe. Both the stripe extraction methods have a limited ability to counteract the shifting effect.

The dynamic threshold method takes advantage of the fact that the threshold is lower in regions with low reflectivity thus maintaining the stripe width. Figure F.5 shows this effect.

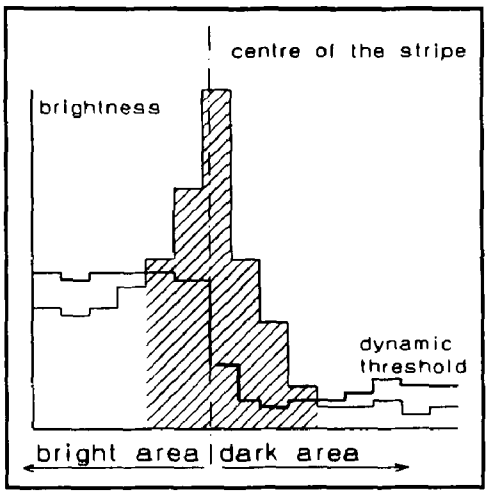

Figure F.5: Maintaining of the stripe width by the dynamic threshold in areas of varying reflectivity

The subtraction method is insensitive to varying brightness conditions if they occur simultaneously and with the same intensity in both the red and the blue channel. After subtraction of the red from the blue channel the changes cancel each other out. If a sudden change in intensity happens in only one channel the centre calculation in both channels will suffer.

Experiments using two different colours with a stripe's centre located at the sharp boundary between the colours show that an error of approximately 1.5 pixel widths is possible. This experiment is performed under extreme conditions which never occur on ulcerated skin. Due to the blurring and scattering properties of skin and flesh sharp colour boundaries are rare and the error is much less.

The same problem arises in both methods when those parts of the surface which are illuminated by a stripe change their slope. When assuming mainly lambertian reflection and a homogenous reflecting surface the amount of reflected light is proportional to the angle of incidence of the stripe. The smaller the angle the less light is reflected.

Two factors prevent the centre of the stripe from being detected wrongly: a) the stripe widens at positions with little angle and b) for the dynamic threshold method the threshold includes into the calculation the dim parts of the stripe (those with little angle of incidence). As a result the centre is nearly correctly detected.

It is tempting to try and correct the varying reflectivity of surface regions by image processing in order to decrease the amount of error induced by unstable reflection properties. Unfortunately this process would introduce more errors than it would eliminate. The first reason for this is again noise.
If a standard stripe passes an area with two different reflectivities, e.g. 80% and 20%, those pixels related to the respective areas have to be multiplied by two different factors to compensate for the variation. Pixels in bright areas have to be multiplied by 1.25 and those in dark areas by 5.0 to achieve a virtual reflection of 100%. This multiplication also multiplies the amount of noise of the respective pixel values. This happens twice as the correction factors obtained from the picture without stripes are also derived from noisy pixel values.
To make things even worse all the pixel values have to be gamma corrected before reflection compensation calculations can take place. As mentioned before this means for darker pixels that their values decrease while their noise contribution stays constant.
For the dynamic threshold method the same mechanism also applies to the threshold values which also have to be processed. Therefore the result of the whole reflection compensation process is even more noisy.

The second reason why reflection compensation produces poor results is vested in the colour filtering properties of the stripe producing slide and the camera. For successful reflection compensation the reflectivity of the skin for a particular stripe colour has to be derived from the picture without stripes which is exposed to white light. This is not perfectly possible since the colour channels of the camera integrate over a certain bandwidth and their output signal does not carry any information about the distribution of the illumination intensity of single wavelengths within the respective channel.
Reflection compensation under these circumstances is possible without errors, only if the white light in the picture without stripes is composed by using filters with exactly the same filter spectra as the stripe producing slide.

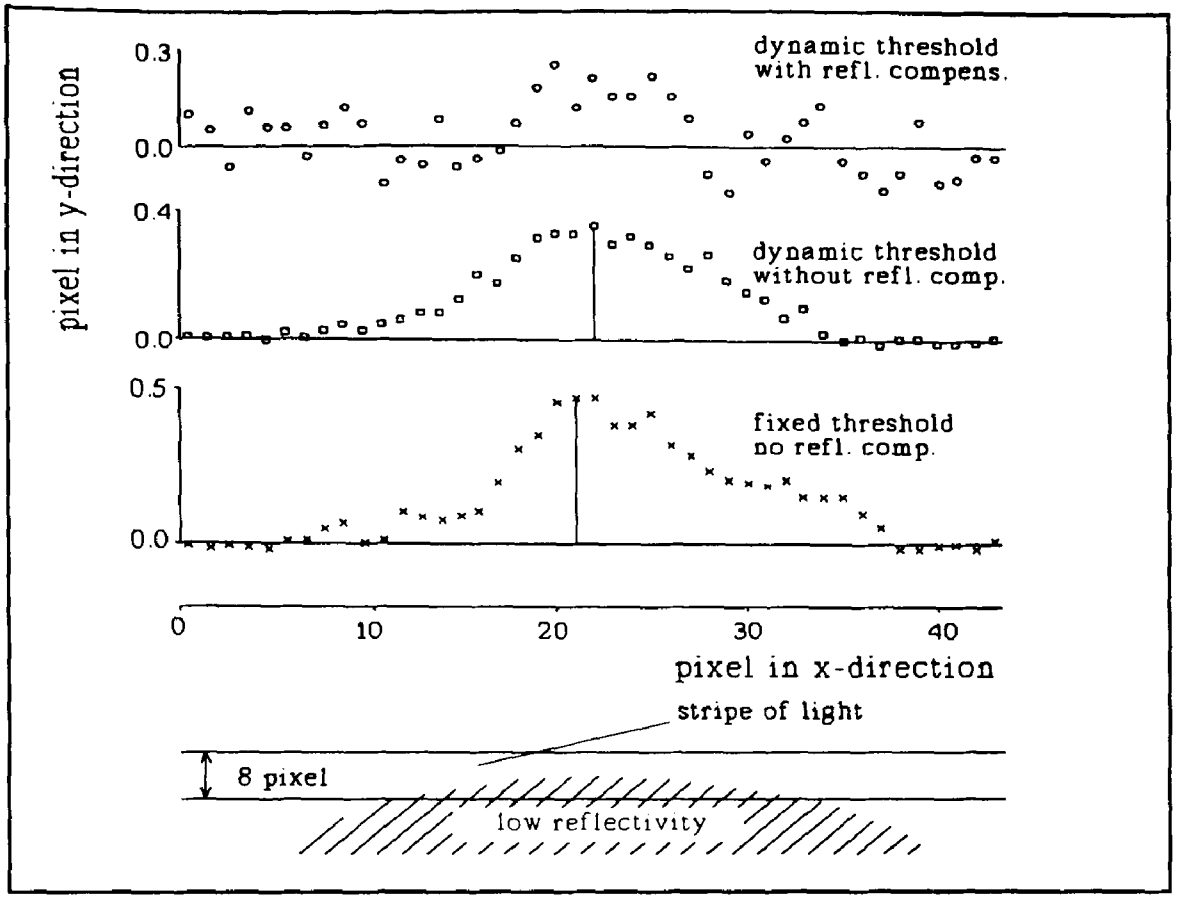

Figure F.6: Comparison of three different approaches to detect the centre of a stripe that passes a region of low reflectivity by the dynamic threshold method

Figure F.6 shows the effect of reflection compensation on the accuracy of the dynamic threshold method. For the subtraction method the result of reflection compensation is almost the same. The figure shows the position where the centre of a stripe was detected with respect to the true centre at 0.0 for three different cases: (x) fixed threshold without reflection compensation, (□) dynamic threshold without reflection compensation and (o) dynamic threshold with reflection compensation.

It can be seen that the reflection compensation process does eliminate the effect of the dark area but significantly more noise is introduced. Due to the blurring properties of human skin (see chapter B.1.5, figure B.6) and the fact that such a harsh contrast as in this example is rather rare on normal skin the effect of varying reflectivity can be ignored. Additionally it is rather unlikely that a sudden change in reflectivity appears exactly in the middle of a stripe where it matters most. The more this event is shifted to one of the rims the less it influences the result.

F.2.2.5 Consequences of Movements of the Sensor During Image Acquisition

In the previous sections it is assumed that the two pictures used to derive stripe and threshold information are in exact spatial coincidence. Both pictures should show a certain surface point at exactly the same position on the monitor. This idealising assumption can not always be met in reality as there is a time interval of 0.45 seconds between the two frames. This is mainly caused by the limited speed at which the slide changing mechanism in the projector can operate. The frame grabbing hardware itself contributes only 0.02 seconds to the delay.
If the projector is held manually and not by a stand a certain displacement between the two pictures due to operator movements will inevitably occur. The patient is normally lying in a bed or the ulcerated area of the body is resting somewhere else and does not contribute to the displacement. On average the displacement is around two pixel width in x- and y-direction, but may sometimes exceed 8 pixel widths. When a stand for the sensor is in use no displacement is measurable. A stand should therefore be used wherever possible.

For the subtraction algorithm a displacement between the two pictures is not important since it uses only the image information of the picture with the stripes. For the dynamic threshold method a problem might arise.
The displacement does not pose a problem to the accuracy of the dynamic threshold method if the skin surrounding the ulcer has homogenous reflection properties. As a result the green stripe will be measured accurately. But in regions with highly varying reflectivity, normally within the ulcer, two consequences are possible:

- The green stripe will partly be undetected due to an inappropriate threshold. If the threshold is too high the COS-algorithm can not start, if it is too low the algorithm will reject the stripe because it appears too wide to be valid. In this case no error is being introduced by the measurement but by subsequent processing steps where the interpolation of missing surface points is attempted. If the interpolating processes are successful some points in the ulcers will be interpolated too high, others too low. It is reasonable to assume that the errors are randomly distributed with an average near zero. The volume calculated from this data should therefore be relatively correct because the errors cancel each other out.
- The stripe's centre will be calculated at slightly wrong positions. As the varying reflectivity of the surface is distributed randomly the miscalculations will also distribute randomly. The consequences are the same as mentioned above.

If the displacement of the two pictures is too big the green stripe will not be detected at all in many places. The interpolation or the labelling algorithm detect this and the measurement attempt fails. The time between taking the pictures and the possible failing of the measurement is approximately one minute with the current computing facilities, so the measurement may be repeated without too much inconvenience to the patient.

F.2.2.6 Summary: Performance of the COS-Algorithm

The task of the COS-algorithm is to deliver the accurate position of the stripes' centres. Table F.8 summarises only those errors that influence the accuracy of the algorithm and are therefore of importance for subsequent processing.

Error	Effect
specular reflection	The main obstacle. At positions with specular reflection the detection of the stripes is suppressed and no centres are calculated.
distortion	Distortion is biggest in corners of the image. It shifts stripe centres 0.4 pixel widths relative to the stripe and max. 1 pixel relative to the reference coordinate system.
noise	Noise produces a standard deviation of max. 0.17 pixel widths in the position of stripe centres.
chromatic aberration	Chromatic aberration is biggest in corners of the image. It shifts stripe centres max. 0.5 pixels widths relative to each other and max. 0.25 pixel widths relative to the reference coordinate system.
gaps in stripes	Gaps in stripes are closed by interpolation. The interpolated centre of a stripe may be up to 3 pixel widths of its real position.
varying reflectivity of the skin	Varying reflectivity of the surface may cause the centre of a stripe to shift max. 0.32 pixel widths.
wrong positions of sensor components	As a result the distance of all points of the measured surface to the sensor may be miscalculated by 0.32 mm (1.2 pixel widths)

Table F.8: Errors influencing the output of the COS-algorithm

F.2.3 The Influence of Errors on Colour Extraction

The extraction of the three colours in the lesion which may be of interest to the physician is based on accurate colour perception. Consequently all those errors which have an influence on the colour of a pixel affect the extraction algorithm. These error are caused by • noise • the gamma circuit • chromatic aberrations • specular reflections • and background lighting.

The term 'colour' describes both the ratio between the three principle components red, green and blue of each pixel and their respective value. Approximately the same amount of noise is imposed on each of the three principle components of every pixel of the image. Dark components are more falsified than bright ones. As soon as one component is relatively dark the ratio between the components also becomes very noisy. Another severe obstacle is clipping caused by specular reflections. The extraction of the ulcer's colours works reliably only in those parts of the image where the ratio between the colour components is not noisy. This can be seen in figure Pv.3 and Pv.4 on page 148.

Before the ratio between the three colour components can be calculated correctly each of them has to be gamma-corrected. As already mentioned this correction amplifies the influence of noise on darker colour components (see chapter F.2.2.3, table F.6). This effect significantly decreases the reliability of colour extraction in dark areas of the image.

Where specular reflections occur they cause clipping and blooming of the affected image points. Both effects completely annihilate both colour ratio and brightness information. Areas affected by specular reflection are therefore excluded from the colour extraction process.

Background Lighting may change the colour impression of an ulcer. Normal lighting in a room tends to be close to white and the change is marginal because the light source of the projector is normally much stronger.
The effect of background lighting can be eliminated because of the magnesium oxide chip which acts as a colour reference. From a shift in its colour appearance correction parameters may be calculated to correct falsified colours.

F.2.4 The Influence of Errors on the Spline Reconstruction Method

The main reason for the observable variation in volume data when measuring the same object is caused by the process of reconstruction of the healthy surface. This section analyses the reasons why the reconstruction algorithm produces such varying results.

The spline interpolation algorithm uses two sets of data for surface reconstruction:

- A representation of the ulcerated skin is obtained by triangulation using the positions of the centres of the stripes.
- Additionally the algorithm needs information about the area of the skin which is actually affected by the ulcer. This area is normally not identical to the ulcer itself. It includes parts of the healthy skin which might be swollen or otherwise affected in its shape.

These two sets of data are subject to a variety of fluctuations and errors. Their influence is discussed in the following.

F.2.4.1 The Influence of Errors in Stripe Centre Positions

Figure F.7 shows a cross section out of three dimensional surface data. Two reconstruction attempts are shown: one with the original surface data (line a), a second one with the same data but with the surface point (p1) closest to the ulcer being elevated by an error of 0.1 mm (line b). Since the spline depends on the gradient (and the position) between surface points a difference of more than 1 mm occurs in the middle of the reconstructed region (Figure F.7 exaggerates the elevation for better illustration). This may not appear much, but when this additional 1 mm is apparent over the whole area of a typical ulcer of 25 cm^2 this deviation causes an additional volume of approximately 1 cm^3.

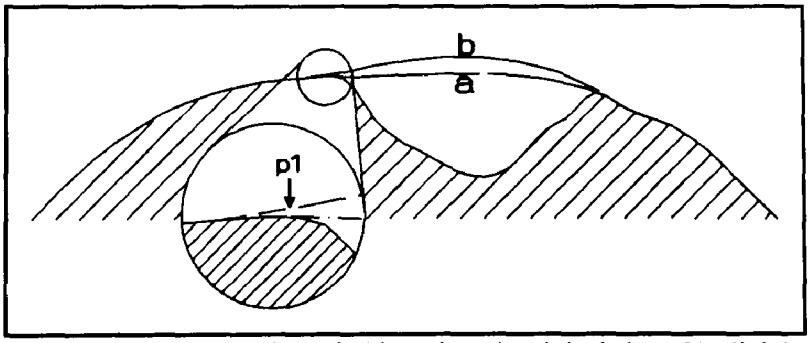

Fig.F.7: Reconstruction of skin using a) original data, b) slightly changed data

If the ulcer has a real volume of 15 cm^3 this is equivalent to an error of nearly 7%. Fortunately this can not happen in reality as several scans, parallel and at 2.2 mm distance to each other, are made. Some might enclose too little, others too much volume. On average the errors should cancel each other out if they are randomly distributed (e.g. noise induced). Systematic errors in contrast do cause a faulty but repeatable measurement.

In the light of these findings the influence of faulty surface data from the COS-algorithm may be examined. According to table F.8 seven effects influence the stripe centre detection. They may be divided into two classes:
a) effects that change the position of all surface points in the same way
b) and effects which influence each surface point differently.

a) Effects that alter the position of all points in the same way, i.e they virtually shift the whole surface as a whole towards or away from the sensor, do not influence the reconstruction algorithm as it uses the relative position of surface points with respect to each other. The absolute position and orientation of the surface is irrelevant. Such effects are distortions, chromatic aberrations and wrong determination of the position of sensor components.

- Distortion. In chapter D.5.1 a geometrical model to approximate the error was introduced. The correction formula, derived from the model, shows that the error caused by distortion is greater in the corners of an image than at its centre. After correcting the measurement points by the correction equation (D.8) and (D.9) the amount of distortion in the corners of an image is reduced to about 1 pixel width. Since the geometrical model that leads to the correction equation is an approximation to the real nature of the error a better compensation can not be achieved.
  In spite of this deficient compensation the spline reconstruction algorithm is only marginally affected because the remaining error affects neighbouring measurement points in the same way. The interpolated surface shifts as a whole, together with the measured surface below, uniformly in one direction. The enclosed volume does not change.

- Chromatic aberration does not affect the COS-algorithm. Stripe centres, relative to the pixels of the stripe, are detected almost correctly. But since the stripes as a whole are shifted by chromatic aberration the positions of the detected centres relative to other stripes are shifted. Especially stripes of different colours show a relative shift towards each other. Fortunately the effect is relatively small (a maximum of 0.5 pixel widths in the corners of an image, where the aberration is biggest). The area around an ulcer is normally relatively close to the optical axis of the camera's lens where the aberration becomes smaller. At a radius of half the image width the effect is hardly measurable by the existing experimental means. The effect fades into the average background noise. Since the spline reconstruction algorithm is not sensitive to errors far away from the boundary of the lesion, the effect of chromatic aberration may be ignored.

- Wrong determination of the positions of camera and projector does not affect the reconstruction process at all. In contrast to the above errors, this error affects all measured surface points in a linear way. The result is a virtual tilting of the surface which does not affect the relative positions of the surface points towards each other. Therefore the reconstruction algorithm is not affected.

b) Other than the effects above the following influences have a noisy characteristic. They may severely influence the reconstruction of one cross section of surface data. But due to their noisy characteristics they tend to cancel each other out. Such effects are noise, gaps in stripes, varying reflectivity of the skin and specular reflections

- Noise and quantisation error combined cause the centre of a stripe to fluctuate around its real position with a standard deviation of a maximum of 0.17 pixel widths. The consequence on the reconstruction algorithm depends mainly on two factors: the widths of the ulcer at the respective position and the amount of error on other measured surface points used for reconstruction. Experiments on plaster models show (see figure E.1 in section E.3) that in repeated measurements some parts of the spline may actually fluctuate about 2 mm.
  If by chance one or more neighbouring reconstruction splines are shifted in the same direction a volume error arises.

- Gaps in stripes are infrequently distributed and do not affect the measured positions of all surface points. They normally occur due to specular reflection or insufficient contrast of the stripes. These effects happen inside the ulcer and at the rims of a limb rather than at the border of the ulcer. Their influence is therefore limited. If a gap occurred at a point which is being used for spline interpolation the interpolated position of this point may be up to three pixel width wrong. Therefore this point is omitted for reconstruction purposes. A neighbouring unaffected one is then used by the algorithm. This might result in a widening of the span to interpolate by some millimetres and consequently increase the amount of uncertainty of the reconstruction but otherwise some parts of the spline curve might go severely wrong.

- Varying reflectivity of the skin might cause the centre of a stripe to be detected wrongly by up to 0.35 pixel widths (0.12 mm). This is less than the error introduced by noise and may therefore be neglected.

- Specular reflections cause gaps in stripes. The consequence of specular reflections are therefore the same as the those by other causes resulting in gaps in stripes.

Summarising the above, it can be said that all but one of the errors which falsify the centre of a stripe may be ignored. A significant effect on the accuracy of the reconstruction algorithm is imposed only by noise.
In the following subsection it will be shown that other factors caused by the nature of the ulcerated skin result in much bigger errors.

F.2.4.2 Varying Determination of Ulcer Boundaries

When using a plaster model of an ulcer with a flat, uncurved surface around the ulcer, the error in volume measurement is indeed small. Only the measurement errors mentioned above influence the result of the reconstruction algorithm. The precision (repeatability) of the experiments can not be achieved with real ulcers. One reason for this is the fact that in practice it is impossible to define a clear boundary around the area whose surface is somehow affected by the ulcer.

The definition of the area that is affected by the ulcer is being performed by a human operator. In repeated measurements a given surface point in the boundary region might therefore sometimes be defined as affected and sometimes not. The closer the boundary is shifted towards the ulcer the higher is the likelihood of wrong basis data for reconstruction. The further away the boundary is drawn the greater the reconstruction area and the reconstruction errors grow.
The amount of error which is actually added to the error caused by wrong determination of stripe centres can be assessed by repeated calculations of extracted surface data from one ulcer where only the boundary definition is changed between calculations. Fluctuating boundaries appear to contribute another error of up to around 1% to the standard deviation of the volume obtained by experiments on model ulcers.

F.2.4.3 The Influence of Flexible Skin on the Reconstruction Algorithm

The worst error is added by the object of interest itself. The surface of the body is not a rigid structure and might vary between measurements. Its matrix is flexible and responds to multiple stimuli: position of the limb, dressings and bandages and many other factors cause changes and shifts in the surface.
As a result the 3-D map of a given area will always be different. The difference may be little. Especially the surface of the leg is quite rigid and little error is introduced by its limited flexibility when measuring leg ulcers. Lesions at the back or at the coccyx in contrast are extremely flexible. Their volume might change over 50% between two measurements. The figures Pv.1 and Pv.2. on plate V at the end of this chapter (page 148) show two such cases. In these cases the volume definition used in this work is not an appropriate parameter to assess the status of an ulcer.

Errors caused by such influences as imprecise determination of the area to reconstruct and the mechanical behaviour of the skin are independent of the instrument. Even a completely accurate surface scanner would not be able to overcome them as an absolutely correct reconstruction is impossible. An indication for the performance of the instrument can only be given for the accuracy of the mechanism that scans the 3-D data of the skin.

F.2.5 Errors Influencing the Area and Volume Calculation Algorithm

The accuracy of area and volume calculation depends on two factors:
firstly the data which has been extracted in preceding processing steps such as boundary definition and the accuracy of the surface scanning process and secondly by errors caused by the calculation algorithms themselves.

F.2.5.1 The Influence of Mechanical Errors

Mechanical errors influence both the accuracy of the surface scanning process and the final calculation of area and volume. The effect of mechanical errors on the surface scanning process are discussed in the previous section. This section discusses the consequences of two mechanical error sources which in effect lead to a false calculation of the distance from the sensor to the surface to measure: wrong determination of the positions of the camera's and the projector's focal points and displacement of the position of the projection slide.

Since the underlying measurement principle of the structured light technique is triangulation the absolute coordinates of the **camera's and projector's focal points** are of special importance for the accuracy of the measurement. With the equipment available it is possible to determine the coordinates of the sensor components within an uncertainty of 1 mm.

Figure F.8 shows how the measurement of a plane surface positioned parallel at 5 cm distance from the bottom of the sensor is affected by such a wrong determination of the positions of projector and camera. The graph shows the measurement error in z-direction (distance) that occurs if the camera is measured 1 mm to the right and 1 mm below its real position and the projector is measured 1 mm to the left and 1 mm above its real position.

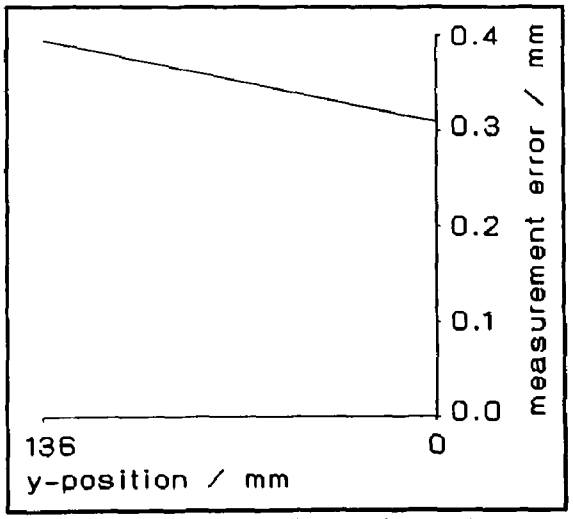

Fig. F.8 Maximum error in z-position calculation of a plane at 5 cm distance caused by wrong determination of camera and projector positions

The error is linear. It has the effect of tilting the representation of the plane surface in the computer memory by a certain amount.

As this systematic error affects all surface points in a linear way the relative position of the surface points towards each other is still correct. This conclusion is of importance for the surface reconstruction algorithm which is not affected by such an error since it relies on the accurate position of surface points relative to each other. The absolute error in distance calculation however, is of importance for the area and volume calculation since the surface area occupied by a pixel changes with the distance (and the orientation) of the surface to the observing camera. If the surface distances are calculated wrongly the resulting figure for the ulcer's area will inevitably be false.
Under the current geometrical constraints of the instrument the maximum offset in area and volume calculation caused by an error of 0.4 mm in depth position calculation is constant and approximately 0.4% of the respective volume or area.

Wrong determination of the component's focal points is only one error source which causes wrong distance values. The experiment on **slide displacement** (chapter F.1.1) delivers a standard deviation of 0.1 pixel units in y-direction. Similar to the focal point errors, the error caused by slide displacement affects the whole image equally but is much smaller. The distance values for all surface points will all be shifted in the same direction. The following calculation gives an assessment of the amount of error caused by slide displacement:

in order to obtain the greatest possible error two cases may be examined. In the first case a stripe is displaced in both, the reference and the measurement projection, in such a way that its positions are shifted towards each other. Consequently the distance of the measured surface point will be calculated too small. In the second case the opposite may have happened: the positions where the stripe is detected in the reference and the measurement picture are shifted apart from each other. The distance measured is too great.
Using the worst case position parameters from the example above and assuming A_y to be 1 mm and B_y in equation (D.12) to be 27 mm in reality a maximum deviation of 0.035 mm results in a difference of 0.14 mm in depth.
In addition to the offset caused by wrong determination of the focal positions of camera and projector there is a statistically distributed error of approximately 1% of the area or volume resulting of the fluctuating slide positions.

F.2.5.2 The Influence of Quantised Surface Data

The measured surface is quantised in two directions: the amount of stripes which hit the surface limit the resolution in vertical direction. Due to the geometrical constraints vertical displacement is equal to depth. On average the stripes have a distance of approximately 8 pixel widths. This is equivalent to a depth resolution of 2.2 mm.

Horizontally every sixth pixel is used as a sampling point. Since the pixel width in horizontally is slightly more than vertically direction this is also equivalent to approximately 2.2 mm. Thus, on a flat surface the sampling points form a grid of squares, 2.2 x 2.2 mm each.

For calculation each square is divided into two triangles. Such a triangle has an average area of 2.4 mm^2 and is the basic cell used for calculation. Figure D.15 (see D.5.4) shows such a mesh of triangles which is superimposed on the ulcerated area. Only triangles which are entirely inside the ulcer are part of the mesh. As a result the area of the ulcer is measured too small. This is taken into account by the calculation algorithm by adding half of the areas of the border cells, which are only partly inside the ulcer. Thus the real borderline of the ulcer is approximated. Some halved border cells are actually too big while others are too small. On a sufficiently big ulcer the errors cancel each other out.

The same effect assists the calculation of the ulcer's volume. The original smooth surface of the wound is represented by the straight sides of the triangles. The triangle's planes sometimes virtually 'cut' through the real surface and sometimes float above it. The mean error is zero for a great number of triangles but with decreasing size of the area and volume of the lesion the possible quantisation error increases. The experimental results which are documented in the figures E.3, E.4 and E.5 in chapter E demonstrate this.

Identical results may be found in repeated runs and the only variation is caused by the boundary definition itself. With these stored pictures an average standard deviation of approximately 3% of the volume is obtainable for most measurements. As in the experiment that uses ulcer models, the percentage of deviation increases with increasing area and decreasing volume. An additional offset may be caused by the complexity of the area surrounding the lesion.

For a reliable assessment of the boundary induced error more clinical trials are necessary. At present only the above estimations and qualitative descriptions are possible.

F.2.6 Summary: Influence of Errors on the Overall Performance of the Instrument

Table F.9 below summarises the findings of the discussion on the influence of errors on the measurement results.

Effect	Influence on	
	Area Calculation	Volume Calculation
Flexibility of skin and ulcerated area	Highest proportion of error. Might make measurement of the lesion inappropriate.	
distortion	negligible	small, less than 0.5% after correction
wrong determination of the positions of the focal points of camera and projector	Might add up to 0.4% offset error	
fluctuations in slide positions	contributes up to 1% fluctuating error	
specular reflections	jeopardises the measurement, might add up to 5% error on volume calculation in rare cases	
defining the boundary of an ulcer	around 2-4% for areas over 10 cm^2	nil
defining the boundary of the area which is affected by an ulcer	negligible	around 2-5% for lesions with an area/volume ration of more than 0.4

Table F.8: Effects, influencing the measurement results of the instrument

PLATE IV: Specular Reflection

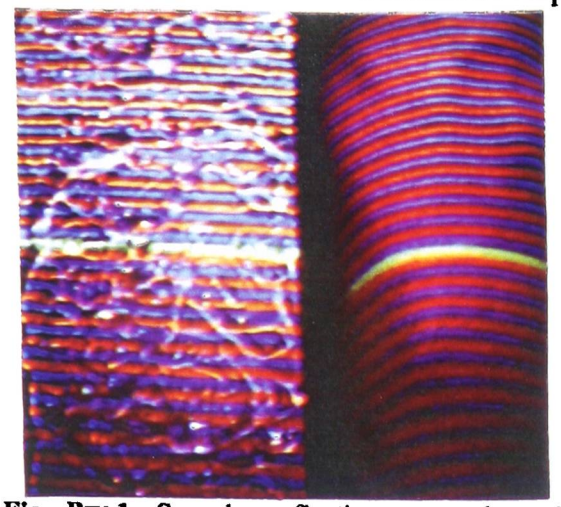

Fig. PIV.1: Specular reflections cause by gel (left), comparison: skin without gel (right)

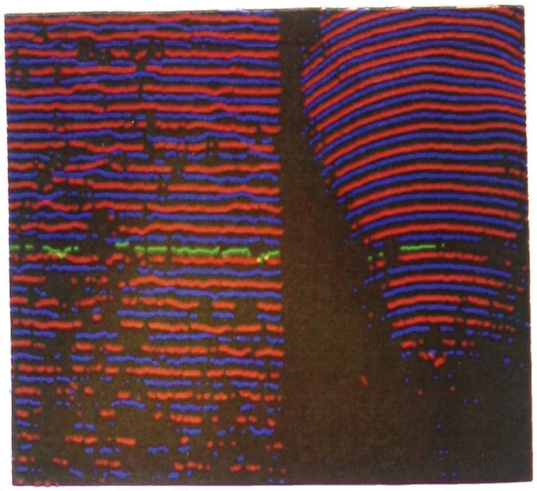

Fig. PIV.2: Stripe centres extracted from figure PIV.1

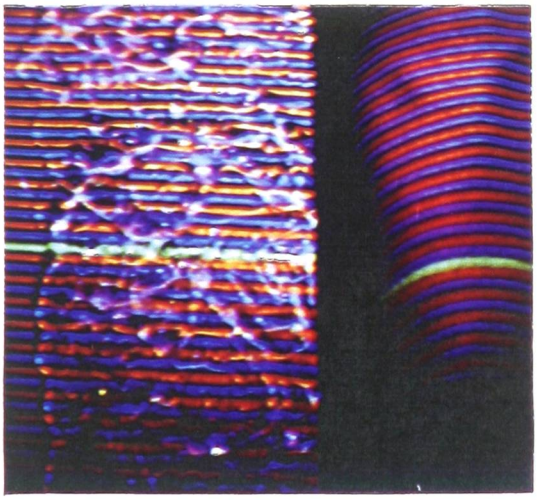

Fig. PIV.3: Specular reflections partly eliminated by a polarising filter

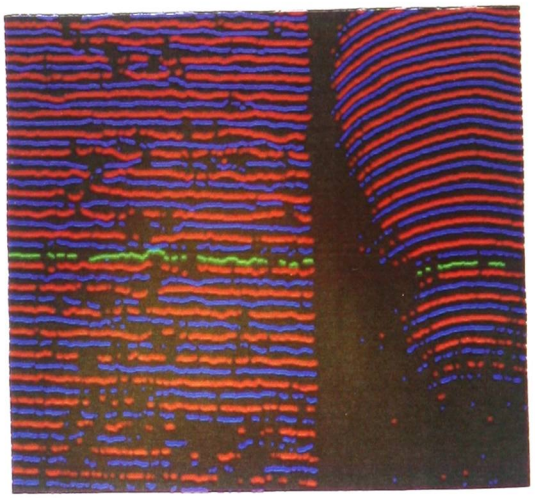

Fig. PIV.4: Stripe centres extracted from figure PIV.3

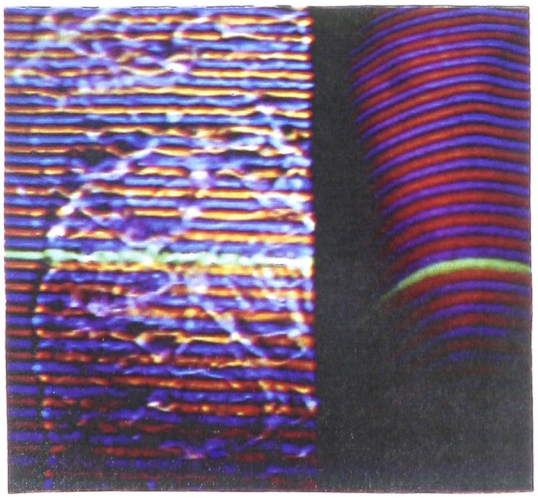

Fig. PIV.5: Specular reflections eliminated by two polarising filters at camera and projector

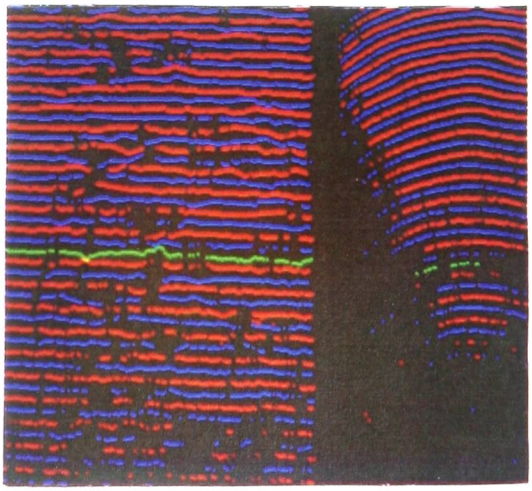

Fig. PIV.6: Stripe centres extracted from figure PIV.5

Plate V: Flexible Wounds and Automatic Ulcer Detection

Fig. Pv.1: Flexible pressure sore at the coccyx.

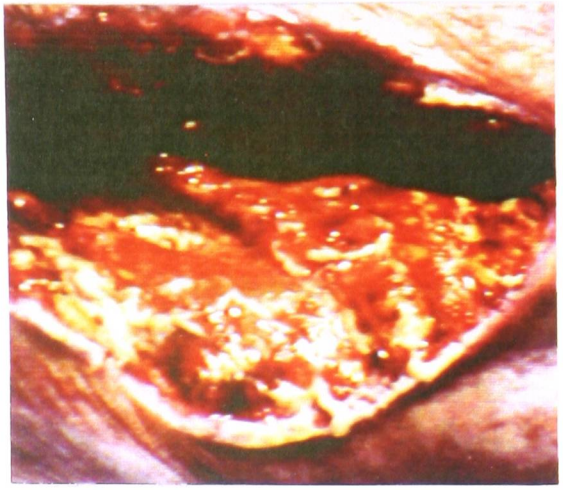

Fig. Pv.2: A flexible operation wound at the abdomen

Fig. Pv.3: Image of a leg ulcer

Fig. Pv.4: Leg ulcer of Pv.3 with ulcer automatically detected and marked (blue)

G: Discussion

The previous chapters gave a description of the hardware and software which is used with this particular instrument, tested its performance by some experiments and analysed a number of error sources which influence the results of the measurement process.
In this chapter the strengths and weaknesses of the three dimensional measurement method by colour coded structured light are discussed with regard to the intended application of the method as a means to measure area and volume of skin ulcers and pressure sores.

- In a first section, G.1, the effectiveness and performance of the most important single procedures of the measurement process are examined.

- A second section, G.2, discusses the combined performance of the single procedures with regard to accuracy, capabilities and restrictions of other competing, conventional methods.

- Section G.3 assesses the potential value of the method to the physician in the light of the above discussion and experimental findings. It reviews practical experiences achieved with the instrument.

G.1 The Main Procedures of the Measurement Process

G.1.1 Digital Filtering

Since the raw image data in the frame memory is corrupted by a certain amount of noise the need for filtering out these unwanted components is obvious. In F.2.2.3 and F.2.3 the consequences of noisy image data on the performance of the COS-algorithm and on colour extraction are evaluated. The moving average filters in use are apparently not entirely successful in their noise suppressing abilities. This is caused by the fact that every analogue or digital filter is a compromise between sometimes opposing demands such as speed of computation, time lag, simplicity, minimised pass- and stopband ripple and small transition bandwidth.

Figure G.1 shows the unfiltered output of the camera's blue channel for a vertical scan through a set of horizontal stripes of light.

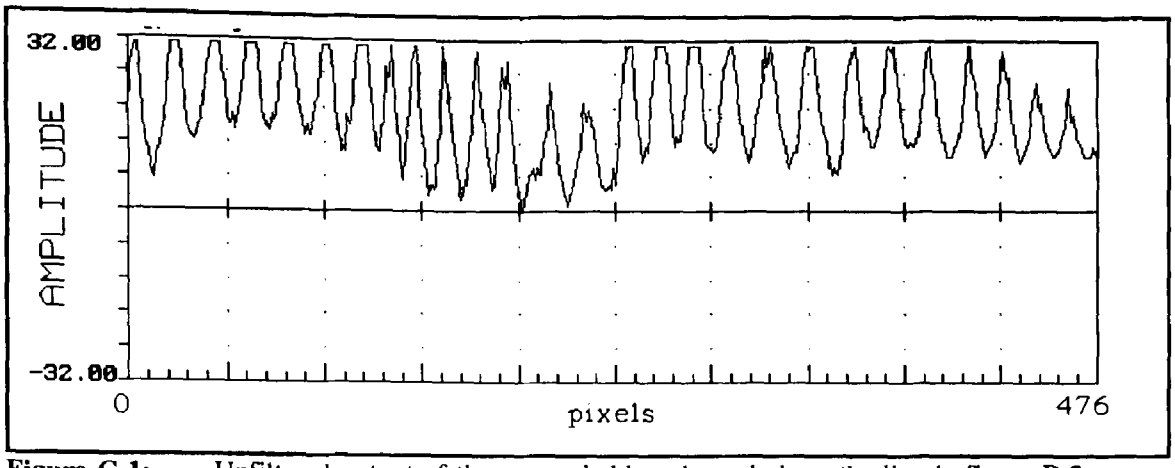

Figure G.1: Unfiltered output of the camera's blue channel along the line in figure D.3.

Note that the scan line is not smooth but due to noise slightly rippled with its peaks partly cut off due to clipping.

In figure G.1 the y-axis which is labelled in pixel units may be replaced by a time scale. Using this analogy the time domain signal may be transformed into a spatial frequency spectrum by applying a discrete Fourier transform. The spatial frequency spectrum is useful to find suitable filter parameters. By analysing the frequency spectrum of several typical scans through striped images the filter parameters may be chosen in order that the low frequency information about the stripes is preserved but noise is suppressed. The spatial frequency spectrum of the scan in figure G.1 is shown in figure G.2.

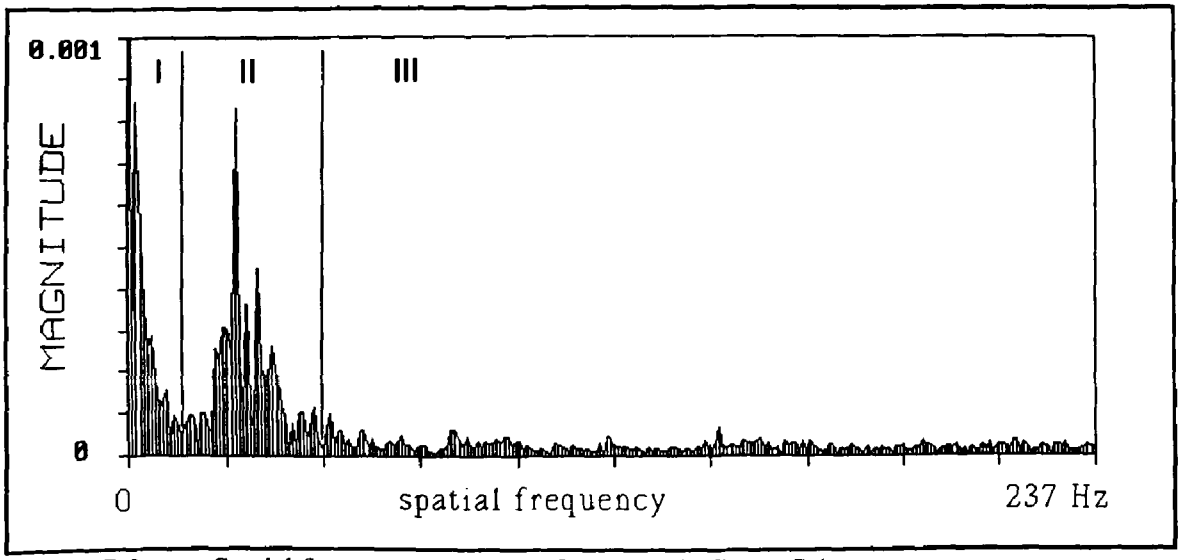

Figure G.2: Spatial frequency spectrum of the scan in figure G.1

The spatial frequency spectrum has three prominent areas: in area **I** at f=0 the mean of the signal produces a considerable peak. The low frequencies of the underlying scene brightness fill the rest of area **I**. Area **II** between f=10 and f=50 Hz reflects the frequency at which the stripes occur on the surface and area **III** beyond 50 Hz indicates noise and those high frequencies produced by the sudden discontinuities in the time domain signal where clipping occurs.

A filter which suppresses frequencies beyond approximately 50 Hz may be of relatively low order as no sharp decay in the transition band is required and some ripple in the passband may be tolerated. As an example figure G.3 shows the characteristics of a second order Butterworth low pass filter with a bandwidth of approximately 40 Hz, transition bandwidth of 40 Hz and a stopband attenuation of 10 dB.

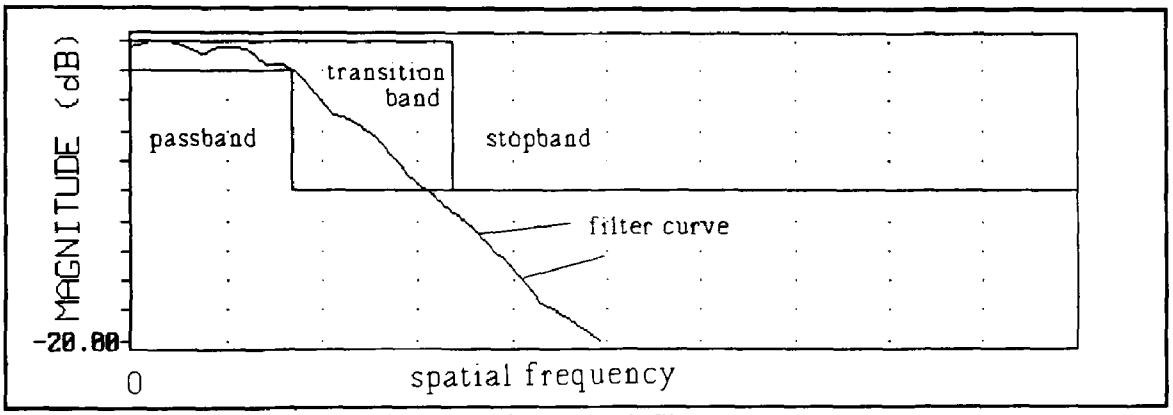

Figure G.3: Characteristic of a 2nd order Butterworth filter

A standard filter design procedure [117] (p.54 ff) or a filter design software package may be used to realise the filter in figure G.3 by choosing the parameters for the general pulse transfer function G(Z) and the final implementation into a software routine.

For the above example the following loop, written in the C language, is a digital representation of an analogue 2nd order Butterworth filter:

```
for(i=2; i<476; ++i)
  {
  y[i]=C*(x[i] + 2*x[i-1] + x[i-2]) + 1.177*y[i-1] - 0.428*y[i-2];
  }
```

where x[ ] is the array of the unfiltered input data and y[ ] is the array of the filtered output data. y[0] and y[2] are 0.

The result of this filtering process is shown in the Fourier analysis of the output signal in figure G.4. Those parts of the frequency spectrum which are located beyond approximately 60 Hz are successfully suppressed. The result is better than the one obtained with the moving average filter which is in use with the current programme.

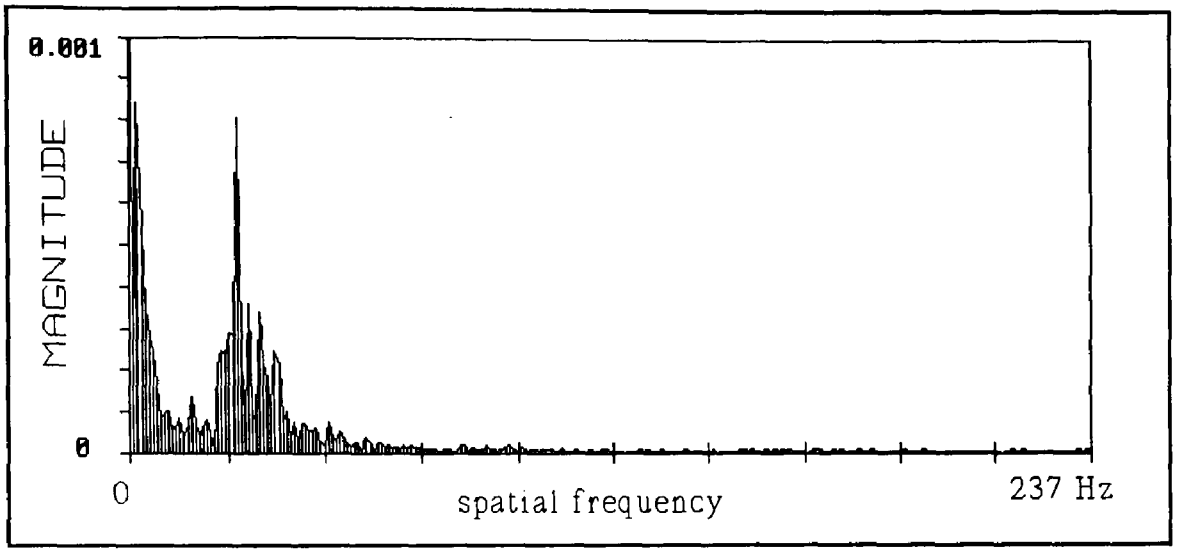

Figure G.4: The frequency spectrum of the filtered output

The time domain scan in figure G.5 makes the improvement in signal quality even more obvious. The clipped plateaux of figure G.1 are now smoothed and the curve is significantly less rippled indicating reduced noise.

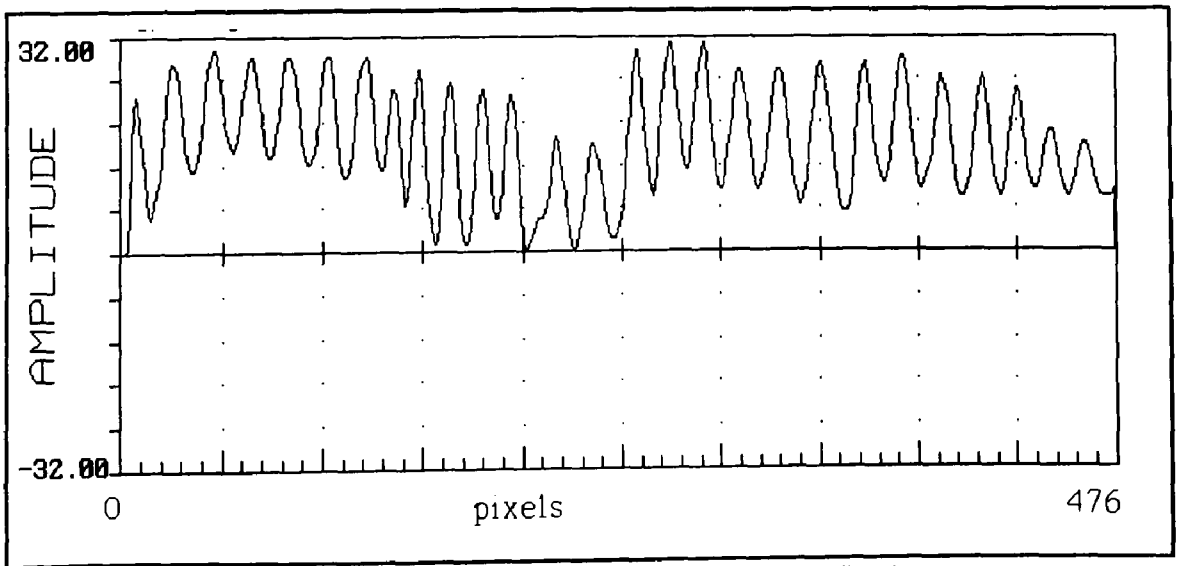

Figure G.5: The output signal of the camera's blue channel after filtering

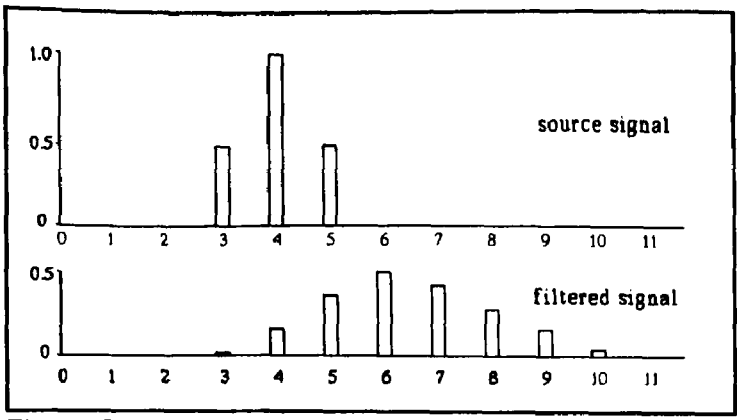

Figure G.6: The time delay caused by a Butterworth filter

The main reason why the Butterworth filter is not used is not immediately apparent: the Butterworth filter, like many other filters inevitably produces a frequency dependent phase shift between the input and the output signal. As a result the peaks in the filtered output signal are not longer at the same position as in the input signal. Figure G.6 illustrates this effect. The stripe appears broadened, dimmed and shifted. The shift of the stripe causes errors in later processes where its position is used as a base for calculations. The shift caused by the Butterworth filter which is used in this example is not correctable by subsequent calculations. A way to overcome the problem is the use of filters which do not cause time delays or have a constant, calculable delay that may be used to correct the result.

Bessel filters, for example, have a constant time delay for all frequencies but consume much more computing time than other filters. The speed of computation for the moving average filter is the main reason why this filter is in use.

A median filter also has no time delay and is fast to compute. Its performance is almost as good as the moving average filter but it does not smooth the clipped plateaus in the peaks of the stripes and its noise reduction properties are slightly worse.

Table G.1 shows the computing time for stripe extraction in an average stripe image with the current equipment.

FILTER	no filter	mov.aver.	median	Butterworth	Bessel
COMPUTATION TIME	48 sec	59 sec	63 sec	193 sec	260 sec

Table G.1: Comparison of the computation time for stripe extraction by four different digital filters.

G.1.2 Stripe Detection

The two stripe detection methods introduced in this work, dynamic threshold and subtraction methods, are much more sensitive and error tolerant than conventional methods (see experiments in E.2). Nevertheless their performance is far from perfect. Both algorithms have increasing difficulties when the images of the stripes degrade from their optimum shape.

Stripes may not be detectable if they become too **dim**. A combination of a camera with a higher dynamic range and a projector with a brighter light source would significantly enhance the performance of the stripe detection process.

Widening of the stripes due to scatter within the skin or due to the angle between the surface and the stripe of light also causes problems in stripe detection. If the stripe detection algorithms are altered to accept these wide stripes the chances of misdetecting other features which are somehow similar to a broad stripe (e.g. small bright areas on the skin) also increase. This problem may be eased by using a slide with thinner stripes. Again, a brighter light source is necessary.

Too little **distance** between the stripes may also endanger their detection. This problem might be overcome by more sophisticated programming, which at present is very straightforward and does not accept stripes which are less than 15 pixels apart. This is mainly a precaution to ensure the accuracy of the centre of stripe finding algorithm but further investigations may reveal that the benefit of increased stripe detection performance is worth the penalty of reduced accuracy.

G.1.3 The COS Algorithm

The finding of the centre of a stripe by calculating the centroid of specific parts of the brightness scan is a well known approach. First mentioned by Takagi and Hata in 1987 [122] it spread fast and is now a well established tool for the structured light technique. Its accuracy is definitely higher (10 times or more) than any of the stripe thinning approaches proposed so far.

The finding of the centre of a stripe is handicapped by three possible sources of error: varying reflectivity of the measured surface, the definition of the boundary of a stripe and the gradient of the stripe with respect to the cross section used for the calculation. In the present version of the measurement process the treatment of all three error sources is not entirely satisfactory.

The compensation of **varying reflectivity** of the observed surfaces is not possible with the current hardware arrangement. In H.2.1 a method to overcome the problem is suggested. At present the amount of error introduced by varying reflectivity of the surface is reduced by the dynamic threshold that maintains the true width of a stripe of light and the similar ability of the subtraction method. The **boundaries of the stripes** are approximately conserved but a residual error is inevitable.

The **gradient of a stripe** with respect to the cross section scan used for centroid calculation is not at present taken into account. An ideal cross section through a stripe should always be perpendicular to its run, i.e a horizontal stripe of light should be scanned exactly vertically. Due to the shape of the measured surface the stripes deviate in some areas from the ideal horizontal run. As a result the cross section through it becomes wider, which decreases the likelihood of detection and increases the error in centre calculations.
A computing procedure which considers this effect would need to operate in two stages: a first stage to establish the slope of the stripe at a given position and a second one that actually calculates its centre. Compared with the present approach such a procedure triples the length of the programme code and increases tenfold the computing time for stripe extraction and centre calculation from at present 1 minute to approximately 10 minutes per frame. A faster computer with the capability of storing whole images in its main memory or a more sophisticated frame grabber card with on-board computing abilities would overcome this obstacle.

G.1.4 Automatic Ulcer Detection

Automatic ulcer detection is desirable to eliminate the influence of errors which are caused by the operator of the instrument when manually defining the boundary of an ulcer. Figure PV.3 on plate V at the end of chapter F (page 148) shows an example of such an automatic ulcer detection. The algorithm decides whether or not a certain pixel belongs to the wound by calculating its position in the RGB-colour cube (see figure D.5 in section D.4.2) where particular regions are defined as "ulcer colours". In this example the colour of the wound is notably different from the colour of the skin and the boundary is sharp and clearly detectable.

Thus the ulcerated region can be detected with high precision. The only problem is caused by specular reflections which corrupt the colour information. The resulting holes in the detected area may be identified and closed by subsequent image processing as long as they are entirely surrounded by detected area.
Some small areas of the skin may show colours which are very similar to those of the ulcer and the detection algorithm might misinterpret them as ulcer areas. The areas are normally small and insulated from each other and thus easily to detect and to eliminate.
Problems arise when the colour of the skin becomes very similar to the wound in large areas. This may happen due to inflammation or by blood and other wound fluids spreading into healthy areas of the skin. In such cases automatical wound detection is difficult or even impossible. Thorough cleaning of the lesion prior to measuring solves the problem but often may be not advisable due to medical reasons.

An automatic ulcer detection algorithm can only be an additional option to the existing programme. It may be possible that trained neural networks are able to decide whether a wound can be detected automatically but unless this capability has not been established a human operator has to decide whether the area of the ulcer should be defined manually or by automatically.

G.1.5 Surface Reconstruction

The surface reconstruction algorithm by cubic splines is the core process of volume measurement. The experiments in E.3 show the superiority of the spline method over other interpolation methods for the task of skin approximation.
The cubic spline is only one member of the family of splines. Some other splines deserve a closer investigation with regard to their suitability of virtual skin reconstruction.

- **Splines of higher order**, i.e. of fifth degree or higher, oscillate more than cubic splines. The dashed line in figure G.7 shows such a spline of fifth order. It is definitely less suitable for surface reconstruction than its cubic relative. Furthermore its computation consumes much more time and the programming code is more complex.

- Splines that do not pass through the measurement points but approximate a **best fitting curve** on the base of a fitting algorithm (e.g. least square method) run into the same difficulties as the bezier approximation in figure E.1 shown in section E.3. They produce large errors when the surface to be reconstructed is curved.

- A different class of splines are **generalised cubic splines**. In contrast to the common cubic spline they may also use functions other than polynomials of third order for the piecewise interpolation process. The functions are twice continuously differentiable and the cubic spline is only a special sub-class of the generalised cubic splines.
  Generalised cubic splines may also introduce a special tension parameter p_k that simulates a pulling force at the end of the interpolated curve. This is shown for different values of p_k in figure G.7. A high value for p_k eliminates unwanted inflection points in the curve but also generates sharper corners.

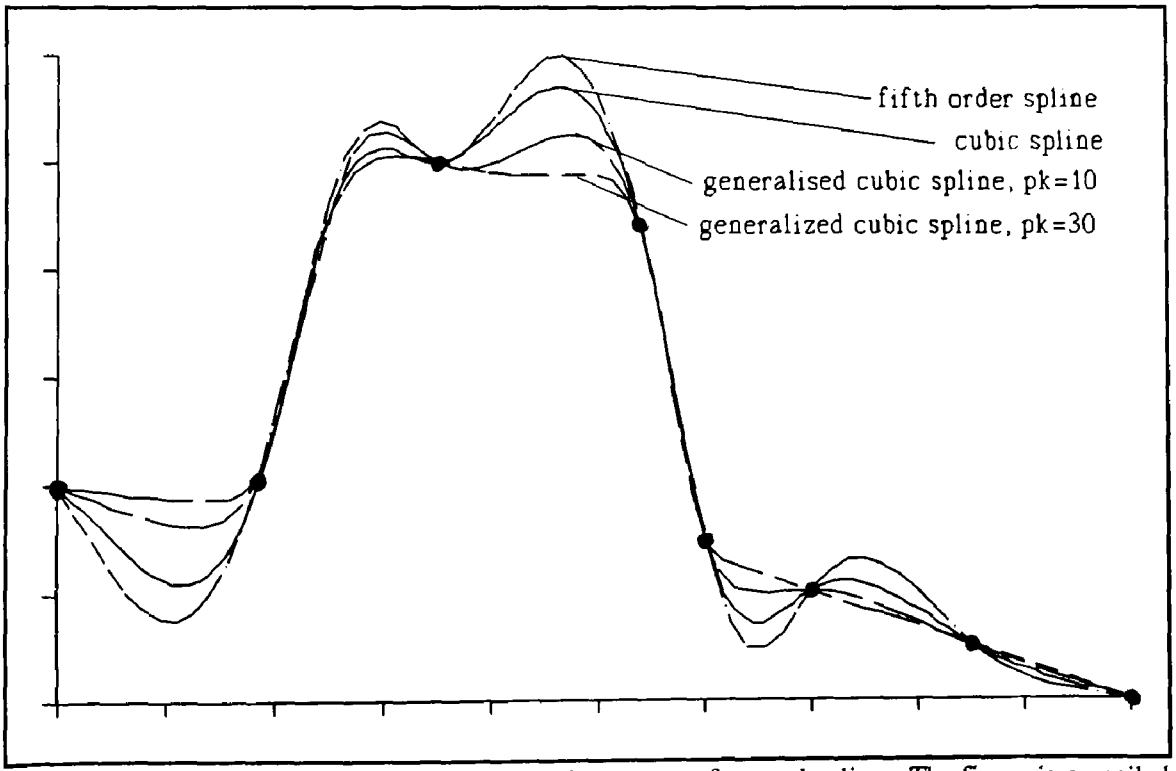

Figure G.7: A comparison of the interpolation curves of several splines. The figure is compiled from figures 40 and 55 of [117]

Generalised cubic splines offer vast opportunities for the virtual reconstruction of surfaces and a future investigation into their potential is definitely worthwhile. At present there is not enough data about ulcerated surfaces available to allow statements about their usefulness.

- A special variety of splines are the two dimensional cubic splines which interpolate over a whole grid of measurement points rather than a one dimensional slice. The major disadvantage of the two dimensional spline interpolation is the huge demand for computer memory and computing time. Future research should nevertheless take the bicubic splines into consideration since they are a much better approximation to the three dimensional reality, especially as they may be programmed using generalised bicubic splines which also offer the opportunities to apply a tension factor p_k to the generated surface.

G.2 Comparison of the Performance of the Measurement Method with Existing Methods

G.2.1 Precision and Accuracy of Area Measurements

For an assessment of the performance of the measurement method presented in this work it is necessary to draw a comparison with other approaches for measuring area and volume of ulcers and pressure sores which have been tested in clinical trials.

area/cm²	structured light	stereophoto-grammetry	direct tracing	photography
12	7.5%	1.8%	10.5%	11.5%
20.5	5.5%	1.9%	8.6%	11.0%
32.6	4.5%	2.0%	10.2%	11.0%
35.4	4.0%	2.2%	6.3%	12.0%
63.8	3.5%	1.7%	6.7%	11.1%

Table G.2: Comparison of the precision of four area measurement methods

Table G.2[36] compares three established area measurement methods with the structured light technique. The percentage figures in the table reflect the precision (standard deviation of single readings around their mean, repeatability) of the measurements and are presented as the 95% confidence interval which is approximately 1.96 times the standard deviation of the measurements.

Notably the stereophotogrammetry results are significantly better than the results obtained with the structure light method. This may be attributed to the better resolution of the colour slides in use with the method, compared with the resolution of a monitor screen. From the slides an operator manually extracts the boundary information in a process analogue to the one of the structured light method where a monitor is used[37].

Another cause of the better precision is the smaller quantisation interval between the measurement points. Furthermore the method was first introduced in 1976 by Beard and Dale [18] and has had more than 10 years to develop.

---

36 The figures for the three other methods are extracted from table 2 on page 441 [26].
Equal to the experiment in E.4.1 which delivers the figures for the structured light method the figures for the three competing methods are obtained from measurements on models thus allowing for direct comparison.

37 This extraction takes 20 minutes (see B.1.3.4). The same process with the method proposed in this work takes approximately 1 minute.

The structured light method definitely produces better results than the direct tracing or direct photography method. The photographic method does not only perform worst in terms of precision, but the absolute accuracy is also limited since the three dimensional shape of the measured area can not be taken into account. The average accuracy is 11.4%. On small areas it may even reach 43%.
The accuracy figures for the other methods are in line with the precision figures: according to the experiment in E.4.1 the accuracy results of the structured light method have a standard deviation always of less than 2% of the area. This translates into an accuracy of less than 4% in the 95% confidence interval. The figure for the stereophotogrammetric method is 0.81%. The direct tracing method produces similar results to the photographic method: 11.7%.

G.2.2 Precision and Accuracy of Volume Measurements

For **volume measurement** the picture is similar. On ulcer models the stereophotogrammetry method produces an average precision of 1.7% (95% confidence interval) while the structured light method precision ranges from 4% to 10% for most volumes. The results for three different volumes are shown in table G.3.

volume / cm^3	structured light	stereophotogrammetry
10.2	5%	1.3%
26.1	4%	1.1%
60.4	4%	2.2%

Table G.3: Comparison between the precision of the structured light and the stereophotogrammetric method

The figures are not directly comparable since the precision of the structured light method is also a function of the area of the lesion (see figure E.5 in section E.4.2.2) whereas no such information is available from the source of figures for the stereophotogrammetric method[38].
The third available volume measurement method performs worse than the structured light method: clinical trials with the transparent film method of Berg delivered a precision of approximately 22%[39].

---

38 The figures are extracted from table 3 on page 441 [26]. Figures for the structured light method refer to areas of 30, 50 and 70 cm^2.

39 The figure is calculated from the data of sore 4 (with a volume of approximately 17 cm^3) in figure 2 on page 1446 of [19].

The figure for measurements on plaster models might be better since Bulstrode et al. observe that the results of clinical trials are always worse than those obtained from models.

For the transparent film method accuracy figures for volume measurement are not available. The other two methods produce similar figures: the structured light method produces measurements with a standard deviation of less than 3% of the volume, approximately 6% deviation in the 95% confidence interval. Bulstrode et al. claim that their stereophotogrammetric method achieves a mean accuracy of 5.2% on models.

Apart from the higher accuracy and precision of the stereophotogrammetric method it has at present the advantage of being able to measure a greater range of areas and volumes. Area measurement is possible from 0.1 to 140 cm^2 compared with the range of 10 to 70 cm^2 where reliable results are obtainable with the structured light method.
Volume measurements are possible from 0.01 to 650 cm^3 with the photogrammetric approach while the structured light method is at present restricted to a range from 10 to 60 cm^3.
Further developments of the instrument should therefore focus on both increasing the precision and the range of the instrument.

The greatest disadvantage of the stereophotogrammetric approach is the time consuming process of film processing before the actual measurement scan can take place. The scanning of one wound requires an additional 20 minutes. The results of the structured light method in contrast are available after less than 5 minutes (with a 286 processor at 10 MHz).

G.2.2 Capabilities and Restrictions

In spite of its prototype status the current version of the instrument already performs better in many areas than most of the traditional measurement methods. At present the instrument is only able to handle a restricted variety of lesions. Especially dry wounds with gently sloping walls and clear boundaries on a homogeneously curved and inflexible limb which are fully visible are suitable for measurement. If all the conditions

- dry wound
- clearly defined boundaries
- inflexible limb
- area/volume ratio greater than 1
- gently sloping walls
- homogeneously curved limb
- full visibility
- area smaller than 70 cm^2

are met the measurement results are reliable and accurate (see figures E.3, E.4 and E.5). The further one or more of the above conditions move away from this ideal state the more problems arise.

Therefore there is a huge scope for further developments of the method. The following paragraphs identify a number of problem areas where the instruments either meets its principle limits or encounters problems which may be overcome by future developments.

- **Visibility.** The instrument's major limitation lies in the fact that it is unable to measure surface features which are either invisible to the camera or not accessible to the stripes of the structured light projector. Ulcers sometimes undermine the epidermis, forming cavities. Measurement of these cavities is impossible with any optical measurement method. In such a case the only way to obtain a result is by guessing the percentage of invisible cavity and add it to the visible and the measurable volume. This is the only situation where the method of filling the wound with saline may produce more reliable results.

- **Occlusions.** Similar to the above problem are occlusions. They occur when prominent surface features such as the rims of a lesion intersect with the planes of structured light so that they can not illuminate the base of the ulcer. A triangular shaped region of the ulcer's volume is then excluded from the calculation. Again it is the task of the operator to assess the amount of error and add it to the measured value. The percentage of error is smaller than with hidden cavities and depends on the size and shape of the lesion.

- **Shape of the wound.** When the edge of an ulcer slopes more than approximately 30 degrees other problems arise. As long as the angles are not too steep no occlusions occur but two other consequences are likely. They depend on the orientation of the slope toward the projector. The surface may be tilted away or towards the projector.
  - In the first case where the surface is tilted away from the projector, the stripes may intersect the surface under an angle of less than 10 degrees. Their image expands and becomes darker. As a result the COS-algorithm may be unable to detect stripe centres any longer.
  - In the second case where the surface is tilted towards the projector the images of the stripes are shifted very closely towards each other and as a result become extremely bright. Due to the scattering properties of the skin the stripes begin to blur into each other and the stripe detection algorithms can not distinguish them any longer.

  Both cases are partly dealt with by the linking algorithm which tries to interpolate missing surface points (see D.4.4). This interpolation introduces errors and limits the overall accuracy of the measurement. In order to reduce the interpolation error the algorithm does not try to interpolate over more than three stripes. If the gap is bigger the interpolation attempt will fail and the measurement process has to be repeated.

- **Projector problems.** A minor restriction is imposed on the instrument due to the limited brightness of the projector. In bright daylight, sunny places and close to windows for example, the ambient brightness limits the contrast between surface areas illuminated by a plane of light and those which should stay dark. In rooms with normal artificial lighting this problem does not arise.

  Nevertheless a brighter light source in the projector could be helpful to overcome the colour crosstalk effect which is addressed in F.1.2.2. A brighter light source in conjunction with a set of narrow banded filters might resolve the crosstalk problem and the associated accuracy problems. Narrow banded stripes of light also offer the opportunity of using a greater number of different stripe colours thus enhancing the stripe coding possibilities and consequently the robustness of the stripe labelling algorithm. In H.2.1 a method is proposed to establish such a projector for multicoloured narrow banded stripes of light.

Another problem is caused by the fact that the stripes of light are projected onto the surface to measure under an angle of approximately 45 degrees. As a result the stripes can not be focused accurately over the entire field of projection. As an additional complication the stripes at the far side are broader, more dim and have a greater distance from each other. A simple solution for this problem is the use of a special *perspective control lens* which simultaneously counteracts all these effects.

- **Specular Reflections.** The detection of stripes and the proper classification of wound colours are often obstructed by specular reflections in wet parts of the lesion. In F.1.4.1 it is shown that specular reflection can be entirely suppressed by using a set of two polarising filters. The current version of the instrument is incapable of avoiding specular reflections. Due to the limited brightness of the projector only one polarising filter is used which only slightly reduces the influence of specular reflections.

- **Field of view.** The present version of the software is not capable of merging information from pictures taken from different angles. This ability should be included in further developments of the instrument. Several techniques for merging pictures from multiple views are known from research into two camera stereo systems. Since the implementation of the specialised algorithms is time consuming and nothing new may be learned from copying these existing techniques their adaption for this task is not considered to be worthwhile in the context of this work. In a fully developed version of the instrument, however, this feature should be included as ulcers may stretch around a limb and are only partly visible from any point in space.
  Instead of taking two sets of pictures from different angles, one after the other, this may be done by an additional second sensor set. This would double the costs and the weight of the sensor and should be considered with caution.
  At present the field of view is restricted to a rectangle of 12 cm x 15 cm. The maximum size of wounds measurable with the instrument is restricted to an area with in a rectangle of approximately 10 cm x 8 cm because a sufficient amount of healthy surface outside the wound has to be available as a base for surface reconstruction.

- **Boundary definition.** The accurate definition of both the boundary of the lesion and the boundary of the area which is affected by it are of pivotal importance for the performance of the measurement process. Automatic detection of these areas could restrict the error which at present is introduced by the manual definition process. In chapter H.2.1 such an automated process is proposed.

The above limitations reflect the present status of the instrument. Some of the problems may be solved by further development. Projector problems, specular reflections and an insufficient field of view are manageable by hardware alterations while increased accuracy and stripe detection are achievable by improvements in the software.

Some proposals for these alterations and improvements are made in H.2. Only the problems caused by limited visibility and the shape of the wound are intrinsic to the method itself and can not be overcome.

G.3 Review of Practical Experiences

During the development process of the system a total of 25 different ulcers and pressure sores were measured. It appears that even the present prototype version of the instrument with its many cables and separate components is easily installed within few seconds at the patients bedside. An additional benefit is the small size of the hand held sensor which allows uncomplicated access to any part of the patient's body.

The measurement of leg ulcers appears to work without problems as long as the ulcers do not extend around the leg. With the current software it is not possible to merge the extracted surface information from multiple views at different angles into one.

Sores in the coccyx region are more difficult because they are usually deep and have a small open surface. As a result the rays from the stripe projector are not focused over the entire depth range and parts of the ulcer walls are not illuminated. If in such a case the software is incapable of producing a complete surface map of the sore the operator is often able to assist the system by manually editing the extracted stripe pattern. This manual interference involves a great deal of guesswork and the resulting figures for area and volume of the wound must be treated with some care.

The manual editor is of great value if only relatively small gaps, which are often caused by specular reflections, in the extracted stripes appear (between 7 approximately and 20 mm) which the software is unable to close. Small gaps may be closed by an operator with a steady hand with astonishing accuracy. Tests with smooth surfaces where such gaps are simulated reveal that the deviation from the real stripe position is rarely more than 2 pixel widths (approximately 0.6 mm).
After manually establishing the shape of a coccyx sore the system always encounters a second difficult stage when it tries to reconstruct the former healthy surface. The result is often obviously wrong, caused by the complicated shape of the coccyx area. For the measurement of coccyx pressure sores the usefulness of the instrument is therefore considerably restricted.

H: Conclusions

H.1 General

The instrument which is described in this work is the physical manifestation of a variety of principles, methods and techniques. It is the combination of a number of well established and well understood phenomena rather than the invention of a single new concept that constitutes the value of this measurement technique. The principles of optics, biomedical facts about the skin and human perception, solid state physics, computer programming techniques and knowledge of electronic engineering are the main ingredients for the realisation of the described concept.

The main objective of this work was the design of an instrument for the three dimensional measurement device for the non-contact measurement of leg ulcers. This aim could be achieved and in the course of the research undertaken it appeared that other medical objects such as pressure sores and operation scars may also be measured.

Apart from simply applying, adapting and amalgamating well known approaches into one concept two new suggestions are made and implemented in the instrument: the recognition of stripes of light by two adaptive extraction techniques and the reconstruction of the ulcerated area by spline algorithms.
Both techniques are more capable, flexible and accurate than approaches known at present. The full potential of both techniques has not yet been fully exploited and some work is still necessary to maximise their performance. This is described in the following section.

H.2 Future Developments and Improvements

This section establishes the scope for further developments and improvements in order to increase the capabilities and the possible value of the instrument to the physician. Based on the experienced restrictions and limitations of the instrument the following list of proposals may be used as a guideline for further research.

H.2.1 Projector Improvements

The first alteration concerns the problems caused by the non-perpendicular projection of the stripes onto the surface. A perspective control lens, in spite of being more complex and expensive than the projecting lens which is at present in use, eliminates the disturbing effects described before.

A second improvement to the projector which does not require a massive change in the structure of the instrument or major amendments of the controlling computer programmes is the replacement of the halogen tungsten lamp by an electronic flash. The flash needs to be synchronised with the frame rate of the camera and requires an additional flash-time control circuit to ensure the correct exposure of a single frame. Both measures are relatively simple to impose as some off-the-shelf flashes are equipped with both an internal exposure control circuit and a connector for external triggering.

A flash does not require the strong and heavy power supply which is necessary at present. This would reduce the costs and the complexity of the system. An additional benefit is the increased brightness of the projected stripes of light. Greater brightness allows the introduction of two polarising filters with perpendicular polarisation axis to eliminate specular reflections and to reduce the sensitivity of the instrument to bright ambient light. Furthermore it allows the projection of narrower stripes thus avoiding most of the problems which are caused by inappropriate wide stripes.

A complete redesign of the projector is inevitable in order to suppress the colour crosstalk effect which is caused by the broad banded filtering properties of the stripe producing slide. The idea is to further reduce the bandwidth of the three colours which are used at present by a set of three small banded resonance filters. The resonance filters are mounted on a fast spinning flywheel which is located between the slide and the projector's lens. The wheel rotates at the frequency of the camera's frame rate so that the camera's CCD array is exposed to light of all three colours during the acquisition of one frame. The wheel also has to be synchronised with the mentioned above flash. Each time a filter on the flywheel passes the optical axis of the projector a flash must be produced. Tungsten lamps can not be used since they are not bright enough to compensate for the reduced bandwidth and the dimming caused by double filtering.

This arrangement produces three major advantages

1. Totally elimination of channel crosstalk. Associated problems such as lack of accuracy are consequently also avoided.

2. If the same flywheel is used to produce the picture without stripes the dynamic threshold method will perform perfectly. At present the method is handicapped by the differences in the spectral distribution of the light emerging from both images. As a result the picture without the stripes is not an accurate description of the underlying reflectivity of the scene for a certain colour. This problem does not appear if the spectral distribution of the light which is perceived by a specific colour sensor in the CCD array is identical for both pictures. As a result the performance of both stripe detection and accuracy of centre detection should improve significantly.

3. The lack of any colour crosstalk enables the possibility of using all three colours instead of only two for colour coding thus improving the robustness of the labelling algorithm. Even the projection of multiple reference stripes is possible by using different unique sequences of the three colours.

As a result of the projector improvements described above a set of highly defined stripes is projected. The clear boundaries in the spectral and the space domain drastically reduce the majority of disturbing influences which at present cause a great collection of errors.

One disadvantage of the flywheel projector is that the picture without stripes is no longer suitable for assessment by a human observer since most of the colour content of the image is lost. Extraction of the ulcer's colours will also prove to be difficult. Recent progress in the frame grabber technology for personal computers fortunately results in greatly increased memory space for the storage of digitised pictures.

Frame grabbers with a storage capacity of four or even more pictures are now available at reasonable prices. A four picture frame grabber card, for example, may be organised as follows:

Frame 1: Image of the ulcer, illuminated with white light. Source of information for colour extraction and basis for assessment by the physician. May be stored on computer disc for later reference.

Frame 2: The image without stripes, illuminated by the flywheel filters. Source of the dynamic threshold for stripe extraction.

Frame 3: Picture with stripes, produced by the striped slide in conjunction with the flywheel filters. Source of position information of the stripes.

Frame 4: A second picture with stripes, produced by a second, but different slide. The stripes of this slide are located at the same positions as in the first slide but with the colours shifted to different positions. At a given stripe position the combination of the colours of the two stripes in frame 3 and 4 allow the (time-) coding of the stripes. Since 'no stripe' is also a valid information a total of four stripe colours may produce $2^4=16$ possible combinations of which only 15 are usable since the combination of two 'no-stripes' does not deliver any position information.

The hardware arrangement outlined above would further improve the performance of the labelling algorithm at the costs of slightly increased image processing time.

H.2.2 Camera Improvements

CCD cameras are capable of detecting electromagnetic waves in the near infrared up to a wavelength of around 1000 nm. This capability might be exploited to obtain more information on the status of healing of a lesion, an approach which follows the experiments of Afromowitz et al.[2,3] on burn wounds. The significance of the results obtained from burn wounds might not be transferrable to ulcers and unless real experiments with such an IR-sensitive camera are made the possible value of such an approach is only speculative.

If an IR sensitive camera is used the benefits obtained from using visible light are still available. An infrared-cut filter may be used to produce pictures in the visible spectrum. A visible band filter may be used to produce pictures from the near infrared spectrum. Using the infrared picture it might be possible, for instance, to assess the amount of blood perfusion in certain parts of the observed skin. Information which is surely of some value to the physician.

H.2.3 Software Improvements

A number of measures may be taken to improve the performance of some software algorithms.

- The matrix which represents the measured surface within the computer memory has meshes with an approximate side length of 2.2 times 2.2 mm. The distance in y-direction is given by the positions of the stripes on the measured surface. It is possible to double the amount of matrix rows by interpolating between the existing rows.
  The distance in x-direction may be decreased without interpolation purely by increasing the amount of columns that contribute to the matrix. A doubling of both rows and columns would significantly reduce the amount of quantisation error which at present is experienced especially with objects of small area and volume.
  The calculation time for such a matrix with finer grating would increase by around three seconds with the current equipment.

- Both stripe extraction algorithms may be improved further. The set of rules which exist within the subtraction algorithm may be fine tuned or even be replaced by a completely different approach. An extraction method which, for example, uses the analogy of a ball that roles along the scan which is produced by subtracting the red from the blue camera channel might be more successful. The imaginary ball gets stuck in every trough of the scan thus detecting red stripes provided that certain parameters such as its size are carefully adapted.
  The dynamic threshold algorithm may be improved by considering detections at previous scan lines. At these positions the search in the following scan lines may be intensified.

- The accuracy of the centre of stripe finding algorithm may be improved by a two stage process. In the first stage the orientation of the stripe at a given position is established and in the second step the stripe is scanned perpendicular to this orientation rather than always vertically as at present.
  The disadvantage of this method lies in its significantly increased computing time.

- The colour extraction algorithm that sorts the lesions colours into three groups in order to classify the ulcer has to be deduced through a larger number of samples. The present algorithm incorporates the knowledge obtained from only 25 ulcers and pressure sores. The value of the classification scheme itself is currently subject to some discussion, partly because the current method uses polaroid instant prints with its dubious colour reproducing abilities.

- A software development which is not directly related to the measurement software is the creation of a data management system that allows storage, search and retrieval of pictures of ulcers and associated area, volume and classification figures together with some selected patient data.

- Finally the process of volume calculation by adding up triangular shaped bodies may be simplified by calculating areas enclosed by the spline curve and the measured surface using, for example, Simpson's rule. This would make the calculation much faster and more accurate since the quantisation error could be reduced significantly.

The above list makes it obvious that there is a significant scope for further improvement of the software. The improvement of both hardware components and software procedures might allow the structured light measurement technique to achieve at least the accuracy and precision of the stereophotogrammetric methods which at present is the most accurate method available.
The combined benefits of high accuracy and fast measurements together with the opportunity of instant storage and retrieval of valuable picture information and associated patient and wound data are unique and will assist clinical research into the treatment of skin ulcers and pressure sores.

H.3 Applications and Possible Spin-Offs

A structured light measurement system that is able to deal with surfaces as complicated as ulcerated skin has possible fields of other applications as well. In the medical field the instrument was able to measure and document the size of operation scars. Two other areas where the measurement system may be used are automated assembly and documentation of environmental damage.

In the field of robot vision and automated assembly the scope for applications is virtually unlimited. Distance sensing, quality control and automated inspection of components are problems which are often encountered in automated assembly lines. For industrial use however, the present version of the measurement process is too slow. The whole measurement process is required within seconds rather than minutes. This demand can be met by implementing some time consuming core processes, e.g. stripe extraction and thinning in hardware.

Acid rain and air pollution result in a lot of damage to buildings and sculptures. A three dimensional measurement system could be of some value for conservationists to document and establish the amount of damage caused by acid rain on stone.

Further needs for three dimensional measurements exist in museums and art galleries where it is sometimes of interest to establish whether or not two sculptures were carved by the same artist. A full three dimensional representation of a piece of art may be stored in computers and transferred to other places without the need to move the valuable and often delicate objects. Such an application, however, is beyond the limits of the present version of the instrument.

The main focus of further research should nevertheless stay on the application for which the instrument has been designed. Applications in other areas would involve many changes, alterations and adaptations.

H.4 Summary

Skin ulcers and pressure sores are common in a hospital population. Accurate figures are rarely obtainable but different studies show that between 5% and 8% of all bedridden and chairbound patients develop pressure sores. Patients with pressure sores require more medical resources and stay between 3 and 5 times longer in a hospital than patients without these complications.

Skin ulcers are favoured by diseases or side effects of treatments which affect the skin. Reduced blood perfusion due to smoking, varicose veins, and damaged vein flaps reduce the supply of nutrients to the skin and certain agents such as steroids used to treat other diseases damage the structure of skin tissue. A weakened immune system is another factor which may influence the development of a skin ulcer. If some or all the above factors come together a minor injury or infection is sufficient to induce ulceration of the skin.

Skin ulcers and pressure sores are extremely painful and difficult to cure. Months rather than days are normal for the healing process. There are many different agents and methods in use for the treatment of the lesions but no single treatment procedure is generally adopted. The lack of an objective measurement method for the area and the volume of the wound makes it more difficult for physicians to compare different treatments and select the best approach for a specific lesion at a specific state of healing. This is the motivation for the development of a three dimensional measurement instrument described in this work.
Any measurement method for skin ulcers and pressure sores should be non-invasive to minimise the risk of damage or contamination of the wound. A non-contact measurement furthermore reduces the pain experienced by the patient. In addition the measurement device should be portable, rugged and simple to operate.

Based on these criteria the colour coded structured light technique has been employed as the underlying tool for measurement. To accommodate the technique to the difficult optical properties of ulcerated skin two specialised stripe extraction algorithms have been developed. Assisted by special tools such as labelling algorithms and lens error compensation calculations, structured light delivers a three dimensional representation of the ulcerated skin's surface.

The volume of the lesion is enclosed between the measured surface and a calculated surface which imitates the shape of the former healthy skin. This virtual surface is produced by cubic spline interpolation which experimentally produces surfaces similar to the shape of real skin.

Experiments and initial clinical tests prove the general suitability of the colour coded structured light technique for the measurement of skin ulcers and pressure sores. The present version of the instrument is able to measure wounds of up to 70 cm^2 where the area/volume ratio is greater than 1. If wounds become too shallow or too deep the results become inaccurate or the measurement simply fails. Special problems are encountered when the lesion undermines the skin so that the resulting cavities are no longer visible to the observing camera.
The instrument is a reliable tool for measuring skin areas which are relatively rigid, i.e. arms and legs. Parts of the body which are very flexible such as the back vary their shape with the position of the patient. A coccyx sore, for instance, may vary its volume drastically just by repositioning the patient between two measurements.

Some future research is still necessary in order to exploit the full capabilities of the method. Improvements on the hardware side include a refined version of the structured light projector in order to suppress specular reflections, improve the detectability of the stripes and to eliminate colour channel crosstalk. Together with a refined version of some software algorithms the performance and the capabilities of the instrument should improve significantly.

With an accurate and reliable instrument for the measurement of ulcers and pressure sores the physician has a valuable tool at his disposal to monitor the effects of treatment. This will enable him to quickly assess if a patient is responding to treatment and changes are necessary. The objective comparison between different treatment strategies will eventually result in an optimised regime for the management of skin ulcers and pressure sores thus reducing the enormous costs and even more important the suffering and pain in these patients.

Appendix

Published Papers Related to this Thesis:

P. Plassmann, B.F. Jones
An Aid for Reconstructing Damaged Sculptures by Estimating the Shape and Volume of a Missing Fragment
Journal of Photographic Science, March/April 1992

P. Plassmann, B.F. Jones
Measuring Area and Volume of Human Leg Ulcers by Colour Coded Structured Light
Proc. 1st European Conference on Advances in Wound Management
4-6 September 1991, Cardiff

An Aid for Reconstructing Damaged Sculptures by Estimating the Shape and Volume of a Missing Fragment

P. Plassmann and B. F. Jones

Department of Electronics and Information Technology, The Polytechnic of Wales, Pontypridd, CF37 1DL

ABSTRACT: *The authors present a non-contact automatic or semi-automatic surface reconstruction method that includes:*

i) a measurement system for 3-dimensional objects,

ii) procedures to obtain knowledge about the area to reconstruct, as well as general information about the object of interest,

ii) and specialized reconstruction algorithms.

An adequate representation of a real object is created in a computer memory using a structured light scanning system with simultaneously projected stripes of light. The method is fast and reliable, and capable of measuring the height of certain surface points within an uncertainty of 0.05% of the total size.

The system characterizes the 3-D structure of the object and determines the area of damage from colour or shading of the reflected light.

1 Introduction

The original objective of this work was to measure area and volume for a medical application: assessing the healing of a skin ulcer. Ulcers may heal from the sides or from the base, measurements of area and volume are therefore important indications to a physician.

True measurement of a cavity requires the reconstruction of the original surface. The cavity's volume is the difference between the actual measured and the reconstructed surface.

Logically a computerized reconstruction method for damaged surfaces also offers a wide range of other applications ranging from estimating the influence of acid rain eroding the stone of sculptures and buildings, to the reconstruction of broken pottery from an incomplete puzzle of parts.

Independent of the actual task, processing by a computer anticipates knowledge of at least two sets of data on the object of interest:

— information about the object's properties (those parts considered to be damaged, and those which are not)

— an accurate three dimensional representation of the object within the computer's memory.

Acquisition of this data should be fast, simple, reliable and non-destructive to the surface. The final computing of the data in order to reconstruct the surface is highly dependent on the actual task.

A method of measurement, applicable to any material, uses the technique of structured light, which was used first in 1970 by Pennington and Will.[1] Reconstruction of the original form of the undamaged object may be made by mathematical interpolation techniques. In many cases the undamaged surface is assumed to follow a cubic spline.

Paper presented at the RPS conference "Imaging Science and the Visual Arts", Bath, November 1990.

2 Method

Three-dimensional measurement is possible with a wide variety of methods. Our approach uses colour coded structured light, with the equipment shown in Fig. 1.

A common slide projector is used to project a set of coloured, parallel stripes of light onto the object of interest. A camera observes the scene from a certain angle and transmits the picture data to a computer system, where a three dimensional representation of the object's surface is calculated by simple triangulation (see Fig. 2).

The whole process of surface reconstruction is divided into four steps: image acquisition, image processing, surface reconstruction and, if required, calculation of area and volume of the damaged part of the object (Fig. 3).

3 Image Acquisition

The slide projector illuminates the scene with two different patterns, producing two pictures which are stored in the computer for later processing.

3.1 Picture one: For the first picture the projector illuminates the whole scene with a bright, homogeneous beam of light. From this picture the following information will be extracted in later image processing:

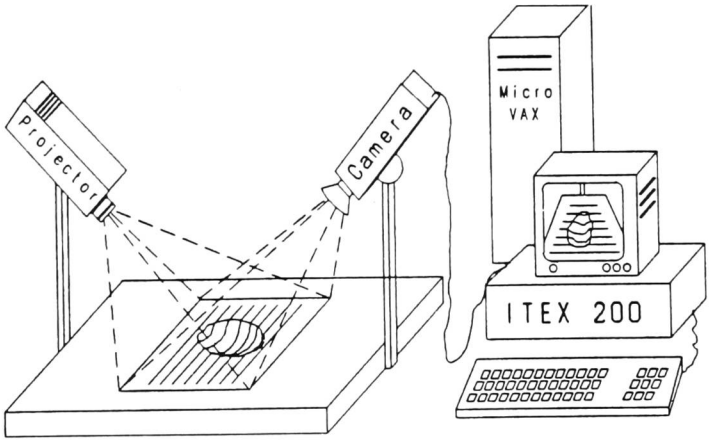

Fig. 1. 3-D structured light measurement system.

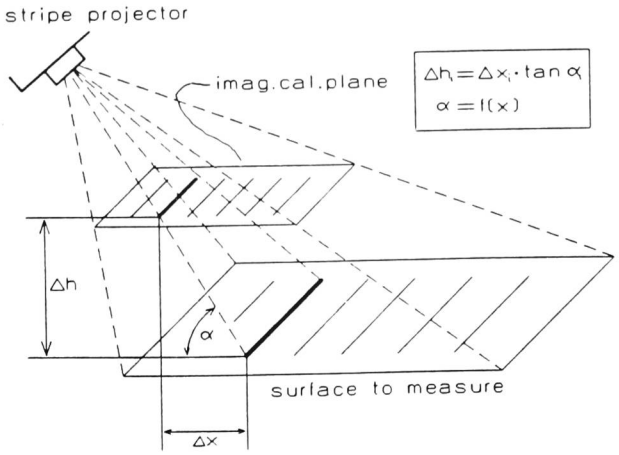

Fig. 2. Depth measurement by structured light.

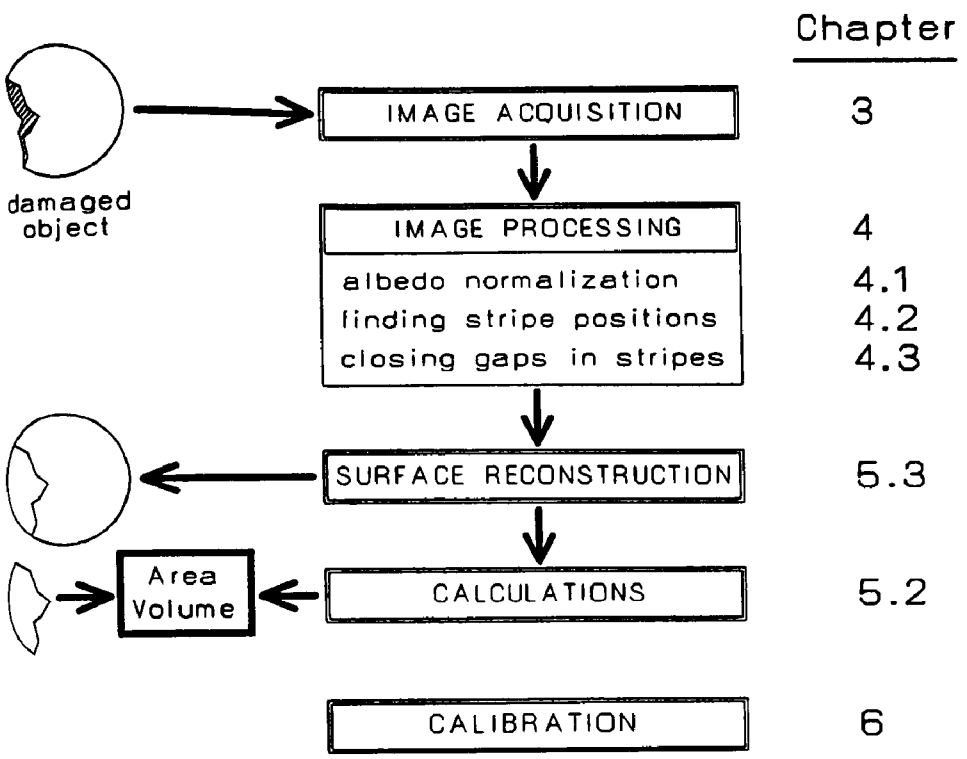

Fig. 3. Processing a damaged surface.

— Boundaries of the object
— Parts of the object to be reconstructed
— Reflectance properties of the object.

3.2 **Picture two:** This time a set of approximately 80 parallel stripes of colour coded light are projected onto the object. The term colour coded[2] describes the system's capability of recognizing the three kinds of stripes coded in the primary colours, red, green and blue. These stripes appear in order on the slide. Only one stripe is coded in white as a reference mark. The purpose of colour coding the stripes is to aid the detection of a given stripe over the object's surface. In areas where the albedo (reflectance) is small, or at edges of the object the stripes may disappear, so that an algorithm must be developed for redrawing the missing parts, and linking the right ends of the stripes together.

Speed of image acquisition is an important parameter here, because the object's position relative to the camera's focal plane must not change during the acquisition process. Otherwise the albedo normalization map obtained from picture one and the striped image in picture two are not in coincidence. Future developments will perform the image acquisition process in $\frac{1}{50}$ sec.

Taking into account the data of both pictures, depth information of the object may be obtained with the procedure described in the following sections.

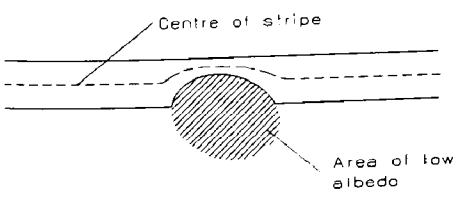

Fig. 4. A stripe of light before albedo normalization.

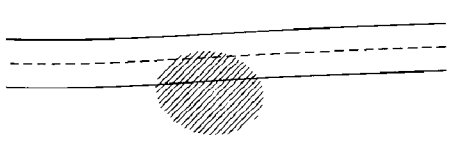

Fig. 5. Stripe of light after albedo normalization.

4 Image Processing

Image processing is a three stage task.

4.1 Stage one: Albedo normalization

Albedo normalization is a process to counteract and to eliminate the effect of varying reflectivity of the observed object.[3] The need for normalization becomes obvious when considering the following effect. Fig. 4 shows a stripe of light passing a region of low reflectivity. For later processing it is essential to find the centre of this stripe with high accuracy. It is clear that this centre will be detected at a wrong position as indicated by the dotted line.

Another reason for normalization is colour. A coloured surface reflects light of its own colour with preference, thus making the detection of colour coded stripes of light impossible, because the colours of the stripes tend to vary or even to fade out with different surface colours. Because of this the surface has to be 'whitened' in the computer memory (i.e. for a red surface: red brightness values have to be decreased while green and blue values have to be increased).

After albedo normalization the stripe will appear as shown in Fig. 5. Now the centre will be precisely detected. As a side effect, the number of gaps in a stripe, caused by regions of low reflectivity is significantly reduced.

4.2 Stage two: Finding the centre of a stripe

The contrast between those parts of the object which are illuminated by the stripes and those which are not is very high. By choosing an appropriate threshold, features of the object will be suppressed and only the stripes remain. Fig. 6 shows the appearance of a horizontal stripe of light which is scanned vertically. With an appropriate threshold level for brightness, a typical stripe of light is approximately 5 pixel wide. Its centre is defined to be its centroid and may be found by using a formula first described by Takagi and Hata.[4] Other formulae based on the intensity distribution of a stripe of light and probability methods[5,6] might produce even better results, but have not yet been tested. These methods take much longer

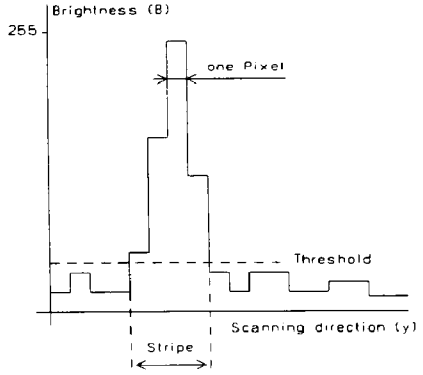

Fig. 6. Brightness of a stripe of light.

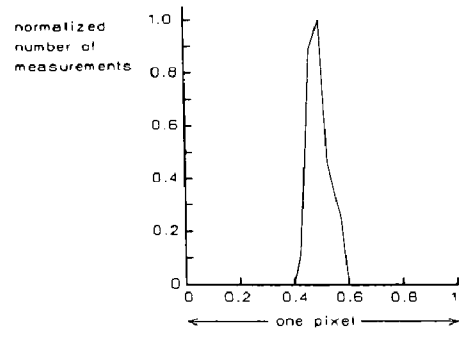

Fig. 7. Position, where the centre of a stripe was found in 250 measurements.

Example A: Restoration of a cavity using cubic splines

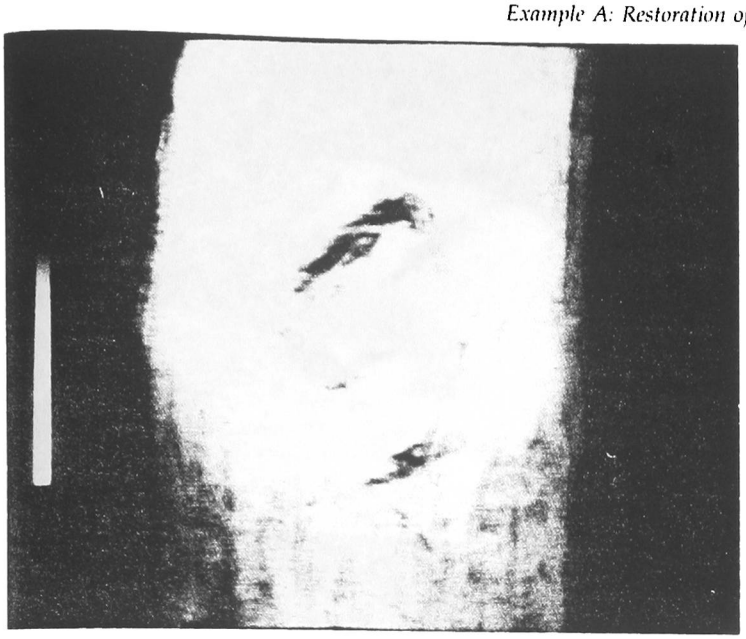

Fig. 8. Model of a cavity (10 cm).

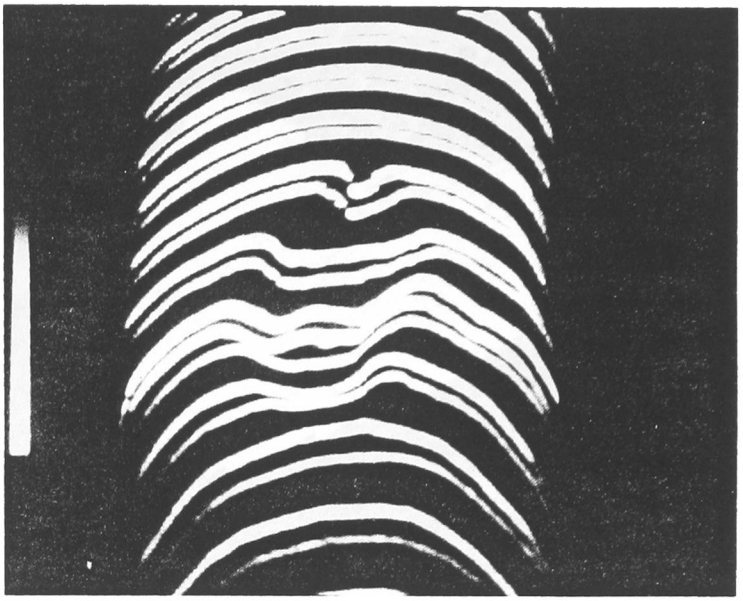

Fig. 9. Stripes projected onto the cavity (blue plane).

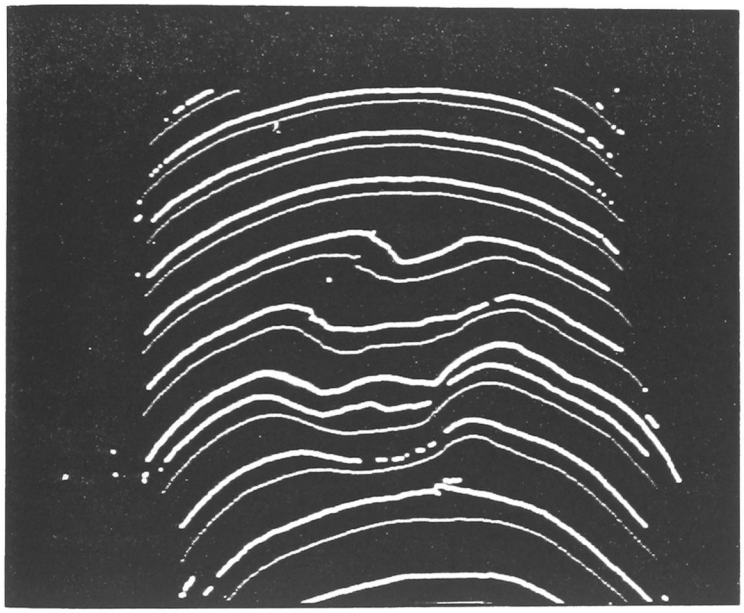

Fig. 10. Stripes extracted.

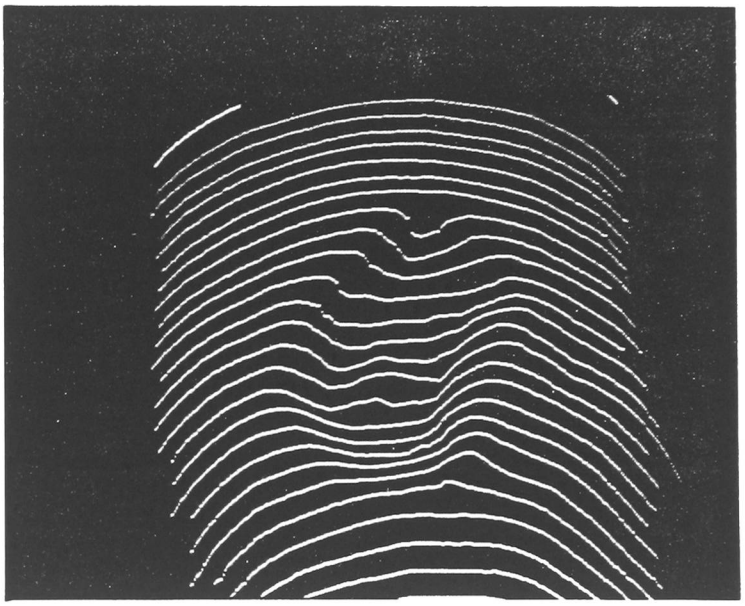

Fig. 11. Stripes linked.

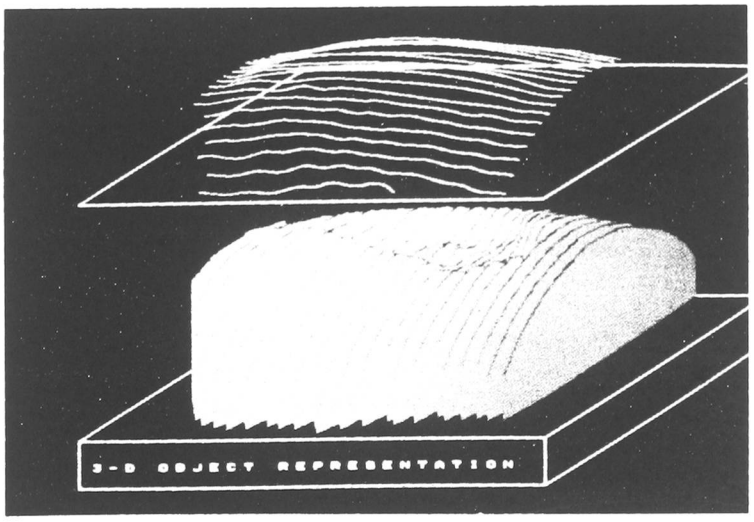

Fig. 12. Representation of the cavity (bottom) and the reconstructed surface (top).

Example B: Restoration of a sphinx's nose using external data

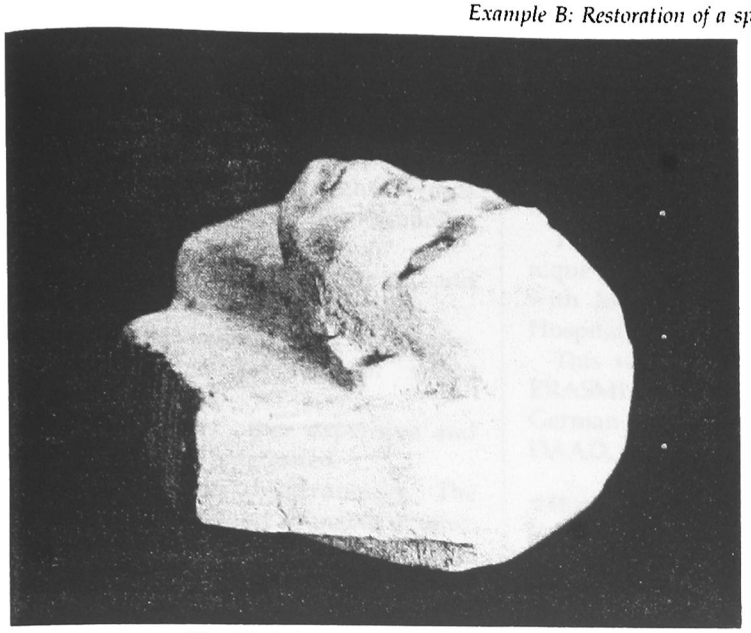

Fig. 13. Sphinx with damaged nose.

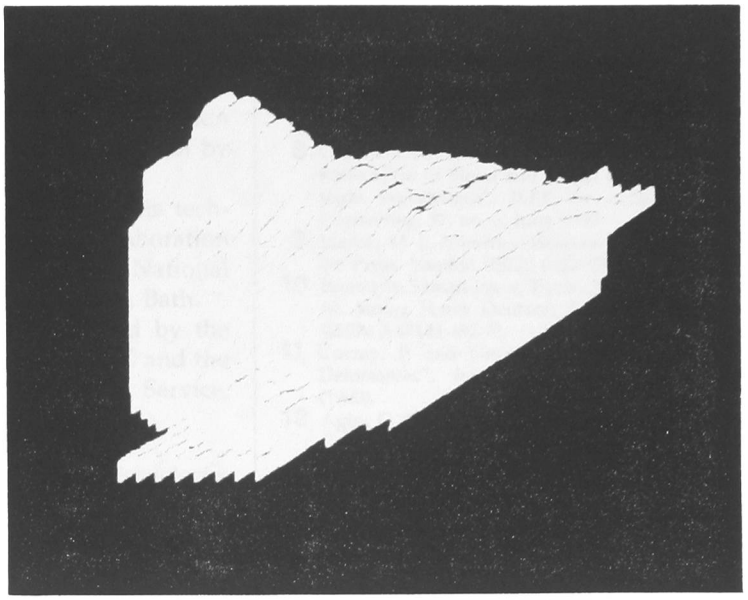

Fig. 14. Sphinx, nose reconstructed.

to compute for only a slight improvement in accuracy.

The consistency with which the centre of each stripe can be determined depends on noise. Repeated measurements show that the centre of the stripe can be located to within ±0.1 pixel. This is equivalent to an accuracy in depth measurement of ±0.02 mm for a 10×10 cm object covering the whole array of 512×512 pixels. Fig. 7 shows the position where the centre of a stripe was located in a sample of 250 measurements.

4.3 Stage three: Closing gaps

Despite albedo normalization a stripe of light may occasionally show a gap, either because of extremely low reflectance or steep angles of an object surface. A linking algorithm using the colour information of the stripes detects the corresponding parts of each stripe.

The algorithm uses a set of three simple rules:

- Only stripes with the same colour may be connected.
- Crossing of stripes is not allowed.
- Linking over unlikely distances (more than three times the minimum distance between stripes) is not accepted.

At present the linking process we have designed does interpolate to fill the gap with a suitable curve. This is subject to further development.

5 Surface Reconstruction

Surface reconstruction is performed in three stages: feature extraction, depth calculation and the actual restoration of the damaged surface.

5.1 Feature extraction

The features of interest are edges and damaged parts of the object. These parts may be found by significant differences in colour ratios or polarization of the reflected light. Applied to human skin ulcers colour ratios may be used to determine the damaged tissue.[7,8] In certain cases, extraction of these features may also be possible by template matching. Under these conditions the system acts automatically. In cases where automatic processing is difficult or impossible, a database supported input by the human operator may be required.

5.2 Depth calculation

After extracting the features of interest, depth calculation is executed by using simple triangulation, as shown in Fig. 2. The data of the triangulation model results in a three dimensional map of the surface.

5.3 Reconstruction

Once the three dimensional properties of the object are derived from the depth calculation, these data may be processed by a variety of algorithms. The restoration of the damaged surface is highly dependent on the kind of object. The operator may choose between three methods:

5.3.1 Reconstruction by cubic splines
This will be the method of choice if the original surface was curved smoothly. Cubic splines interpolate so that the reconstructed surface will have a minimum curvature,[9,10] exactly as skin under normal tension from all sides will cover a limb. This is shown in example A, Figs. 8-12.

5.3.2 Database assisted reconstruction
In case of a missing structure, the necessary data may well be obtained by using a 3-D database, which derives its information from symmetry relations (i.e. an object which is a mirrored counterpart of an existing structure) or from another, identical or similar object. This is shown in example B, Figs. 13 and 14, where the nose of a sphinx is reconstructed using data obtained from the nose of a human subject.

5.3.3 Manual reconstruction
In an interactive process the programme operator may model the missing or damaged part. This method is the subject of further development.

6 Calibration

Before performing a measurement the system must be calibrated. This is to compensate for lens errors in the camera and projector and mechanical alterations caused by shocks or vibrations.

The system is made to compare a pattern which is stored in the computer memory with the same one in a special calibration fixing. Any space and colour deviations will be detected and computed to an error correction map. This map is used to correct the acquired pictures.

7 Discussion

The structured light technique has proved to be a powerful tool for three dimensional measurement.[11] Nevertheless, other techniques, such as the time of flight of light,[12] stereo vision,[13] holography,[14] Moire fringe,[15] or rasterstereography techniques,[16] are also possible to obtain the underlying 3-D data, but have disadvantages. Three dimesional measurement by structured light is a well documented approach. In this context we believe, with other authors[17-19] that, compared with other methods, it offers the following advantages.

Ability to work on objects with low

contrast and ambiguous surrounding lighting conditions, by replacing these through controlled lighting with known spectral properties.

Scanning the object by a CCD camera, together with a simultaneous projection of a set of stripes of light, avoids complicated mechanical scanning systems.

The system is inexpensive, fast, and needs negligible maintenance.

The method itself avoids the corresponding-points problem of stereo vision.

No laser or any other expensive and complex device is required.

There are some disadvantages. The structured light method is unable to operate in bright daylight, since the contrast between a bright surface and the projected stripes is too low to allow location and identification. This problem may be overcome, if necessary, by using an extremely bright light source for the projector (e.g. a flash cascade).

At present, the system cannot merge two or more pictures of the same object to obtain a complete description of the whole object. Processing is limited to the area of the object that is visible both to the camera and the projector.

The object may not move with respect to the system during the acquisition phase of the two pictures necessary for processing. The time taken depends on the performance of the frame-grabbing hardware ($\frac{1}{50}$ sec.).

Acknowledgements

The authors wish to thank Mr. Viv Cole for his assistance in photography and the production of striped slides. The research was carried out on an ITEX* 200 Vision system kindly placed at our disposal by Datacell Inc., Reading.

The medical application for this technique is being assessed in collaboration with Mr. E. F. J. Ring, Royal National Hospital for Rheumatic Diseases, Bath.

This work is partly supported by the ERASMUS programme of the EC and the German Academic Exchange Service, DAAD, grant no. 312 009 625 1.

*ITEX is a trade mark of Imaging Technologies Inc.

References

1 Pennington, K. S. and Will, P. M., "A Grid-Coded Technique for Recording 3-Dimensional Scenes Illuminated with Ambient Light", *Opt. Comm.*, **2**, 167-169 (1970).

2 Boyer, K. L. and Kak, A. C., "Color Encoded Structured Light for Rapid Active Ranging", *IEEE Trans. on Pattern Recognition and Machine Intelligence*, **9**, 14-28 (1987).

3 Horn, B. K. P. and Sjoberg, R. W., "Calculating the Reflectance Map", *App. Opt.*, **18**, 1770-1779 (1979).

4 Takagi, Y. and Hata, S., "High Speed Precise 3-D Vision Sensor Using Slit Light Method", *Proc. of Int. Workshop on Industrial Application of Machine Vision*, p.235-239 (1987).

5 Keely, A. and Morehouse, C., "Structured Light Technique Applied to Solder Paste Height Measurement", *Optics, Illumination and Image Sensing for Machine Vision II, SPIE Proc.*, **850**, 88-92 (ISBN 0-89252-885-0).

6 Alexander, B. F. and Kim Chew Ng, "3-D Shape Measurement by Active Triangulation Using an Array of Coded Light", *Optics, Illumination and Image Sensing for Machine Vision II, Proc. SPIE*, **850**, 199-209 (1987).

7 Afromowitz, M. A., Callis, J. B. and Heimbach, D. M., "Multispectral Imaging of Burn Wounds", *Medical Imaging II, Proc. SPIE*, **914**, 500-504 (1988).

8 Cui, W., Ostrander, L. E. and Lee, B. Y., "In Vivo Reflectance of Blood and Tissue as a Function of Light Wavelength", *IEEE Trans. on Biomedical Engineering*, **37**, no. 6, June 1990.

9 Maron, M. J., *Numerical Analysis*, Collier Macmillan Press, London (ISBN 0-02-475670-9).

10 Bronstein Semandejew, *Taschenbuch der Mathematik*, Verlag Harry Deutsch, Frankfurt und Thun (ISBN 3-87144-492-8).

11 Curran, P. and Groves, D., "Assessing Spinal Deformities", *Image Processing*, **2** (2), 14-16 (1990).

12 Agin, G. J., "Representation and Description of Curved Objects", Thesis, AIM-173, Stanford AI-Lab (1972).

13 Cheung, Chi-Cong and Brown, W. A., "3-D Shape Measurement using Three Camera Stereopsis", *Optics, Illumination and Image Sensing for Machine Vision II, Proc. SPIE*, **850**, 128-135 (ISBN 0-89252-885-0) (1988).

14 Jalkio, J. A., Kim, R. C. and Case, S. K., "Triangulation Based Range Sensor Design", *Proc.SPIE Int. Soc. Opt. Eng.*, **728**, 243-247 (1986).

15 Takasiki, H., "Moire Topography", *App; Opt.*, **12** (4), 845-850 (1973).

16 Frobin, W. and Hierholzer, E., "Rasterstereography: A Photogrammetric Method for Measurement of Body Surfaces", *Photogrammetric Engineering and Remote Sensing*, **47** (12), 1717-24 (1981).

17 Popplestone, R. J. and Brown, C. M., "Forming Mod. of Plane-and-Cylinder Faceted Bodies from Structured Light", *Proc. 4th YJCAI*, 664-668 (1975).

18 Lewis, J. R. T. and Sopwith, T. "Measuring the Human chest with Structured Lighting", *3rd Int. Conf. on Pattern Recognition*, **4** (5), 359-366 (ISSN: 0167-8655) (1985).

19 LeMoigne, J. and Waxman, A. M., "Projected Light Grids for Short Range Navigation of Autonomous Robots", *Proc. 7th Int. Conf. on Pattern Recognition*, 203-206 (1984).

1ST EUROPEAN CONFERENCE ON ◆ ADVANCES ◆ IN WOUND MANAGEMENT

4-6 September 1991

University of Wales
College of Cardiff

PROCEEDINGS

SPONSORSHIP PROVIDED BY

Smith+Nephew

Measuring area and volume of human leg ulcers by colour coded structured light

P. Plassman and B.F. Jones

Department of Electronics and Information Technology, Polytechnic of Wales, Pontypridd, Mid Glamorgan, UK

Summary

This paper describes a non-contact semi-automatic leg ulcer measurement and management system. Besides measuring the area of an ulcer it can also evaluate its volume by calculating the difference between the virtual reconstruction of the former healthy skin and the actual measured surface.

An adequate representation of a real ulcer is created in a personal computer memory using a structured light scanning system with simultaneously projected stripes of colour coded light. The method is fast and reliable, and capable of evaluating area and volume with an uncertainty of 5% of the total size.

Means for ulcer classification, healing time forecast and patient data management may be included into the system.

INTRODUCTION

Ulcers of the human skin may be induced by a weakened immune system, age, certain diseases or medical treatment. They are favoured by illnesses that force the patient to remain nearly motionless in one position exposing parts of the body to a constant pressure. These are generally focal areas over bony prominences. The blood supply to the skin is then reduced significantly which contributes to the likelihood of development of a pressure sore.

In an average hospital population up to 8% of all bedridden or chairbound patients suffer from pressure sores causing long lasting pain to the patients.[1] Such wounds heal very slowly. Several months rather than weeks are normal for the healing process. Some patients suffer even longer due to drawbacks during treatment and may have to live with the lesion for several years. Patients with pressure sores stay between 3.5 and 5 times longer in a hospital than normal.[2]

The costs for this are an enormous burden to the NHS in excess of £100 million annually (1989). An American survey[3] revealed that the costs for one patient alone are between $2000 and $10 000. The total figure for the United States was estimated as $3–5 billion (1980).

Doctors generally agree on two main phases for ulcer

treatment: a first cleansing phase followed by a granulation/epithelialisation phase.[4]

During the first phase, which lasts approximately two weeks, surgery and cleaning by enzymes is appropriate. The wound is usually treated with 0.9% sodium chloride solution (saline) or dextranomer beads.[5] The second phase of ulcer treatment may last several months but '. . . there is surprisingly little agreement about subsequent management'.[6]

A 1988 survey by Knight[7] concludes that '. . . there are literally hundreds of agents that are touted to improve healing, but until an adequate trial can prove the efficacy of these agents, conservative treatment remains the preferred method'.

Only a few well controlled studies have been carried out to obtain objective information on the suitability of several treatment methods, mainly due to the lack of appropriate measurement methods and devices.

EXISTING MEASUREMENT METHODS

In the past several attempts have been made to measure area and volume of skin ulcers. Photography or digitised thermography[8] are unable to deliver any three dimensional volume information and are restricted to areas where the skin is relatively flat.

Berg *et al.*[6] proposed a method where a transparent and adhesive film completely covers the sore. The volume between film and wound is then filled with a measured amount of saline solution. Similar to other contact making methods it is painful for the patient, may damage the wound and risks additional infection.

The most advanced non-contact approach uses stereophotogrammetry.[9] The results of photogrammetric measurement are not available instantly as photographic processing and at least 20 minutes of image scanning by a trained human operator are necessary.

THE MEASUREMENT TECHNIQUE

An ulcer measurement system should avoid any contact with the patient. It should be fast and reliable in producing an accurate three-dimensional representation of the lesion.

Our approach uses the structured light triangulation method.[10] A set of parallel stripes of light is projected onto the surface of interest under a certain angle as shown in Figure 1.

A camera, which is connected to a PC based imaging system, observes the scene from above. The relative positions of camera and projector, the projection and the observation angles are known to the computer. Using this geometrical information together with the observed intersections of the planes of light with the surface, the computer can calculate the relative positions in space of those surface points being hit by light. The sensor houses a specialised stripe projector and a colour CCD camera. The portable PC (an 80286 processor with mathematical co-processor at 10 MHz) is equipped with additional hardware for image capture, processing and display. Except for the stripe projector all elements are common industrial components. As a result the system is relatively cost efficient.

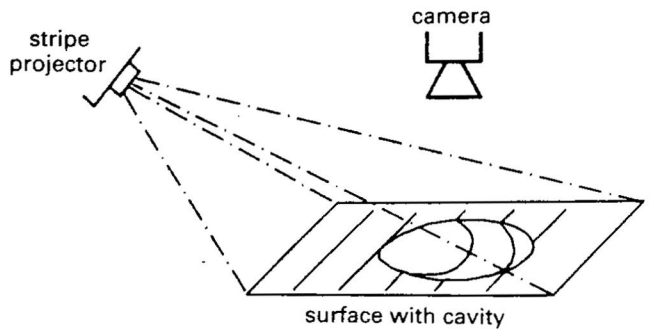

Figure 1. The principle of three-dimensional measurement by structured light.

THE MEASUREMENT PROCESS

The process of ulcer measurement is divided into four steps: image acquisition, image processing, surface reconstruction and calculation of area and volume.

Image acquisition

The slide projector illuminates the scene with two different patterns, producing two pictures which are stored in the computer for later processing.

Picture 1

To obtain the first picture the projector illuminates the scene with a bright, homogeneous beam of light. From this picture the boundaries of the ulcer which are required for area and volume calculation will be extracted in later image processing steps. A reflectance map will also be obtained from this picture. The map provides reflectance data for each point of the scene and is vital for later image processing.

Picture 2

To obtain the second picture a set of approximately 60 parallel stripes of colour coded light are projected onto the skin. The term 'colour coded'[11] describes the system's capability of recognising three kinds of stripes coded in the primary colours, red, green and blue. These stripes appear in order on the slide. Only one stripe is coded in white as a reference mark. The purpose of colour coding the stripes is to aid the detection of a given stripe over the object's surface. In areas where the reflectance is small, or at edges of the object, the stripes may disappear, so that an algorithm must redraw the missing parts linking the right ends of the stripes together. From this picture depth information will be calculated. Figure 2 shows a plaster model of an ulcer with these stripes.

The time necessary to acquire both pictures is approximately 0.1 s. This is an important parameter as the patient's position relative to the camera must not change during the acquisition process. Otherwise the image data obtained from pictures 1 and 2 will not be in spatial co-incidence.

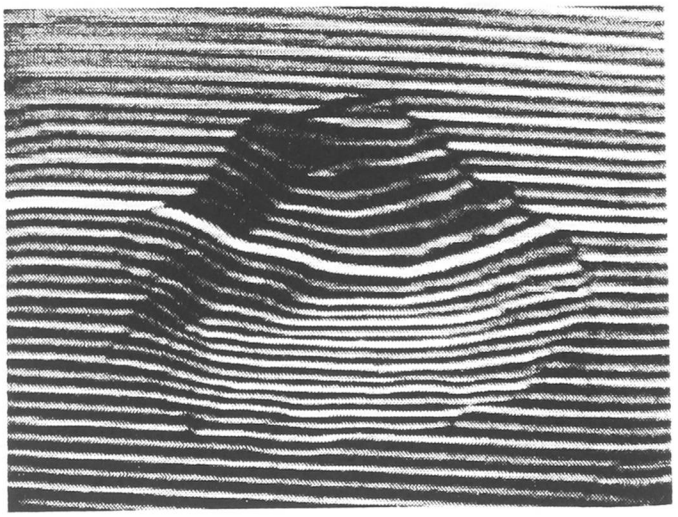

Figure 2. A computer generated image of a plaster model of an ulcer with stripes projected on it.

Image processing

Once the two pictures have been taken computer algorithms correct for camera non-linearity (γ-correction) and lens errors (chromatic and monochromatic aberrations).

After this pre-processing the effects of varying reflectivity of the observed surface have to be compensated for using the reflectance map obtained from picture 1.[12] The need for this becomes obvious when considering that the accuracy of the structured light technique depends on its ability to find the centre of the projected lines precisely. Figure 3 shows a stripe of light passing a region of low reflectivity. This region partly darkens the projected stripe. Thus its centre will be detected at the wrong position.

As a side effect of the compensation process, the number of gaps in a stripe, caused by regions of low reflectivity, is significantly reduced.

Another reason for reflection compensation is colour. A coloured surface reflects light of its own colour with preference thus making the detection of colour coded stripes of light difficult as the colours of the stripes tend to vary or even to fade out with different surface colours. Reflection compensation results in a virtual 'whitening' of the surface in the computer memory (i.e. for a red surface: red brightness values have to be decreased while green and blue values have to be increased).

After reflection compensation the projected stripes of picture 2 appear more clearly and evenly. Nevertheless they have a certain width and their centres have to be detected.

Figure 4 shows the brightness distribution of a horizontal stripe of light, scanned vertically. The contrast between those parts of the skin hit by the stripes and those which are not is very high. A dynamic threshold for stripe extraction automatically adapts itself to the underlying brightness of the scene. Thus features of the object are being suppressed and only the stripes remain.

A typical stripe of light is approximately 5 pixels wide. Its centre is defined to be its centroid and may be found with sub-pixel accuracy using the formula in Figure 4.

The consistency with which the centre of each stripe can be determined depends on noise inevitably produced by camera electronics, quantisation errors, etc. Repeated measurements under ideal circumstances show that the centre of the stripe can be located to within ± 0.1 pixel. This is equivalent to an accuracy in depth measurement of ± 0.02 mm for a 10 × 10 cm object covering the whole array of 512 × 512 pixels. Figure 5 shows the position where the centre of a stripe was located in a sample of 250 measurements.

On real skin, however, this accuracy cannot be achieved. Scattering within the optically heterogeneous skin adds a

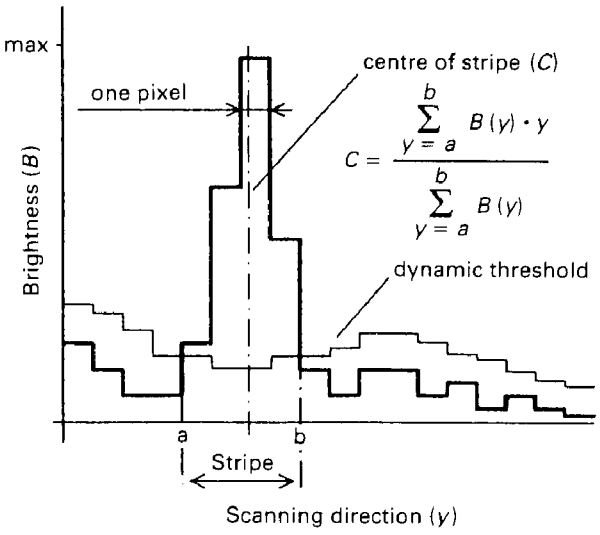

Figure 4. Detection of the centre of a stripe of light with sub-pixel accuracy.

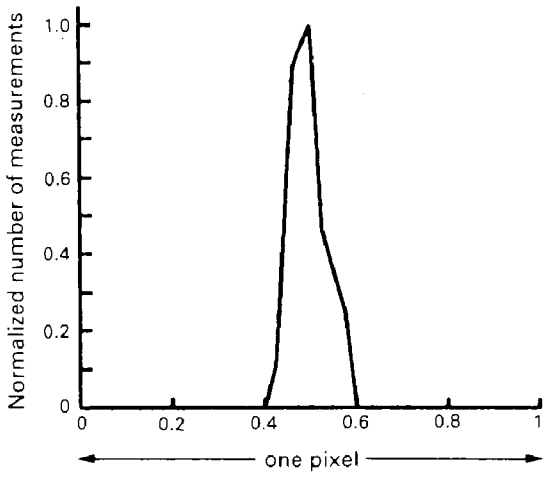

Figure 5. The position where the centre of a stripe was located in a sample of 250 measurements under ideal conditions.

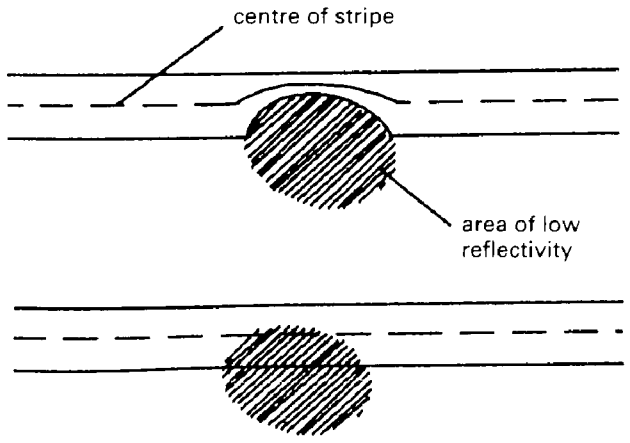

Figure 3. The centre of a stripe before and after reflection compensation.

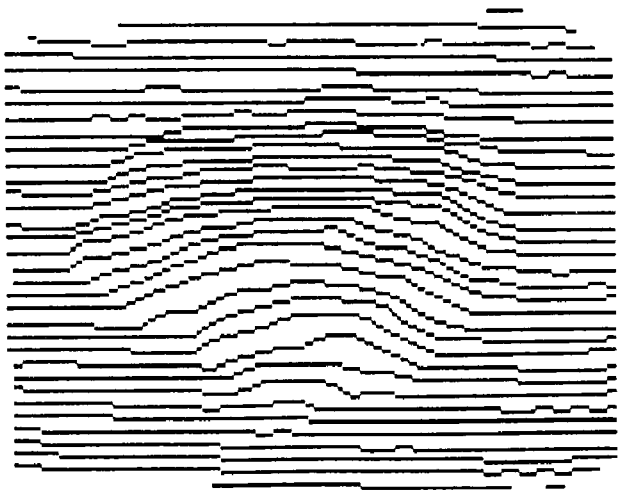

Figure 6. Extracted, thinned and linked stripe image of a plaster model.

certain amount of uncertainty and noise to the measurement leading to an accuracy of ± 0.4 mm in the worst cases.

In a final image processing step an algorithm closes gaps in the stripe pattern. These appear when a stripe of light passes a region of extremely low reflectance or steep slopes of the ulcerated skin. The linking algorithm uses a set of three simple rules:

- only stripes with the same colour may be connected
- crossing of stripes is not allowed
- linking over unlikely distances is not accepted.

Image processing results in a stripe map as shown in Figure 6. The depth information of the measured ulcerated skin is encoded in the positions of the stripes.

Surface reconstruction

The volume of an ulcer is the difference between its actually measured surface and the former healthy surface. Therefore the healthy surface has to be virtually reconstructed in the computer's memory. In a first step the boundary of the ulcer has to be extracted from the image data. At present this is done manually using a pointing and drawing device commonly known as a 'mouse'. In future this process may be performed automatically using colour information, shading or polarisation (wet parts) of the ulcerated area.

The second step is the virtual reconstruction itself. Third order cubic splines interpolate the healthy skin over the damaged area and produce a surface with minimum curvature (Figure 7). This imitates the behaviour of skin under normal tension from all sides.

Calculation

The final step is the calculation of area and volume of the ulcer. Area calculation uses the extracted boundary of the ulcer and takes the curvature of the surface into account. The volume of the ulcer is derived from the difference between the measured and reconstructed surface. Repeated measurements on a plaster model produced results with a mean error of less than 5%.

FURTHER DEVELOPMENT

At present the accuracy of measurement is not completely satisfactory but can be increased. By doubling the number of projected stripes the accuracy also doubles. Refining some image processing algorithms will also result in a higher accuracy.

Taking pictures with a colour camera under controlled lighting conditions offers the opportunity to design a scheme for ulcer classification. A similar attempt has been made by Arnqvist and his group[4] using colour photographs.

Afromowitz *et al.*[13] suggested a method to predict the healing time of an ulcer using red/infra-red *versus* green/infra-red diagrams. As a common CCD camera is also sensible in the near infra-red this feature may also be included in the system in the future.

Finally a patient data managing system will be introduced. Its ability to store a whole patient's history file including colour pictures on computer media offers the physician a tool for finely controlled studies into the treatment of ulcers.

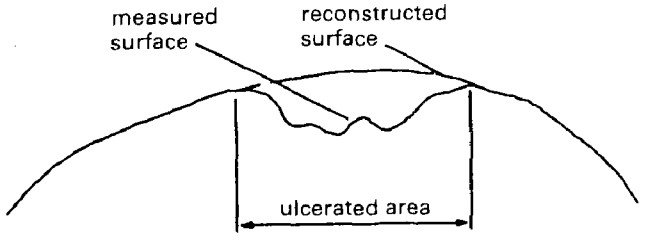

Figure 7. Reconstruction of the healthy surface by cubic spline interpolation.

DISCUSSION

The structured light technique itself has proved to be a powerful tool for three dimensional measurement.[14] Other techniques such as stereo vision[15] and Moire fringe[16] can also be used to obtain the underlying three dimensional data, but have disadvantages when being used for ulcer measurement.

A disadvantage of the structured light method is its inability to operate under bright daylight conditions as the stripe contrast becomes too low to allow accurate location and identification. This problem may be overcome, if necessary, by using an extremely bright light source for the stripe projector.

Furthermore the system cannot merge two or more scans of the same ulcer stretching around a limb to obtain a complete description of the whole lesion. Processing is limited to the area of the ulcer that is visible both to the camera and the projector.

Ulcers which are partly covered by skin cannot be measured.

Acknowledgements—The authors wish to thank Mr Francis Ring from the Royal National Hospital for Rheumatic Diseases in Bath and Dr Rajan from the Cottage Hospital in Pontypridd for their help and advice in medical questions. This work in partly supported by the German Academic Exchange Service, grant no. 312009 625 1.

REFERENCES

1 Barbenel, J.C., Jordan, M.M., Nicol, S.M., & Clark, M.O. (1977): Incidence of pressure-sores in the Greater Glasgow Health Board area. *Lancet* ii, 548–550.
2 Allman, R.M., LaPrade, C.A., Noel, L.B., Walker, J.M., Moorer, C.A., Dear, M.R. & Smith, C.R. (1986): Pressure sores among hospitalized patients. *Annals of Internal Medicine* **105**, 337–342.
3 Constantin, M.B. (ed) (1980): *Pressure Ulcers: Principles and Techniques of Management*. Boston: Little Brown.
4 Arnqvist, J., Hellgren, L. & Vincent, J. (1988): Semiautomatical classification of secondary healing ulcers in multispectral images. In *Proceedings of the 9th International Conference on Pattern Recognition*, pp. 459–461.
5 Erikson, G., Eklund, A.E., Lidén, S. & Zetterquist, S. (1984): Comparison of different treatments of venous leg ulcers: a controlled study using stereophotogrammetry. *Current Therapeutic Research* **35**, 678–684.
6 Berg, W., Traneroth, C., Gunnarson, A. & Lossing, C. (1990): A method for measuring pressure sores. *Lancet* **335**, 1445–1446.
7 Knight, A.L. (1988): Medical management of pressure sores. *Journal of Family Practice* **27**, 95–100.
8 Ring, E.F.J. (1985): Video thermal imaging. In *Thermological Methods*, pp. 101–111. Heidelberg: Verlag Chemie.
9 Bulstrode, C.J.K., Goode, A.W. & Scott, P.J. (1986): Stereophotogrammetry for measuring rates of cutaneous healing: a comparison with conventional techniques. *Clinical Science* **71**, 437–443.
10 Popplestone R.J., Brown, C.M. *et al.* (1975): Forming models of plane-and-cylinder faceted bodies from structured lighting. In *Proceedings of the 4th YJCAI*, pp. 664–668.
11 Boyer, K.L. & Kak, A.C. (1987): Color encoded structured light for rapid active ranging. *IEEE Transactions on Pattern Recognition and Machine Intelligence* **9**, 14–28.
12 Horn, B.K.P. & Sjoberg, R.W. (1979): Calculating the reflectance map. *Applied Optics* **18**, 1770–1779.
13 Afromowitz, M.A., Callis, J.B. & Heimbach, D.M. (1988):

Multispectral imaging of burn wounds. In *Proceedings of the SPIE (Medical Imaging II)* **914**, 500–504.
Lewis, J.R.T. & Sopwith, T. (1985): Measuring the human chest with structured lighting. *3rd International Conference on Pattern Recognition* **4**, 359–366.
Curran, P. & Groves, D. (1990): Assessing spinal deformities. *Image Processing* **2** (2), 14–16.
16 Cheung, C.C. & Brown, W.A. (1988): 3D shape measurement using three camera stereopsis. In *Proceedings of the SPIE (Optics, Illumination and Image Sensing for Machine Vision II)* **850**, 128–135.
17 Takasiki, H. (1973): Moire topography. *Applied Optics* **12**, 845–850.

References

[1] Abdou,I.E. Pratt,W.K.
Quantitative Design And Evaluation Of Enhancement Edge Detectors
Proc.IEEE, vol.67, no.5, p.753-763, May 1979

[2] Afromitz,M.A. James,B.C. Heimbach,D.M et al.
Multispectral Imaging of Burn Wounds
Proc.SPIE Medical Imaging II
vol.914, p.500-504, Feb. 88, ISSN: 0-89252-949-0

[3] Afromowitz,M.A. Van Liew,G.S. Heimbach,D.M.
Clinical Evaluation Of Burn Injuries Using An Optical Reflectance Technique
IEEE Transactions on Biomedical Engineering
vol.BME-34, p.114-127, Feb.1987

[4] Agapakis,J.E. Epstein,G.N. Friedman,J.M. Katz,J.M. et al.
Adaptive Robot Welding Using Preview Vision Sensing of Joint Geometry
Proc. SPIE: Intelligent Robots and Computer Vision: Fifth in a Series
vol.726, p.566-575, Oct. 1986, ISSN: 0277-786x

[5] Agin,G.J. Binford,T.O.
Computer Description Of Curved Objects
Proc. Int. Joint Conf. on artificial Intelligence
p.629-640, 1983

[6] Agin,G.J.
Representation and Description of Curved Objects
Ph.D Thesis
Oct. 1972, AIM-173, Stanford AI-Lab

[7] Alexander,B.F. Kim Chew Ng
3-D Shape Measurement by Active Triangulation Using an Array of Coded Light
Proc. SPIE: Optics, Illumination and Image Sensing for Machine Vision II
vol.850, p.199-209, 1987

[8] Allman,R.M La Prade,C.A. Noel,L.B. et al.
Pressure Sores Among Hospitalized Patients
Ann. Intern. Med., vol.105, p.337-342

[9] Aloimonos,J. Weiss,I. Bandyopadhyay,A.
Active Vision
Int. Journal of Computer Vision (Netherlands)
vol.1, part 4, p.33-56, 1988
Kluver Academic Publishers, Boston

[10] Altschuler,M.D. Altschuler,B.R. Taboada,J.
Laser Electro-optic System For Rapid 3-D Topographic Mapping Of Surfaces
Optical Engineering
vol.20, part 6, p.953-961, 1981

[11] Amelio,G.F.
Charge-Coupled Devices
CCD, The Solid State Technology
p.177-187, Fairchild Semiconductor Ltd.

[12] Amini,Afshin Tewfik,Ahmed H.
Comparison of Parametri and Non-Parametric Edge Detection Algorithms
Proc. on Image Processing Algorithms and Techniques
vol.1244, p.417-428, 1990, ISBN: 0-8194-0291-5
SPIE (Editor: Pennington,K.S.)

[13] Anderson,R.Rox Parrish,John A.
The Optics of the Human Skin
The Journal of Investigative Dermatology
vol.77, p.13-19, 1981

[14] Anderson,R.R. Hu,J. Parrish,J.A.
Optical Radiation Transfer in Human Skin
Bioengineering and the Skin (Editors: Marks,R. Payne,P.A.)
p.253-265, ISBN 0-85200-314-5
MTP Press, Ltd (Lancaster, England)

[15] Arnquist,J. Hellgren,L. Vincent,J.
Semiautomatical Classification of Secondary Healing Ulcers
Proc. 9th Int. Conf. on Pattern Recognition
p.459-461, 1988, IEEE, New York, NY

[16] Barbenel,J.C. Jordan,M.M. Nicol,S.M. et al.
Incidence of Pressure-sores in the Greater Glasgow Health Board Area
Lancet 1977, p.548ff

[17] Baruch, Orit
Line Thinning by Line Following
Pattern Recognition Lettters (Netherlands)
vol.8, part 4, p.271-276, Nov. 1988

[18] Beard,L.F.H. Dale,P.F.
A portable Stereophotographic Camera for Clinical Measurement
Medical and Biological Illustration
vol.26, p.107-110, 1976

[19] Berg,W. Traneroth,C. Gunnarson,A. Lossing,C.
A Method for Measuring Pressure Sores
Lancet, vol.335, p.1445-46

[20] Blais,F. Rioux,M.
BIRIS: A simple 3-D Sensor
Proc.SPIE: Optics, Illumination and Image Sensing for Machine Vision
vol.728, p.235-242, 1986
Cambridge, MA, USA

[21] Bolle, Ruud M. Vemuri, Baba C.
On Three-Dimensional Surface Reconstruction Methods
IEEE Trans. on Pattern Analysis and Machine Intelligence
vol.13, p.1-13, Jan.1991, IEEE Log Number 9040358

[22] Boyer,K.L. Kak,A.C.
Color Encoded Structured Light for Rapid Active Ranging
IEEE Transactions on Pattern Recognition and Machine Intelligence
vol.PAMI-9, p.14-28, 1.Jan. 1987

[23] Boyle,R.D. Thomas,R.C.
Computer Vision, A First Course
1988, ISBN 0-632-01577-2
Blackwell Scientific Publications

[24] Breukmann, Bernd
Computer-Gestützte optische Meßsysteme in der 3-D Meßtechnik
MIOP '88: Microwaves and Optoelectronics (Conference Proceedings)
p.1-6

[25] Bronstein,Il'ja N. Semendjajew,K.A.
Taschenbuch der Mathematik
ISBN 3-87144-492-8
Verlag Harry Deutsch, Thun

[26] Bulstrode,C.J.K. Goode,A.W. Scott,P.J.
Stereophotogrammetry for Measuring Rates of Cutaneous Healing:...
Clinical Science, vol.71, p.437-443

[27] Cameron, John R. Skofronick, James G.
Medical Physics
John Wiley & Sons, Inc., 1978

[28] Chan,K.K
Implementation of Fast Cosine Transform With Digital Signal Processing
Proc. SPIE: Medical Imaging II
p.782-785, 1988

[29] Chen, Y.C. Yang, C.W. Hen, C.F.
An Ultrasonic Imaging System for 3-D Object Recognition
Proc.IECON: Int. Conf. on Industrial Electronics
vol.2, p.690-697, Conference held: 3.-6.Nov.1987

[30] Cheung, Chi Cong Brown, William A.
3-D Shape Measurement Using Three Camera Stereopsis
Proc.SPIE: Optics, Illumination and Image Sensing for Machine Vision II
vol.850, p.128-135, 1988, ISBN 0-89252-885-0

[31] Chiaradia,M.T. Distante,A. Stella,E.
3D Surface Reconstruction Using Orientation Map and Sparse Depth...
Proc.SPIE: Intelligent Robots and Computer Vision
vol.848, p.366-377, 1987, ISBN 0-8952-883-4

[32] Chin-Tu Chen Jin-Shin Chou Wei-Chung Lin Pelizarr,C.A.
Edge and Surface Searching in Medical Images
Proc.SPIE: Medical Imaging II
vol.914, p.594-599, Feb. 88

[33] Constantin,M.B. (Editor)
Pressure Ulcers: Principles and Techniques of Management
Little Brown, Boston, 1980

[34] Cooper,David B. Hung,Yi-Ping Taubin,Gabriel
A New Model-based Stereo Approach for 3D Surface Reconstruction
Second Int. Conf. on Computer Vision, 5-8. Dec.1988
p.74-83, ISBN: 0-8186-0883-8
IEEE Comp. Soc. Press, Washington/USA

[35] Cui, Weija Ostrander,Lee E. Lee,Bok Y.
In Vivo Reflection of Blood and Tissue as a Function of Light Wavelength
IEEE Transactions on Biomedical Engineering
vol.37, no.6, p.632-639, June 1990, IEEE Log Number 9034762

[36] Curran, Paul Groves, David
Assessing Spinal Deformities
Image Processing p.14-16 October 90

[37] Davies,E.R. Plummer,A.P.N.
Thinning Algorithms: A Critique and a New Methodology
Pattern Recognition, vol.14, p.53-63 , 1981
Pergamon Press Ltd.

[38] Deng, Tung-chiang Bergen, Trudy L.
Accuracy of Position Estimatation by Centroid
Intelligent Robots and Computer Vision
vol.848, p.141-150, 1987, ISBN: 0-8954-833-4

[39] Dodd,G.G. Rossol,L. (Editors)
Computer Vision and Sensor-Based Robots
1979, ISBN 0-306-40305-6
Plenum Press, New York

[40] Duda, R.O. Hart, P.E.
Pattern Clasification and Scene Analysis
1973, ISBN 0-471-22361-1
John Wiley & Sons, New York

[41] Edwards, Thomas R.
Two Dimensionbal Convolute Integer Operators for Digital Image Processing
Proceedings on Image Processing Algorithms and Techniques
vol.1244, p.26-44, 1990, ISBN: 0-8194-0291-5
Proc.SPIE (Editor: Pennington, K.S.)

[42] EG & G RETICON
Solid State Camera Products
1989

[43] Eriksson,G. Eklund,A.E. Liden,S. Zetterquist,S.
Comparison of Different Treatments of Venous Leg Ulcers: ....
Current Therapeutic Research
vol.35, p.678-684, April 1984
Therapeutic Research Press, Inc.

[44] Errikson,G. Eklund,A.-E. Torlegard,K. Dauphin,E.
Evaluation of Leg Ulcer Treatment with Stereophotogrammetry
British Journal of Dermatology
vol.101, p.123-131
British Assoc. of Dermatologists

[45] Fan, Ting-Jun Medioni,G. Nevatia, Ramakand
Matching 3-D Objects Using Surface Descriptions
Proc. of the 1988 IEEE Int. Conf. on Robotics and Automation
vol.3, p.1400-6, 1988

[46] Feather,J.W. Dawson,J.B. Barker,D.J. Cotterill,J.A.
A Theoretical and Experimental Study of the Optical Properties of in vivo Skin
Proceedings of the Symposium on Bioengineering and the Skin
p.275-281

[47] Ferguson,J. Barbenel,J.C.
Skin Surface Patterns and the Mechanical Properties of the Dermis
Bioengineering and the Skin (Editors: Marks,R. Payne,P.A.)
p.83-92, ISBN 0-85200-314-5
MTP Press, Ltd (Lancaster, England)

[48] Frantz, Rita A. Johnson, David A.
Stereophotography and Computerized Image Analysis: A Three Dimensional Method of Measuring Wound Healing
Wounds: A Compendium of Clinical Reasearch and Practice
vol.4, p.58-64, Feb. 1992

[49] Freeman,H. Potmesil,M.
Curved Surface Representation Utilizing Data From Photographic Images
Workshop on the Representation of Three Dimensional Objects, 1-2. May 1979
p.1-26, May 1979

[50] Frobin,W. Hierholzer,E.
Rasterstereography: A Photogrammetric Method for Measurement of Body Surfaces
Photogrammetric Engineering and Remote Sensing
vol.47, p.1717-24, 12.Dec.81
Amer. Soc. of Photogrammetry

[51] Gilblom, David L.
Special Scanning Modes in CCD Cameras
Proc.SPIE: Optics, Illumination and Sensing for Machine Vision IV
vol.1194, p.52-61, 1989, ISBN 0-8194-0233-8

[52] Girod, Bernd Scherock, Stephen
Depth from Defocus of Structured Light
Proc.SPIE: Optics, Illumination and Image Sensing for Machine Vision IV
vol.1194, p.209-215, 1989, ISBN 0-8194-0233-8

[53] Goharla'ee,M. Raaberg,M.
Applications Of Structured Lighting For Volume Measurement
Proc.SPIE: Optics, Illumination and Image Sensing for Machine Vision
vol.728, p.65-73, Oct. 1986, ISBN 0277-786x

[54] Groen,F.C.A. Ekkers,R.J. DeVries,R.
Image Processing with Personal Computers
Signal Processing
vol.15, p.279-291, 1988
Elsevier Science Publishers B.V. (North Holland)

[55] Naruse,N. Nomura,Y. Yamamoto,T.
High-Accuracy Distance and Inclination Measurement Using Slit-Ray Projection
Systems and Computers in Japan
vol.18, no.12, p.1-9, Dec. 1987, ISSN 0882-1666
Scripta Technica, Inc.

[56] Hansen,Charles Ayache,Nicholas Lustman,Francis
Towards Real-time Trinocular Stereo
p.129-133, ISBN: 0-8186-0883-8
IEEE Computer Society Press, Washington/USA

[57] Haralick,R.M. Chu,Y.H.
Solving Camera Parameters from Perspective Projection of a Parameteric Curve
Pattern Recognition
vol.17, no.6, p.637-645, 1984

[58] Healey, Glenn Binford, Thomas O.
A Color Metric for Computer Vision
Proc. CVPR '88: The Computer Soc. Conf. on Comp. Vis. & Patt. Rec.
p.10-17, 1988,

[59] Hecht, Eugene
Optics, Second Edition
1987, ISBN 0-201-11611-1
Addisson-Wesley Publishing Com., Inc.

[60] Hoff,William Ahuja, Narendra
Surfaces from Stereo: Integrating Feature Matching Disparity Estimation, and Contour Detection
IEEE Transactions on Pattern Analysis and Machine Intelligence
vol.11, no.2, p.121-136, Febr. 1989
IEEE Log Number: 8824799

[61] Hopwood,R.K.
Minicomputers and Microprocessors in Optical Systems
Proc.SPIE, vol.230, 1980

[62] Horn,B.K.P.
Robot Vision, 1986, ISBN 0-262-08159-8
MIT Press

[63] Horn,B.K.P. Sjoberg,R.W.
Calculating the Reflectance Map
Applied Optics
vol.18, no.9, p.1770-9, 1.June 1979

[64] Houkes, Zweitze Korsten, Maarten J.
Considering Shape from Shading as an Estimation Problem
Proc. on Image Processing Algorithms and Techniques
vol.1244, p.56-67, 1990, ISBN: 0-8194-0291-5
SPIE (Editor: Pennington, K.S.)

[65] Ide, Masao Masuzawa, Nobuyoshi
Multiple Section Tomograms Simultaneous Display Ultras. Diag. Equ.
Proc. Ultrasonics International Conference, Brighton
p.40-48, 1977, ISBN 0-902852-76-0
IPC Science and Technology Press

[66] Ikeuchi,Katsushi Kanade,Takeo
Applying Sensor Models to Automatic Generat. of Obj. Recog. Progs.
p.228-237, ISBN: 0-8186-0883-8
IEEE Comp. Soc. Press, Washington/USA

[67] Ishizaka, Yukuta Shimonura, Shoji

High-speed Pattern Recognition System Based on template Matching
Proc. SPIE Int. Soc of Opt. Eng (USA)
vol.849, p.202-208, 1988

[68] Jalkio,J.A. Kim,R.C. Case,S.K.
Threee Dimensional Inspection Using Multistripe Structured Light
Optical Engineering
vol.24, no.6, p.966-974, Nov/Dec 1985

[69] Jalkio,J.A. Kim,R.C. Case,S.K.
Triangulation Based Range Sensor Design
Proc.SPIE: Optics, Illumination and Image Sensing for Machine Vision
vol.728, p.243-247, 1986
Cambridge, MA, USA

[70] James,M.
Pattern Recognition
1987, ISBN 0-636-01885-2
BSP Professional Books, Oxford, Lond.

[71] Jarvis,R.A.
A Perspective On Range Finding Techniques For Computer Vision
IEEE Transactions on Pattern Recognition and Machine Intelligence
vol.PAMI-5, no.2, p.122-139, March 1983

[72] Jou, Jinn-Yeu Bovik, Alan C.
Improving Visible-Surface Reconstruction
Proc. CVPR 1988: The Comp. Soc. Conf. on Computer Vision
p.138-143, 1988

[73] Kaidbey,K.H. Agin,P.P. Sayre,R.M. Kligman,A.M.
Photoprotection by Melenin - a Comparison of Black and Caucasian Skin
Journal of the American Acadamy of Dermatology
vol.1, p.249-260

[74] Keeler, Elaine K.
Three-Dimensional Magnetic Resonance Imaging of the Head
Proceedings on Biostereometric Technology and Applications
vol.1380 , p.24-32, Conf. 7-8.Nov 1990, ISBN 0-8194-0447-0
SPIE, Editor Herron, R.E.

[75] Keely, Catherine A. Morehouse, Charles C.
Structured Light Technique Applied to Solder Paste Height Measurement
Proc.SPIE: Optics, Illumination and Image Sensing for Machine Vision II
vol.850, p.88-92, 1988, ISBN 0-89252-885-0

[76] Knight,Aubrey L.
Medical Management of Pressure Sores
The Journal of Family Practice
vol.27, p.95-100
Appleton & Lange

[77] Kuppenheim, Hans F. Heer, Raymond R.
Spectral Reflectance of White and Negro Skin Between 440 and 1000 μm
Journal of Applied Physiology
vol.4, p.800-806, 1952

[78] Lanir,Y.
The Fibrous Structure of the Skin and its Relation to Mech. Behav.
Bioengineering and the Skin (Editors: Marks,R. Payne,P.A.)
p.93-95, ISBN 0-85200-314-5
MTP Press, Ltd (Lancaster, England)

[79] Lapreste,J.T. Cartoux,J.Y Richetin,M.
Face Recognition from Range Data by Structural Analysis
Nato ASI Series: Ssyntactic and Structural Pattern Recognition
vol.F45, p.303-314, 1988
Springer Verlag, Berlin

[80] Lawrence,P.D. Yeung,K.K.
A Low-Cost Three Dimensional Vision System Using Space Encoded Spot Projection
Proc.SPIE: Optics, Illumination and Image Sensing for Machine Vision
vol.728, p.160-172, 1986
Cambridge, MA, USA

[81] LeMoigne,J. Waxman,A.M.
Projected Light Grids For Short Range Navigation Of Autonomous Robots
Proc. of the 7th Int. Conf. on Pattern Recognition
p.203-206, July/August 1984

[82] Lewis,J.R.T Sopwith,T.
Measuring the Human Chest with Structured Lighting
3rd. Int Conf. on Pattern Recognition
vol.4, part 5, p.359-366, Sept.1985, ISSN: 0167-8655

[83] Maron,M.J.
Numerical Analysis
ISBN: 0-02-475670-9
Collier Macmillan Press, London

[84] Maruyama, Minoru Abe, Shigeru
Range Sensing by Projecting Multiple Slits with Random Cuts
Proc.SPIE: Optics, Illumination and Image Sensing for Machine Vision IV
vol.1194, p.216-224, 1989, ISBN 0-8194-0233-8

[85] McClellan, Jay
Charact. and Correction of Image Acquisition System Response for Machine Vision
Proc.SPIE: *Optics, Illumination and Image Sensing for Machine Vision IV*
vol.1194, p.62-73, 1989, ISBN 0-8194-0233-8

[86] McVey,E.S. Lee,J.W.
Some Accuracy And Resolution Aspects Of Computer Vision Distance Measurement
IEEE Transactions on Pattern Analysis and Machine Intelligence
vol.PAMI-4, no.6, p.646-649, Nov.1982

[87] Miyamoto,K. Kobayashi,Y. et al.
Non-Contact High Precision Surface Measurement Instrument
Bull. Japan Soc. of Prec. Engg.
vol.2, no.2, p.121-122, June 1986

[88] Moring,I. Ailisto,H. Heikkinen,T. et al.
Acquisition and Processin of range Data Using a Laser .... System
Proc.SPI: Optics, Illumination and Image Sensing for Machine Vision II
vol.850, p.174-183, 1987, ISBN 0-89252-885-0

[89] Morrirssey-Golas,B.M.
Introduction to Color Image Processing
Electronic Imaging '88: Int. Electr. Imag. Exposition and Confer.
vol.1, p.66-68, Conf.: 3-6.Oct.'88
(Advance printing of paper summaries)

[90] Morris, Peter G.
Nuclear Magnetic Resonance Imaging in Medicine and Biology
1986 ISBN 0-19-855155-X Clarendon Press, Oxford

[91] Nakagawa,Y. Shiohara,M. Gotoh,T. Ohta,R.
A Hybrid Image Compression Method For Medical Images
Proc. SPIE: Medical Imaging II
vol.914, p.815-822, 1988

[92] Nayar, Shree K. Sanderson, Arthur C.
Determining Surface Orientatation of Specular Surfaces by Intensity Encoded Illummination
Proc.SPIE: Optics, Illumination and Image Sensing for Machine Vision II
vol.850, p.122-127, 1988, ISBN 0-89252-885-0

[93] Novak, Carol L. Shafer, Steven A. Willson, Reg G.
Obtaining Accurate Color Images for Machine Vision Research
Proc. Perceiving, Measuring and Using Color
vol.1250, p.54-68, 1990, ISBN 0-8194-0297-4
SPIE (Editor: Brill, Michael H.)

[94] Oppenheim, Allan V. Schafer, Ronald W.
Digital Signal Processing
1975, ISBN 0-13-214107-8
Prentice / Hall International, Inc.

[95] Parkhinen,J. Jaaskelainen,T. Kuittinen,M.
Spectral Representation of Color Images
Proc. 9th Int. Conf. on Pattern Recognition
vol.2, p.933-935, IEEE Cat 88CH 2614-6
Conference held: 14-17 Nov. 1988, Rome

[96] Pavy Jr., Henry,G. Smith, Stephen W. von Ramm, Olaf T.
An Improved Real Time Volumetric Ultrasonic Imaging System
Medical Imaging V: Image Physics
vol.1443, p.54-61, 1991, ISBN 0-8194-0538-8
SPIE, Editor: Schneider, Roger H.

[97] Pennington,K.S. Will,P.M.
A Grid-Coded Technique For Recording 3-Dimensional ScenesIlluminated with Ambient Light
Optics Communication
vol.2, no.4, p.167-169, Sept.1970

[98] Pentland, A.P.
Local Shading Analysis, Technical Note
Artificial Intelligence Centre SRI, Menlo Park, CA
1982

[99] Popplestone,R.J. Brown,C.M. et al.
Forming Models of Plane-And-Cylinder Faceted Bodies from Structured Light
Proc. 4th YJCAI
p.664-668, Sept.1975

[100] Posdamer,J.L. Altschuler,M.D.
Surface Measurement By Space Encoded Beam Systems
Computer Graphics and Image Processing
vol.18, p.1-17, 1982

[101] Pugh,A. (Editor)
Robot Sensors
1986, ISBN 3-540-16125-2
Springer Verlag, Berlin

[102] Puskorius,G.V. Feldkamp,L.A.
Camera Calibration Methodology Based on a Linear Perspective Transf. Model
Proc. of the IEEE Conf. on Robotics and Automation
vol.3, p.1858-60, 1988
IEEE

[103] Quian,Richard Xu,GuangYou
Investigation on Calibration Problem
Proc. IAPR Workshop on Computer Vision
p.249-252,Conference held: Tokyo, 12-14 Oct. 1988

[104] Richard,M.J. Allard,J. Ghosh,S.K. Bougouss,M.
Three-Dimensional Reconstruction of Human Limbs from Tomogr. Views
Computers and Biomedical Research (USA)
vol.22, p.26-35
Academic Press Inc.

[105] Rienecker, Wolfgang
Prüfen mit Licht
MM Maschinenmarkt
vol.4, 26.Jan.1988
Vogel-Verlag, Würzburg, Germany

[106] Ring,E.F.J. Hughes,H.
Real-Time Video Thermography
Journal of Medical Engineering and Technology Supplement
p.86-89, 1986
Taylor and Francis

[107] Ring,E.F.J.
Video Thermal Imaging
Thermological Methods
p.101-111, 1985
Verlag Chemie, Edition Medizin, Heidelberg

[108] Rosenfeld,J.P. Tsikos,C.J.
High Speed Space Encoding Projector for 3-D Imaging
Proc.SPIE: Optics, Illumination and image Sensing for Machine Vision
vol.728, p.146-1518, 1986
Cambridge, MA, USA

[109] Rostenberg, A. Wasserman, E. Medanski,R.S.
Sugar Paste in the Treatment of Leg Ulcers
Arch. Dermatol.
vol.78, p.94ff

[110] Schroeder, H.E.
Practical Illumination Concept and Technique for Machine Vision Applications
(also published in EG&G RETICON: Solid State Camera Products 1989)
June 84
Soc. of Manufacturing Engineers

[111] Schumaker, Larry L.
Reconstruction of 3D Objects Using Splines
Proc. on Curves and Surfaces in Computer Vision and Graphics
vol.1251 p.130-140 1990 ISBN: 0-8194-0298-2
Editor: Ferrari, L.A.

[112] Seitz,G. Titziani,H. Litschel,R.
3-D Koordinatenmessung durch optische Triangulation
Feinwerktechnik und Messtechnik
p.433-437, 1986
Stuttgart, Germany

[113] Shea, J.D.
Pressure Sores: Classification and Management
Clinic. Orthop.
vol.112, p.89-100

[114] Shrikhande,N. Stockman,G.
Surface Normals from Striped Light
Proc. 5th Scandinavian Conf. on Image Analysis, Stockholm
vol.2, p.649-60, 2.-5.June 87
Nat. Defense Res. Inst., Linkoping, Sweden

[115] Smith,Daniel J. Bhat,Shailash Bulgrin,Jeffrey P.
Video Image Analysis of Wound Repair
Wounds: A Compendium of Clinical Research and Practice
vol.4, p.6-15, Jan 1992

[116] Spann, M. Nieminen, A.
Adaptive Gaussian Weighted Filtering for Image Segmentation
Pattern Reckognition Letter (Netherlands)
vol.8, part 4, p.251-5, Nov. 1988

[117] Späth, Helmuth
Spline Algorithmen zur Konstruktion glatter Kurven und Flächen
3. Edition, 1983, ISBN 3-486-39473-8
R. Oldenbourg Verlag, München

[118] Stewart,Charles V. Dyer,Charles R.
The Trinocular General Support Algorithm: A Three-Camera Stereo...
p.134-138 ISBN: 0-8186-0883-8
IEEE Computer Society Press, Wash.USA

[119] Stockman,G. Hu,G.
Sensing 3-D Surface Patches Using A Projected Grid
IEEE Conf. on Computer Vision and Pattern Recognition
p.602-607, 1986, Conf. held: Miami Beach, Florida

[120] Svetkoff, Donald J.
Image Quality Evaluation of Machine Vision Sensors
Proc.SPIE: Optics, Illumination and Image Sensing for Machine Vision II
vol.850, p.54-61, 1988, ISBN 0-89252-885-0

[121] Tagare, Hemant D. deFigueiredo, Rui J.P.
On the Localization Performance Measure and Optimal Edge Detection
Proc. on Image Processing Algorithms and Techniques
vol.1244, p.408-428, 1990, ISBN: 0-8194-0291-5
SPIE (Editor: Pennington K.S.)

[122] Takagi,Y Hata,S
High Speed Precise 3-D Vision Sensor Using Slit Light Method
Proc. of Int. Workshop on Industrial Application of Machine Vision...
Tokyo, Japan, p.235-239, 1987

[123] Takasiki, H.
Moire Topography
Applied Optics
vol.12, no.4, p.845-850, 1973

[124] Takatani, Setsuo Graham, Marshall D.
Theor. Analysis of Diffuse Reflect. from a Two-Layer Tissue Model
IEEE Transactions on Biomedical Engineering
vol.BME-26, no.12, p.656-664 , Dec. 1979

[125] Terrel, Trevor J.
Introduction to Digital Filters
1988, ISBN 0-333-44322-5
Macmillan Education Ltd, London

[126] Wang,Y,F. Mitiche,A. Aggarwal,J.K.
Computation of Surface Orientation and Structure of Objects....
IEEE Transactions on Pattern Analysis and Machine Intelligence
vol.9, no.1, p.129-137, 1.Jan.1987

[127] Wang,Y.F. Aggarwal,J.K.
3D Object Recognition From Stripe Coding and Multiple Views
Proc. of the 5th Scandinavian Conf. on Image Analysis, Stockholm
vol.2, p.669-682, 1987
Nat. Defense Res.Inst., Linkoping, Sweden

[128] Welford, W.T.
Aberrations of the Symmetrical Optical System
1974 ISBN 0-12-742050-9
Academic Press, London

[129] Weng,Juyang Ahuja,Narendra Huang,Thomas S.
Two-View Matching
p.64-73, ISBN: 0-8186-0883-8
IEEE Comp. Soc. Press, Washington/USA

[130] Woodcock,J.P.
Instrumentation for the Invest. of the Extracranial Carotid Circul
Clin. Phys. Physiol. Meas. (UK)
vol.10, suppl.A, p.5-14, 1989

[131] Yanh,H.S. Boyer,K.L. Kak,A.C.
Range Data Extraction And Interpretation By Structured Light
Proc. First Conf. on Artificial Intelligence Applications
p.199-205, Dec. 1984, ISBN: 0 8186 0624 x
IEEE Comput. Soc., Silver Springs,USA

[132] Zisk,N.H. Wittels,N.
Camera Edge Response
Proc.SPIEE: Optics, Illumination and Image Sensing for Machine Vision II
vol.850, p.9-16, 1988, ISBN 0-89252-885-0